

Experimental studies of  
bypass transition and its control

by

Fredrik Lundell

February 2003  
Technical Reports from  
KTH Mechanics  
Royal Institute of Technology  
S-100 44 Stockholm, Sweden

Akademisk avhandling som med tillstånd av Kungliga Tekniska Högskolan i Stockholm framlägges till offentlig granskning för avläggande av teknologie doktorsexamen fredagen den 14:e mars 2003 kl 10.15 i Kollegiesalen, KTH, Stockholm.

©Fredrik Lundell 2003

Universitetsservice AB, Stockholm 2003

F. Lundell 2003, Experimental studies of bypass transition and its control

KTH Mechanics, Royal Institute of Technology  
S-100 44 Stockholm, Sweden

## Abstract

Bypass transition, *i.e.* transition of a boundary layer at subcritical Reynolds numbers, has been studied. Fundamental studies of the phenomenon as such have been performed side by side with experiments aimed at controlling, *i.e.* delaying, transition. The experiments have been performed in three different flow facilities, two with air as the working fluid (a plane channel flow and a wind-tunnel) and one with water (a water channel).

From the water channel data the well known low-speed streaks appearing in a boundary layer under a turbulent free stream are found to be correlated with upward motion in the boundary layer.

The streaks are found to scale in proportion to the boundary-layer thickness in both the streamwise and wall-normal directions. The streamwise length is around hundred boundary-layer thicknesses.

It is found that the secondary instability of the streaks grows slower for disturbances consisting of less than four wavelengths, as compared to continuous wavetrains.

Elongated low-speed structures are controlled, first in the plane channel flow and then by a reactive system in the wind-tunnel. In the channel, the breakdown of generated streaks is delayed by applying localized suction under the regions of low velocity. Measurements of the disturbance environment with and without control applied show that both the growth of the secondary instability and its spreading in the spanwise direction are reduced when applying the control. In order to be successful, the control has to be applied to a narrow region (about  $1/10^{\text{th}}$  of a streak width) around the position of minimum velocity.

The reactive system in the windtunnel, comprising four upstream sensors and four suction ports downstream, inhibits the growth of the amplitude of the streaks for a certain distance downstream of the suction ports. After the inhibited growth the disturbances start to grow again and far downstream the streak amplitude returns to close to the uncontrolled values.

**Descriptors:** Fluid mechanics, Active control, Laminar-turbulent transition, Free-stream turbulence

## Preface

This thesis considers experimental studies of bypass transition and its control and is based on the following papers:

**Paper 1** AYUMU INASAWA, FREDRIK LUNDELL, MASAHARU MATSUBARA, YASUAKI KOHAMA & P. HENRIK ALFREDSSON, Velocity statistics and flow structures observed in bypass transition using stereo PTV *To appear in Experiment in Fluids*

**Paper 2** FREDRIK LUNDELL & P. HENRIK ALFREDSSON Streamwise scaling of streaks in laminar boundary layers subjected to free-stream turbulence *Submitted for publication*

**Paper 3** FREDRIK LUNDELL Streak oscillations of finite length: disturbance distribution and growth

**Paper 4** FREDRIK LUNDELL & P. HENRIK ALFREDSSON Experiments on control of streamwise streaks *Submitted for publication*

**Paper 5** FREDRIK LUNDELL Reactive control of free-stream turbulence induced transition: an experimental study

**Paper 6** FREDRIK LUNDELL, AYUMU INASAWA, SATOSHI KIKUCHI & YASUAKI KOHAMA Streak control by a surface-mounted piezo-ceramic flap

**Paper 7** FREDRIK LUNDELL Pulse-width modulated blowing/suction as a flow-control actuator

The first part of this thesis consists of an introduction to the subject, reviews of relevant work and a summary of the results presented in the papers. The second part consists of the seven papers.

## Division of work between authors

### **Paper 1**

The idea of the experiment was MM's. The water channel was designed by MM and built by MM and AI. MM, AI and FL performed the initial instrumentation. The measurement procedure and evaluation was developed by AI and MM. The figures were produced mainly by AI in cooperation with MM and FL. The manuscript was written mainly by FL with feedback from MM and AI, except for the introduction, which was written by MM. All authors commented the manuscript in different phases of its production.

### **Paper 2**

The measurements, evaluation and writing was done by FL. HA assisted during the writing.

### **Paper 4**

The initial idea of the experiment was HA's. The instrumentation, measurements, evaluation and writing was done by FL. HA assisted during the writing.

### **Paper 6**

The experiments were performed by FL, AI and SK in a cooperation on equal basis. The paper was written by FL.

## Conference contributions

### Paper 1

The results were presented by AI at *TSFP-2* in Stockholm, June 2002<sup>1</sup>.

### Paper 3

Parts of the results were reported by FL at *Svenska Mekanikdagarna* in Stockholm, June 1999, at the *3rd ERCOFTAC SIG 33 Workshop: New and Emerging Techniques for Transition Prediction* in Ravello, April 2000, at the *EUROMECH Colloquium 423: Boundary layer transition in Aerodynamics* in Stuttgart, April 2001, at the *ERCOFTAC Workshop on Flow Control* in Abisko, April 2001, and at *TSFP-2* in Stockholm, June 2001<sup>1</sup>.

### Paper 4

The work has been presented by FL at the *Workshop on Flow Control and Design* in Abisko, April 1998, at the *IUTAM Symposium on Mechanics of Passive and Active Flow Control* in Göttingen, Germany, September 1998, at the *IUTAM Symposium on Laminar-Turbulent Transition* in Sedona, September 1999<sup>1</sup>, at the *EUROMECH Colloquium 415: Shear-Flow Control* in Berlin, July 2000, and at the *Workshop on Drag Reduction on Aircraft and Ground Transportation* in Sendai, August 2000.

### Paper 5

The results were presented by FL at the *55<sup>th</sup> Annual Meeting of the Division of Fluid Dynamics (DFD) of American Physical Society (APS)* in Dallas, November 2002.

### Paper 6

The results were presented by FL at *Svenska Mekanikdagarna* in Linköping, June 2001, and at the *54<sup>th</sup> Annual Meeting of the DFD of APS* in San Diego, November 2001.

---

<sup>1</sup>With written contribution to the conference proceedings.

*Till Michaela, mamma och pappa*



# Contents

<b>Abstract</b>	iii
<b>Preface</b>	iv
<b>Division of work between authors</b>	v
<b>Conference contributions</b>	vi
<b>Chapter 1. Introduction</b>	1
1.1. Fluids engineering and flow control	1
1.2. Laminar-turbulent transition	2
1.3. Flow control	3
1.4. Scope of thesis	4
<b>Chapter 2. Basic concepts</b>	5
2.1. Theory and governing equations	5
2.2. Experimental fluid dynamics	8
2.3. Two generic setups for transition studies	12
2.4. Concluding remarks	14
<b>Chapter 3. Free-stream turbulence induced transition</b>	15
3.1. Transition scenarios	15
3.2. Transient growth	16
3.3. Secondary instabilities and breakdown	17
3.4. Relations to the regeneration cycle of turbulence	19
3.5. Prospects for flow control	21
<b>Chapter 4. Boundary layer flow control</b>	22
4.1. General characteristics of flow control	22
4.2. Passive flow control	24
4.3. Non-reactive flow control	26

## CONTENTS

4.4. Reactive control	28
4.5. Concluding remarks	36
<b>Chapter 5. Methodologies of the present work</b>	<b>37</b>
5.1. Why experiments?	37
5.2. The flow apparatuses	37
5.3. Experimental techniques	40
<b>Chapter 6. Results</b>	<b>43</b>
6.1. Free-stream turbulence induced transition	43
6.2. Control	48
<b>Chapter 7. Discussion and outlook</b>	<b>55</b>
7.1. Free-stream turbulence induced transition	55
7.2. Control of transition and turbulence	56
<b>Acknowledgments</b>	<b>59</b>
<b>References</b>	<b>60</b>
<b>Paper 1. Velocity statistics and flow structures observed in bypass transition using stereo PTV</b>	<b>71</b>
<b>Paper 2. Streamwise scaling of streaks in laminar boundary layers subjected to free-stream turbulence</b>	<b>95</b>
<b>Paper 3. Streak oscillations of finite length: disturbance evolution and growth</b>	<b>111</b>
<b>Paper 4. Experiments on control of streamwise streaks</b>	<b>137</b>
<b>Paper 5. Reactive control of free-stream turbulence induced transition: an experimental study</b>	<b>161</b>
<b>Paper 6. Streak control by a surface-mounted piezo-ceramic flap</b>	<b>199</b>
<b>Paper 7. Pulse-width modulated blowing/suction as a flow control actuator</b>	<b>209</b>

## CHAPTER 1

# Introduction

### 1.1. Fluids engineering and flow control

Engineers specializing in fluid mechanics make designs so that interaction between the fluid and the construction gives rise to a specific outcome. Such outcomes can be the lift on an airfoil, the drag on a car or the heat transfer in a heat exchanger. One may say that the success of a fluids engineer relies on his/her ability to control the flow within certain design constraints. For instance in the design of a wing, not only lift is important, but also drag and geometrical constraints. Similarly, in the aerodynamic design of a car many different constraints have to be accounted for. In the design of a heat exchanger there is always a balance between the heat transfer needed and the allowable pressure loss as well as space limitations.

The term “flow control”, however, has often a more specific meaning. It usually refers to means affecting the flow in a given geometry by passive or active measures. One of the driving forces in flow control has been the possibility to reduce friction drag on vehicles (airplanes and ships) or in pipelines. In these cases, the main emphasis has been on reduction of the skin friction by manipulation of the turbulence in the boundary layer close to the wall. One may say that the idea of controlling near-wall turbulence stems from the research on near-wall coherent structures which was done several decades ago. This research showed that near-wall turbulence is highly non-isotropic: close to the wall it consists of streamwise elongated regions of high- and low-speed flow. The structures are connected to so called bursting events, during which most of the turbulence production occurs. The idea behind most control attempts has been to limit the bursting events (*e.g.* by reducing their strength and/or frequency of occurrence) by affecting the streaky structures near the wall. There are however several practical complications if this is to be done, mainly because the physical size of these structures is extremely small (of the order of a fraction of a millimetre), not only in the applications but also in most laboratory experiments. In addition, care has to be taken so that the measurements are accurate enough to carefully determine the control effect.

In the present thesis some flow situations with streaky structures near the wall will be studied and the effect of some control attempts presented. An advantage with the flow situations studied in this thesis is that the spatial

## 1. INTRODUCTION

scales of the flow structures are much larger than in a real, turbulent flow. This simplifies both control and measurements. One of the cases – a laminar boundary layer subjected to free-stream turbulence – is also an interesting engineering case and the study of this case can be motivated as such.

### 1.2. Laminar-turbulent transition

Laminar-turbulent transition is the process through which a flow transfers from a laminar state to a chaotic turbulent motion. One example is water streaming out from the water tap; at low velocities the flow is laminar but at higher velocities, the flow gets turbulent. Laminar-turbulent transition can also be studied from a sailing yacht if there is a thin layer of oil on the water surface (bio-degradable vegetable oil can be poured on the water in front of the yacht if no "natural" oil is available). Close to the bow, the oil will form a thin layer along the hull. Further abaft, the layer thickens and even further astern of the bow, the layer will become irregular due to laminar-turbulent transition of the flow closest to the hull. Transitions between laminar and turbulent flow appear in many engineering situations, for instance in boundary layers on solid walls (airplane wings, ship hulls, turbine blades, heat-exchanger surfaces etc.).

The goal of the research presented in this thesis is to explore the possibilities to control transition induced by Free-Stream Turbulence (FST). Transition induced by FST is characterized by the growth and breakdown of high and low-speed streaks inside the boundary layer. Delaying transition may be of interest in applications where a laminar flow is preferable, *e.g.* to reduce friction or heat transfer. As will be shown, the flow structures observed in a boundary layer subjected to FST are similar to those appearing near the wall in turbulent boundary layer flows. The understanding and control/delay of FST induced transition thus may have implications also to other flow cases, specifically information on what is needed to achieve control of wall-bounded, fully-developed turbulent flows can be expected.

A paper by Reynolds, which was published 120 years ago (Reynolds 1883), can be viewed as the starting point of transition research. Reynolds performed visualizations of the flow in pipes under laminar, turbulent and transitional conditions. He found that the flow was laminar if a certain dimensionless parameter combination was below a critical value. The dimensionless number has been given his name and is defined as  $Re = UL/\nu$  where  $U$  and  $L$  are characteristic velocity and length scales of the flow situation (mean flow velocity and pipe diameter in Reynolds' case) and  $\nu$  is the kinematical viscosity of the fluid. Even though the knowledge about transition has increased over the years that have passed since Reynolds presented his results, there are still important phenomena related to transition that remain to be understood.

The development of transition and hydrodynamic stability research is illustrated by the development of the texts on the subject. Most of the research has aimed at exploring the stability of wall-bounded flows. Four standard

text books on hydrodynamic stability have been published over the last 50 years: Lin (1955), Chandrasekhar (1961), Drazin & Reid (1981) and Schmid & Henningson (2001). Through the development of direct numerical simulations, increased measurement possibilities and theoretical development, the field has changed from studying linear single-mode instabilities analytically to describing the full non-linear transition scenario. The present thesis contributes with some results regarding transition under the influence of FST, addressing open questions in the field.

### 1.3. Flow control

Drag reduction using polymer additives in water was a strongly pursued research area during the 1960's and 1970's. The interest originated from the result that minute concentrations (10 ppm) of certain polymer additives mixed with the fluid reduced the drag in turbulent flows with up to 80%. This dramatic effect sparked the search for other ways to reduce drag.

The research field of reactive flow control arose with the early experimental studies reported by Liepmann *et al.* (1982), who used a heating strip to cancel single-mode, 2-dimensional instability waves. The initial wave was successfully cancelled by out of phase disturbances introduced further downstream and natural transition in a low-disturbance (low FST) environment was delayed. If reactive control should be implemented for more complicated disturbances, it is probably necessary that both sensing and actuation are made at the wall. So called MEMS technology (Micro-Electro-Mechanical-System) has ignited the hope for a large number of sensors and actuators to be designed and manufactured inexpensively, similarly to microelectronic components. The sensors and actuators would thereafter be mounted on the surface where control is attempted. A number of review articles and books dealing with flow control issues have been published since 1989, see for instance Gad-el-Hak (1989, 1996, 2000), Bushnell & McGinley (1989), Ho & Tai (1998), Joslin (1998) and Löfdahl & Gad-el-Hak (1999).

Only a few experimental studies of reactive control of more complicated (as compared to 2D instability waves) disturbances in the transitional or turbulent flow regime have been made and the results from the existing studies are so far inconclusive. On the other hand many studies using Direct Numerical Simulations (DNS) to control the Navier-Stokes equation have been done and good control results have been obtained. DNS allow the control algorithms to be tested without actually building the complicated sensor/actuator systems and fast processing units necessary for physical implementation. However, many of the sensing and actuation schemes chosen in the numerical simulations seem to be impossible to realize physically in the near future. The emphasis of the present thesis is therefore to show how or if available technology can be used to successfully realize reactive flow control of streaky structures in boundary-layer flows. The progress in numerical work shows large energy-saving potentials if

## 1. INTRODUCTION

reactive control could be applied to turbulent flows. However, in order to maximize the fluids engineering potential, numerical and experimental work on reactive flow control should join forces and aim towards efficient, realizable control schemes. Successful experimental demonstrations will hopefully help the forces to be joined.

### 1.4. Scope of thesis

In summary the work performed within the framework of the present thesis has had the following objectives:

- To study the nature of FST induced transition in order to gain further knowledge of the process.
- To perform experiments in which disturbances, modelled after the ones appearing naturally in a boundary layer subjected to free-stream turbulence, are generated. Such simplified disturbances, generated at predetermined positions at selected times, can, if properly designed, increase the understanding of the processes behind transition to turbulence.
- To control model disturbances in order to evaluate actuator performance and control strategies.
- To implement and evaluate the performance of a reactive control system in a flat-plate boundary layer subjected to FST designed to reduce the disturbance level and eventually delay transition.

The main experiments have been designed so that they allow studies on more than one objective in parallel.

Chapter 2 gives some basic theoretical and experimental background to the work, whereas chapter 3 is a brief review of results on transition in boundary-layer flows, with an emphasis on FST induced transition. Chapter 4 gives an introduction to various control methods and strategies. The flow apparatuses and measurement techniques of the present work are described in chapter 5 and the main results are summarized in chapter 6. Chapter 7 gives an outlook and discusses future possibilities for transition and control research.

## CHAPTER 2

### Basic concepts

The equations describing the flow of Newtonian fluids are well established and have a history of more than 150 years. Unfortunately, the equations are non-linear and cannot, except in some special cases, be solved analytically. With supercomputers it is possible to simulate fluid flow with both full time and space resolution for simple flow cases at low Reynolds numbers. More complicated flow situations as well as high Reynolds numbers have to be studied via simplified theories and/or experiments. In this chapter a short presentation of the governing equations and experimental methods with special relevance to the present work will be made.

#### 2.1. Theory and governing equations

##### 2.1.1. Navier-Stokes equations

In this work, incompressible flow of a Newtonian fluid with constant viscosity is considered. The equations of motion of such a fluid are the Navier-Stokes equations,

$$\frac{\partial \tilde{u}_i}{\partial t} + \tilde{u}_j \frac{\partial \tilde{u}_i}{\partial x_j} = -\frac{1}{\rho} \frac{\partial \tilde{p}}{\partial x_i} + \nu \frac{\partial^2 \tilde{u}_i}{\partial x_j \partial x_j} \quad (2.1)$$

together with the continuity equation:

$$\frac{\partial \tilde{u}_i}{\partial x_i} = 0 \quad (2.2)$$

where  $\tilde{u}_i$  denotes the velocity components,  $\tilde{p}$  the pressure,  $\rho$  the fluid density and  $\nu$  the kinematical viscosity of the fluid. The velocity vector consists of the components  $\tilde{u} = \tilde{u}_1$ ,  $\tilde{v} = \tilde{u}_2$  and  $\tilde{w} = \tilde{u}_3$  in the  $x = x_1$ ,  $y = x_2$  and  $z = x_3$  directions. The coordinates are usually chosen so that  $x$  is the streamwise,  $y$  the wall normal and  $z$  the spanwise direction.

To solve a given problem equation 2.1 together with equation 2.2 should be integrated in time using proper initial and boundary conditions. For laminar flows this can usually be done without problems but for high Reynolds numbers the flow will become turbulent and the solution will be time dependent. To get useful results it will be necessary to average (time, space or ensemble averaging) the quantities of interest (mean velocity distribution, wall friction etc.). Due to the non-linearities of the equations and the multitude of scales present in

## 2. BASIC CONCEPTS

turbulent flow, a direct integration of the equations, resolving all scales in time and space, put large demands on the computational power, why it can be done only for simple cases. Such a simulation can serve as a complement or alternative to experiments, and are called Direct Numerical Simulations (DNS).

### 2.1.2. The Orr-Sommerfeld and Squire equations

For flows which undergo a transition from laminar flow to turbulence, a useful approach is to study the behaviour of small disturbances to see whether they grow or not. Such small disturbances can be with linear stability theory. If the disturbance amplitude grows, the flow is unstable and one would expect transition to turbulence. The advantage with this approach is that the equations can be linearized which make them accessible for theoretical analysis. First, the velocity components are decomposed into a mean  $(U, V, W)$  and a fluctuating part  $(u, v, w)$ , *i.e.*

$$\tilde{u} = U + u \quad (2.3)$$

and similarly for  $\tilde{v}$  and  $\tilde{w}$ .

For the disturbance analysis, we can assume the steady and laminar base flow to be parallel and dependent on one spatial coordinate only:

$$(U, V, W) = (U(y), 0, 0) \quad (2.4)$$

and the disturbances to be of the form

$$u(x, y, z, t) = \hat{u}(y) \exp [i(\alpha x + \beta z - \omega t)]. \quad (2.5)$$

With these assumptions, one can derive the Orr-Sommerfeld (OS) equation:

$$\left[ (-i\omega + i\alpha U)(D^2 - k^2) - i\alpha U'' - \frac{1}{Re}(D^2 - k^2)^2 \right] \hat{v} = 0 \quad (2.6)$$

together with the Squire equation

$$\left[ (-i\omega + i\alpha U) - \frac{1}{Re}(D^2 - k^2) \right] \hat{\eta} = i\beta U' \hat{v} \quad (2.7)$$

from equations (2.1) and (2.2). Above,  $D$  and prime denote derivation with respect to  $y$ ,  $k^2 = \alpha^2 + \beta^2$  and  $\hat{\eta}$  is the normal vorticity defined as

$$\hat{\eta} = \beta \hat{u} - \alpha \hat{v}. \quad (2.8)$$

The Reynolds number,  $Re$ , is defined as

$$Re = \frac{U_\infty L}{\nu} \quad (2.9)$$

where  $U_\infty$  and  $L$  are the velocity and length scales used to non-dimensionalize the variables. The OS and Squire equations constitute an eigenvalue problem: for a given Reynolds number  $Re$  and wavenumber pair  $(\alpha_k, \beta_k)$ , there exist eigenvalues  $\omega_k$  with corresponding eigenfunctions  $\hat{u}_k(y)$ . From equation (2.5) it follows that the stability of such an *eigenmode* is given by the imaginary part of  $\omega_k$ : if it is positive, the amplitude of the disturbance grows exponentially

## 2.1. THEORY AND GOVERNING EQUATIONS

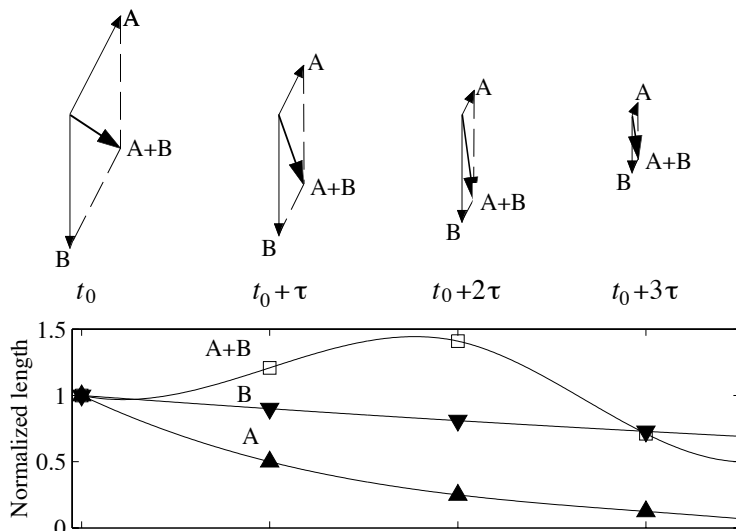


FIGURE 2.1. Transient growth. Even though the lengths of the vectors  $A$  and  $B$  both decrease exponentially, their sum  $A+B$  exhibits an initial growth before it decays.

and if it is negative, the amplitude decays. The analysis can also be performed in a spatial context by fixing  $\omega_k$  and solve for the eigenvalue  $\alpha_k$  together with its eigenfunction  $u_k(y)$ .

From the derivation and reasoning above, it could be believed that it is enough to study the stability of individual modes in order to determine whether a flow will stay laminar or not. This is however not the case and the reason is that the eigenfunctions  $u_k(y)$  are non-orthogonal. Due to this fact, a sum of eigenmodes might show an initial growth Even if linear stability theory predicts that all eigenmodes decay exponentially. The process is sketched in figure 2.1. Mathematically it is understood such that a disturbance  $u_N$  made up of  $N$  modes with weights  $a_k$ , *i.e.*

$$u_N(x, y, z, t) = \sum_{k=1}^N a_k u_k(y) \exp[i(\alpha_k x + \beta_k z - \omega_k t)], \quad (2.10)$$

might increase in amplitude (as measured by *e.g.*  $\int_x \int_y \int_z u_N^2$ ) even though all imaginary parts of  $\omega_k$  are negative. This mechanism is denoted *transient growth*. The linear dynamics are thus sufficient for disturbance growth to appear even if all eigenmodes are stable. After the growth of disturbance amplitude by linear mechanisms, non-linear mixing becomes important for the regeneration of turbulence.

## 2. BASIC CONCEPTS

### 2.2. Experimental fluid dynamics

Before the computers were fast enough to simulate the Navier-Stokes equations, so called Direct Numerical Simulation (DNS), the knowledge of fluid motion had to be increased by a mutual development of theory and experiments. The development is indeed mutual: in some cases, a phenomenon has been observed experimentally and later been explained by a theory while in other cases, a clever theoretical investigation has predicted a phenomenon, later to be confirmed by a suitably designed experiment. Since this thesis is based on experimental studies, the fundamentals of fluid mechanical experiments will be discussed in general. An overview of the experimental techniques used in the present work will also be given.

#### 2.2.1. *Experiment design*

There are two ways to gain knowledge from an experiment. Perhaps the most obvious way is to come up with a question and then design an experiment answering this specific question. For such an experiment to be successful, the question has to be simple enough, so that it can be answered by a single experiment. If not, the question has to be divided into subquestions, answerable one by one. Once a question of suitable complexity has been isolated, the experiment has to be designed. The experiment should be complex enough to answer the question, but preferably not more complex than that.

The second way to gain knowledge from experiments is to identify a phenomenon to be studied, design an experiment containing this phenomenon and perform measurements capturing it. Such an experiment is usually done in the laboratory but can sometimes also be observations of natural phenomena (such as the atmospheric boundary layer). With the data securely in the notebook, on film or on disk, it is possible to study the phenomenon in the detail allowed by the data. This process is usually highly iterative: after studying the initial data it might be necessary to perform complementary measurements to answer new questions.

For any experiment, the investigator has to choose a suitable combination of measurement techniques providing enough information of the flow with a reasonable investment of money and time. The factors determining such decisions can be the complexity of the flow or the necessary accuracy and time resolution as well as the equipment available in the laboratory.

#### 2.2.2. *Data evaluation and presentation*

An experienced experimentalist usually has some idea, even if it is vague, of what to do with the data after the measurements. Distributions of mean and fluctuating quantities are obvious and natural. So are spectra, which give information of the frequency content of the signals. Correlations can provide important information on typical length scales as well as flow structures and

## 2.2. EXPERIMENTAL FLUID DYNAMICS

wavelets allow for studies of structures or oscillations appearing intermittently. In order to study repeated features of the flow, ensemble or conditional averaging can be useful.

### 2.2.3. *Measurements techniques*

The quantities of interest in a flow experiment are one or more of the pressure, the velocity, the shear stress at a wall or the temperature. For all properties, both mean and fluctuating quantities might be of interest. There are a number of possible techniques available to measure them and below follows a brief introduction to the methods used in the present work. The presentation is intended for the reader with little experience of fluid dynamic experiments. All methods are, to various extents, susceptible to general problems such as accuracy and resolution in frequency and space. To evaluate an experiment correctly one needs information on how the techniques have been applied as well as on the flow apparatus used. To correctly interpret experimental results and their shortcomings an extensive experience is usually also necessary.

2.2.3a. *Visualization.* Flow visualization can for some flow situations give a very good overall idea of the flow. In order to perform a visualization, particles (often called markers or tracers) have to be inserted in the flow and the particles chosen are assumed to move with the flow. This means that the density and size have to be chosen such that the fluid force (viscous drag) on the particle is large enough for the particle to follow the flow accurately. One possibility is to introduce the markers in a controlled manner. Smoke in air and dye in water can be injected through an opening at the surface or a thin wire stretched through the flow can be used to generate smoke in air or hydrogen bubbles in water. The displacement of the particles with time can then be viewed and interpreted in terms of motion of the fluid. Another possibility is to mix reflective particles into the fluid so that their collective behaviour gives qualitative information on the flow behaviour. Similarly a smoke sheet moving around a bluff body or along the surface of a rigid body gives a qualitative picture of the flow.

Today flow visualization is usually registered on digital video and modern image processing techniques make it possible to perform advanced analysis of images, allowing also quantitative data to be deduced from visualizations. Structures seen in flow visualizations must however be interpreted with care, since they do not necessarily result from the local flow field. However a good visualization sequence can say more than weeks of measurements and is also often useful before a measurement campaign is started.

2.2.3b. *Pressure measurements.* Measurements of the mean pressure is a standard method in all fluid laboratories. The static pressure in a fluid is most easily measured through a small hole drilled in a surface. The fluctuating pressure

## 2. BASIC CONCEPTS

must usually be measured directly at the wall by having a small microphone membrane mounted flush with the wall.

The simplest transducer, which can be used to determine a mean pressure, is a ruler together with a U-shaped tube filled with a liquid. The pressure to be measured is connected to one end of the tube and the other end is connected to a known pressure. In this way the U-tube can be said to be a differential transducer. Electrical gauges can also be used. Among the principles available for conversion of the pressure to an electrical signal are capacitive (measuring the capacitance between two surfaces, one of which is moved if the pressure is changed), resistive (such as a strain gauge on a membrane), light intensity (a mirror is moved if the pressure is changed) or frequency (the eigenfrequency of a structure changing with pressure). Furthermore, paints that change color, reflectance or other properties with pressure are available. The time response of the paints is typically of the order of 1 s, while electrical gauges (such as microphones) usually can respond to frequencies up to several kHz.

*2.2.3c. Velocity measurements.* The velocity of a flow can be measured in several ways. The methods can be categorized as methods based on pressure, heat transfer or displacement/movement of particles following the flow.

*Pressure-based methods.* The dynamic pressure,  $\frac{1}{2}\rho u^2$ , *i.e.* the pressure difference between a pressure hole facing the flow and one positioned in a wall parallel to the flow can be used to measure the velocity by Prandtl or Pitot tubes. In the present work this technique is used *e.g.* to determine the flow velocity in the free stream of the wind-tunnel.

*Hot-wire anemometry.* The heat transfer from a heated body to a flowing fluid is the basis for hot-wire anemometry. In practise a thin (0.6-20  $\mu\text{m}$ ) wire, typically made of tungsten or platinum is heated to a temperature of 100-200 degrees above the ambient temperature. The velocity is then given by the heat transfer from the wire, which can be detected thanks to the fact that the resistance of the wire increases with temperature. Most often this is done by keeping the wire at a constant resistance, *i.e.* temperature, (Constant Temperature Anemometry, CTA). After calibration of the system, the instantaneous velocity can be deduced from the voltage over the wire. By arranging two or several wires close together at different angles to the flow direction, not only the magnitude but also the direction of the velocity can be measured.

Typical advantages of hot wires are quick time response and the possibility to perform time-resolved measurements. The main disadvantages are that in order to get quantitative data the wire has to be calibrated. Also the wire has to be hold in the flow by some kind of probe support potentially disturbing the flow and the approximate flow direction must usually be known beforehand.

*Laser Doppler Velocimetry.* Laser Doppler Velocimetry (LDV) utilizes the Doppler shift in frequency of the light scattered by particles moving in the intersection of two laser beams. The method provides the velocity without

## 2.2. EXPERIMENTAL FLUID DYNAMICS

any calibration: knowing the frequency of the light in the laser beams and their angle of intersection, the velocity can be obtained by detecting the light scattered by the moving particle. With laser beams of different colours, the velocity can be measured in more than one direction. The method provides accurate measurements of the velocity of particles passing the measurement volume. If the particles follow the flow, that measure also gives the flow velocity.

The advantages are that optical access to the measurement area is sufficient, no probes have to be put in the flow. In addition, the measurements can be performed without calibration. The price one has to pay is that there have to be particles in the fluid and that the velocity is obtained only when particles are passing the measurement volume. Therefore it is not straightforward to perform time resolved measurements.

*Particle Image Velocimetry.* The third major method used for velocity measurements is Particle Image Velocimetry, PIV, which has evolved dramatically during the last ten years thanks to the development of digital cameras and fast data processing units. It is now possible to set up close to automatic measurement systems based on this technique. In PIV, a light sheet is used in order to take two images of a plane of the particle-filled flow. The images are taken with a small time interval. Cross-correlation of selected areas of the images can then be used to deduce the displacement of the particles from the first image to the other. (In some systems, a double exposed image is used and the displacements calculated from the autocorrelation of this image.) The displacement together with the known time interval between the images or exposures give the velocity of the particles in the area of the image under study. The advantage is the distribution of the measurements: with two cameras and stereo imaging techniques, all three velocity components can be measured simultaneously in a plane. The main disadvantages are low data rates and resolution/accuracy.

One may say that PIV has replaced what was earlier denoted PTV or Particle Tracking Velocimetry. In the latter technique individual particles are followed and velocities are calculated from their subsequent positions. With many particles in the flow there are problems to know the identity of particles from one picture to the next. This problem is overcome by the PIV technique. In the present thesis a new technique where tracers are released in a controlled manner, facilitating the identification of particles from one image to the next, has been developed. This may be seen as a development of the PTV technique.

2.2.3d. *Shear-stress measurements.* The shear stress (friction) at a wall is often of great interest, both for performance measurements, diagnostics of a flow or flow physics investigations. The shear stress is also often used as input in reactive control loops, since it can be measured non-intrusively at the wall. In order to measure the shear stress, one can in principle measure the force on a small part of the wall (floating element) or use other, more intricate methods.

## 2. BASIC CONCEPTS

Whether the mean or fluctuations of the shear stress are to be measured, different methods are used. If only the mean is needed and the flow is turbulent, *Preston tubes*, *i.e.* tubes mounted at the wall, parallel to the flow (so that their openings are normal to the flow), can be used. A floating element can also be used in these cases. Another possibility for measuring the mean shear stress is to use the oil-film method, in which the development of a thin oil film on the wall is studied by the movements of the fringes appearing when it is illuminated by monochromatic light. There are also shear-stress sensitive paints available, which change color depending on the shear stress applied to them.

Time resolved (fluctuation) measurements of the shear stress are typically made by thermal sensors, similar to the hot wires/films used for velocity measurements but mounted at or in the close vicinity of the wall. This kind of sensor is the standard in reactive flow control experiments.

### 2.3. Two generic setups for transition studies

In order to investigate fundamental aspects of the flow physics in different processes, such as laminar/turbulent transition, different model setups are used in experiments as well as DNS. Two generic setups for transition and control studies are the plane channel flow (plane Poiseuille flow) and the flat-plate boundary-layer flow (Blasius boundary layer). Both these are used in the present work and are described in some detail below.

#### 2.3.1. *The Poiseuille flow channel*

Two rigid walls with fluid moving between them constitute a Poiseuille flow channel as illustrated in figure 2.2 (a). The flow through the channel is driven by a pressure gradient balancing the friction forces on the walls. If the Reynolds number is low ( $Re = U_\infty h / \nu < 1000$ ), the flow between the walls will be laminar independently of the disturbance environment. The velocity variation between the walls will then take the form of a parabola, with the velocity being zero at the walls and showing a maximum in the centre of the channel. Ideally, the length and the spanwise width of the channel are infinite, which in an experiment is translated to “large enough”. To get the fully developed parabolic profile the development length from the inlet has to be of the order  $100\text{-}200h$ , the higher the  $Re$  the longer the inlet length. For stability work the width should preferably be larger than  $50h$ .

In a direct numerical simulation, the flow is usually decomposed into periodic Fourier modes, why the simulated channel tend to be periodic (*i.e.* the flow in a wide enough channel flanked by channels with identical flows on both sides). Such periodic boundary conditions are usually used both in the stream-wise and spanwise directions.

### 2.3. TWO GENERIC SETUPS FOR TRANSITION STUDIES

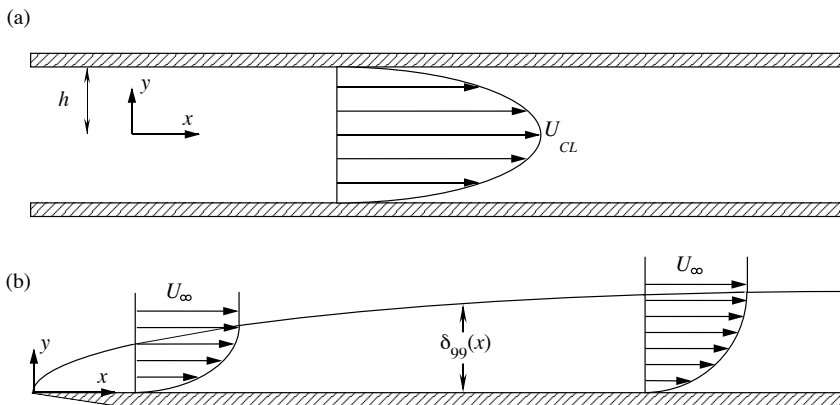


FIGURE 2.2. Two generic flow cases for transition studies, (a) plane channel (Poiseuille) flow and (b) flat-plate boundary-layer (Blasius) flow.

#### 2.3.2. The Blasius boundary layer

A boundary layer forming on a flat plate under a free stream of constant velocity is denoted a Blasius boundary layer. As in the channel, the velocity is zero at the plate and increases away from the plate, ultimately reaching the free-stream velocity far away. With the free-stream velocity being constant, there are no pressure gradients present why the friction at the wall is balanced by the growth of the boundary layer; the boundary-layer thickness increases (*i.e.* the fluid velocity further away from the plate is decreasing) with the downstream direction. The thickness of the boundary layer can be characterized by different measures. The displacement thickness, *i.e.* the distance streamlines outside the boundary layer are displaced because of the growing boundary layer, is defined as

$$\delta^* = \int_0^\infty \left[ 1 - \frac{u(y)}{U_\infty} \right] dy. \quad (2.11)$$

Another important measure is the momentum loss thickness,

$$\theta = \int_0^\infty \frac{u(y)}{U_\infty} \left[ 1 - \frac{u(y)}{U_\infty} \right] dy, \quad (2.12)$$

the growth of which is related to the friction drag on the plate. In this thesis, the lengthscale  $\delta = \sqrt{x\nu/U_\infty}$  is often used. The displacement and momentum thicknesses for a Blasius boundary layer are related to  $\delta$  so that  $\delta^* = 1.72\delta$  and  $\theta = 0.66\delta$ . Other measures of the thickness can be used, such as  $\delta_{99}$  indicated in figure 2.2, the height at which the velocity has reached 99% of the free-stream velocity.

## 2. BASIC CONCEPTS

### **2.4. Concluding remarks**

There are three approaches to gain knowledge of fluid flow — theory, experiments and simulations — obviously each has its own unique difficulties and pitfalls. Different aspects of a phenomenon are more or less suited for different approaches, and so are different phases of the investigation. Due to the physical nature of an experiment, there are parameters which do not suit themselves for variation in an experiment, such as geometry. However, other parameters can be scanned very quickly in an experimental setup, since the flow response to the new parameter setting is more or less immediate.

## CHAPTER 3

### Free-stream turbulence induced transition

#### 3.1. Transition scenarios

Transition to turbulence in boundary layer flows may follow different routes depending on the flow situation. In all cases disturbances enter the boundary layer which grow in amplitude whereupon transition may occur. The simplest and most studied case is two-dimensional wave disturbances which can be theoretically studied through the linearized equations of the flow, the OS-equation (2.6). Such waves are denoted Tollmien-Schlichting (T-S) waves, which either decay or grow exponentially. If they grow they will soon reach high enough amplitudes for non-linearities to set in and trigger transition. The starting point of this scenario, the amplification of T-S waves, was studied theoretically in the 1930's by Tollmien (1935) and Schlichting (1935). An experiment by Schubauer & Skramstad (1948) confirmed that 2D waves in a boundary layer will be amplified under approximately the conditions predicted by Tollmien and Schlichting. Even though the experiment confirmed the main results of the theory, it was not until the DNS study by Fasel & Konzelmann (1990) and the experiment by Klingmann *et al.* (1993) that it was finally agreed upon that the OS-equation was sufficient to describe the physics of the problem.

After the initial growth of single modes of the disturbance equations, different routes are possible, depending on the disturbance environment. Generally, nonlinear interactions set in when a T-S wave has reached a level ( $u_{rms}$ ) of 1–2% of the free-stream velocity. For a detailed description of the transition process and relevant references the reader is referred to Schmid & Henningson (2001).

Transition scenarios which do not start with T-S waves are usually denoted bypass transition and one such is transition which occurs at high free-stream turbulence levels. In that case low-frequency oscillations in the streamwise velocity appear in the boundary layer. These oscillations are due to streamwise streaks of alternating high and low-velocity and flow visualization studies show that the streaks meander slowly sideways and thereby give rise to the observed low frequency variations. If the energy of the streamwise velocity fluctuations is measured in the boundary layer, it is found to have its maximum in the centre of the boundary layer and to exhibit an initial amplification which is linear with downstream distance, in contrast to amplified T-S waves which grow

### 3. FREE-STREAM TURBULENCE INDUCED TRANSITION

exponentially. The streak spacing in the spanwise direction is of the order of the boundary layer thickness and the streaks reach peak-to-peak amplitudes of the order of 50% or more of  $U_\infty$  prior to transition. The process of transition is not undisputed, but there are strong indications that the streaks are susceptible to a secondary instability which is of inflectional (in the spanwise direction) origin. Such an instability may grow rapidly and give breakdown which would lead to formation of turbulent spots and finally a fully developed turbulent boundary layer.

Free stream turbulence induced transition is typically studied by placing a grid, creating free-stream turbulence, in a wind-tunnel upstream of the leading edge of the plate or airfoil over which the boundary layer develops. Measurements have been performed by *e.g.* Kendall (1990), Roach & Brierly (1990) and Westin *et al.* (1994), Alfredsson & Matsubara (2000) and Matsubara & Alfredsson (2001), and the field have been reviewed by Kendall (1998). Jacobs & Durbin (2001) performed a DNS of free-stream turbulence induced transition, which successfully reproduced most of the results of Roach & Brierly (1990). As always, a DNS gives detailed information about flow structures etc. Also in the DNS-study streaks are the dominant feature of the boundary layer before breakdown to turbulent spots. However, Jacobs & Durbin did not observe secondary instabilities prior to breakdown, instead they argue that turbulence spots are formed due to “backward jets” in the boundary layer, interacting with the small scales in the turbulence in the free stream.

#### 3.2. Transient growth

The appearance of streaks in shear flows is a phenomenon studied not only for its importance to free-stream turbulence induced transition. Streaks are present also in turbulent shear flows, and the mechanism creating them is believed to be “lift up”, a conception coined by Landahl (1980) although the mechanism was already recognized by Ellingsen & Palm (1975). The process is easy to interpret: a wall-normal velocity disturbance lifts slow fluid from close to the wall to regions of higher velocity in the shear flow. This is a linear and inviscid mechanism and the mathematical background is the coupling between the wall-normal velocity and the normal vorticity in the Squire equation (2.7). Mathematically the eigenmodes to the coupled eigenvalue problem, given by equations (2.6) and (2.7), are not orthogonal, why transients, appearing due to initial cancellation of nearly parallel modes, can be of major importance to the disturbance evolution.

In transition studies, the concept of transient growth was adopted by Hultgren & Gustavsson (1981) who explored transient growth in plane channel flow. Gustavsson (1991) continued with three dimensional disturbances and Butler & Farrell (1992) performed the analysis for both plane channel flows and parallel boundary layers. Luchini (2000) and Andersson, Berggren & Henningson (1999) calculated the optimal disturbance for Blasius boundary-layer

### 3.3. SECONDARY INSTABILITIES AND BREAKDOWN

flow. The optimal disturbance is the initial condition maximizing the ratio of some disturbance-energy measure between two points and was found to be a weak streamwise vortex. The wall normal disturbance profile obtained from the theory agrees well with the disturbance profiles measured in boundary layers subjected to free-stream turbulence.

Brandt, Henningson & Ponziani (2002) performed a non-linear receptivity analysis which showed that wave-like disturbances in the free stream can generate streaks via non-linear interactions. This receptivity process takes place downstream of the leading edge. The results show that disturbances in the free stream above a boundary layer can introduce streaks in the boundary layer.

#### 3.2.1. *Model experiments of transient disturbances*

The response of a boundary layer to localized forcing through a hole in the wall was studied by Grek *et al.* (1985), who concluded that three different kinds of disturbances can be generated. The one related to transient growth is long structures of near constant spanwise width, at first growing in amplitude but decaying further downstream. The two others are T-S wave packets of Gaster type and the immediate formation of turbulent spots. In contrast to the transient disturbance, both the wave packet and the turbulent spot grow significantly in the spanwise direction while propagating downstream.

A localized disturbance in laminar flow was studied by Gad-el-Hak & Husain (1986) who intended to model the sub-layer streaks of a turbulent boundary layer by transiently growing intermittent streaks generated from a hole in a plate under a laminar boundary layer. Breuer & Haritonidis (1990) disturbed the boundary layer with a flexible membrane moving upwards or downwards. Bakchinov *et al.* (1998) used two kinds of disturbance generation; first they generated a disturbance in the free-stream and then they compared the development of this disturbance with the development of a disturbance introduced from a hole in the plate. In all experiments, the same observation is made: a long structure is formed, which at first grows in amplitude to a maximum whereupon it decays in amplitude while it propagates downstream. During its development, the length of the disturbance is constantly growing. Similar results were obtained by Elofsson, Kawakami & Alfredsson (1999) who introduced continuous suction through a spanwise array of holes in a channel flow. They observed longitudinal streaks which first grew in amplitude and then decayed.

### 3.3. Secondary instabilities and breakdown

The elongated, transiently growing disturbances generated by localized disturbances decay after the initial growth, rather than developing into turbulent spots as seen in a boundary layer subjected to free-stream turbulence. Thus, transient growth is not providing the complete description of the transition

### 3. FREE-STREAM TURBULENCE INDUCED TRANSITION

process. For turbulence to occur, there has to be some secondary mechanism acting on the streaks, or a primary instability unrelated to the streaks. This is an open question and relevant work is reviewed below.

#### 3.3.1. *Experiments*

The first candidate for providing high frequency oscillations eventually leading to the formation of a turbulent spot are T-S waves. Boiko *et al.* (1994) generated 2D T-S waves in a boundary layer subjected to FST and found that the growth factors of the 2D disturbances are considerably lower as compared to what is predicted by linear theory for a Blasius boundary layer without streaks. This was also found in the simulations by Cossu & Brandt (2002), where a boundary layer with stable streaks, generated by optimal disturbances, was studied.

A boundary layer containing streamwise streaks generated by upstream roughness elements was studied by Bakchinov *et al.* (1995). They found a competition between 2D T-S waves and a new instability appearing at higher frequencies, traveling with the local velocity at the position of maximum amplitude. The maximum amplitude was found at the position of maximum spanwise shear. These facts indicate that the new instability is an inflectional instability of the streaks.

Westin *et al.* (1998) found that transient, localized disturbances (presumably similar to individual streaks in a boundary layer subjected to FST) can be driven to breakdown if 2D T-S waves are present. The transient disturbance was found to interact with the T-S wave, generating oblique structures eventually leading to a process similar to oblique transition, studied by e.g. Schmid & Henningson (1992), Berlin, Wiegel & Henningson (1999) and Elofsson & Alfredsson (2000). From the visualization images of FST induced transition presented by Matsubara & Alfredsson (2001), there seems to be a secondary instability acting on the streaks, assumed to be similar to the secondary instability of streaks found in other flows with streak like structures (*e.g.* curved channel flow). The secondary instability of velocity streaks in a plane channel flow was studied by Elofsson *et al.* (1999) whereas Asai, Minagawa & Nishioka (2002) studied the secondary instability of low-speed streaks in a Blasius boundary layer. In the plane channel used by Elofsson *et al.* (1999), only the anti-symmetric mode was amplified. Asai *et al.* (2002) used two streaks of different width and forced both the symmetric and the anti-symmetric mode. It was found that the width of the streak is critical for the mode selection: the symmetric mode was most strongly amplified for the wide streak, whereas the opposite was valid for the anti-symmetric mode. The visualizations of the anti-symmetric mode from the controlled model experiment of Asai *et al.* (2002) show an astonishing similarity with the single “wobble” captured in a high-speed video sequence by Matsubara & Alfredsson (2001).

### 3.4. RELATIONS TO THE REGENERATION CYCLE OF TURBULENCE

#### 3.3.2. Theory

It is well known that streak-like mean velocity disturbances can be subject to exponentially growing disturbances. One example is the velocity pattern created by Görtler vortices, the secondary instability which was studied by Bottaro & Klingmann (1996). The secondary instability can be either symmetric or anti-symmetric, and in the case of the quickly developing Görtler vortices, the most unstable mode is found to change from the antisymmetric to the symmetric with downstream distance.

The secondary instability of streaks generated by the optimal disturbance in a laminar boundary layer was studied by Andersson *et al.* (2001). The streaks were found to be subject to exponentially growing disturbances once they reached a threshold amplitude of 26%. The most unstable mode was an antisymmetric oscillation of the low-velocity streaks.

In the comprehensive study of Schoppa & Hussain (2002), it was found that the secondary instability of velocity streaks is subject to a transiently growing disturbance, *i.e.* that a wiggle of a streak grows linearly at first before single mode exponential growth sets in. The possibility of an initial quick transient growth for exponentially unstable cases is also emphasized by Schmid & Henningson (2001).

#### 3.3.3. Numerical studies

The scenario sketched above, first growth of streaky structures and thereafter the appearance of a secondary instability, is questioned by Jacobs & Durbin (2001) based on data from their numerical simulations. Rather than a secondary instability, they claim that breakdown of the low-speed structures in the boundary layer (denoted “backward jets”) is forced through an interaction between the streaks (jets) and small scales in the free stream.

The T-S wave scenario was studied numerically by Fasel (2002). He shows that the structures appearing during the breakdown process are fairly unchanged by the presence of the streaks.

Finally, the process of breakdown suggested by the experimental and theoretical studies has been simulated. Brandt & Henningson (2002) forced the secondary instability of a streak created by the optimal disturbance and studied the growth of the secondary instability and its breakdown to turbulence. The structures created in the latter part of the breakdown process showed similarities with other types of breakdown.

### 3.4. Relations to the regeneration cycle of turbulence

The cause and relevance of sub-layer streaks in turbulent boundary layers are a large research area and have been reviewed by *e.g.* Panton (2001). It may be hypothesized that the dynamics of such streaks and the dynamics in a boundary layer subjected to free-stream turbulence are similar, why a short review of the

### 3. FREE-STREAM TURBULENCE INDUCED TRANSITION

subject is relevant in this thesis. If the dynamics are similar, the control results in this thesis are relevant not only for transition delay, but also for control of turbulence.

Visualizations and correlation measurements near the wall in turbulent boundary layers by *e.g.* Kline *et al.* (1967) show the existence of low velocity streaks. The reason for and significance of these streaks have been the subject of intense study through the years. Landahl (1990) gives a review of a number of theoretical explanations for sublayer streaks and Johansson, Alfredsson & Kim (1991) show quantitative results for streaks obtained from the analysis of data bases obtained from DNS. One model for the creation and re-creation of streaks is that the streaks are one of the stages in a regeneration cycle, according to which a streak is generated by streamwise vorticity and growing until it breaks down, generating strong high frequency oscillations, either by a secondary instability or by some other, non-linear mechanism. After the bursting, non-linear mechanisms redistribute the vorticity so that new streaks are formed and the cycle continues. This cycle was studied in data from a DNS of low Reynolds number turbulent channel flow by Hamilton, Kim & Waleffe (1995) who concluded that the low-velocity streak breaks down due to a secondary instability. The secondary instability of instantaneous low velocity streaks in turbulent flow has also been studied by Skote, Haritonidis & Henningson (2002), who concluded that there exists a symmetric instability, occurring due to the inflectional normal velocity profile.

An alternative scenario is the parent-offspring scenario, according to which streaks are induced by older streaks. Jiménez (1994) studied the structure of near wall flow and found a regeneration cycle in which streak generation is one vital ingredient. The second ingredient is shear tilting of vertical vorticity blobs originating from the streaks, forming almost horizontal vorticity. The horizontal vorticity then generates a new streak.

Schoppa & Hussain (2002) study necessary conditions to be fulfilled for a low-velocity streak to be unstable and find a universal criterion for a streak to be unstable, namely that the “streak lift-up angle” has to be larger than a certain value. Statistics from DNS data bases show that few streaks stronger than the threshold value exist.

Low-dimensional mathematical models illustrating the cyclic behaviour of systems like the regeneration cycle described above have been studied by Waleffe (1995, 1997).

The importance of both the linear and non-linear terms in the Navier-Stokes equations for turbulence regeneration is highlighted in a numerical experiment performed by Kim & Lim (2000). They performed DNS of a turbulent channel flow, and studied the flow when the linear coupling between mean streamwise shear and wall-normal velocity was turned off. In a second experiment, they turned off the non-linear terms instead. By observing the

### 3.5. PROSPECTS FOR FLOW CONTROL

development of random initial conditions in the two cases, they concluded that the linear coupling is responsible for the streak generation, and that the non-linear terms are responsible for the regeneration process. Both are necessary for self-sustained turbulence, why it is enough to cancel one of them in order to inhibit the regeneration cycle. Various regeneration cycle scenarios are reviewed by Panton (2001).

#### **3.5. Prospects for flow control**

The dynamics of the streaks found in free-stream turbulence might be similar to streaks found in turbulent boundary layers. It is agreed in both cases that the streaks are generated by lift up whereas several mechanisms, parent-offspring, backward jets or secondary instabilities (symmetric or anti-symmetric modes, transiently or exponentially growing) have been proposed for regeneration and breakdown of the streaks. The exact process of breakdown of streaks is not of paramount interest from a control perspective, since a control system limiting streak growth will delay transition and/or reduce turbulence independent of the details of the breakdown process.

## CHAPTER 4

# Boundary layer flow control

### 4.1. General characteristics of flow control

As mentioned in chapter 1 there are many different types of control, however in the flow control literature, the categorization of control methods is not unambiguous. In figure 4.1 four different situations are described, (a) a system to which no control is applied, (b) a system where the fluid properties or boundaries have been changed, but there are no external energy usage, (c) non-reactive control where external energy is supplied to the system and finally (d) reactive control where information from the system together with external energy are used to control the system.

The underlying idea of flow control is that small design modifications, or minute energy input, can improve the performance of a given system. The aim can be to decrease drag or increase lift. Other aims can be to improve mixing or suppress noise. In order to obtain the target, the system can be manipulated in different ways.

All physical systems are subjected to external disturbances which will affect the output of the system. Some examples are surface vibrations, acoustic noise, free-stream turbulence outside a boundary layer or variations of the flow rate. Each system also has its internal dynamics. The control objectives can be reached by changing the system dynamics and/or by counteracting the input noise.

#### 4.1.1. *Passive methods*

A passive method controls the flow by changing the system itself. Two examples are placing riblets on a surface to effect the near-wall turbulent structures and adding polymers to the fluid in order to decrease turbulent friction drag, *i.e.* by changing the rheological properties of the fluid. An important application area for passive methods is control of separation. A well known example is vortex generators on the upper surface of airfoils generating vortices which enhance mixing in the boundary layer so that separation is avoided. Another example is the surface structure of golf balls, where the dimples promote transition to turbulence which delays separation and thereby decreases the drag.

#### 4.1. GENERAL CHARACTERISTICS OF FLOW CONTROL

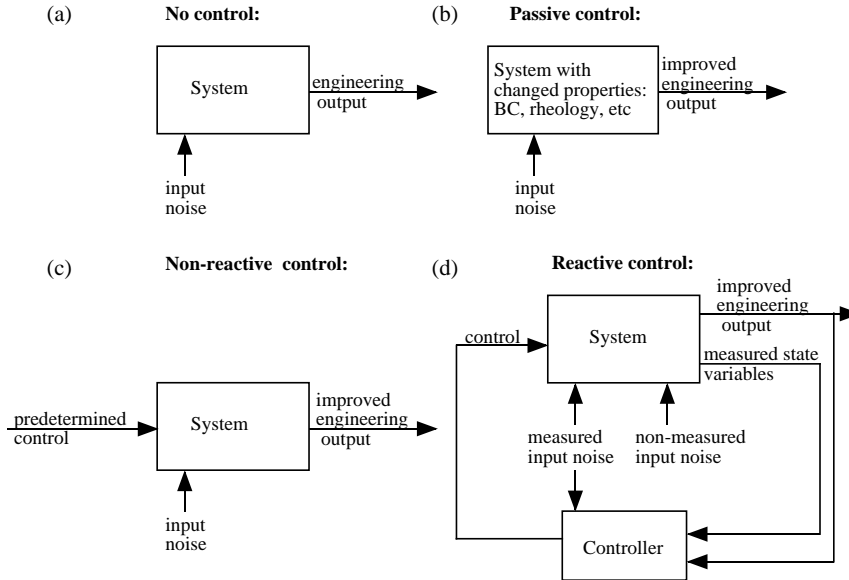


FIGURE 4.1. Different control approaches.

A number of passive methods which aim either to reduce turbulent drag or delay transition are reviewed in section 4.2.

##### 4.1.2. *Non-reactive methods*

Non-reactive methods are characterized by the fact that they use energy in order to obtain the control purpose. The underlying idea is of course that the energy savings or quality improvements thanks to the control shall at least compensate the energy spent on the control. Examples of such methods are steady surface suction or predetermined surface movement. Such examples are reviewed in section 4.3.

##### 4.1.3. *Reactive methods*

Reactive methods are different from non-reactive in that they respond to the instant state of the system or the time-varying external disturbances, as is illustrated in figure 4.1(d). In a physical system this means that both the sensing and actuation are localized. Depending on the input to the controller, the system is feedforward (if it utilizes the measured input noise only) or feedback (if it uses the measured state of the system and/or the engineering output). The distinction between feedforward and feedback is not distinct, and that categorization will not be emphasized in the following.

## 4. BOUNDARY LAYER FLOW CONTROL

In a physical experiment or application, three elements have to be available in order to build a reactive control system, namely sensors, actuators and the controller. Numerical studies, on the other hand, automatically have access to full flow information. In a simulation, it is also straightforward to apply body forces anywhere in the flow or apply blowing/suction at the wall which can be distributed on the scale of the computational grid. Simulations of control with wall-movements can also be performed in codes made for the purpose. It is thus natural, that numerical studies tend to concentrate on the design of controllers, while most experimental work have concentrated on different kinds of actuators. Physical realizations of reactive control systems are so far very few.

There are many methodologies available for controller design. Physical insight, neural networks, linear optimal control, linear cancellation or direct optimization over time horizons varying from very short to infinity are some of the possibilities. In the review of reactive control of turbulence and transition in section 4.4, sensor and actuator technology are reviewed together with controller design.

### 4.2. Passive flow control

There are several methods which fit under the heading “Passive flow control” and all methods appearing in this section have been studied for several decades. This section has no intention to give a complete review of the field and only a few papers have been referred to for each method.

#### 4.2.1. *Polymer additives*

The pressure needed to drive a turbulent water flow through a pipe can be dramatically decreased by the addition of elastic polymers, Paterson & Abernathy (1970). The reduction in shear stress can be up to 80% and the phenomenon has been studied extensively but there is yet no complete explanation. Den Toonder *et al.* (1997) compared two different models for the effect of the polymers in direct numerical simulations and compared the results with experimental data. They concluded that the viscous anisotropy introduced by the polymers is important for drag reduction to occur whereas the elasticity is not. However, Sreenivasan & White (2000) managed to reproduce both the onset of drag reduction and the maximum drag reduction asymptote found in experiments, using a theory which is based on elastic effects.

After 50 years of research and some 2500 papers devoted to the phenomenon, Sreenivasan & White (2000) state that to gain more knowledge, “. . . one requires new experiments at high Reynolds numbers, an integral part of which should be the characterization of the polymer. Such experiments must be directed towards problems that have a chance of being posed adequately in theoretical terms – such as the ones chosen here – rather than to the exploration

## 4.2. PASSIVE FLOW CONTROL

of a whole range of fascinating but ill-posed problems.”. The importance of using experiments, theory and simulations hand-in-hand when planning future studies can be extrapolated to all flow control studies!

### 4.2.2. Riblets

Riblets are ridges in the surface and are known to decrease the drag in turbulent boundary layer flows. In order to obtain the drag reduction, the riblets have to have proper dimension and be aligned with the flow. An extensive experimental investigation by Bechert *et al.* (1997) varied all relevant parameters in a turbulent channel flow and a drag reduction of 9% was achieved for the optimal parameter settings. The mechanism behind the drag reduction is not clear and under continuous investigation, see Falcomer & Armenio (2002). Another experimental study of the flow over riblets is Choi (1989), where the results indicate that the riblets inhibit spanwise movements of the near-wall streaks, decreasing the bursting and thereby reducing the drag.

For transition studies, riblets mounted across the flow has proven to somewhat delay the later stages of transition induced by T-S waves (Grek *et al.* 1995). In a later experiment by Grek *et al.* (1996), the same riblets were found to dramatically decrease the growth of streamwise streaks induced by surface roughnesses.

### 4.2.3. LEBUs

A Large Eddy BreakUp device (LEBU) is a wing profile mounted in the outer part of a boundary layer and has been proposed to give drag reduction by, as the name indicates, breaking up the large eddies in the boundary layer. The underlying idea is that the bursting in the boundary layer is triggered by the large scales and that their destruction would decrease the bursting activity. Some preliminary studies showed large overall drag reduction and many different research groups around the world became excited by the prospects of LEBUs and got involved in this research. Several groups also showed that behind the LEBUs there were a strong decrease in the local skin friction, however in order to get a positive drag reduction effect the integrated skin-friction reduction has to be larger than the penalty drag on the LEBUs themselves. Careful towing tank experiments by Sahlín, Alfredsson & Johansson (1986); Sahlín, Johansson & Alfredsson (1988) showed that no positive effect on total drag was achieved when using LEBUs. This method has thereafter, at times, been denoted “the cold fusion of turbulence research”.

### 4.2.4. Compliant surfaces

The swimming performance and speed of dolphins have always fascinated man. Through estimates of the muscle power of dolphins, it was found that the power available was too small to overcome the assumed friction of the swimming

## 4. BOUNDARY LAYER FLOW CONTROL

dolphin. This led to the idea that the soft and elastic skin of the dolphin could reduce drag. Since then research on the effect of compliant surfaces on both laminar and turbulent boundary layers has been pursued and most of the work is reviewed by Gad-el-Hak (2000). For instance it is suggested from theoretical considerations and verified in experiments that compliant coatings can reduce the growth of instability waves and thereby increase the transition Reynolds number with almost an order of magnitude.

Compliant coatings have also been suggested to decrease the friction drag of a turbulent boundary layer. In an experimental study, Choi *et al.* (1997) found a drag reduction of 7% in a turbulent boundary layer over a compliant coating. The fluctuations of the velocity, shear stress and pressure were also reduced. Recently, Endo & Himeno (2002) performed numerical simulations of the phenomenon and concluded that the drag reduction in a turbulent channel flow momentarily reached 7% and 2.7% in the mean. The possibilities to optimize the parameters of the compliant coatings can probably improve the performance.

### 4.3. Non-reactive flow control

The methods cited so far are all passive in the sense that there is no need for external energy input in order to drive the control system; the methods rely on passive utilization of the flow dynamics. However, allowing oneself to use external energy to control the flow the possibilities increase.

#### 4.3.1. Steady suction

One control concept is to use steady and continuous suction through the wall in order to change the mean flow and thereby obtain the desired control effect. According to Schlichting & Gersten (2000), with a suction velocity at the wall of  $1.2 \times 10^{-4}U_\infty$ , the boundary layer is stable to T-S waves and will remain laminar. The drag reduction obtained is then 60–80% depending on the Reynolds number. For other types of disturbances, such as those introduced by free-stream turbulence, much stronger suction is needed in order to obtain stabilization. Some recent work on transition delay using the method of steady suction is reviewed below.

4.3.1a. *Experimental work.* Fransson (2001) performed experiments on the effect of continuous suction in a boundary layer subjected to free-stream turbulence. With a FST level of 1.4%, he found that a suction velocity of  $2.5 \times 10^{-3}U_\infty$  was necessary in order to inhibit disturbance growth in the boundary layer. This value is 20 times larger than the value given by Schlichting & Gersten (2000). This shows that the disturbances introduced in the boundary layer by the free-stream turbulence need much stronger control as compared to the T-S waves accounted for in earlier studies.

### 4.3. NON-REACTIVE FLOW CONTROL

The ultimate goal of transition control is not necessarily to maintain laminar flow over the whole surface, *e.g.* turbulent flow might be preferable at some point in order to avoid separation. Nelson *et al.* (1997) experimentally demonstrated the use of multiple suction strips together with an iterative algorithm in order to move the transition point to a predetermined position.

In a practical application suction is usually performed through a perforated surface with discrete holes. This means that the suction is not uniformly distributed over the surface, but instead rather localized. The effect of such localized suction was studied by MacManus & Eaton (2000) who showed that the suction rate through individual holes may not exceed a critical value, above which the flow induced by the sharp sides of the hole can generate large disturbances in the flow.

4.3.1b. *Theoretical studies.* The suction distributions minimizing the disturbance amplitude growth of a disturbance (or selected group of disturbances) have been obtained by optimization processes by Balakumar & Hall (1999) and Pralits, Hanifi & Henningson (2002). Their results show that for a given energy consumption, the maximum effect, as measured by the growth of disturbances in the flow, usually is obtained if most of the suction is used upstream and the suction rate then is decreased downstream.

Cathalifaud & Luchini (2000) calculated the steady blowing/suction distribution which most efficiently decreases the growth of optimal disturbances. It was found that the actuation should be of high amplitude at the upstream end of the region over which transpiration was applied. The study only considers steady (infinitely long) optimal disturbances.

#### 4.3.2. *Non-reactive structure manipulation*

Applying steady suction changes the mean flow to a more stable state. Turbulence or transition can however be affected also by actuation affecting mainly structures in the flow.

4.3.2a. *Spanwise oscillation.* If the wall below a turbulent boundary layer oscillates in the spanwise direction, the turbulence activity inside the boundary layer has been observed to decrease for certain parameter values (frequency and amplitude). This effect has been studied experimentally by Jung *et al.* (1992). The numerical study of Laadhari *et al.* (1994) showed a drag reduction of up to 40% by oscillating the wall. Later studies by Choi, DeBisschop & Clayton (1998) and Choi & Clayton (2001) confirm the drag reduction results and show that the underlying mechanism is that the oscillating wall tilts vorticity towards the spanwise direction. The thus created spanwise vorticity alters the mean velocity profile by decreasing the velocity close to the wall and

#### 4. BOUNDARY LAYER FLOW CONTROL

increasing it further out from the wall. At the same time, the spanwise vorticity obstructs the streak-creating longitudinal vortices, thereby reducing the bursting activity.

4.3.2b. *Transverse traveling waves.* Schoppa & Hussain (1998) show in a numerical simulation that a spanwise traveling wave, obtained through blowing and suction at the wall of a turbulent channel flow, may reduce the friction drag. This is equivalent to a spanwise traveling surface wave. The amplitude of their actuation is fairly high and the best results were obtained with a blowing/suction amplitude of 6% of the centreline velocity. Du *et al.* (2002) reports result from a simulation, showing that a spanwise traveling wave can reduce turbulent drag. At optimal conditions, the spanwise traveling wave reduced the drag with 30%. The control scheme can be realized by moving walls or electromagnetic forces in conductive media, such as salt water.

#### 4.4. Reactive control

The reason for suggesting reactive control of flow instabilities is that the energy spent for controlling can be used more efficiently if knowledge of the flow state is used. The potential of reactive control is illustrated by Bewley *et al.* (2001), who found that a turbulent channel flow can be relaminarized by suction/blowing at the wall, if it at each instant is adjusted to minimize future flow oscillations (accessible in advance via DNS). The basic idea is that the state of the flow is measured by a sufficient number of sensors whereupon an appropriate control action is calculated by a controller. Finally this control action is applied via blowing/suction at the wall or some other actuation method.

When entering the field of reactive flow control, a comment has to be made regarding the choice of method: experiments or DNS. In flow studies, the approaches differ in the data they provide: a DNS provides full field data of certain parameter values whereas an experimental study typically provides data from chosen positions, but possibly for a larger number of parameter settings. In flow control, additional differences appear. Numerically, distributed actuation can be applied, whereas the experimental approach has to rely on localized actuation. The localized actuation tend to create a near-field, especially close to the wall, in which the global flow field does not affect the velocity variation. This disparity does not only hinder the comparison of experimental and numerical data, but also the experimentalists who wish to make use of progress from numerical studies.

It is well known that transition induced by T-S waves can be delayed by introducing anti-phase waves. The anti-phase wave can be introduced by oscillating suction/blowing through a slot, a vibrating ribbon or intermittent heating and the concept has been demonstrated experimentally by Milling (1981) (vibrating ribbon) and Liepmann, Brown & Nosenchuck (1982) (intermittent heating). In a follow up experiment, Liepmann & Nosenchuck (1982) showed

#### 4.4. REACTIVE CONTROL

how transition induced by 2D wave disturbances can be delayed by reactive control systems relying on linear wave cancellation.

The localized nature of flow disturbances appearing in some transition scenarios and turbulence, makes it necessary to produce large quantities of sensors and actuators. MEMS (Micro-Electro-Mechanical-Systems) promise to enable the production of sensors and actuators in large quantities (Ho & Tai 1996; Löfdahl & Gad-el-Hak 1999).

MEMS are built utilizing the techniques of the fabrication of integrated chips. Three dimensional structures with beams, membranes, flaps, etc. can be built on silicon substrates. The ultimate goal is to build sensors, actuators and the necessary controller electronics on the same chip. So far, hot-film sensors for shear stress and different pressure sensors have been produced (Löfdahl & Gad-el-Hak 1999) whereas there are few (if any) successful experiments with integrated control systems comprising sensors and actuators manufactured with MEMS-technology. A self cleaning valve, designed for use in aeronautic applications, has however been successfully built and tested (Kerho 2002).

A selection of studies on reactive control of turbulent and transitional flows are summarized in table 1, where the sensor/sensed quantity, controller and result are shown for a selection of references. The sensors are fairly well developed. The situation is different when it comes to actuators and controllers. The controller is the algorithm used to calculate the actuation based on measurements (*c.f.* figure 4.1).

##### 4.4.1. *Sensors*

Time resolved information of the flow for control purposes should be obtained from non-intrusive sensors and is therefore typically obtained from wall wires or hot films. Such sensors give information of the instantaneous wall shear stress. Even though the frequency response of such sensors can vary with the frequency, as pointed out by Alfredsson *et al.* (1988), they are suitable for detecting flow structures in the near-wall region.

It has been shown by Bewley & Protas (2002) that it is necessary to combine shear stress measurements with pressure measurements at the wall if the flow field above the wall is to be efficiently estimated. This means that in addition to the shear-stress sensors, pressure sensors such as microphones might have to be used.

##### 4.4.2. *Actuator principles*

There are a multitude of mechanisms, which can be used to affect a flow for control purposes. Some have already been touched upon, such as vibrating ribbons or intermittent heating, which have been used to reduce the amplitude of T-S waves. The most important ones used for transition and turbulence control will be described below, together with reviews of the results obtained.

4. BOUNDARY LAYER FLOW CONTROL

Reference	Flow information	Actuation	Controller	Result
<b>Simulations</b>				
Bewley <i>et al.</i> (2001)	full flow field	modulated & distributed blowing/suction	direct optimization	relaminarization
Högberg <i>et al.</i> (2002)	full flow field	modulated & distributed blowing/suction	linear optimal control	inhibited transition
Lee <i>et al.</i> (1998)	$(\frac{\partial w}{\partial y})_{y=0}$ $(\frac{\partial p}{\partial z})_{y=0}$	modulated & distributed blowing/suction	suboptimal control	22 % drag red.
Choi <i>et al.</i> (1994)	$v(y^+ = 15)$	modulated & distributed blowing/suction	linear proportional (opposition control)	25% drag red.
Lee <i>et al.</i> (1997)	$(\frac{\partial w}{\partial y})_{y=0}$	modulated & distributed blowing/suction	neural network	20% drag red.
Kang & Choi (2000)	$v(y^+ = 15)$ $(\frac{\partial w}{\partial y})_{y=0}$	vertical wall motion	linear proportional & suboptimal	17% drag red.
Lee <i>et al.</i> (2001)	$(\frac{\partial u}{\partial y})_{y=0}$	modulated & distributed blowing/suction	optimal control (reduced order)	17% drag red.
Joshi <i>et al.</i> (1997)	$(\frac{\partial u(x_i, z)}{\partial y})_{y=0}$ at $x_i = x_1, x_2 \dots$	blowing/suction strips in spanwise direction	systems theory	stabilization of Poiseuille flow
Endo <i>et al.</i> (2000)	$v(y^+ = 15)$ $(\frac{\partial^2 w}{\partial y \partial z})_{y=0}$	vertical wall motion with physical constraint	linear proportional	12% drag red.
<b>Experiments</b>				
Rathnasingham (1997)	wall wires (four sensors)	pulsating jets (sign insensitive)	linear system identification	7% drag red.
Kerho <i>et al.</i> (2000)	hot films (five by five)	localized suction (five by five)	triggered on threshold	22 % drag red. (momentum loss)

TABLE 1. Summary of some of the numerical and experimental studies on reactive flow control. All numerical studies are on laminar or turbulent channel flow. The experiments are all made in boundary layer flows.

#### 4.4. REACTIVE CONTROL

4.4.2a. *Localized suction and/or blowing.* Spatially and temporally modulated suction and/or blowing have been used in numerical work as well as in experiments. Suction through a narrow streamwise slot or a hole in a boundary layer plate have been used to inhibit bursting of generated structures by Gad-el-Hak & Blackwelder (1989). Myose & Blackwelder (1995) delayed transition of Görtler vortices by applying suction below the low velocity regions. A similar technique was used by Egami & Kohama (1999) who delayed transition induced by cross-flow vortices.

Tardu (2001) experimentally studied the effect of periodic suction/blowing through a spanwise slot on a turbulent boundary layer. It was found that periodic blowing, oscillating between zero and a certain amplitude, had similar effects on the mean flow as continuous blowing with the same integrated amplitude. However, the time dependent forcing had interesting effects during the cycle: at certain positions and periods of time, the flow seemed to relaminarize.

Rebbeck & Choi (2001) studied the effect of sudden blowing through a hole on structures in a turbulent boundary layer. The actuator was activated with a fixed frequency and the randomly appearing structures were detected by a wall wire. In the post processing, time excerpts in which the structure appeared at similar times relative the actuator were ensemble averaged. By this method, the effect of the actuator could be tried without the need of reactive control. It was found that properly applied, the actuation inhibited the bursting of the streaks and smeared out the rapid deceleration typically occurring during the bursting process .

Transition of transiently growing low velocity disturbances in a laminar boundary layer has been inhibited by suction through a hole by Bakchinov *et al.* (1999). Later experiments (Bakchinov *et al.* 2000) showed that the opposite also works, *i.e.* that blowing can be used to decrease the amplitude and inhibit breakdown of high-speed streaks.

4.4.2b. *Vertical wall motion.* Suction/blowing have shown to be an efficient actuation technique. In applications, such as on an aircraft wing or in a pipe line, it might however be unpractical. Therefore, vertical wall motion with the same velocity as the blowing/suction has been proposed, since the boundary condition becomes the same, provided the curvature of the wall is small. Breuer, Haritonidis & Landahl (1989) showed that the growth of a transient disturbance can be inhibited by vertical motion instead of suction (compare with the results of Gad-el-Hak & Blackwelder (1989) and Bakchinov *et al.* (1999) above). A streamwise array of membranes was moved down one after another with a suitable time delay. The breakdown of a disturbance generated by a similar membrane upstream of the others, moved in the opposite direction, was successfully inhibited.

## 4. BOUNDARY LAYER FLOW CONTROL

The motions introduced by the sudden upwards movement of a part of the wall was studied by Hofmann & Herbert (1997). The simulations aimed at examining the flow patterns produced by an experimentally realizable actuator.

Vertical wall motion has also been tested in numerical studies of turbulence control. This will be touched upon under the review of controllers.

4.4.2c. *Synthetic jets.* On average, a high frequency oscillating zero-mass-flux suction/blowing through a hole generates a pair of streamwise vortices together with a jet. This effect was used by Rathnasingham & Breuer (1997) (together with a linear system identification scheme to be described below) to decrease bursting in a turbulent boundary layer. Glezer & Amitay (2002) review the use of such synthetic jets and illustrate its ability to control separation on a cylinder.

4.4.2d. *Flap based configurations.* Jacobson & Reynolds (1998) used an actuator based on an electromagnetically driven flap, which was placed over a cavity. The two gaps on the sides of the flap were of different width and when the flap was moving up and down at resonance, a pair of streamwise vortices were generated over the narrow gap, somewhat similar to the synthetic jets. The vortices created by the actuator can be made to interact with longitudinal wall structures for flow control purposes.

4.4.2e. *Electromagnetic actuation.* Among others, Rossi & Thibault (2002) report on the use of electromagnetic forcing, which can be used in conductive media such as salt water. Such a device can generate localized as well as more homogeneous body forces and thereby act as a flow control actuator.

### 4.4.3. Controller design and its evaluation

With sensors and actuators available, the third component in a control system, the controller, determining what control action to apply based on the sensor signal(s), has to be designed. It can be designed based on physical arguments or from a mathematical analysis. The methods below are the most important ones tried.

4.4.3a. *Opposition control.* The perhaps most obvious control is to apply an action which opposes structures which have been identified as critical in the flow. This approach is called opposition control and was tried by Choi *et al.* (1994). They performed a DNS and set the normal velocity at the wall to the opposite of the normal velocity at a suitable distance from the wall. The distance at which the measurements were taken was found by tuning. Drag reduction of up to 25% was obtained in the turbulent channel flow under study. The scheme is however not realizable in a physical experiment, since distributed measurements of the wall-normal velocity at a distance above the wall cannot be performed.

#### 4.4. REACTIVE CONTROL

A similar controller used together with vertical wall motion and some physical constraints on amplitude and size of the wall elements to be moved, was found to give a drag reduction of 12% in the simulation of Endo *et al.* (2000). Reference simulations showed that the decrease in efficiency as compared to Choi *et al.* (1994) was due to the physical constraints and not due to the change of actuation principle.

Chang *et al.* (2002) applied the opposition control scheme at different Reynolds numbers. At low Reynolds numbers, the opposition control scheme managed to relaminarize the flow whereas at higher Reynolds numbers, a drag reduction, decreasing with Reynolds number, was obtained.

4.4.3b. *Other cancellation schemes.* Opposition control has developed into a benchmark method in control of turbulence for drag reduction. The idea of cancellation has however been used also in other ways, both experimentally, in simulations and in more theoretical work and some examples will be given below.

In an experimental demonstration of reactive control of turbulence, Kerho *et al.* (2000) showed that suction, triggered by the time derivative of the streamwise wall shear stress from upstream sensors, can be used to reduce the drag. It was assumed that quick acceleration (fast increase of the shear stress) is related to upward motions, which in turn create streaks. The suction is then supposed to cancel the upward motion. The scheme was tried in a turbulent boundary layer and drag reduction of up to 22%, based on mean profile measurements, was reported.

A second reactive control experiment is the one by Rathnasingham & Breuer (1997). Also this study relies on a cancellation scheme. But instead of an assumed physical behaviour, as in the case of Kerho *et al.* (2000), the actual development of disturbances in the turbulent boundary layer under study is modeled. In the experiments of Rathnasingham & Breuer (1997), the streamwise velocity at some distance above the wall downstream of the sensors is modeled from the sensor signals by FIR (finite impulse response) filters, *i.e.* weighted sums. Similar filters are used to model the velocity variation resulting from the actuator output. The filters can be used to apply actuator output designed to cancel the expected velocity variation, which first is modeled from the sensor signals. Rathnasingham (1997) report drag reduction of 7% in a turbulent boundary layer. Also here, the drag reduction was deduced from mean flow profiles. The approach relies on the assumption that the dynamics are linear in the sense that the response to actuation does not change with the flow.

Koumoutsakos (1997) proposed and made numerical studies of a scheme based on the vorticity flux in and out from the wall. The actuation was applied such that a preset vorticity flux at the wall was obtained. Simulations showed that the method can extinguish near-wall vortices. With a vortex flux into the

## 4. BOUNDARY LAYER FLOW CONTROL

wall, near-wall vortices are found to be sucked into the wall (*i.e.* the flow, not the fluid).

Gmelin & Rist (2001) delayed transition in a simulation by measuring the normal vorticity at the wall and apply the opposite as a boundary condition with a time delay found to be optimal. The scheme showed to be more robust to non-linear features of the flow as compared to schemes using the velocity or streamwise shear instead of the vorticity.

Using the spanwise wall shear stress as input and body forces in the flow, Lee & Kim (2002) obtained a drag reduction of 35%. If the scheme is to be implemented in low conducting media, such as salt sea water, the body force cannot be too large and Lee & Kim mention that a realistic drag reduction, leading to a net gain, is of the order of 20%.

4.4.3c. *Neural network.* A neural network is a tool which can be used to obtain controllers. It consists of an input layer, some hidden layer(s) and an output layer. A signal arriving at the input layer is transferred to the output layer via the hidden layers. At the hidden layers, different linear and/or nonlinear transformations of the signal are made. During the tuning (training), the transformations are tuned so that the output gives the desired result. Once tuned (trained), the neural network can be used as a controller. Lee *et al.* (1997) trained a neural network to minimize the drag in a turbulent channel. A drag reduction of 20% was obtained and in this study, only measurements at the wall were used. The resulting network was found to be exchangeable with simple proportional controllers.

4.4.3d. *Direct optimization.* The methods so far have relied on some simple intuitive or empirical models to design the controller. However, since the governing equations are known to be the Navier-Stokes equations, they can be used for the controller design. In complexity, the opposite of the opposition control is direct optimization, which means that among all possible control actions, the one minimizing a suitable performance measure is chosen. Bewley *et al.* (2001) performed a simulation applying such a control. At each timestep, an iteration had to be performed in order to find the optimal control action. During the iteration, simulations had to be performed in order to obtain the result of the control. This very time consuming and information arduous controller proved to be successful: optimally applied blowing and suction proved to be able to relaminarize the turbulent channel flow used as a test case.

4.4.3e. *Linear optimal control.* Linear optimal control theory provides the optimal feedback gains to be applied to a linear system so that some objective function is minimized. The general theory is explained by Doyle *et al.* (1989) and was applied to the discretized Navier-Stokes equations by Bewley & Liu (1998). The methodology has also proven to be successful in transitional flows

#### 4.4. REACTIVE CONTROL

studied by Högberg, Henningson & Bewley (2002) and Högberg & Henningson (2002), where transition could be delayed substantially. Högberg has also managed to relaminarize a turbulent channel flow with the optimal controller (private communication).

A reduced order optimal controller was tried by Lee *et al.* (2001) together with blowing/suction. A drag reduction of 17% was obtained. The development of reduced order controllers is a necessary step if the controllers are to be implemented physically.

4.4.3f. *Suboptimal control.* The suboptimal control strategy differs from the direct optimization in the way that the control is optimized over a very short time-scale, a time horizon of only one time step is usually used. This approach was used by Lee *et al.* (1998) who report a drag reduction of 22% in a turbulent channel flow.

4.4.3g. *Systems theory.* Joshi *et al.* (1997) derived a single-input/single-output system from the linearized Navier-Stokes equations, describing the development of a single mode from an input position to a downstream output one. The derived system was written on traditional transfer-function form, so that the feedback control of the system could be studied within the framework of systems theory. A compensator built up of a constant feedback gain together with an integrator, was shown to stabilize the system. However transients, potentially driving the system to transition, occurred due to the feedback.

##### 4.4.4. Estimation

If controllers designed by optimal control are to be realized in physical experiments, the whole flow field has to be estimated from the available measurements. Estimation is thus a crucial step if the advances from numerical studies are to be implemented physically.

One approach is to run a simulation of the flow (complete with all dynamics or with simplified dynamics) and numerically force this simulation (the estimator) towards the state of the real flow from which some measurements are taken. The control to be applied is then based on the states in the simulated flow (the estimate). The quality of the estimate is found to be crucial in order to obtain good control results (Högberg *et al.* 2002).

The use of Wiener filters for estimation was tested by Amonlirdviman & Breuer (2000), who showed that the streamwise velocity can be fairly well predicted from the spanwise wall shear stress. This is in agreement with the prediction results of Rathnasingham & Breuer (1997), who managed to predict the low frequency fluctuations of the streamwise velocity near the wall in a turbulent boundary layer very well from a wall wire mounted in the streamwise direction, *i.e.* parallel to the flow.

#### 4. BOUNDARY LAYER FLOW CONTROL

An additional candidate for estimation of the flow field from sparse measurements is Proper Orthogonal Decomposition (POD). In POD analysis, orthogonal modes of the measurements from the system are sought, so that, at any level of truncation, as much as possible of the fluctuation energy is contained. POD analysis of a turbulent channel flow was done by Podvin & Lumley (1998). It was concluded that if wall shear stress measurements with a resolution possible to obtain in an experiment was used, the mean error of the estimate as compared to the real flow was about 20%. An additional complication with the POD approach is also that, as control is applied, the system changes and POD modes obtained without control applied are not the correct ones anymore (Prabhu *et al.* 2001).

In this context, it is appropriate to remind of the result of Bewley & Protas (2002). They used Taylor expansions of the flow to show that when estimating the flow over a wall, the streamwise shear stress, the spanwise shear stress and the pressure all provide unique and valuable information. This indicates that in order to get a good estimation of the flow above a wall, all three quantities may have to be measured.

#### 4.5. Concluding remarks

Control of fluid flow in order to achieve certain design goals can be done with different methods, in this thesis categorized as passive, non-reactive and reactive. The methods differs in the use of external energy and the use of information of the state of the flow. For turbulent drag reduction, the addition of polymers in the fluid can give very large (60% or more, Sreenivasan & White (2000)) reductions in the friction drag. Surface modifications such as riblets can give a drag reduction of up to 9% (Bechert *et al.* 1997) and similar values have been reported for compliant surfaces (Choi & Clayton 2001). Non-reactive methods, such as spanwise oscillation or transverse waves, have proven to give drag reduction of up to 30%. The energy penalty for applying the control is however fairly large. On the other hand, reactive methods show the possibility to relaminarize low Reynolds-number turbulence and reduce the drag at higher Reynolds numbers with less penalty. Relaminarization typically results in drag reduction on the order of 60–80%, while the typical value for reactively controlled non-relaminarized turbulence seems to be around 20–25%.

When it comes to transition delay, transition induced by T-S waves can be delayed by reactive control, using ribbons, blowing/suction or heating to introduce out-of-phase disturbances. The transition delay is substantial. Compliant coatings is another mean to delay transition to four or six times higher Reynolds numbers.

Reactive control of transition induced by FST has not been studied previously, although some numerical studies on the control of optimal disturbances have been performed. These show that if optimal disturbances are to be controlled, much larger actuator strength is needed, as compared to what is needed

#### 4.5. CONCLUDING REMARKS

to delay transition induced by T-S waves. The numerical findings are complemented by the experimental study of Fransson (2001), who showed that the steady wall suction needed to inhibit disturbance growth in a boundary layer subjected to FST is 20 times the value stabilizing T-S waves.

## CHAPTER 5

### Methodologies of the present work

#### 5.1. Why experiments?

After reading the review on flow control, or simply after studying table 1, it should be obvious that the gap between physically implemented control systems and the ones studied numerically is large. Also, the experimental studies on simple reactive controllers usually lack the detail in the measurements of the effect necessary to draw safe conclusions of how the physical processes are affected. Therefore, the aim of the present project has been to control FST induced transition. Once a successful control system was designed, detailed measurements have been performed to study the control effect.

In order to isolate a phenomenon appearing randomly in the real application, model disturbances have been used. The relevance of such studies is of course related to the similarity between the randomly appearing disturbances and the model disturbance. In the present work, the use of model disturbances made it possible to study the effect of actuation without the need of reactive control.

#### 5.2. The flow apparatuses

As opposed to the rest of the thesis, the flow apparatuses are presented in order of appearance, *i.e.* the order the author came to work with them.

##### 5.2.1. Poiseuille flow channel

Papers 3 and 4 consider work performed in a plane Poiseuille flow channel. The channel consists of two glass plates separated 8.2 mm by aluminum bars. In between the glass plates, air is blown by a centrifugal fan. The channel has been used for numerous previous experiments, *e.g.* Elofsson & Alfredsson (1998), Elofsson, Kawakami & Alfredsson (1999) and Talamelli, Westin & Alfredsson (2000). The present experiments make use of the streak generation technique developed by Elofsson *et al.* (1999). The aim was to study the possibilities to control streamwise streaks by localized suction (Paper 4) and the growth of streak instabilities limited to a few wavelengths (Paper 3).

## 5.2. THE FLOW APPARATUSES

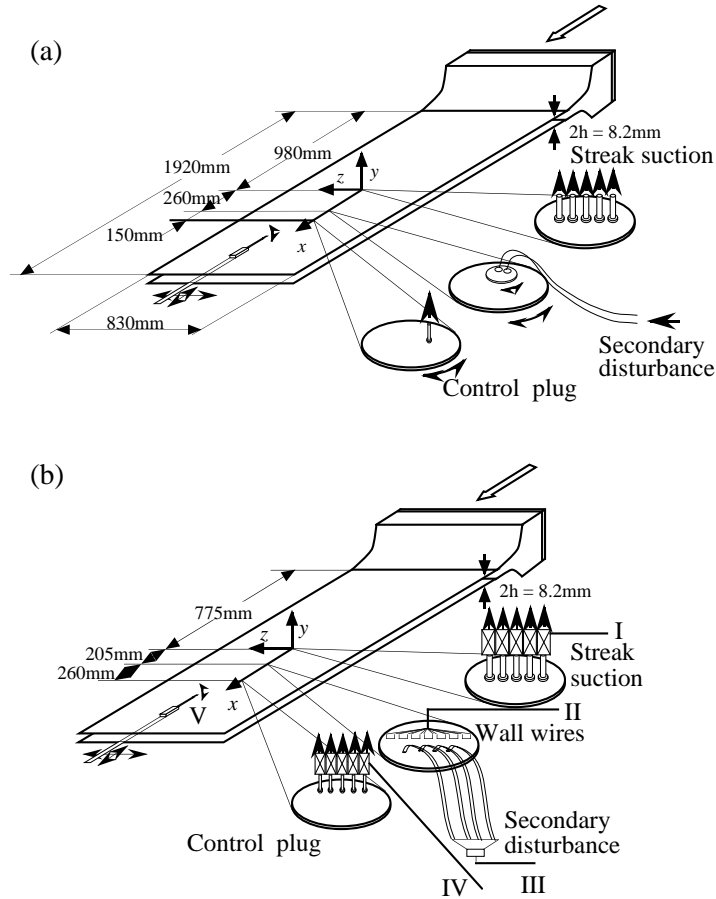


FIGURE 5.1. Overview of experimental setup for (a) non-reactive streak control and (b) reactive control.

One of the advantages of the channel was that it was accessible for a long period of time. Also, the existing disturbance generation system used by Eloffsson *et al.* (1999) could easily be adapted to the needs of the present studies. For the present study, the channel was equipped for random disturbance generation, making it possible to randomly force streaks as well as their secondary instability. The control system used suction through a spanwise array of holes or streamwise slots, turned on and off by fast solenoid valves based on measurements of the oscillations of the streamwise shear stress upstream of the actuators.

## 5. METHODOLOGIES OF THE PRESENT WORK

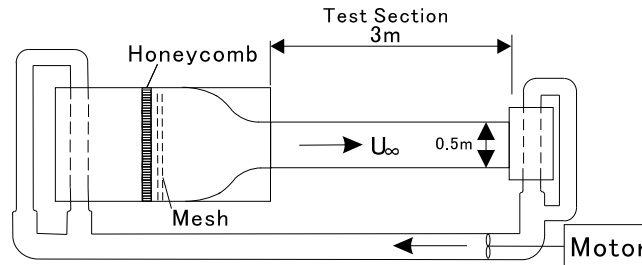


FIGURE 5.2. Top view of water channel.

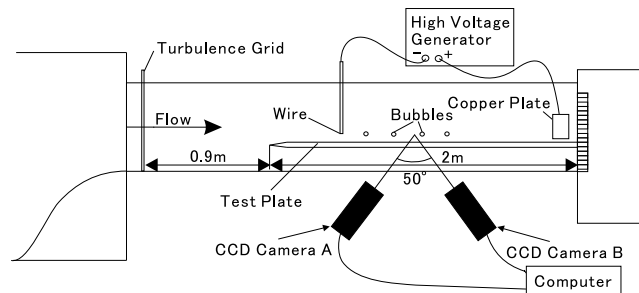


FIGURE 5.3. Test section setup with PTV-system.

### 5.2.2. The water channel in Sendai

Paper 1 reports measurements in a water channel (see figure 5.2), which was designed by Dr. Masaharu Matsubara and built mainly by him and Mr. Ayumu Inasawa at the Institute of Fluid Science at Tohoku University in Sendai, Japan. During a four month visit of Fredrik Lundell in 1999 the channel was completed, trimmed and equipped with a flat plate (the set up is shown in figure 5.3). The water channel was dedicatedly designed to allow time resolved measurements of the wall-normal velocity in a zero-pressure-gradient boundary layer under a turbulent free stream.

The main advantage of the water channel as compared to air apparatuses is that typical time scales are much longer. The development of the structures can be studied with the eye if suitable markers are present in the flow and time resolved stereo digital Particle Tracking Velocimetry (PTV) could be performed utilizing off-the-shelf products for digital video production.

### 5.2.3. The MTL wind-tunnel

The MTL (Minimum Turbulence Level) wind-tunnel at KTH was inaugurated in 1990. Free-stream turbulence induced transition has been studied in it by Westin *et al.* (1994), Alfredsson & Matsubara (2000), Matsubara & Alfredsson

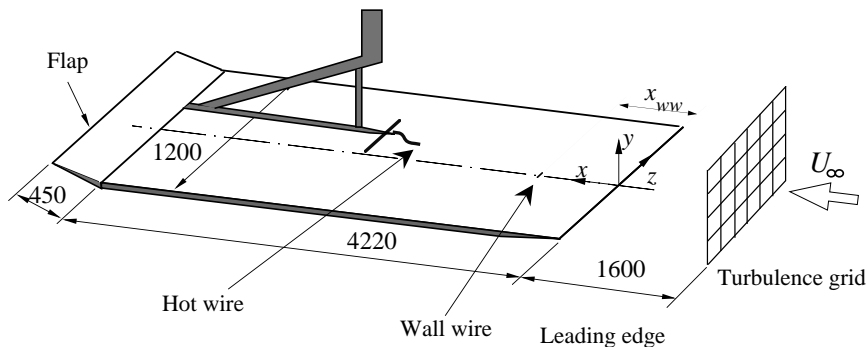


FIGURE 5.4. Setup in MTL wind-tunnel.

(2001), Fransson (2001) and Yoshioka, Fransson & Alfredsson (2003). The tunnel is equipped with a five axis traverse system. The flat plate setup and hot-wire measurements are well established from previous studies. Also, a number of turbulence generating grids are available. During the present experiments, instrumental plugs with sensors and actuators have been designed and built for the plate.

### 5.3. Experimental techniques

#### 5.3.1. Velocity measurements

5.3.1a. *Hot-wire anemometry.* For all experiments in air, the velocity was measured by a single hot wire measuring the streamwise velocity component. The reasons for choosing the hot wire were the time resolution and the simple synchronization of the measurements with other measurements, control systems and disturbance generation.

5.3.1b. *Bubble tracking velocimetry.* In order to measure the wall-normal velocity in the water channel, a stereo particle tracking system was designed and built. The system consists of two cameras, viewing chains of hydrogen bubbles, generated by a straight wire, under different angles. Stereo-viewing techniques were then used to reconstruct the three-dimensional position of the bubble chain, by which both the streamwise and wall-normal velocity could be deduced. The system allowed time resolved measurements of the instantaneous spanwise distribution of both the streamwise and wall-normal velocity.

5.3.1c. *Laser Doppler Velocimetry.* A Laser Doppler Velocimeter was used to confirm the accuracy of the bubble-image velocimetry system. The advantage of the LDV system was that measurements could be performed without calibration, thus being the perfect reference.

## 5. METHODOLOGIES OF THE PRESENT WORK

### 5.3.2. *Skin-friction sensing with wall wires*

In Paper 4 and 5, reactive control is studied. In both studies, the fluctuating wall shear stress is used as input to the controller. The fluctuating wall shear stress was sensed with wall wires. Even though special considerations have to be taken if the wall-shear stress is to be measured correctly with a wall wire, it is a convenient sensor for flow control studies due to its fast frequency response and high signal-to-noise ratio. A similar wall wire was used also in Paper 2, where correlations between a wall wire and a traversable hot wire were used to study the development of disturbances inside the boundary layer.

### 5.3.3. *Model disturbances*

5.3.3a. *Velocity streaks in the channel.* In the Poiseuille flow channel, velocity streaks were generated by applying suction through five streamwise slots, separated in the spanwise direction. Further downstream, the secondary instability of the streaks was forced by speakers. If the secondary instability is forced at a suitable frequency and the streak amplitude is large enough, breakdown to turbulence occurs after an amplification of the secondary instability. Both the streak generation and secondary instability forcing could be made random, simulating disturbances appearing in a boundary layer subjected to FST.

5.3.3b. *Localized disturbances in the wind-tunnel.* Model disturbances have also been used in the MTL wind-tunnel, where they were generated by blowing and suction through a hole in the plate. If high frequency noise was added to the disturbance, the high frequency fluctuations were amplified and the disturbance developed into an incipient spot. The disturbances were used to investigate the possibility to delay breakdown by a piezo-ceramic flap actuator.

### 5.3.4. *Actuation*

5.3.4a. *Localized suction.* In both the control Papers 4 and 5, suction through holes or narrow slots is used for actuation. Suction through holes has been used by previous investigators, and in the present work suction was first confirmed to be able to decrease the amplitude of steady and randomly appearing streaks in the channel (Paper 4). It was thereafter used for reactive control of FST induced transition (Paper 5). The suction was maintained by an air pump and turned on and off by solenoid valves. The main disadvantages are that it does neither allow amplitude-modulated nor opposite (blowing) actuation.

5.3.4b. *Piezo-ceramic flap.* With proper activation, a piezo-ceramic flap showed to successfully inhibit breakdown of streaky disturbances generated in the boundary layer. The results are presented in Paper 6. The piezo flap promises to provide amplitude modulated actuation as well as actuation action of both signs (downward motion and upward motion). These aspects were however not explored during this work.

### 5.3. EXPERIMENTAL TECHNIQUES

5.3.4c. *Pulse-width modulated blowing/suction.* Amplitude modulation can also be achieved by using pulse-width modulation. Within the present work, pulse-width modulated blowing/suction was tried as an actuator and a high correlation between the generating signal and the response of an undisturbed boundary layer was obtained. The results are presented in Paper 7.

## CHAPTER 6

### Results

In this chapter, the results from Papers 1–7 are presented briefly. For details and further discussions, the papers enclosed in the thesis should be consulted. The results are separated into two sections. First, fundamental studies related to FST induced transition are studied. The relevant papers are Papers 1–3. In the second section of this chapter, the flow control results from Papers 4–7 are reviewed.

#### 6.1. Free-stream turbulence induced transition

##### 6.1.1. *Streak growth*

Figures 6.1 and 6.2 from Paper 1 show velocity data from the boundary layer measured in the water channel. In figure 6.1, the mean velocity ( $\bar{U}$ ) and disturbance ( $u_{rms}$ ) profiles in the boundary layer are shown. There is good agreement between the stereo-PTV measurements and the LDV data as well as with theory. This also illustrates the accuracy of the newly developed stereo-PTV system.

Simultaneous time traces of the streamwise,  $u$ , and wall-normal,  $v$ , velocities and their product ( $uv$ ) at a point in a boundary layer subjected to FST, as measured by the PTV-system, are shown in figure 6.2. Strong fluctuations are seen in the streamwise velocity component, as streaks of high and low-velocity pass the measurement position. Note that the scale varies for the three components:  $v$  is amplified ten times as compared to  $u$ . The wall-normal velocity is seen to be negatively correlated with the streamwise component. This illustrates the concept of lift up, *i.e.* that the low-speed streaks are generated as low-velocity fluid is moved by a positive (upwards) wall-normal velocity disturbance to higher regions in the boundary layer and vice versa for high-speed streaks. Studying figure 6.1 in more detail, it is seen that high-speed disturbances start before the generating wall-normal disturbance while low-speed disturbances exist also after the corresponding period of positive wall-normal velocity fluctuation. The mechanism behind this effect is yet to be described. The observation serves as an illustration of the intriguing dynamics and kinematics of the low frequency disturbances under study.

The  $zt$ -distributions of the velocity disturbances in the boundary layer (figure 6.3) show that the fluctuations seen in figure 6.2 are related with elongated

### 6.1. FREE-STREAM TURBULENCE INDUCED TRANSITION

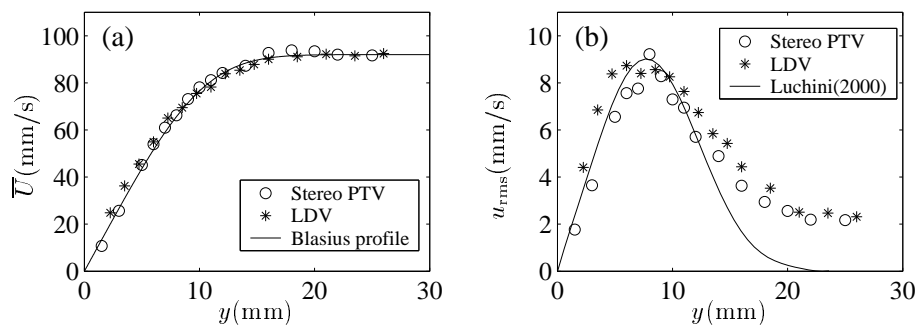


FIGURE 6.1. Profiles of (a)  $\bar{U}$  and (b)  $u_{rms}$  measured by PTV and LDV in the boundary layer,  $x = 800$  mm,  $U_\infty = 0.092$  m/s and  $Tu = 3.4\%$ .

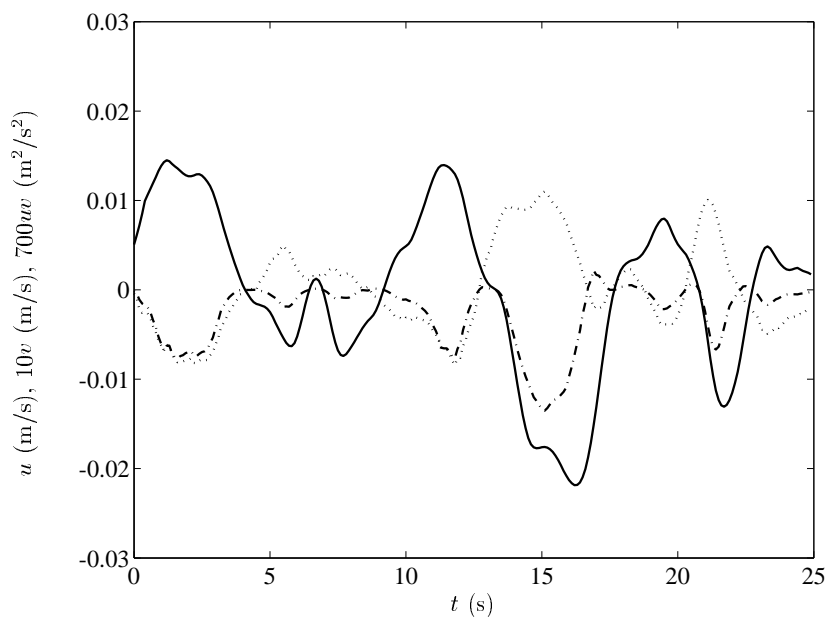


FIGURE 6.2. Simultaneous time signals of  $u$  (—),  $v$  ( $\cdots$ ), and  $uv$  ( $\cdot-\cdot-$ ) in a boundary layer subjected to  $3.4\%$  of FST. Data from  $y/\delta^* = 1.48$ .

structures in the boundary layer. Time resolved, spanwise distributed measurements of the streamwise and wall-normal velocity components in a boundary layer subjected to FST have not been performed before.

## 6. RESULTS

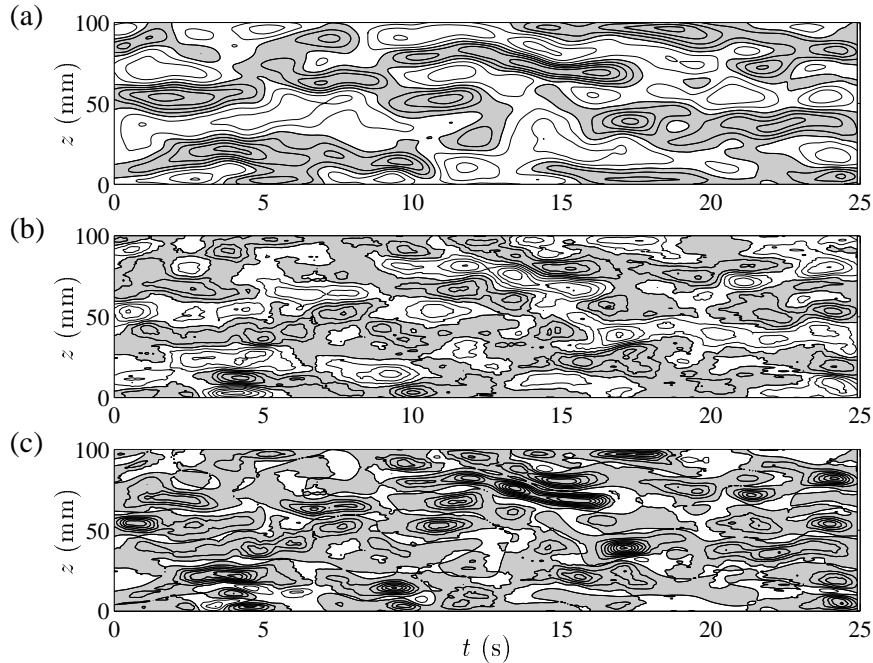


FIGURE 6.3. Contour maps of (a)  $u$ , (b)  $v$  and (c)  $uv$  at  $y/\delta^* = 1.48$ . Data taken by the stereo PTV-system in the water channel,  $U_\infty = 0.108$  m/s,  $Tu = 3.4\%$ . Contour levels: (a),  $\pm 5, 10, \dots$  mm/s, (b),  $\pm 0.3, 0.6, \dots$  mm/s and (c),  $\pm 3, 6, \dots$  mm<sup>2</sup>/s<sup>2</sup>. Negative contours are filled with grey.

In Paper 2, the streamwise scaling of such structures is studied. The correlation between a wall wire and a traversable hot wire is used to study the development of the structures over the flat plate in the MTL wind-tunnel. The structures were found to scale as the boundary-layer thickness in both the streamwise and wall-normal direction. The mean correlation structure is shown in figure 6.4(a) together with its propagation speed along constant non-dimensional  $y$ . The wall-normal coordinate in the boundary layer is now scaled with  $\delta$ .

The velocities in figure 6.4(b) show that the structures propagate downstream at a speed which is constant and equal to the mean flow velocity around  $y = 2.6$ . At other  $y$ ,  $U_{struc}$  varies with the streamwise position.

Due to the growth of the boundary layer, the kinematics of the disturbances are non-intuitive. The variation of the propagation velocity, both through the boundary layer and in the streamwise direction, can be explained by the

## 6.1. FREE-STREAM TURBULENCE INDUCED TRANSITION

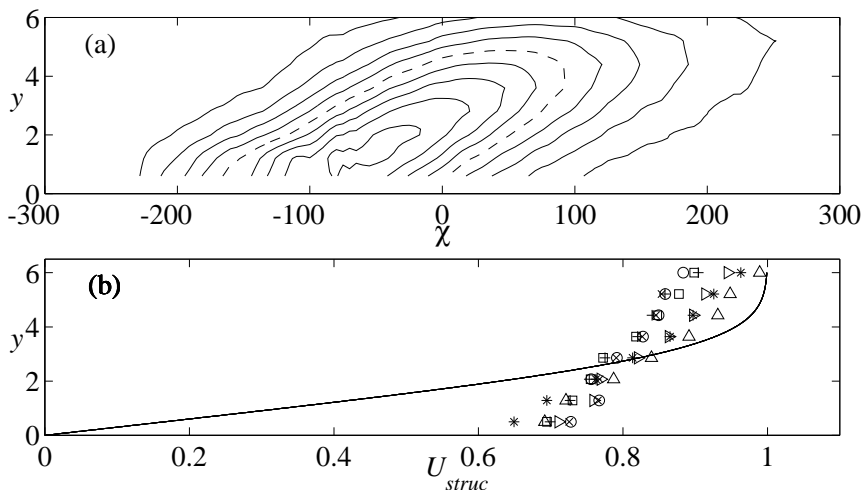


FIGURE 6.4. Mean correlation distribution (a) and structure propagation speed (b) for different wall-wire positions and  $Tu$ . The symbols in (b) are:  $Tu=1.8\%$ ,  $x_{ww}^*=214$  (\*), 414 (+), 484( $\square$ ), 764( $\circ$ ), 834 mm ( $\times$ ) and  $Tu=1.1\%$ ,  $x_{ww}^*=214$  ( $\triangle$ ), 484 mm ( $\triangleright$ ).

assumption of self-similar structures developing in the boundary layer. Further details are found in Paper 2.

### 6.1.2. Streak breakdown

Having studied the generation mechanism and scaling of streaks in boundary layers in Papers 1 and 2, an aspect of the breakdown of streaks due to the growth of a secondary instability is studied in Paper 3. The steady velocity streaks in the Poiseuille channel are forced by a known noise signal. At certain times, the disturbance signal exhibits (instantaneously) a frequency amplified by the streaks. At such times, a wiggle with a length of a few wavelengths is observed in the velocity signal. An example of such a disturbance at different streamwise positions is seen in figure 6.5.

In Paper 3, the initial disturbance distribution of such instabilities is found to be similar to what has been observed for infinite wavetrains. However, the dynamics of the leading and trailing edges of a localized disturbance cannot be observed if the streak is forced by infinite wavetrains.

For disturbances longer than four wavelengths, the growth rate was found to be constant and equal to that obtained for infinite wavetrains. The growth of the secondary instability was however found to be slower for disturbances shorter than four wavelengths as shown in figure 6.6. For this figure, the growth

## 6. RESULTS

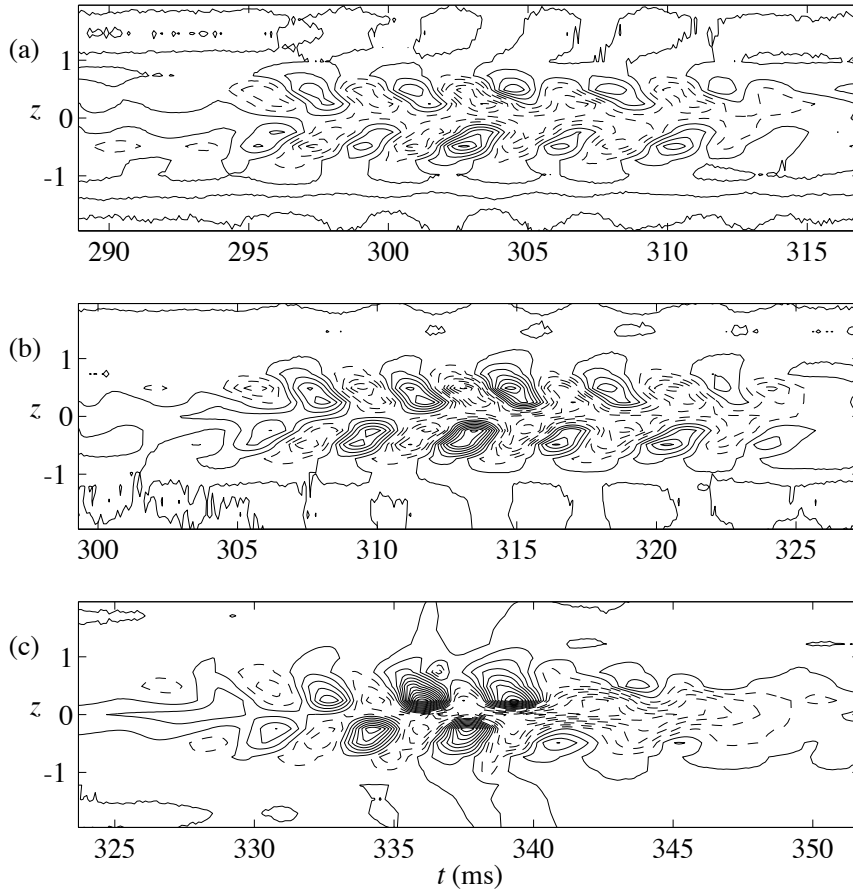


FIGURE 6.5. Data taken on streaks forced by random noise in the Posieuille flow channel. Ensemble-averaged disturbance velocity  $u$  at  $y = 0.36$  and (a)  $x = 88$ , (b) 112 and (c) 161. All coordinates are scaled with the half-channel height. Contour levels are (a, b) 0.3% and (c) 1% of  $U_{CL}$ . Negative contours are dashed. To get a physical aspect ratio the figure, the time axis has to be stretched twice.

rate was measured by forcing the secondary instability with signals consisting of a predetermined number of wavelengths,  $N$ , ranging from 0.5 to 30.

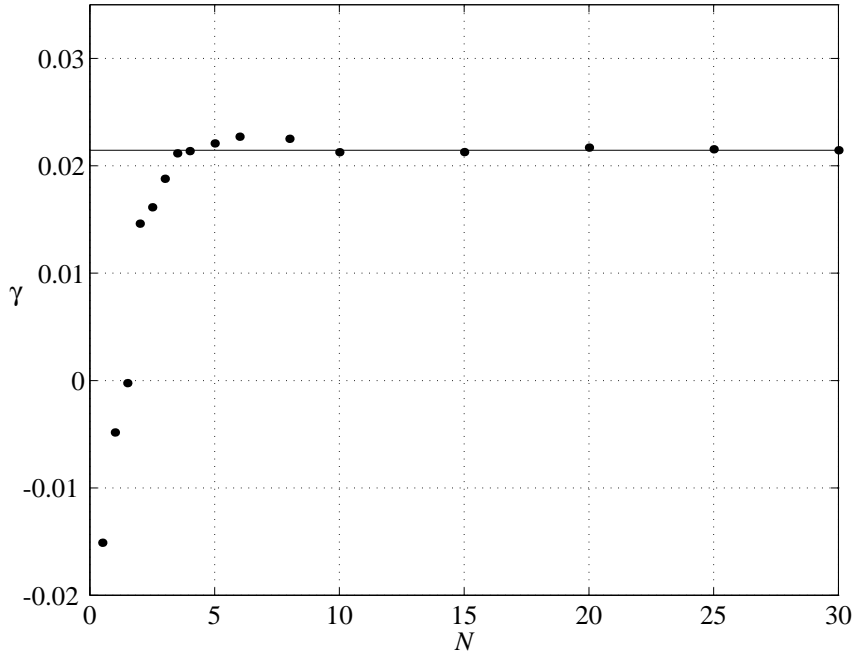


FIGURE 6.6. Growth factor of wavy disturbances as a function of number of wavelengths. The line denotes the value obtained for  $N = 30$ .

## 6.2. Control

### 6.2.1. Channel flow results

The first control results are presented in Paper 4 and considers delay of transition in the Poiseuille flow channel. In figure 6.7, the streaks generated in the channel are shown (a) with and (b) without control applied. The control, which is localized suction applied under the low velocity streaks, is seen to slightly decrease the peak-to-peak amplitude (in the spanwise direction) of the streaks. Studying the corresponding amplitudes of the secondary instability in figure 6.7(b) and (d), the control is seen to radically reduce the amplitude of the secondary instability and substantially delay the breakdown to turbulence.

In figure 6.8 the streamwise development of the amplification factor  $N$ , defined as  $\ln(u_{rms}/u_{rms,min})$  is shown both with and without control applied and the instability is seen to grow exponentially in both cases. Without control, the amplitude of the secondary instability grows as  $\exp(0.082x)$  and level out around  $x = 150$ , where a turbulent wedge starts to form. With control applied, the growth factor is reduced with a factor of three and the disturbance hence

## 6. RESULTS

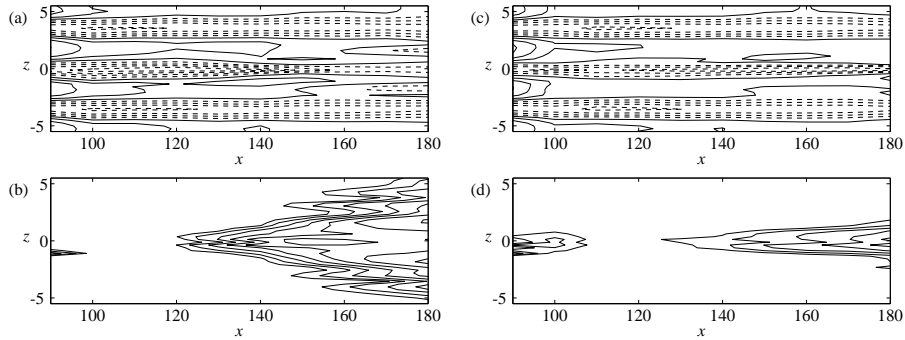


FIGURE 6.7. Mean velocity disturbance (a, c) and velocity *rms* (b, d) of the streaks in the channel without (a, b) and with (c, d) control applied. The velocity contours in (a) and (c) are  $\pm 5\%$ ,  $\pm 15\%$  of  $U_{CL}$  after subtraction of the mean velocity in the region  $90 < x < 180$ ,  $-3.6 < z < 3.6$ ; the *rms*-contours in (b) and (d) are logarithmic 1.75%, 2.5%, 3.8%... of  $U_{CL}$ . Data is taken at  $y = 0.6$ .

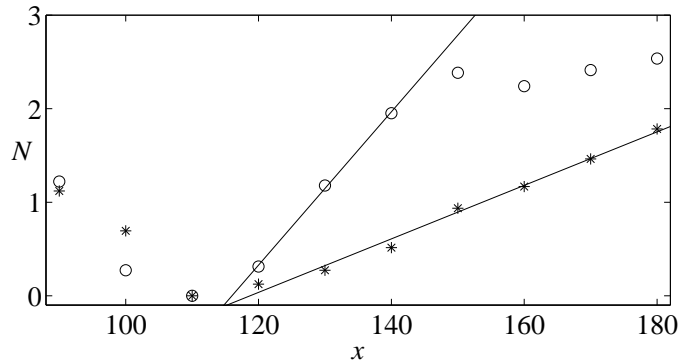


FIGURE 6.8. Growth of the secondary instability ( $\circ$ ) without and ( $*$ ) with control applied. The lines have slopes 0.082 and 0.029, respectively.  $N$  is calculated as  $\ln(u_{rms}/u_{rms,min})$ . At each spanwise position, the disturbance level is chosen as the maximum of  $u_{rms}$  in the spanwise direction at  $y = 0.6$ .

grows much slower. Consequently, breakdown is delayed to downstream of  $x = 180$ .

In order to achieve the positive control results reported in figures 6.7 and 6.8, the control suction has to be applied within a narrow region close to the

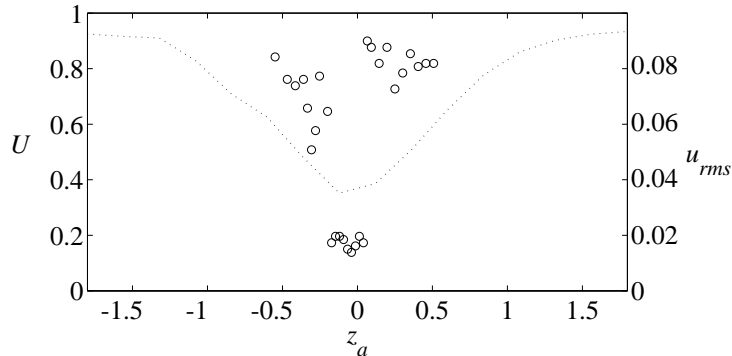


FIGURE 6.9. Velocity fluctuations as a function of actuator position  $z_a$ ,  $U(x = 145, y = 0.6, z = z_a)$  ( $\cdots$ , left scale) and  $u_{rms}(x = 145, y = 0.6, z = 0)$  for different actuation positions ( $\circ$ , right scale).

centre of the low-speed streak. This is illustrated in figure 6.8 where the fluctuation level at  $x = 145$  is shown as a function of the position at which the control suction is applied ( $z_a$ ).

### 6.2.2. Boundary layer results

The boundary layer results demonstrate the use of a reactive control system to delay FST induced transition, a flow case which may give insights towards the control of fully turbulent boundary layer flows as well. The system consists of four wall-wire sensors, four suction holes and a controller. Figure 6.10(a) shows the streamwise development of the integrated disturbance energy in the boundary layer,  $E$ , with and without control. The control is applied at  $x = 450$  mm. The control is seen to inhibit the disturbance growth for about 200 mm. After  $x = 600$  mm, the fluctuations grow towards the uncontrolled value again. In relative terms, the maximum reduction in disturbance energy is around 27%, as seen in figure 6.10(b). The length  $\Delta x$  shown in figure 6.10(c) is the distance the disturbance development is delayed by the reactive control. It is seen that the delay is approximately 200 mm for a long distance downstream of the actuator. In this work, a very simple threshold controller were used.

In the controller, three parameters was used: the threshold on streamwise shear for suction to be applied, the delay between detection and actuation and the suction velocity.

## 6. RESULTS

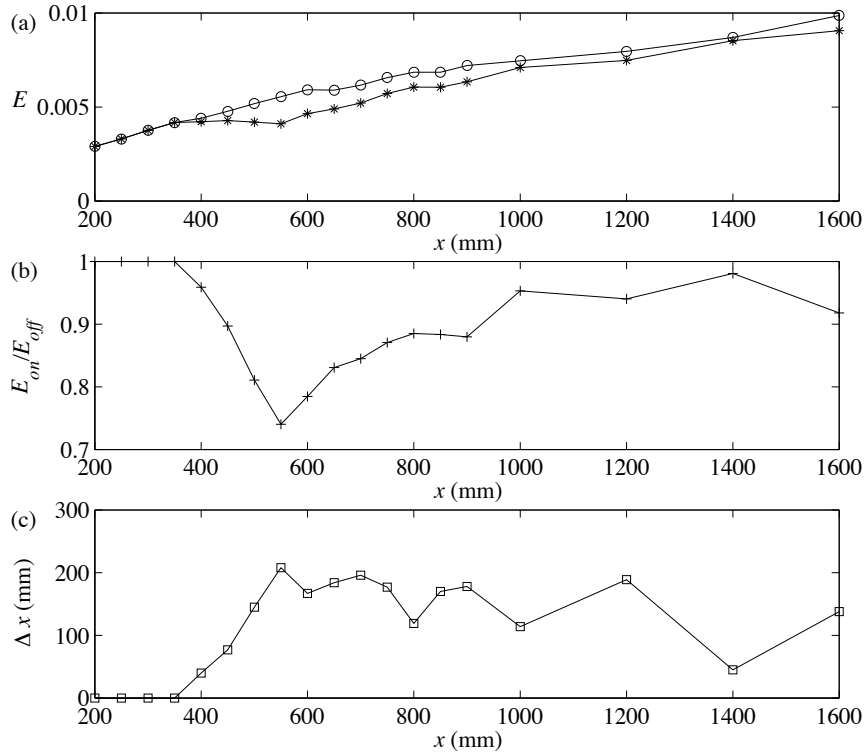


FIGURE 6.10. Streamwise development of the disturbance energy  $E = \int_0^{y=6} u_{rms}(y, z = 0)^2 dy$ ; (a) control on ( $*$ ) and off ( $\circ$ ), (b)  $E_{on}/E_{off}$  and (c)  $\Delta x$ , the distance disturbance growth is delayed by the control.

### 6.2.3. Control of a model disturbance with a flap

In addition to the suction used in the experiments above, two other actuator principles were also tried within the present work. The first was a surface-mounted piezo-ceramic flap, which was used to inhibit breakdown of streamwise elongated model disturbances in the boundary layer. Figure 6.11 shows velocity traces from different streamwise positions. In (a), the development of the model disturbance is seen. At  $x = 230$  mm, a low velocity structure is seen. Following the structure downstream, the structure appears at later and later times. At  $x = 600$  mm, some high frequency oscillations can be seen around  $t = 0.15$  s. This oscillation is amplified downstream and the structure ultimately turns into a turbulent spot, the trace of which is seen at  $x = 2000$  mm.

If, however, the flap is activated in a suitable manner, the development into a turbulent spot can be inhibited, as seen in figure 6.11(b). It is seen that the

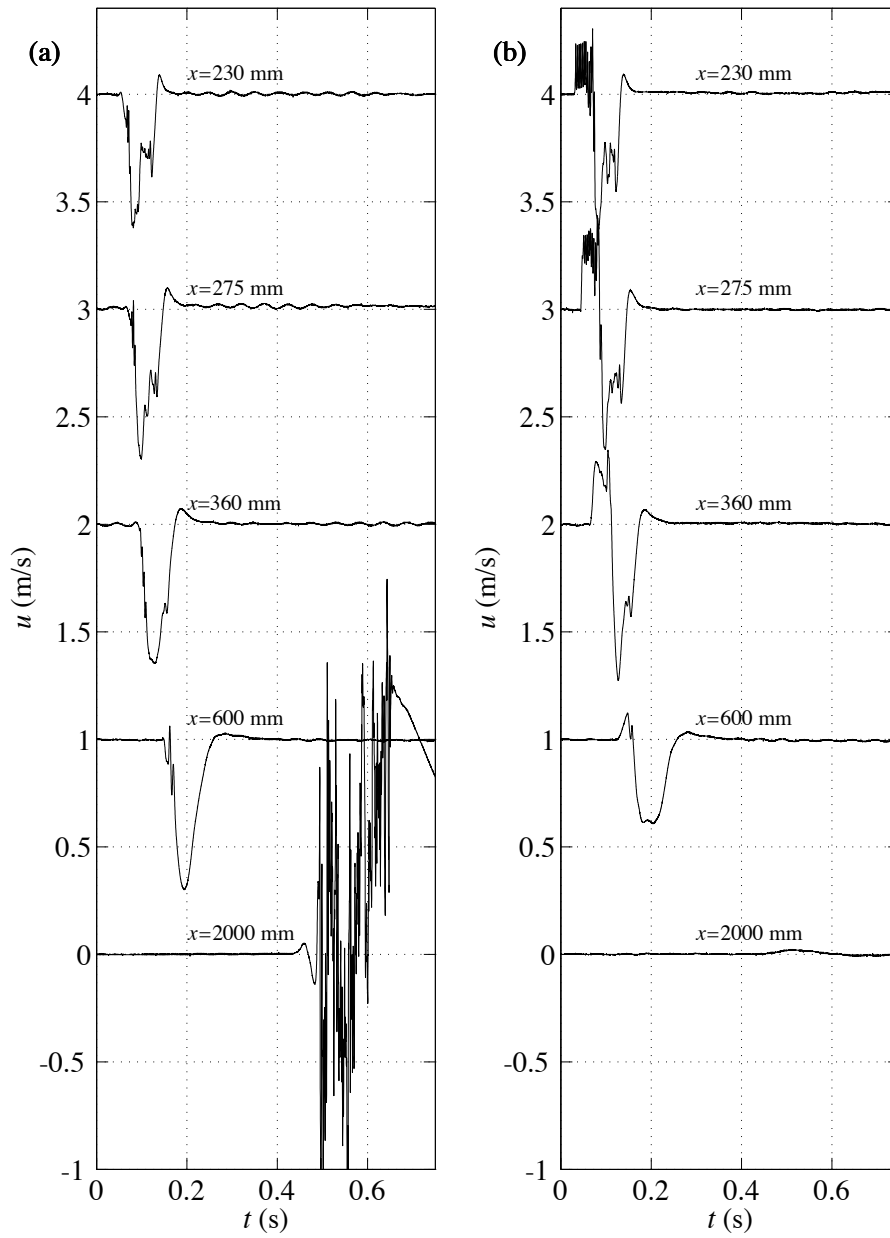


FIGURE 6.11. Velocity signal (a) without and (b) with control applied. Traces are separated 1 m/s.

## 6. RESULTS

flap generates a high velocity disturbance in front of the low velocity structure. This inhibits the appearance of high frequency oscillations at  $x = 600$  mm and at  $x = 2000$  mm, there is no trace of a turbulent spot.

### 6.2.4. *Pulse-width modulated blowing/suction*

The last actuation principle which has been studied is Pulse-Width-Modulated (PWM) blowing/suction. The reason to try it is the wish for an amplitude-modulated actuator, which is capable to produce actuation of both signs even for an on/off actuator (such as a solenoid valve). PWM blowing/suction is a candidate for such an actuator. In figure 6.12 the correlation between the generating signal and the response of the streamwise velocity is shown for various time-delays between the signals.

As seen in figure 6.12, the PWM blowing/suction creates an elongated structure in the boundary layer, which tilts down as time proceeds (a-f). Close to the hole, through which the blowing/suction is performed (positioned at  $x = 450$  mm), the correlation between the velocity variation in the boundary layer and the generating signal is up to 90%. The *rms*-amplitude of the velocity variation generated by the PWM blowing/suction is 3% of  $U_\infty$ .

## 6.2. CONTROL

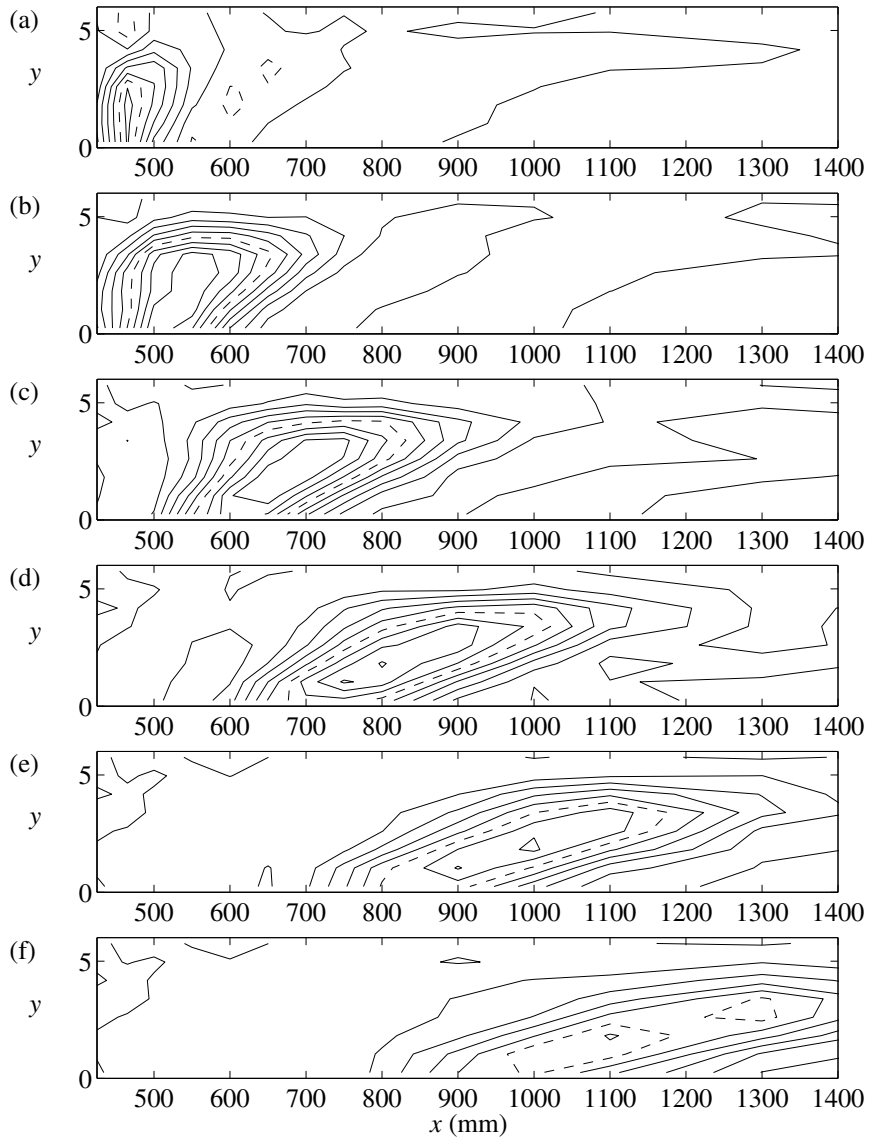


FIGURE 6.12. Spatio-temporal development of correlation between the hot-wire signal and the signal generating the PWM blowing/suction. Delay between signals are (a) 0, (b) 25 ms, ..., (f) 125 ms. Contours are 10% apart, negative contours and the 50% contour are dashed.

## CHAPTER 7

### Discussion and outlook

#### 7.1. Free-stream turbulence induced transition

The main features of FST transition are well known and were outlined in the review (chapter 3). The present thesis give some further information on the physical processes involved. The main contributions of the present work, which will be discussed in more detail below, are:

- The correlation and spatial distribution of the wall-normal and streamwise velocity in a boundary layer subjected to FST has been obtained with a newly developed experimental technique, Paper 1.
- The development of the streamwise length of FST induced structures, and the propagation speed have been determined. The observed propagation speed of the structure has been explained kinematically, Paper 2.
- It has been shown that also short, localized wave disturbances on streaks can be viewed as a secondary instability, Paper 3.

The spanwise and temporal correlations of the wall-normal and streamwise velocity shown in Paper 1, show that the wall-normal disturbance is more localized than the streaks in the streamwise velocity, generated by lift up. Furthermore, the time traces of the streamwise and wall-normal velocities show that for high-speed streaks, the wall-normal disturbance appears at the rear end of the streaks. Low-speed streaks on the other hand are trailing the wall-normal disturbance which created it. The results are probably of significance also for turbulent boundary layers, since lift up is the mechanism also behind sub-layer streaks in turbulent flow (Johansson, Alfredsson & Kim 1991). For control systems where the wall shear stress serves as input, this is also important information.

From temporal spectra, Matsubara & Alfredsson (2001) deduced that the streamwise length of the streaks in FST transition grows in linear proportion to the boundary-layer thickness. Their conclusion was based on the validity of Taylor's hypothesis which may be questionable for this type of disturbance. However, the spatial correlation measurements presented in Paper 2 confirm this finding and also shed some light on the propagation velocity of the structures, which is far from obvious due to their scaling. The disturbances in the

## 7.2. CONTROL OF TRANSITION AND TURBULENCE

boundary layer are seen to scale as the boundary-layer length scale throughout their development. This result shows that if FST induced transition is to be modeled correctly, long, but intermittent, disturbances have to be studied.

The flow visualizations of Matsubara & Alfredsson (2001) indicate that a wave-like secondary instability seems to precede breakdown of streaks in FST induced transition. The present results corroborate that such short disturbances can indeed amplify and trigger non-linearities which may lead to breakdown.

The central mechanism of transition induced by FST, *i.e.* the growth of long streamwise structures, is now well established and future studies should aim towards explaining the mechanism introducing the disturbances into the boundary layer together with more conclusive studies of the breakdown process. This includes measuring and explaining the size distribution of the streaks together with the influence of the turbulence in the free stream. In part, such studies can be made numerically, but experiments are necessary to get long time records for statistical accuracy. At a first stage, details of the breakdown can probably be accessed from existing databases, obtained by DNS and in wind-tunnel experiments.

### 7.2. Control of transition and turbulence

In this thesis, control of transitional flow structures are reported. The main results are summarized as:

- The breakdown of generated streamwise streaks in a plane Poiseuille flow can be delayed by localized suction, however, the suction is only effective within a small spanwise range below the low velocity streak, Paper 4.
- A reactive control system has been designed and used to inhibit the growth of velocity streaks in a laminar boundary-layer subjected to FST, Paper 5.
- A surface mounted piezo-ceramic flap has shown to suffice to inhibit breakdown to turbulence of streaky structures, Paper 6.
- Pulse-width modulated blowing/suction has been shown to produce amplitude modulated actuation of both signs in a laminar flow, Paper 7.

The measurements reported in Papers 4 and 5 provide more detailed measurements than previous experimental studies when it comes to the effect of the control. This has been possible to achieve thanks to well-documented disturbances, controlled experimental conditions and automated measurement procedures.

Paper 5 shows that the amplitude of randomly appearing and transiently growing streaks in FST induced transition can be decreased by reactively controlled localized suction. The results on control of FST induced transition are however not as striking as results obtained for individual model disturbances (Gad-el-Hak 1989; Bakchinov *et al.* 2000). In addition to this, the reactive

## 7. DISCUSSION AND OUTLOOK

control system which have been used decreases the disturbance amplitude far less than the optimal controller using full state information which was applied to optimal disturbances in a DNS by Högberg & Henningson (2002). Since the numerical study uses a lot more information from the flow as input to the controller and applies the actuation modulated and distributed over the wall, an experimental result at the level of the result from the numerical study cannot be expected. The discrepancy to the model-disturbance results can be explained by the continuous forcing from the free stream and from the uncontrolled areas at the sides. This is of course also an important difference compared to the DNS control of an optimal disturbance.

Since flow control is a subject inherently connected to engineering, it is impossible not to discuss the engineering possibilities appearing in the light of this thesis and other work on flow control aiming towards control of turbulence. Even though some numerical studies, either utilizing full flow information or studying low Reynolds numbers, report relaminarization of the flow (Bewley *et al.* 2001; Chang *et al.* 2002), the typical result at slightly higher Reynolds numbers and/or using simpler controllers and less information, is a drag reduction of 25% or less (Choi *et al.* 1994; Lee *et al.* 1997, 1998, 2001; Kang & Choi 2000; Endo *et al.* 2000; Chang *et al.* 2002). The 25% should be compared to the optimal riblets, found to give a drag reduction of 9% by Bechert *et al.* (1997). An important difference is of course that riblets have to be designed for a rather specific operating condition, while a reactive control system can give good results over a larger design range.

The experimental studies of Rathnasingham & Breuer (1997) and Kerho *et al.* (2000) were both made in turbulent boundary layers and both show reductions in skin friction, namely 7% and up to 25%, respectively. However skin friction is hard to measure accurately and the skin friction reductions reported need to be independently confirmed. Their results still indicate that drag reduction by reactive control is possible also in physical experiments, and that a reduction of the friction drag of the order of 20-25% may be achievable. Still this is far less than the 60-80% which can be obtained by polymer additives.

The design of a practical control system is a true challenge, which, if it is to be tackled successfully, probably involves carefully scheduled experiments together with numerical and theoretical studies. The numerical simulations done today use input data and actuator output that are not feasible for experimental implementation. On the other hand the experiments are in heavy demand for numerical support from simulations. A starting point would be to decide on a promising durable low-power actuator. The response of this actuator must then be studied experimentally, aiming to build a database of the interaction between the actuator and the flow. From such a data base, a numerical model of the actuation can be developed and used in the simulation. With the dynamics of the system thus determined, various control theories can be tried to determine a control scheme which gives a suitable result.

## 7.2. CONTROL OF TRANSITION AND TURBULENCE

The process outlined above includes several years of carefully scheduled experiments and simulations. But if an energy efficient demonstrator of reactive control is to be built, such an approach is probably necessary.

## Acknowledgments

The Swedish Research Council and KTH has provided the economical means without which this thesis would not have been written. The support is gratefully acknowledged.

I would like to thank my supervisor Henrik Alfredsson, who introduced me to the field of free-stream turbulence induced transition and initialized the project. At critical times during the experiments, evaluation or writing, Henrik has provided constructive ideas on how to move on and improve the work. He also kindly demonstrated the importance of superior technique during Halvvasan.

I would also like to thank Masaharu Matsubara, who taught me some of the experimental fluid dynamics they never mention in text books and the difference between "good enough" and "perfect". The Matsubara family has also given me quite a few hands-on experiences of Japanese life — my gratitude to you extends from the first Wollaston wire in 1997 to the "Nabe" in 2002.

It has been a pleasure to work with Ayumu Inasawa and enjoy his patience.

It was most giving to cooperate with Dr. Satoshi Kikuchi and share his experience with the piezo-ceramic flaps.

The hospitality of professor Yasuaki Kohama during my visits in Sendai has been extraordinary. I will never forget the Obon-fireworks outside Matsushima.

Marcus Gällstedt and Ulf Landén at KTH and Mr. Yamabe at IFS have provided quick and high quality work in the workshops.

The courses and environment provided and maintained by my other teachers in fluid dynamics at KTH Mechanics, Gustav Amberg, Fritz Bark, Tony Burden, Anders Dahlkild, Dan Henningson, Arne Johansson, Barbro Muhammad Klingmann, Lars Söderholm and Nils Tillmark, have been very good and instructive. Another good tutor has been Viktor Kozlov, whose enthusiastic demonstrations of control and transition has been a great source of inspiration.

To my family, friends and colleagues who has been around in the laboratories and elsewhere, Alberto, Alessandro, Alex, Alicia, Björn, Bosse, Calle, Claes, Daniel, Davide<sup>2</sup>, Kristoffer, Henrik, Gustaf, Ivano, Jens<sup>2</sup>, Johan<sup>2</sup>, Jun<sup>2</sup>, Katti, Kristian, Lovisa, Luca<sup>2</sup>, Kiura, Mehran, Mia<sup>2</sup>, Michael<sup>2</sup>, Olle, Paku, Per, Pontus, Richard, Roland, Shuya, Simagaki, Thomas, Timmy<sup>3</sup>, Vera<sup>2</sup>..., thank you all for support and distraction, laughs and sorrows, help and instructions, and proof-reading.

Tack mamma och pappa för allt stöd ni gett mig genom mitt liv och min utbildning.

Tack Michaela för stöd och kärlek under de avslutande åren av min utbildning och i alla andra aspekter av tillvaron.

---

<sup>2</sup>Your uniqueness is not in your name.

<sup>3</sup>There is only one Timmy, and he read and commented the whole thesis on an early stage.

## References

- ALFREDSSON, P. H., JOHANSSON, A. V., HARITONIDIS, J. H. & ECKELMANN, H. 1988 The fluctuating wall-shear stress and the velocity field in the viscous sub-layer. *Phys. Fluids* **31**, 1026–1033.
- ALFREDSSON, P. H. & MATSUBARA, M. 2000 Free-stream turbulence, streaky structures and transition in boundary layer flows. *AIAA-paper 2000-2534*.
- AMONLIRDVIMAN, K. & BREUER, K. S. 2000 Linear predictive filtering in a numerically simulated turbulent flow. *Phys. Fluids* **12**, 3221–3228.
- ANDERSSON, P., BERGGREN, M. & HENNINGSON, D. S. 1999 Optimal disturbances and bypass transition in boundary layers. *Phys. Fluids* **11**, 134–150.
- ANDERSSON, P., BRANDT, L. & HENNINGSON, D. S. 2001 On the breakdown of boundary layer streaks. *J. Fluid Mech.* **428**, 29–60.
- ASAI, M., MINAGAWA, M. & NISHIOKA, M. 2002 The instability and breakdown of a near-wall low-speed streak. *J. Fluid Mech.* **455**, 289–314.
- BAKCHINOV, A. A., GREK, G. R., KLINGMANN, B. G. B. & KOZLOV, V. V. 1995 Transition experiments in a boundary layer with embedded streamwise vortices. *Phys. Fluids* **7**, 820–832.
- BAKCHINOV, A. A., KATASONOV, M. M., ALFREDSSON, P. H. & KOZLOV, V. V. 1999 Control of boundary layer transition at high FST by localized suction. In *IUTAM Symposium on Mechanics of Passive and Active Flow Control* (ed. G. E. A. Meier & P. R. Viswanath), pp. 159–164. Dordrecht: Kluwer Academic Publishers.
- BAKCHINOV, A. A., KATASONOV, M. M., ALFREDSSON, P. H. & KOZLOV, V. V. 2000 Control of streaky structures by localized blowing and suction. In *IUTAM Symposium on Laminar-turbulent transition* (ed. H. F. Fasel & W. S. Saric), pp. 159–164. Heidelberg: Springer Verlag.
- BAKCHINOV, A. A., WESTIN, K. J. A., KOZLOV, V. V. & ALFREDSSON, P. H. 1998 Experiments on localized disturbances in a flat plate boundary-layer. Part 2. Interaction between localized disturbances and TS-waves. *Eur. J. Mech. B/Fluids* **17**, 847–873.
- BALAKUMAR, P. & HALL, P. 1999 Optimum suction distribution for transition control. *Theor. Comp. Fluid Dyn.* **13**, 1–19.
- BECHERT, D. W., BRUSE, M., HAGE, W., VAN DER HOEVEN, J. G. T. & HOPPE,

## REFERENCES

- G. 1997 Experiments on drag-reducing surfaces and their optimization with an adjustable geometry. *J. Fluid Mech.* **338**, 59–87.
- BERLIN, S., WIEGEL, M. & HENNINGSON, D. S. 1999 Numerical and experimental investigation of oblique boundary layer transition. *J. Fluid Mech.* **393**, 23–57.
- BEWLEY, T. R. 1999 Linear control and estimation of nonlinear chaotic convection: Harnessing the butterfly effect. *Phys. Fluids* **11**, 1169–1185.
- BEWLEY, T. R. & LIU, S. 1998 Optimal and robust control of linear paths to transition. *J. Fluid Mech.* **365**, 305–349.
- BEWLEY, T. R., MOIN, P. & TEMAM, R. 2001 DNS-based predictive control of turbulence: an optimal benchmark for feedback algorithms. *J. Fluid Mech.* **447**, 179–225.
- BEWLEY, T. R. & PROTAS, B. 2002 Skin friction and pressure: the "footprints" of turbulence. In *Proceedings of the 3rd Symposium on Smart Control of Turbulence. Tokyo*. Accessible from <http://turbulence.ucsd.edu/references.html>.
- BOIKO, A. V., WESTIN, K. J. A., KLINGMANN, B. G. B., KOZLOV, V. V. & ALFREDSSON, P. H. 1994 Experiments in a boundary layer subjected to free stream turbulence. Part 1. The role of T-S waves in the transition process. *J. Fluid Mech.* **281**, 219–245.
- BOTTARO, A. & KLINGMANN, B. G. B. 1996 On the linear breakdown of Görtler vortices. *Eur. J. Mech. B/Fluids* **15**, 301–330.
- BRANDT, L. & HENNINGSON, D. S. 2002 Transition of streamwise streaks in zero-pressure gradient boundary layers. *J. Fluid Mech.* **472**, 229–262.
- BRANDT, L., HENNINGSON, D. S. & PONZIANI, D. 2002 Weakly nonlinear analysis of boundary layer receptivity of free-stream disturbances. *Phys. Fluids* **14**, 1426–1441.
- BREUER, K. S. & HARITONIDIS, J. H. 1990 The evolution of a localized disturbance in a laminar boundary layer, Part I: Weak disturbances. *J. Fluid Mech.* **220**, 569–594.
- BREUER, K. S., HARITONIDIS, J. H. & LANDAHL, M. T. 1989 The control of transient disturbances in a flat plate boundary layer through active wall motion. *Phys. Fluids A* **1**, 574–582.
- BUSHNELL, D. M. & MCGINLEY, C. B. 1989 Turbulence control in wall flows. *Annu. Rev. Fluid Mech.* **21**, 1–20.
- BUTLER, K. M. & FARRELL, D. F. 1992 Three dimensional optimal perturbations in viscous shear flow. *Phys. Fluids A* **4**, 1637–1650.
- CATHALIFAUD, P. & LUCHINI, P. 2000 Algebraic growth in boundary layers: optimal control by blowing and suction. *Eur. J. Mech. B/Fluids* **19**, 469–490.
- CHANDRASEKHAR, S. 1961 *Hydrodynamic and hydromagnetic stability*. Oxford University Press.
- CHANG, Y., COLLIS, S. S. & RAMAKRISHNAN, S. 2002 Viscous effect in control of near-wall turbulence. *Phys. Fluids* **14**, 4069–4080.
- CHOI, H., MOIN, P. & KIM, J. 1994 Active turbulence control for drag reduction in wall-bounded flows. *J. Fluid Mech.* **262**, 75–110.
- CHOI, K.-S. 1989 Turbulent flow over riblets. *J. Fluid Mech.* **208**, 417–458.

## REFERENCES

- CHOI, K.-S. & CLAYTON, B. R. 2001 The mechanism of turbulent drag reduction with wall oscillation. *Int. J. Heat Fluid Flow* **22**, 1–9.
- CHOI, K.-S., DEBISSCHOP, J.-R. & CLAYTON, B. R. 1998 Turbulent boundary-layer control by means of spanwise-wall oscillation. *AIAA J.* **36**, 1157–1163.
- CHOI, K.-S., YANG, X., CLAYTON, B. R., GLOVER, E. J., ATLAR, M., SEMENOV, B. N. & KULIK, V. M. 1997 Turbulent drag reduction using compliant surfaces. *Proc. R. Soc. Lond. A* **453**, 2229–2240.
- COSSU, C. & BRANDT, L. 2002 Stabilization of Tollmien-Schlichting waves by finite amplitude optimal streaks in the Blasius boundary layer. *Phys. Fluids* **14**, L57–L60.
- DEN TOONDER, J. M. J., HULSEN, M. A., KUIKEN, G. D. C. & NIEUWSTADT, F. T. M. 1997 Drag reduction by polymer additives in a turbulent pipe flow: numerical and laboratory experiments. *J. Fluid Mech.* **337**, 193–231.
- DOYLE, J. C., GLOVER, K., KHARGONEKAR, P. P. & FRANCIS, B. A. 1989 State-space solutions to standard  $H_2$  and  $H_\infty$  control problems. *IEEE Trans. Aut. Control* **34**, 831–847.
- DRAZIN, P. G. & REID, W. H. 1981 *Hydrodynamic stability*. Cambridge University Press.
- DU, Y., SYMENOIDIS, V. & KARNIADAKIS, G. E. 2002 Drag reduction in wall-bounded turbulence via a transverse travelling wave. *J. Fluid Mech.* **457**, 1–34.
- EGAMI, E. & KOHAMA, Y. 1999 Control of crossflow instability field by selective suction system. In *IUTAM Symposium on Mechanics of Passive and Active Flow Control* (ed. G. E. A. Meier & P. R. Viswanath), pp. 171–176. Dordrecht: Kluwer Academic Publishers.
- ELLINGSEN, T. & PALM, E. 1975 Stability of linear flow. *Phys. Fluids* **18**, 487–488.
- ELOFSSON, P. A. & ALFREDSSON, P. H. 1998 An experimental study of oblique transition in plane Poiseuille flow. *J. Fluid Mech.* **358**, 177–202.
- ELOFSSON, P. A. & ALFREDSSON, P. H. 2000 An experimental study of oblique transition in a Blasius boundary layer flow. *Eur. J. Mech. B/Fluids* **19**, 615–636.
- ELOFSSON, P. A., KAWAKAMI, M. & ALFREDSSON, P. H. 1999 Experiments on the stability of streamwise streaks in plane Poiseuille flow. *Phys. Fluids* **11**, 915–930.
- ENDO, T. & HIMENO, R. 2002 Direct numerical simulation of turbulent flow over a compliant surface. *J. Turbulence* **3** (007).
- ENDO, T., KASAGI, N. & SUZUKI, Y. 2000 Feedback control of wall turbulence with wall deformation. *Int. J. Heat Fluid Flow* **21**, 568–575.
- FALCOMER, L. & ARMENIO, V. 2002 Large-eddy simulation of secondary flow over longitudinally ridged walls. *J. Turbulence* **3** (008).
- FASEL, H. & KONZELMANN, U. 1990 Non-parallel stability of a flat-plate boundary layer using the complete Navier-Stokes equation. *J. Fluid Mech.* **221**, 311–347.
- FASEL, H. F. 2002 Numerical investigation of the interaction of the Klebanoff-mode with a Tollmien-Schlichting wave. *J. Fluid Mech.* **450**, 1–33.
- FRANSSON, J. H. M. 2001 Investigation of the asymptotic suction boundary layer. TRITA-MEK 2001:11. Department of Mechanics, Royal Institute of Technology.
- GAD-EL-HAK, M. 1989 Flow control. *Appl. Mech. Rev.* **42**, 261–292.

## REFERENCES

- GAD-EL-HAK, M. 1996 Modern developments in flow control. *Appl. Mech. Rev.* **49**, 365–379.
- GAD-EL-HAK, M. 2000 *Flow control*. Cambridge University Press.
- GAD-EL-HAK, M. & BLACKWELDER, R. F. 1989 Selective suction for controlling bursting events in a boundary layer. *AIAA J.* **27**, 308–314.
- GAD-EL-HAK, M. & HUSSAIN, A. K. M. F. 1986 Coherent structures in a turbulent boundary layer. part 1: Generation of "artificial" bursts. *Phys. Fluids* **29**, 2124–2139.
- GLEZER, A. & AMITAY, M. 2002 Synthetic jets. *Annu. Rev. Fluid Mech.* **34**, 503–529.
- GMELIN, C. & RIST, U. 2001 Active control of laminar turbulent transition using instantaneous vorticity signals at the wall. *Phys. Fluids* **13**, 513–519.
- GREK, G. R., KOZLOV, V. V. & TITARENKO, S. V. 1996 An experimental study of the influence of riblets on transition. *J. Fluid Mech.* **315**, 31–49.
- GREK, G. R., KOZLOV, V. V., TITARENKO, S. V. & KLINGMANN, B. G. B. 1995 The influence of riblets on a boundary layer with embedded streamwise vortices. *Phys. Fluids* **7**, 2504–2506.
- GREK, H. R., KOZLOV, V. V. & RAMAZANOV, M. P. 1985 Three types of disturbances from the point source in the boundary layer. In *Laminar turbulent transition* (ed. V. V. Kozlov), pp. 262–272. Springer-verlag.
- GUSTAVSSON, L. H. 1991 Energy growth of three-dimensional disturbances in plane Poiseuille flow. *J. Fluid Mech.* **224**, 241–260.
- HAMILTON, J. M., KIM, J. & WALEFFE, F. 1995 Regeneration mechanisms of near-wall turbulence structures. *J. Fluid Mech.* **287**, 317–348.
- HO, C.-M. & TAI, Y.-C. 1996 Review: MEMS and its applications for flow control. *J. Fluids Eng.* **118**, 437–447.
- HO, C.-M. & TAI, Y.-C. 1998 Micro-electro-mechanical systems (MEMS) and fluid flows. *Annu. Rev. Fluid Mech.* **30**, 579–612.
- HOFMANN, L. M. & HERBERT, T. 1997 Disturbances produced by motion of an actuator. *Phys. Fluids* **9**, 3727–3732.
- HÖGBERG, M. & HENNINGSON, D. S. 2002 Linear optimal control applied to instabilities in spatially developing boundary layers. *J. Fluid Mech.* **470**, 151–179.
- HÖGBERG, M., HENNINGSON, D. S. & BEWLEY, T. R. 2002 Localized feedback control and estimation of transition in plane channel flow. *J. Fluid Mech.* **470**, 151–179.
- HULTGREN, L. S. & GUSTAVSSON, L. H. 1981 Algebraic growth of disturbances in a laminar boundary layer. *Phys. Fluids* **24**, 1000–1004.
- JACOBS, R. G. & DURBIN, P. A. 2001 Simulations of bypass transition. *J. Fluid Mech.* **428**, 185–212.
- JACOBSON, S. A. & REYNOLDS, W. C. 1998 Active control of streamwise vortices and streaks in boundary layers. *J. Fluid Mech.* **360**, 179–211.
- JIMÉNEZ, J. 1994 On the structure and control of near wall turbulence. *Phys. Fluids* **6**, 944–953.
- JOHANSSON, A. V., ALFREDSSON, P. H. & KIM, J. 1991 Evolution and dynamics of shear-layer structures in near-wall turbulence. *J. Fluid Mech.* **224**, 579–599.

## REFERENCES

- JOSHI, S. S., SPEYER, J. L. & KIM, J. 1997 A systems theory approach to the feedback stabilization of infinitesimal and finite-amplitude disturbances in plane Poiseuille flow. *J. Fluid Mech.* **332**, 157–184.
- JOSLIN, R. D. 1998 Aircraft laminar flow control. *Annu. Rev. Fluid Mech.* **30**, 1–29.
- JUNG, W. J., MANGIAVACCHI, N. & AKHAVAN, R. 1992 Suppression of turbulence in wall-bounded flows by high-frequency spanwise oscillations. *Phys. Fluids A* **4**, 1605–1607.
- KANG, S. & CHOI, H. 2000 Active wall motions for skin-friction reduction. *Phys. Fluids* **12**, 3301–3304.
- KENDALL, J. M. 1990 Boundary layer receptivity to free-stream turbulence. *AIAA paper 90-1504*.
- KENDALL, J. M. 1998 Experiments on boundary-layer receptivity to freestream turbulence. *AIAA-paper 98-0530*.
- KERHO, M. 2002 Active reduction of skin friction drag using low-speed streak control. *AIAA paper 2002-0271*.
- KERHO, M., HEID, J., KRAMER, B. & NG, T. 2000 Active drag reduction using selective low rate suction. *AIAA-paper 2000-4018*.
- KIM, J. & LIM, J. 2000 A linear process in wall-bounded turbulent shear flows. *Phys. Fluids* **12**, 1885–1888.
- KLINE, S. J., REYNOLDS, W. C., SCHRAUB, F. A. & RUNSTADLER, P. W. 1967 The structure of turbulent boundary layers. *J. Fluid Mech.* **20**, 741–773.
- KLINGMANN, B. G. B., BOIKO, A., WESTIN, K. J. A., KOZLOV, V. V. & ALFREDSSON, P. H. 1993 Experiments on the stability of Tollmien-Schlichting waves. *Eur. J. Mech., B/Fluids* **12**, 493–514.
- KOUMOUTSAKOS, P. 1997 Active control of vortex-wall interactions. *Phys. Fluids* **9**, 3808–3816.
- LAADHARI, F., SKANDAJI, L. & MOREL, R. 1994 Turbulence reduction in a boundary layer by a local spanwise oscillating surface. *Phys. Fluids* **6**, 3218–3220.
- LANDAHL, M. T. 1980 A note on an algebraic instability of inviscid shear flows. *J. Fluid Mech.* **98**, 243–251.
- LANDAHL, M. T. 1990 On sublayer streaks. *J. Fluid Mech.* **212**, 593–614.
- LEE, C. & KIM, J. 2002 Control of the viscous sublayer for drag reduction. *Phys. Fluids* **14**, 2523–2529.
- LEE, C., KIM, J., BABCOCK, D. & GOODMAN, R. 1997 Application of neural networks to turbulence control for drag reduction. *Phys. Fluids* **9**, 1740–1747.
- LEE, C., KIM, J. & CHOI, H. 1998 Suboptimal control of turbulent channel flow for drag reduction. *J. Fluid Mech.* **358**, 245–258.
- LEE, K. H., CORTELEZZI, L., KIM, J. & SPEYER, J. 2001 Application of reduced-order controller to turbulent flows for drag reduction. *Phys. Fluids* **13**, 1321–1330.
- LIEPMANN, H. W., BROWN, G. L. & NOSENCHUCK, D. M. 1982 Control of laminar instability waves using a new technique. *J. Fluid Mech.* **118**, 187–200.
- LIEPMANN, H. W. & NOSENCHUCK, D. M. 1982 Active control of laminar-turbulent transition. *J. Fluid Mech.* **118**, 201–204.
- LIN, C. C. 1955 *The theory of hydrodynamic stability*. Cambridge University Press.

## REFERENCES

- LÖFDAHL, L. & GAD-EL-HAK, M. 1999 MEMS applications in turbulence and flow control. *Prog. Aerospace Sci.* **35**, 101–203.
- LUCHINI, P. 2000 Reynolds number independent instability of the boundary layer over a flat surface: optimal perturbations. *J. Fluid Mech.* **404**, 289–309.
- MACMANUS, D. G. & EATON, J. A. 2000 Flow physics of discrete boundary layer suction-measurments and predictions. *J. Fluid Mech.* **417**, 47–75.
- MATSUBARA, M. & ALFREDSSON, P. H. 2001 Disturbance growth in boundary layers subjected to free stream turbulence. *J. Fluid Mech.* **430**, 149–168.
- MILLING, R. W. 1981 Tollmien-Schlichting wave cancellation. *Phys. Fluids* **24**, 979–981.
- MYOSE, R. Y. & BLACKWELDER, R. F. 1995 Control of streamwise vortices using selective suction. *AIAA J.* **33**, 1076–1080.
- NELSON, P. A., WRIGHT, M. C. M. & J.-L.RIOUAL 1997 Automatic control of laminar boundary-layer transition. *AIAA J.* **35**, 85–90.
- PANTON, R. L. 2001 Overview of the self-sustaining mechanisms of wall-turbulence. *Prog. Aerospace Sciences* **37**, 341–383.
- PATERSON, R. W. & ABERNATHY, F. H. 1970 Turbulent drag reduction and degradation with dilute polymer solutions. *J. Fluid Mech.* **43**, 689–710.
- PODVIN, B. & LUMLEY, J. 1998 Reconstructing the flow in the wall region from wall sensors. *Phys. Fluids* **10**, 1182–1190.
- PRABHU, R. D., COLLIS, S. S. & CHANG, Y. 2001 The influence of control on proper orthogonal decomposition of wall-bounded turbulent flows. *Phys. Fluids* **13**, 520–537.
- PRALITS, J. O., HANIFI, A. & HENNINGSON, D. S. 2002 Adjoint-based optimization of steady suction for disturbance control in incompressible flows. *J. Fluid Mech.* **467**, 129–161.
- RATHNASINGHAM, R. 1997 System identification and active control of a turbulent boundary layer. PhD thesis, Dep. of Aeronautics and Astronautics, Massachusetts Institute of Technology.
- RATHNASINGHAM, R. & BREUER, K. S. 1997 System identification and control of a turbulent boundary layer. *Phys. Fluids* **9**, 1867–1869.
- REBBECK, H. & CHOI, K.-S. 2001 Opposition control of near wall turbulence with a piston-type actuator. *Phys. Fluids* **13**, 2142–2145.
- REYNOLDS, O. 1883 On the experimental investigation of the circumstances which determine whether the motion of water shall be direct or sinuous, and the law of resistance in parallel channels. *Phil. Trans. Roy. Soc. Lond.* **174**, 935–982.
- ROACH, P. E. & BRIERLY, D. H. 1990 The influence of a turbulent freestream on zero pressure gradient transitional boundary layer development. Part I: Test cases T3A and T3B. Cambridge University Press, *ERCOTAC Workshop, Numerical Simulation of Unsteady Flows and Transition to Turbulence*, Lausanne, pp 319–347.
- ROSSI, L. & THIBAUT, J.-P. 2002 Investigation of wall normal electromagnetic actuator for seawater flow control. *J. Turbulence* **3** (005).

## REFERENCES

- SAHLIN, A., ALFREDSSON, P. H. & JOHANSSON, A. V. 1986 Direct drag measurements for a flat plate with passive boundary layer manipulators. *Phys. Fluids* **29**, 696–700.
- SAHLIN, A., JOHANSSON, A. V. & ALFREDSSON, P. H. 1988 The possibility of drag reduction by outer layer manipulators in turbulent boundary layers. *Phys. Fluids* **31**, 2814–2820.
- SCHLICHTING, H. 1935 Amplitudenverteilung und Energiebalanz der kleinen Störungen bei der Plattenströmung. *Nachr. Ges. Wiss. Göttingen. Math. Phys. Klasse, Fachgruppe I* **1**, 47–78.
- SCHLICHTING, H. & GERSTEN, K. 2000 *Boundary layer theory*. McGraw-Hill.
- SCHMID, P. J. & HENNINGSON, D. S. 1992 Channel flow transition induced by a pair of oblique waves. In *Instability, transition and turbulence* (ed. M. Y. Hussain, A. Kumar & C. L. Street), pp. 356–366. Springer-Verlag.
- SCHMID, P. J. & HENNINGSON, D. S. 2001 *Stability and transition in shear flows*. Springer-Verlag.
- SCHOPPA, W. & HUSSAIN, F. 1998 A large-scale control strategy for drag reduction in turbulent boundary layers. *Phys. Fluids* **10**, 1049–1051.
- SCHOPPA, W. & HUSSAIN, F. 2002 Coherent structure generation in near-wall turbulence. *J. Fluid Mech.* **453**, 57–108.
- SCHUBAUER, G. B. & SKRAMSTAD, H. K. 1948 Laminar boundary layer oscillations and transition on a flat plate. *Tech. Rep.* 909. NACA.
- SKOTE, M., HARITONIDIS, J. H. & HENNINGSON, D. S. 2002 Varicose instabilities in turbulent boundary layers. *Phys. Fluids* **14**, 2309–2323.
- SREENIVASAN, K. R. & WHITE, C. M. 2000 The onset of drag reduction by dilute polymer additives, and the maximum drag reduction asymptote. *J. Fluid Mech.* **409**, 149–164.
- TALAMELLI, A., WESTIN, K. J. A. & ALFREDSSON, P. H. 2000 An experimental investigation of the response of hot-wire X-probes in shear flows. *Exp. Fluids* **28**, 425–435.
- TARDU, S. F. 2001 Active control of near-wall turbulence by local oscillating blowing. *J. Fluid Mech.* **439**, 217–253.
- TOLLMIE, W. 1935 Ein allgemeines Kriterium der Instabilität laminarer Geschwindigkeitsverteilungen. *Nachr. Ges. Wiss. Göttingen. Math. Phys. Klasse, Fachgruppe I* **1**, 79–114.
- WALEFFE, F. 1995 Hydrodynamic stability and turbulence: beyond transients to a self-sustained process. *Stud. Appl. Math.* **95**, 319–343.
- WALEFFE, F. 1997 On a self-sustaining process in shear flows. *Phys. Fluids* **9**, 883–900.
- WESTIN, K. J. A., BAKCHINOV, A. A., KOZLOV, V. V. & ALFREDSSON, P. H. 1998 Experiments on localized disturbances in a flat boundary layer. Part 1. The receptivity and evolution of a localized free stream disturbance. *Eur. J. Mech. B/Fluids* **17**, 823–846.
- WESTIN, K. J. A., BOIKO, A. V., KLINGMANN, B. G. B., KOZLOV, V. V. & ALFREDSSON, P. H. 1994 Experiments in a boundary layer subjected to free

## REFERENCES

- stream turbulence. Part 1. Boundary layer structure and receptivity. *J. Fluid Mech.* **281**, 193–218.
- YOSHIOKA, S., FRANSSON, J. H. M. & ALFREDSSON, P. H. 2003 Evolution of disturbances in a boundary layer with wall suction. In *Turbulence Shear Flow Phenomena 3*. To appear.

P1

Paper 1



# Velocity statistics and flow structures observed in bypass transition using stereo PTV

By **A. Inasawa**<sup>1</sup>, **F. Lundell**<sup>2</sup>, **M. Matsubara**<sup>3</sup>, **Y. Kohama**<sup>4</sup> &  
**P. H. Alfredsson**<sup>2</sup>

<sup>1</sup>Aeronautics and Space Engineering, Tohoku University, 980-8579 Sendai, Japan

<sup>2</sup>KTH Mechanics, S-100 44 Stockholm, Sweden

<sup>3</sup>Department of Mechanical Systems Engineering, Shinshu University, 380-8553  
Nagano, Japan

<sup>4</sup>Institute of Fluid Science, Tohoku University, 980-8577 Sendai, Japan

It is known from smoke visualizations that in a transitional boundary layer subjected to free-stream turbulence, streaks appear and eventually break down to turbulence after wavy motions. In order to observe the streaky structures directly, a stereo particle-tracking velocimetry system using hydrogen bubbles in a water channel has been developed and validated against laser Doppler velocimetry. Mean flow statistics show good agreement with previous results. With the developed measurement system, the instantaneous spanwise distribution of the streamwise and wall-normal velocities can be measured fast enough to resolve the time development of the streaky structures. Measurements of instantaneous spanwise distributions of the streamwise and wall-normal velocity disturbances show strong negative correlation between the wall-normal and streamwise velocities in the streaks.

---

## 1. Introduction

Recently, the process of transition to turbulence in a boundary layer subjected to high levels of free-stream turbulence has been studied both in experiments and numerical simulations. Experimental results (Alfredsson & Matsubara 2000; Matsubara & Alfredsson 2001) which were obtained by flow visualizations, hot-wire measurements and particle image velocimetry, illustrate the scenario of free-stream turbulence induced transition. The scenario starts with the appearance of streamwise elongated streaky structures of high and low velocity inside the boundary layer. The amplitude of the velocity variation of the streaks grows with downstream distance. Further downstream, wavy motions

*A. Inasawa, F. Lundell, M. Matsubara, Y. Kohama & P. H. Alfredsson*

of the streaks are seen, whereupon breakdown to turbulence occurs. This local region of turbulence propagates downstream and grows in both the streamwise and spanwise directions, forming an arrowhead-shaped turbulent spot. The fully developed turbulent boundary layer is obtained when the spots have merged and filled the boundary layer. This process is different from that of modal growth of Tollmien-Schlichting (T-S) waves, and is therefore sometimes referred to as bypass transition.

Direct numerical simulations (Jacobs & Durbin 2001) mostly confirm this scenario, though the wavy motion of the streaky structure was not observed. The breakdown of the streaks seems to be directly triggered by the small scale of the free stream interacting with low-speed structures ("backward jets") in the top of the boundary layer. Also in the numerical calculation, the streaky structures are the dominant disturbances upstream of the turbulent spot generation.

Another recent direct numerical simulation is reported by Fasel (2002). He studies the growth and development of T-S waves in a boundary layer in which streaks are present. From the simulations it was concluded that the breakdown scenario was fairly unchanged compared to the case with no streaks present. Independent of the later stages of transition (secondary instabilities, backward jets or 2D T-S waves amplified in the low-velocity streak) the growth of the streaks is an important feature if transition is to be understood, predicted, or controlled. The experiments (Alfredsson & Matsubara 2000, Matsubara & Alfredsson 2001) report specific properties of the growth rate and spatial scales of the streaky structures. The energy of the streamwise velocity fluctuation ( $\sim u_{rms}^2$ ), in which low-frequency components were dominant, increased in proportion to the streamwise distance from the leading edge. The spanwise width of the streaks, if scaled by the local boundary layer thickness, was decreasing downstream (the numerical value is more or less constant) and seemed to asymptotically approach twice the boundary layer thickness. The streamwise scale of the streaks was proportional to the boundary layer thickness, *i.e.* the square root of the distance from the leading edge. Theoretically, this type of disturbance was first suggested by Landahl (1977, 1980). He extended the idea of the non-modal growth in a shear flow, proposed by Ellingsen & Palm (1975) for streamwise independent disturbances, to local disturbances and offered a physical explanation which he named 'lift-up'. Lift-up is the production of regions of low streamwise velocity by wall-normal velocity disturbances; a positive wall-normal velocity disturbance lifts fluid with low momentum to higher regions of the boundary layer.

The non-modal theory was further developed by Luchini (2000) and Andersson *et al.* (1999) to the viscous case with a Blasius basic flow. They showed that the maximum attainable fluctuation energy with a given energy input is proportional to  $x$  and that the wall-normal position of the maximum fluctuation level is at the middle of the boundary layer ( $y/\delta^*=1.3$ ) where  $\delta^*$  is

*Velocity statistics and flow structures in bypass transition*

the displacement thickness of a Blasius boundary layer. In their analysis, they calculated the optimal disturbance and its downstream development, *i.e.* the disturbance maximizing the energy growth for various spanwise wavenumbers.

In their analysis, the spanwise wavelength of the optimal disturbance is found to be approximately 2.8 times larger than the final boundary layer thickness. This optimal disturbance had the same properties as observed in the experiment in terms of both streamwise proportional energy growth and the profile of the streamwise velocity fluctuation, whereas in the experiments of Matsubara & Alfredsson (2001), the spanwise wavelength divided by the boundary layer thickness decreases downstream and approaches a value of approximately 2.

According to the lift-up mechanism, the spanwise non-uniformity of the wall-normal velocity component in the boundary layer is the source of the energy growth of the streamwise velocity fluctuations. Measurements of the wall-normal velocity fluctuations have been conducted by Roach & Brierly (1990) and Westin (1997) using hot-wire X-probes. In both measurements, the profiles had a local maximum inside the boundary layer. These results do not agree with the direct numerical simulation by Jacobs & Durbin (2001) which shows a monotonic decrease of the fluctuation towards the wall at the most upstream positions. A laser Doppler velocimetry (LDV) measurement performed by Fransson & Westin (2002) also showed a monotonic decrease of the wall-normal fluctuation toward the wall, confirming the results of Jacobs & Durbin (2000). Observe that we, as well as previous studies, present and discuss the fluctuation of the wall-normal velocity only. The mean, appearing due to the growth of the boundary layer, decays as the square root of the distance from the leading edge and is less than one percent of the free-stream velocity at all measurement stations of the present study.

The correlation between the streamwise and wall-normal fluctuations obtained by Westin (1997) using X-wires had strong positive values near the wall, a result obviously contradicting the lift-up effect, according to which a negative streamwise disturbance is created by a positive deviation from the mean of the wall-normal velocity, thus giving a negative correlation. Talamelli *et al.* (2000), developed a method to compensate the X-wire data for the wall-normal shear and the influence of the probe near the wall. They applied the compensation to the data of Westin (1997) and obtained more realistic profiles.

The first purpose of the present study is to demonstrate how a stereo PTV technique can be used for time-resolved measurements of  $u$  and  $v$  in a transitional boundary layer over a flat plate under a turbulent free stream. Once the accuracy of the measurement technique is established, the main purposes are (i) to verify the profile of wall normal velocity fluctuation and the profiles of  $\overline{uv}$  and (ii) to observe the lift-up mechanism, *i.e.* the creation of low velocity streaks

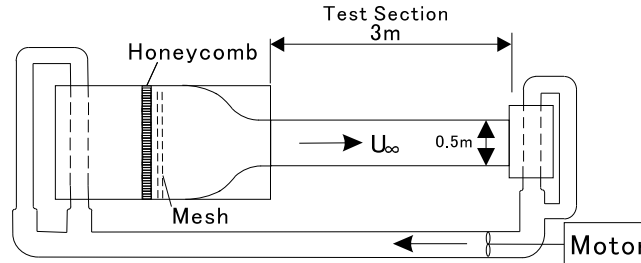


FIGURE 1. Top view of water channel.

by the transport of slow fluid from close to the wall to higher regions in the boundary layer by wall-normal velocity disturbances.

In section 2, the setup is described and in section 3, the PTV-system is explained and validated against an LDV system. Measurements in a boundary layer are presented and discussed in section 4 and finally the conclusions are given in section 5.

## 2. Experimental setup

The experiments were carried out in a water channel (figure 1). An axial pump powered by a 0.75 kW AC motor drove water in the closed system. The rotational speed of the pump was frequency controlled. The water flowed into the settling chamber through the return pipes and entered the settling chamber from a perforated pipe with 10 mm diameter holes. The side shape of the chamber was formed as a Rankine half body and its opening connected to a honeycomb made of 4 mm diameter drinking straws. Three screens with 40 meshes per inch were mounted upstream of the 4:1 contraction. The test section was 500 mm wide, 500 mm high and 3000 mm long. The side and bottom walls of the test section were made of glass for optical access. The test section was built without a lid in order to make it easy to work with the setup in the test section. At the downstream end of the test section a screen and a honeycomb were placed in order to avoid that the surface wave was reflected from the downstream basin to the test section. The water in the downstream chamber was drained through a perforated pipe and flowed back to the pump.

A schematic of the experimental setup is shown in figure 2. In the channel, a 2095 mm long flat acrylic plate was mounted 110 mm above the bottom wall. A symmetric leading edge made of aluminum was attached to the plate. The leading edge was a wedge with  $3^\circ$  opening angle and 95 mm length.

The free-stream turbulence was generated by grids of various sizes mounted in front of the plate in the test section. In the present study, two different grids were used and the data of the grids are given in table 1. The distance from the grid to the plate leading edge was 0.9 m (Grid A) or 0.8 m (Grid B).

*Velocity statistics and flow structures in bypass transition*

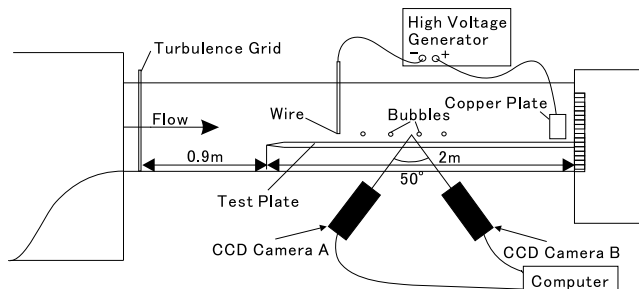


FIGURE 2. Test section setup with PTV-system.

Grid	$Tu$ (%)	$M$ (mm)	$d$ (mm)	Bar geometry	$x_{\text{grid}}$ (m)
A	3.4	50	10	round	-0.9
B	2.5	40	5	round	-0.8

TABLE 1. Characteristics of the grids used.  $M$  is the mesh width,  $d$  the bar diameter and  $Tu$  the turbulence level at  $x = 0$  mm,  $y = 70$  mm.

The turbulence behind a grid is known to reach a nearly isotropic state after around 20 mesh sizes ( $M$ ) (e.g. Groth & Johansson 1988). In our case, the distances are  $18 M$  (Grid A) and  $20 M$  (Grid B). The turbulence level was defined as  $Tu = u_{\infty,rms}/U_{\infty}$  where  $u_{\infty,rms}$  is the root mean square of the streamwise velocity in the free stream and  $U_{\infty}$  is the free-stream velocity.  $Tu$  was measured 70 mm above the leading edge and is  $3.4 \pm 0.2 \%$  (Grid A) and  $2.5 \pm 0.3 \%$  (Grid B) where the variation is over one grid mesh size in the spanwise direction. The free-stream turbulence was thus nearly isotropic and uniform from the leading edge and downstream.

Hydrogen bubbles were used as flow markers both for flow visualization and particle-tracking velocimetry. A gold-plated tungsten wire of 0.03 mm diameter was used as the cathode and a copper plate placed downstream of the measurement position as the anode. The wire and the plate were connected to a high-voltage pulse generator giving pulses of 400 V which created a bubble chain along the wire. The wire was positioned across the test section in the spanwise direction and a stepper motor traversed the wire in the direction normal to the wall.

For PTV, the bubble chains were recorded by two progressive scan cameras positioned under the test section. The two cameras captured images of the

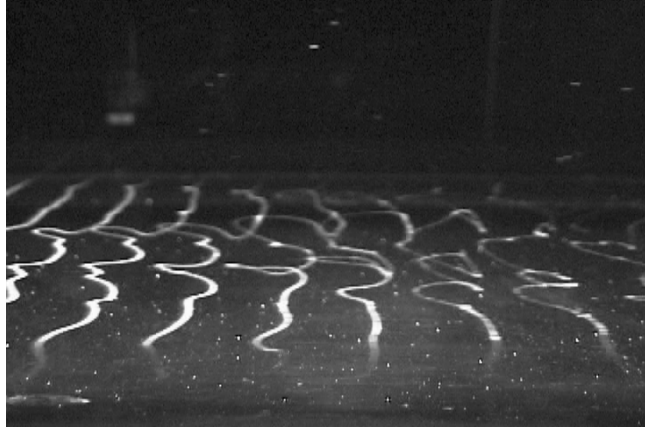


FIGURE 3. Side view of bubble chains. Bubble wire was positioned in the centre of the boundary layer at  $x = 800$  mm,  $U_\infty = 0.12$  m/s and Grid A mounted at  $x = -500$  mm. Flow is from left to right.

bubble chains from the same area under different angles. The cameras were synchronized with the hydrogen bubble lines and the images were captured and stored by a computer.

The coordinates are  $x$  for the streamwise,  $y$  for the wall normal and  $z$  for the spanwise direction. The corresponding velocities are  $U$ ,  $V$  and  $W$ . The Reynolds number is defined as  $Re = xU_\infty/\nu$ , where  $\nu$  is the kinematical viscosity of the water. The  $y$ -coordinate is often normalized by the displacement thickness of a Blasius profile,  $\delta^*$ , calculated as  $1.72\sqrt{x/Re}$ .

The usual decomposition in mean and fluctuation was used, with capital letters denoting the complete signal and small letters denoting fluctuation quantities. An overbar,  $\bar{U}$ , denotes the mean (*i.e.*  $U = \bar{U} + u$ ). The root mean square of a quantity was defined as  $u_{rms} = \sqrt{u^2}$ . The mean is taken in time for the LDV measurements and in time and the spanwise direction for the PTV measurements.

### 3. Flow visualization and quantification of PTV

#### 3.1. Hydrogen bubble flow visualization

Each time a voltage pulse was applied to the bubble wire, a bubble chain was formed. This chain was convected downstream and after a predetermined time delay, a new chain was created by the next pulse. If the velocity of the fluid passing the wire was constant, parallel, straight bubble chains would be seen.

### *Velocity statistics and flow structures in bypass transition*

Figure 3 shows bubble chains created in the centre of the boundary layer over the flat plate. Note that in this explanatory figure, Grid A was not mounted at its standard position ( $x_{grid} = -900$  mm) but at  $x_{grid} = -500$  mm.

The chains were recorded by a CCD camera from the side of the channel. The camera was positioned above the plate and slightly tilted down towards the test plate in order to show the spanwise distribution of the chains. The flow direction was from left to right. When the bubbles that form on the wire were swept away by the flow, they formed a nearly straight chain. As the bubbles were convected downstream by the local velocity of the flow, the chain deformed due to the spanwise velocity variation as is seen in figure 3. Two low velocity streaks are seen as kinks of the chains. It can also be seen that the kinks of the chains develop in three dimensions with a small upward motion. As observed by the stereo-viewing eyes of a human, the low-velocity regions moved away from the wall. This was first evidence of lift-up, *i.e.* that the positive wall-normal velocity disturbance created the large streamwise velocity disturbance.

#### *3.2. Quantification by stereo PTV*

Example images from the two cameras obtained during PTV measurements are shown in figure 4. The size of the area shown is approximately 95 mm in the streamwise (horizontal) and 74 mm in the spanwise (vertical) directions. Note that the images were taken under an angle, which is why their aspect ratio is different from 95:74. The bubble wire was positioned in the middle of the boundary layer and the flow was from left to right. Two low-speed streaks are seen, one slightly above the middle and one a quarter of the way up from the bottom of the images. Since the two images were taken from different viewing angles (from the upstream direction in figure 4(a) and downstream in figure 4(b)), stereo image techniques give not only the streamwise position ( $x$ ) but also the vertical position ( $y$ ) of the bubble chains.

Figure 5 shows how the position of a bubble chain was obtained from a captured image. The original raw image is shown in figure 5(a). A wavy bubble chain is seen in the middle of the image. The evaluation process is shown in the sequence figure 5(b)–(d). First, a binary image was created using a threshold. In order to isolate the bubble-chain, a labeling method, removing white points without white neighbours (in certain directions) was used (b). Multiplying the original image with this image all pixels except for the bubble chain were set to black, figure 5(c). Finally, the centre of the bubble chain was obtained as the centre of mass of the intensity for each row in this figure, and this position was used for the velocity determination (d). The difference in position, as seen by the two cameras, gave the vertical position of the bubble chain.

In figure 6, the three-dimensional positions of the bubble chains in figure 4 are shown. At  $x = 0$ , the straight bubble wire is seen and the curves then



Camera A (see figure 2)



Camera B (see figure 2)

FIGURE 4. Sample images from the two cameras at  $x = 900$  mm,  $y/\delta^*=1.5$ , and  $U_\infty=0.12$  m/s. Flow is from left to right. Grid A mounted at  $x = -900$  mm

represent lines created at  $t = -n\Delta t$ , where  $n$  is increasing with  $x$  and  $\Delta t$  was 160 ms for this figure. All coordinates in this figure are in relation to the bubble wire.

*Velocity statistics and flow structures in bypass transition*

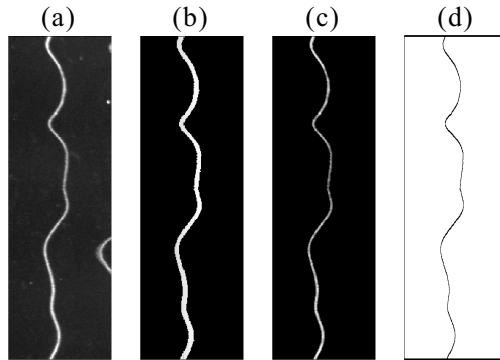


FIGURE 5. Chain detection process.

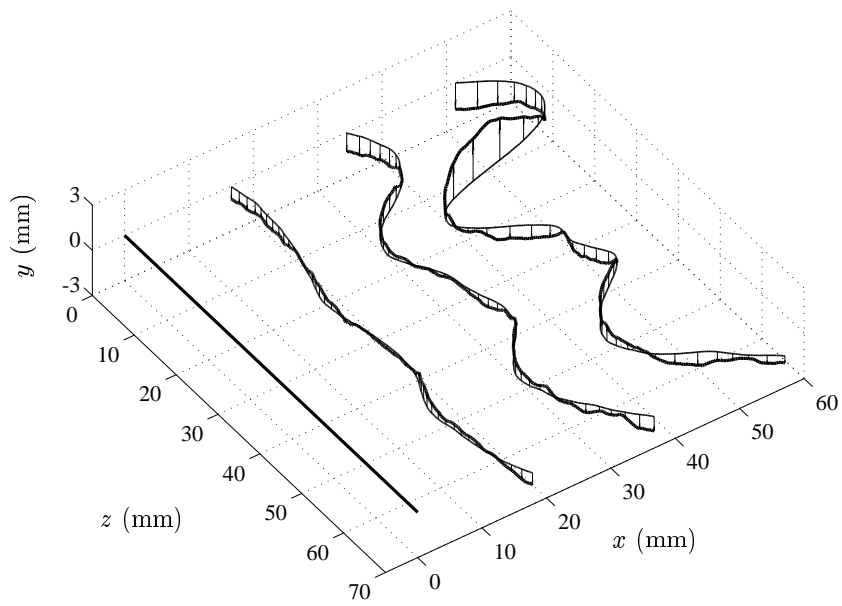


FIGURE 6. Detected bubble lines plotted in three dimensions.

From the  $x$ - and  $y$ -positions of two bubble chains and the known time interval between them, the streamwise velocity  $U(z)$  and wall-normal velocity fluctuation  $v(z)$  were calculated.

Method	$\bar{U}$ (m/s)	$u_{rms}$ (m/s)	$v_{rms}$ (m/s)	$\bar{u}\bar{v}$ (m <sup>2</sup> /s <sup>2</sup> )
LDV	0.0737	0.00616	0.00315	$-5.14 \times 10^{-6}$
Image	0.0749	0.00594	0.00324	$-5.41 \times 10^{-6}$
Discrepancy	1.7%	3.6%	2.9%	5.3%

TABLE 2. Comparison of statistical quantities as measured by PTV and LDV in the outer part of the boundary layer at  $x = 800$  mm,  $y = 20$  mm.

### 3.3. Validation of PTV

LDV measurements were made as a reference in order to estimate the accuracy of the stereo PTV technique. These measurements were performed with a one-dimensional LDV system equipped with a Bragg cell. Three quantities,  $u_{rms}$ ,  $v_{rms}$  and  $\bar{u}\bar{v}$ , were determined by measuring with the optics in three different directions, namely the streamwise direction and two directions inclined  $45^\circ$  from the streamwise direction. The fluctuation of the streamwise velocity,  $u_{rms}$ , was obtained from the measurements in the streamwise direction while the quantities  $v_{rms}$  and  $\bar{u}\bar{v}$  were calculated from

$$v_{rms}^2 = \frac{1}{2 \sin^2 \theta} (\overline{p^2} + \overline{q^2} - 2u_{rms}^2 \cos^2 \theta) \quad (1)$$

$$\bar{u}\bar{v} = \frac{1}{4 \sin \theta \cos \theta} (\overline{p^2} - \overline{q^2}) \quad (2)$$

where  $p$  and  $q$  are the fluctuating part of the velocity measured at the angle  $\theta$  and  $-\theta$ , respectively.

For each direction, the LDV signal was sampled with a frequency of 200 Hz and a sampling time of 600 s. With the stereo PTV, 1000 stereo images were taken with a frequency of 6 Hz, giving a total sampling time of 167 s. The statistics calculated from the PTV measurements were averaged in time as well as over the spanwise extent of the measurement area.

The statistics obtained in the outer part of the boundary layer with stereo PTV and LDV are compared in table 2. In order to create large amplitude velocity fluctuations, comparable to the ones inside a boundary layer subjected to free-stream turbulence, the turbulence generating grid was placed 500 mm upstream of the leading edge (the default position was 900 mm). Measurements were made in the outer part of the boundary layer in order to have a measurable value of  $\bar{u}\bar{v}$ . As can be seen in table 2, the discrepancy of the value between stereo PTV and LDV is less than 2% for  $\bar{U}$  and less than 6% for the fluctuations and correlations.

*Velocity statistics and flow structures in bypass transition*

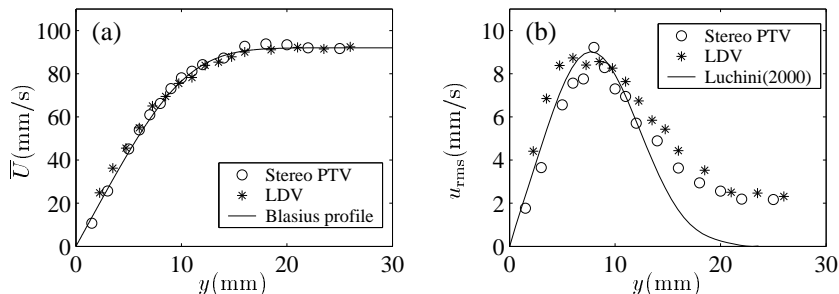


FIGURE 7. Profiles of  $\bar{U}$  and  $u_{rms}$  measured by PTV and LDV in the boundary layer,  $x = 800$  mm,  $U_\infty = 0.092$  m/s, Grid A.

The non-measured spanwise velocity component also introduces errors. The error  $\Delta v$  can be estimated to be

$$\Delta v = \frac{\partial v}{\partial z} w \Delta t \quad (3)$$

where  $\Delta t$  is the time interval between two bubble chains. Assume that the structures to be studied in the boundary layer have a width of  $\Delta z$  and that the maximum value of  $v$  is  $\hat{v}$  so that  $\partial v / \partial z \lesssim \hat{v} / \Delta z$ . In addition, we assume that  $w \lesssim \hat{v}$ . Introducing this in equation (3), we get

$$\Delta v = \frac{\hat{v}}{\Delta z} \hat{v} \Delta t \quad (4)$$

or, by dividing with  $\hat{v}$ ,

$$\frac{\Delta v}{\hat{v}} = \frac{\hat{v} \Delta t}{\Delta z} \quad (5)$$

Typical values from the measurements are  $\hat{v} = 3$  mm/s,  $\Delta t = 0.1$  s and  $\Delta z = 10$  mm which gives  $\Delta v / \hat{v} = 3\%$  as the upper bound of the error. A similar analysis for  $u$  gives the same result.

It should be remembered, however, that stereo PTV provides not only statistics of  $u$  and  $v$  but simultaneous measurements and time traces of both velocity components at all spanwise positions covered by the images. The errors estimated above, which indeed are large compared to what can be achieved in single point measurements, are therefore acceptable.

#### 4. Boundary layer measurements

During the measurements reported in this section, the time between two bubble chains was 0.1 s and the images were captured 0.05 s after the second bubble chain was created. Depending on the  $y$ -position, that bubble line had moved 1-6 mm from the wire when the images were captured. The volume in which bubbles were detected spanned 12 mm in the streamwise direction and 1 mm in

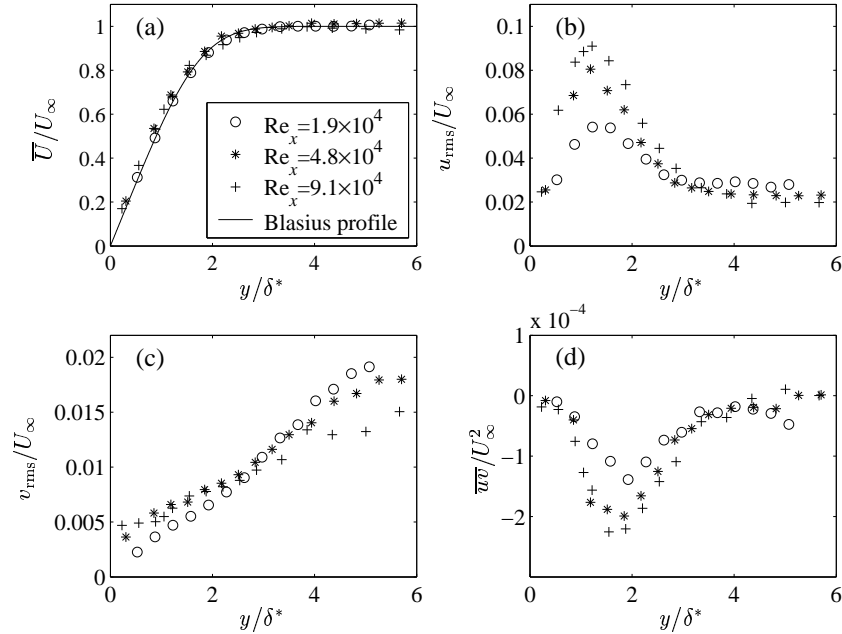


FIGURE 8. Boundary layer statistics measured by PTV. Grid A,  $x = 230, 580$  &  $1070$  mm and  $U_\infty = 0.108$  m/s.  $Re = 1.9 \times 10^4$  ( $\circ$ ),  $Re = 4.8 \times 10^4$  ( $*$ ) and  $Re = 9.1 \times 10^4$  ( $+$ ). The full curve in (a) is the laminar Blasius profile.

the wall-normal direction. The wall-normal extent of the measurement volume is less than 10% of the boundary layer thickness at all measurement stations.

During measurements, the free-stream velocity and turbulence intensity were continuously monitored by the LDV system, whose measurement volume was positioned 70 mm above the tip of the leading edge. For stereo PTV, 1000 stereo images were taken with a frequency of 10 Hz, giving a total sampling time of 100 s.

#### 4.1. Velocity statistics in the boundary layer

In figures 7–12, boundary layer statistics are presented. First, an additional comparison between PTV and LDV is made in figure 7, whereupon stereo PTV measurements from four streamwise measurement stations are presented in figures 8 and 9. Finally, the stereo PTV data is compared with optimal perturbation theory, previous measurements and DNS results in figures 10 – 12.

The profiles of  $\bar{U}(y)$  measured with the two systems in figure 7(a) show good agreement between stereo PTV and LDV measurements. Furthermore,

Velocity statistics and flow structures in bypass transition

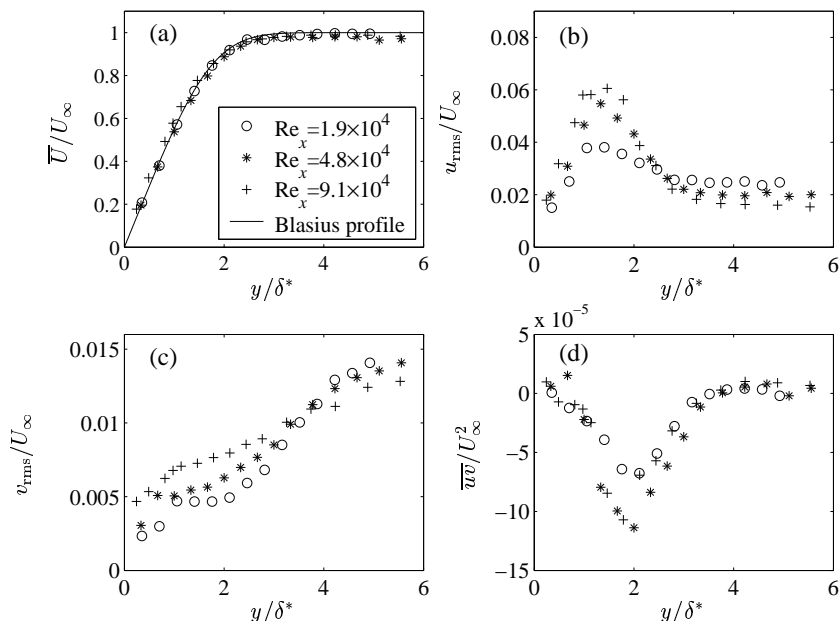


FIGURE 9. Boundary layer statistics measured by PTV. Grid B,  $x = 230, 580$  &  $1070$  mm and  $U_\infty = 0.114$  m/s.  $Re = 1.9 \times 10^4$  ( $\circ$ ),  $Re = 4.8 \times 10^4$  ( $*$ ) and  $Re = 9.1 \times 10^4$  ( $+$ ). The full curve in (a) is the laminar Blasius profile.

the boundary layer profile is seen to fit the Blasius boundary layer solution well. Continuing to the  $u_{rms}$  profile in figure 7(b), the accuracy of the stereo PTV, as compared to the LDV, is confirmed. Also, the well established agreement between the experimental disturbance distribution and the optimal disturbance theory of Luchini (2000) (the arbitrary amplitude of the theoretical curve has been adjusted to fit the data) is demonstrated. The data of figure 7 was obtained at  $x = 800$  mm with  $U_\infty = 92$  mm/s. The free stream turbulence level was  $Tu = 3.3\%$ .

Stereo PTV measurements at three streamwise positions ( $x = 230, 580, 1070$  mm) are shown in figure 8 ( $Tu = 3.4\%$ ,  $U_\infty = 0.108$  m/s) and figure 9 ( $Tu = 2.5\%$ ,  $U_\infty = 0.114$  m/s). The wall-normal distance is normalized by  $\delta^*$ , the displacement thickness of the Blasius boundary layer. Studying the quantities in due order, the mean velocity profiles in plates (a) of the figures show that the boundary layer developing over the flat plate indeed is a Blasius boundary layer. The  $u_{rms}$  distributions in plates (b) show the common features for a boundary layer subjected to free-stream turbulence: a large (order of 10% of  $U_\infty$ )  $u_{rms}$  with maximum amplitude around  $y/\delta^* = 1.4$ .

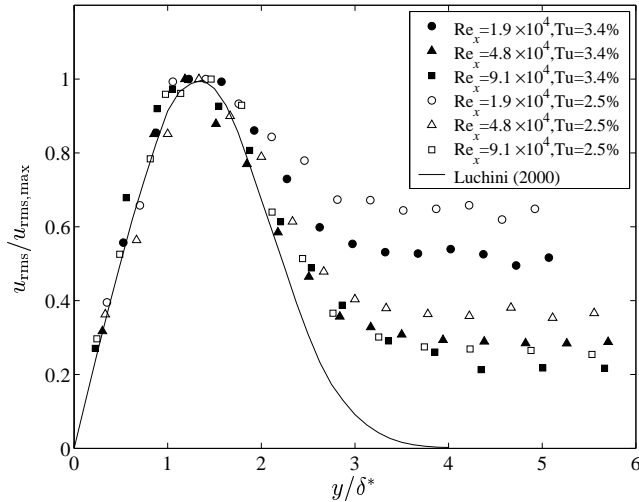


FIGURE 10. Profiles of  $u_{rms}$ , each normalized by its maximum value, compared to the theory of Luchini (2000).

The amplitude of  $u_{rms}$  increases with downstream distance and for the most downstream measurement station, the amplitude saturates.

The  $v_{rms}$  profile is difficult to measure with hot-wire anemometry, since the moving spanwise velocity gradients due to the streaks introduce an error in the measurements of the wall-normal velocity (see Fransson & Westin, 2002). The  $v_{rms}$  profiles in figures 8(c) and 9(c) show that at the most upstream positions  $v_{rms}$  increases from zero at the wall towards the free-stream value, which is reached far out from the wall.

The property  $\overline{uv}$  is shown in figures 8(d) and 9(d). This property can be measured with hot-wire techniques only if corrections are made for the wall-normal velocity gradient (Talamelli *et al.* 2000). The present data was obtained through direct measurements without any corrections. The measurements show a considerable scatter (also seen in the corrected hot-wire data), but still, a clear negative peak around  $y/\delta^* = 1.8$  is seen at all positions.

Profiles of  $u_{rms}$ , each normalized with its maxima, are compared with the optimal disturbance theory of Luchini (2000) in figure 10. The  $u_{rms}$  profiles once again show good agreement with the theory. The disturbances imposed on the boundary layer from the free-stream turbulence are of course not optimal disturbances, but it is known that most initial disturbances develop wall-normal disturbance distributions similar to the optimal one (Luchini 2000).

The  $\overline{uv}$  profiles are compared with the previous experimental data of Talamelli *et al.* (2000) in figure 11. The position of the valley of the present data

Velocity statistics and flow structures in bypass transition

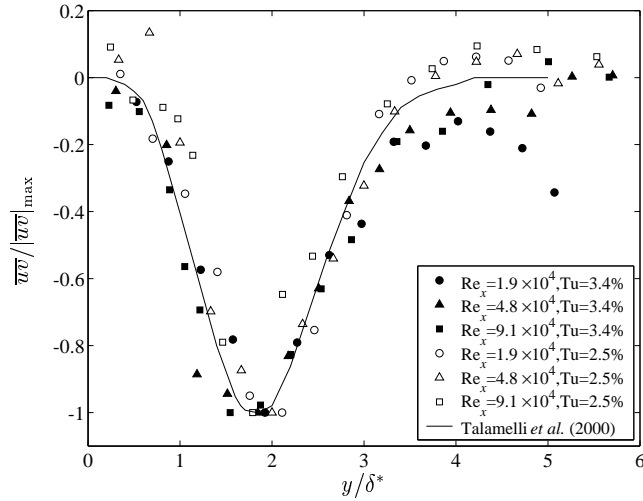


FIGURE 11. Normalized profiles of  $\overline{uv}$  compared to measurements of Talamelli *et al.* (2000).

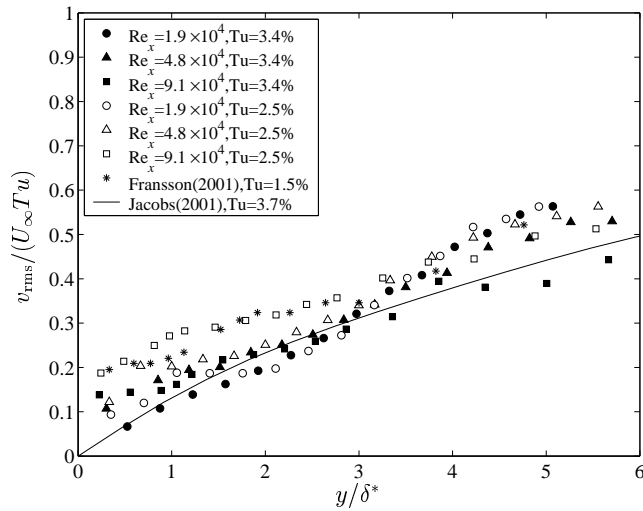


FIGURE 12. Normalized profiles of  $v_{rms}$  compared with LDV data of Fransson & Westin (2002) and DNS data of Jacobs & Durbin (2001).

is seen to coincide with the position found after corrections in the previous experiment.

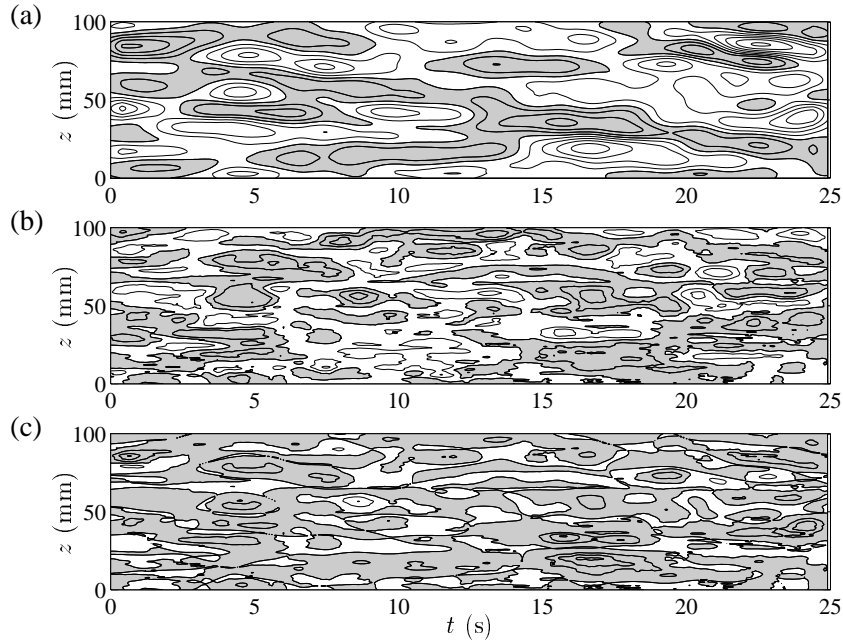


FIGURE 13. Contour maps of (a)  $u$ , (b)  $v$  and (c)  $uv$  at  $y/\delta^*=0.16$ ,  $x = 1070$  mm and  $U_\infty = 0.108$  m/s, Grid A. Contour levels are  $\pm 1.5, 3, \dots$  mm/s for  $u$ ,  $\pm 0.25, 0.5, \dots$  mm/s for  $v$  and  $\pm 1, 2, \dots$  mm<sup>2</sup>/s<sup>2</sup> for  $uv$ . Negative contours are filled with gray.

In figure 12, the  $v_{rms}$  profiles are shown in the same plot together with the LDV data of Fransson & Westin (2002) and the DNS data of Jacobs & Durbin (2001). The profiles are scaled with  $U_\infty Tu$ , *i.e.* the turbulence level in the free stream at the leading edge (or, in the DNS case, at the beginning of the computational box). For the most upstream positions, where  $v_{rms}$  monotonically decays towards the wall, the present data agrees well with the results of previous investigators. When comparing the data of Fransson & Westin and Jacobs & Durbin, we see that, in this scaling,  $v_{rms}$  is higher for the low free-stream turbulence level (Fransson & Westin) than for the case with a high level (Jacobs & Durbin). This trend is seen also in the present data.

#### 4.2. Flow structures

If the main interest is boundary layer statistics, the stereo PTV method has no advantage over other well-established methods, such as *e.g.* two-dimensional LDV. The reason to develop and use the stereo PTV system was the desire to study the creation and spatial development of velocity disturbances in the

*Velocity statistics and flow structures in bypass transition*

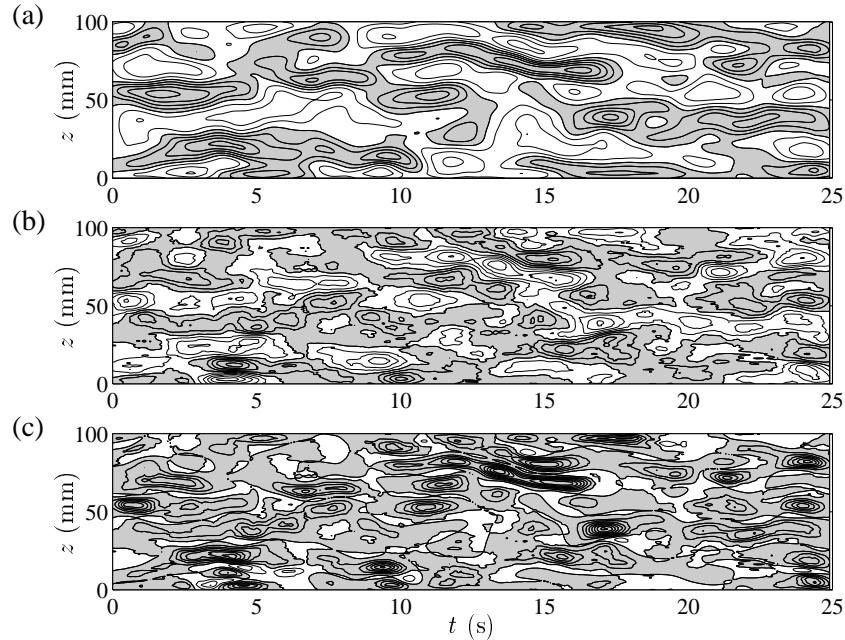


FIGURE 14. Contour maps of (a)  $u$ , (b)  $v$  and (c)  $uv$  at  $y/\delta^*=1.48$ ,  $x = 1070$  mm and  $U_\infty = 0.108$  m/s, Grid A. Contour levels are  $\pm 5, 10, \dots$  mm/s for  $u$ ,  $\pm 0.3, 0.6, \dots$  mm/s for  $v$  and  $\pm 3, 6, \dots$  mm<sup>2</sup>/s<sup>2</sup> for  $uv$ . Negative contours are filled with gray.

boundary layer. The simultaneous measurements of the spanwise distributions of both  $u$  and  $v$  give new and intriguing possibilities for such studies, increasing the understanding of free-stream turbulence induced transition.

During the measurements to be reported in figures 13–17, the free-stream velocity and turbulence level at the leading edge was 0.108 m/s and 3.4 %, respectively. The Reynolds number based on the distance from the tip of the leading edge to the stereo PTV measurement area at  $x=1070$  mm was  $9.1 \times 10^4$ . The boundary layer statistics at this position are shown by the plus markers in figure 8.

Figures 13–15 show contour maps of  $u$ ,  $v$ , and  $uv$  (*i.e.* the velocity fluctuations with the mean in  $z$  and time subtracted) at three different heights ( $y/\delta^* = 0.16, 1.48$  and  $2.80$ ) through the boundary layer. Negative values are filled with gray. At each height, 250 stereo image sets were used to create the temporal velocity maps. It should be emphasized that the measurements at different *heights* were not simultaneous, which is why no comparisons of individual structures can be made in figures 13–15. Also note that the contour

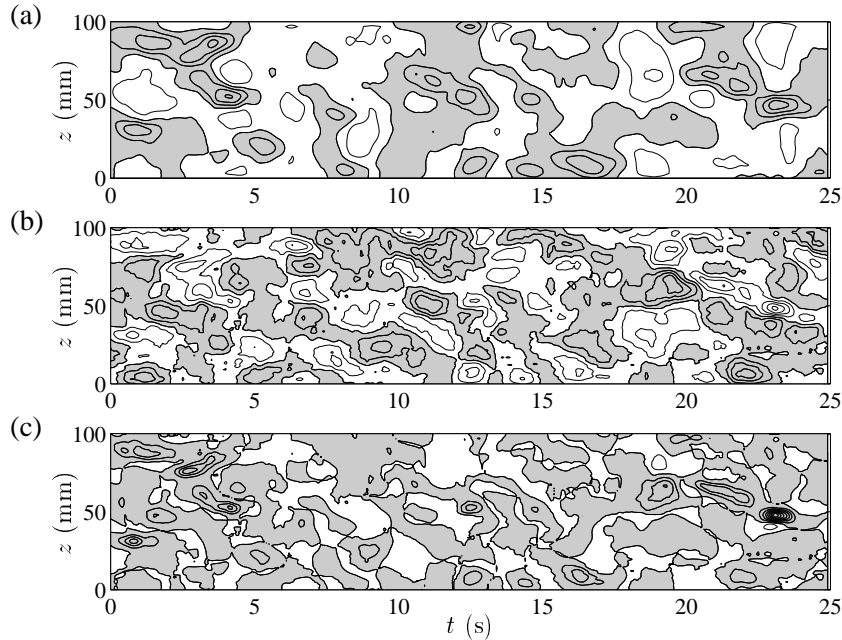


FIGURE 15. Contour maps of (a)  $u$ , (b)  $v$  and (c)  $uv$  at  $y/\delta^*=2.80$ ,  $x = 1070$  mm and  $U_\infty = 0.108$  m/s, Grid A. Contour levels are  $\pm 3, 6, \dots$  mm/s for  $u$ ,  $\pm 0.5, 1, \dots$  mm/s for  $v$  and  $\pm 3, 6, \dots$   $\text{mm}^2/\text{s}^2$  for  $uv$ . Negative contours are filled with gray.

levels are different both for the different components ( $u$ ,  $v$  and  $uv$ ) as well as for the different heights so that the features of the structures at each height can be studied. In figures 13(a), 14(a) and 15(a), the streamwise velocity disturbance is shown. At  $y/\delta^* = 0.16$  and 1.48, figures 13(a) and 14(a), strong low-speed (gray) velocity streaks are clearly seen. At the uppermost height,  $y/\delta^* = 2.80$ , low-speed structures are much less accentuated.

As seen in figures 13(b), 14(b) and 15(b), particularly high values also of the vertical velocity,  $v$ , are seen in isolated regions at  $y/\delta^* = 1.48$ . Comparing figures 14(a) and (b), it can be suspected that a positive  $v$  velocity corresponds to a negative disturbance in  $u$ . This suspicion is confirmed when studying the  $uv$  distribution in figure 14(c), where very strong negative (gray) correlations are seen at the positions of the low-speed streaks in plate (a). At the other heights (figures 13(c) and 15(c))  $uv$  is not as strongly correlated as in the centre ( $y/\delta^* = 1.48$ ) of the boundary layer. The main contribution to the negative peak in  $\overline{uv}$  at  $y/\delta^* = 1.8$  (see figure 11) thus originates from localized regions of negative  $uv$  at positions of low streamwise velocity.

Velocity statistics and flow structures in bypass transition

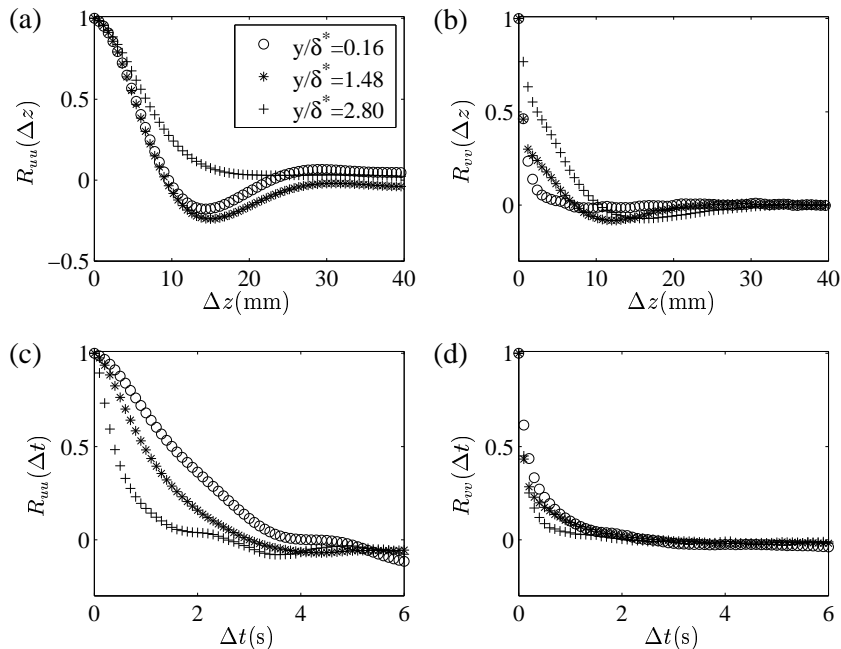


FIGURE 16. Spanwise- and auto-correlations of  $u$  and  $v$  at  $y/\delta^* = 0.16$  ( $\circ$ ), 1.48 ( $*$ ) and 2.80 ( $+$ ),  $x = 1070$  mm and  $U_\infty = 0.108$  m/s, Grid A, (a) spanwise correlation of  $u$ , (b) spanwise correlation of  $v$ , (c) autocorrelation of  $u$  and (d) autocorrelation of  $v$ .

The strong negative correlation in  $uv$  occurring at the low velocity regions strongly indicates that lift up is the mechanism behind the elongated streamwise velocity disturbance seen in free-stream turbulence induced transition.

The spanwise and autocorrelations of the data illustrated in figures 13–15 are shown in figure 16. First, the well-known minimum in the spanwise correlation (*c.f.* Matsubara & Alfredsson, 2001) is seen in figure 16(a). The spanwise correlation of the  $v$ -component in figure 16(b) shows a small minimum for  $y/\delta^* = 1.48$  at  $\Delta z = 12$  mm, but it is not at all as strong as the minimum in the correlation of the streamwise velocity. This shows that even though a structure of high or low streamwise velocity often is flanked by a disturbance of the opposite sign, a disturbance in the wall-normal velocity usually appears alone. Furthermore, the autocorrelations in figure 16(c) and (d) show that the disturbances in  $u$  last for longer times than those in  $v$ , *i.e.* that wall-normal velocity disturbances are much shorter than the regions of positive and negative streamwise velocity variations.

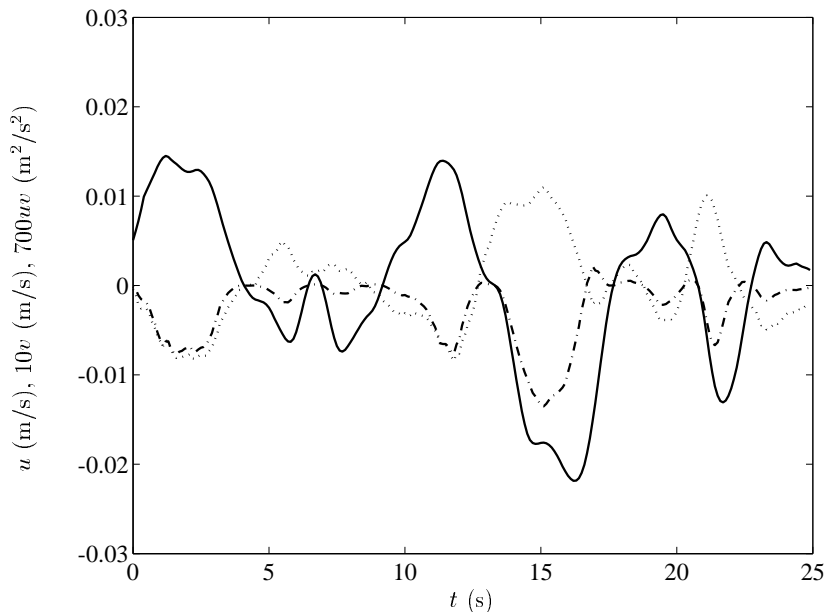


FIGURE 17. Simultaneous time signals of  $u$  (—),  $v$  ( $\cdots$ ) and  $uv$  ( $\cdot - \cdot -$ ) at  $z=70$  mm in figure 14

The observation from the autocorrelations of  $u$  and  $v$  above, namely that the disturbances in  $u$  are longer than those in  $v$ , are seen also in figure 17, where the time signals of  $u$ ,  $v$  and  $uv$  at  $z = 70$  mm in figure 14 is plotted. Regions of low streamwise velocity are seen in periods from  $t = 13$  to  $t = 18$  and 21–23 s. Note that the beginning of the period of negative  $u$  coincides with the start of the positive  $v$  (and, consequently, negative  $uv$ ). However, the period of negative  $u$  is longer than the period of positive  $v$ , *i.e.* the low streamwise velocity is observed not only during the period of positive  $v$ . The extent of the low streamwise velocity period suggests that a normal velocity disturbance gives a momentum deficit which can be observed far downstream.

## 5. Conclusions

Three main conclusions from the present study are

- (i) The stereo PTV measurements successfully regenerate statistical quantities in a boundary layer subjected to free-stream turbulence.
- (ii) The monotonic decrease of  $v_{rms}$  towards the wall was confirmed.
- (iii) The low-velocity streaks are strongly coupled to fluid moving from the wall (*i.e.* positive  $v$ -disturbances).

### *Velocity statistics and flow structures in bypass transition*

The first point above shows that the time resolved measurements of the spanwise velocity distribution  $u(z)$  and  $v(z)$  by the stereo PTV system are accurate enough to study streak development in bypass transition.

The second point confirms the findings of Jacobs & Durbin (2001) and Fransson & Westin (2002) and shows that earlier hot-wire measurements were in error.

The third point is a strong evidence that the ideas of lift-up dating back to Landahl (1977) plays a vital part in free-stream turbulence induced transition. The present results are some of the first direct observations of this effect.

The data obtained from the measurements constitute a database which will be used for future studies, including more correlations and statistics regarding the flow structures in the boundary layer.

## **6. Acknowledgments**

The excellent technical support and patience of Mr. Yamabe are greatly acknowledged. We are grateful to our colleagues at IFS for joining the construction of the water channel. Kristian Angele kindly read, corrected and commented the manuscript. Fredrik Lundell's stay in Japan was partly financed by the Scandinavia-Japan Sasakawa Foundation. Fredrik Lundell's later travels to Japan were supported by JSPS. Dr. Matsubara was supported by JSPS Research Fellowships for Young Scientists.

## References

- ALFREDSSON, P. H. & MATSUBARA, M. 2000 Free-stream turbulence, streaky structures and transition in boundary layer flows. *AIAA-paper 2000-2534*.
- ANDERSSON, P., BERGGREN, M. & HENNINGSON, D. S. 1999 Optimal disturbances and bypass transition in boundary layers. *Phys. Fluids* **11**, 134–150.
- ELLINGSEN, T. & PALM, E. 1975 Stability of linear flow. *Phys. Fluids* **18**, 487–488.
- FASEL, H. F. 2002 Numerical investigation of the interaction of the Klebanoff-mode with a Tollmien-Schlichting wave. *J. Fluid Mech.* **450**, 1–33.
- FRANSSON, J. H. M. & WESTIN, K. J. A. 2002 Errors in hot wire X-probe measurements induced by unsteady velocity gradients. *Exp. Fluids*. In press.
- GROTH, J. & JOHANSSON, A. V. 1988 Turbulence reduction by screens. *J. Fluid Mech.* **428**, 185–212.
- JACOBS, R. G. & DURBIN, P. A. 2001 Simulations of bypass transition. *J. Fluid Mech.* **197**, 139–155.
- LANDAHL, M. T. 1977 Dynamics of boundary layer turbulence and the mechanism of drag reduction. *Phys. Fluids* **20**, 55–63.
- LANDAHL, M. T. 1980 A note on an algebraic instability of inviscid shear flows. *J. Fluid Mech.* **98**, 243–251.
- LUCHINI, P. 2000 Reynolds number independent instability of the boundary layer over a flat surface: optimal perturbations. *J. Fluid Mech.* **404**, 289–309.
- MATSUBARA, M. & ALFREDSSON, P. H. 2001 Disturbance growth in boundary layers subjected to free stream turbulence. *J. Fluid Mech.* **430**, 149–168.
- ROACH, P. E. & BRIERLY, D. H. 1990 The influence of a turbulent freestream on zero pressure gradient transitional boundary layer development, part I. Test cases T3A and T3B. In *Numerical Simulation of Unsteady Flows and Transition to Turbulence*, (ed. O Pironneau *et al.*), pp. 319–347. Cambridge Univ. Press. Editors
- TALAMELLI, A., WESTIN, K. J. A. & ALFREDSSON, P. H. 2000 An experimental investigation of the response of hot-wire x-probes in shear flows. *Exp. Fluids* **28**, 425–435.
- WESTIN, K. J. A. 1997 Laminar-turbulent boundary layer transition influenced by free stream turbulence. PhD thesis, Royal Institute of Technology. *TRITA-MEK 1997:10*

Paper 2

P2



# Streamwise scaling of streaks in laminar boundary layers subjected to free-stream turbulence

By **Fredrik Lundell & P. Henrik Alfredsson**

KTH Mechanics, S-100 44 Stockholm, Sweden

A laminar boundary layer subjected to free-stream turbulence generated by grids upstream of the leading edge has been studied. Correlations between a wall wire and a hot wire in the boundary layer have been obtained. The hot wire has been traversed to 328 positions for each of the five wall-wire positions studied. The length, height and width of the correlation distributions are seen to increase in the downstream direction becoming self similar in coordinates scaled with the boundary-layer length-scale. The propagation speed of the structure is obtained and its variation in the streamwise and wall-normal directions is found to agree with what is obtained from a simple model.

---

## 1. Introduction

Free-stream turbulence (FST) may induce large elongated disturbances into laminar boundary layers which are completely different from Tollmien-Schlichting waves. The main features of such disturbances are that they consist of elongated regions (streaks) of high and low streamwise velocity, that their spanwise wavelength is of the order of the boundary-layer thickness and that the energy (square of the *rms*-value) of the streamwise velocity-fluctuation grows in linear proportion to the downstream distance. All these features agree well with the theory developed by Luchini (1996, 2000) and Andersson, Berggren & Henningson (1999) which describes algebraically (transiently) growing disturbances in laminar boundary-layer flows. Such disturbance growth is due to non-orthogonality of the eigenmodes which may give rise to large growth even at subcritical Reynolds-numbers.

Early work on transition induced by FST has been reviewed by Kendall (1998), whereas two recent papers by Alfredsson & Matsubara (2000) and Matsubara & Alfredsson (2001) used hot-wire anemometry, Particle Image Velocimetry and flow visualization (see figure 1) to give detailed information of



FIGURE 1. Smoke visualization of streaks and spots in a boundary layer subjected to free-stream turbulence. The white smoke is assembled in low-velocity regions and flow is from left to right. From Matsubara & Alfredsson (2001).

the structure of disturbances inside a laminar boundary layer subjected to various free-stream turbulence-levels. From visualization pictures, it was shown that the streaks are fairly steady in the spanwise direction: once created, the streaks move only slowly sideways. The spanwise scale of the streaks seemed to adapt to a width close to the boundary-layer thickness (except near the leading edge). Similar streaks were observed by Jacobs & Durbin (2001) in a direct numerical simulation. Alfredsson & Matsubara suggested that the breakdown of streaks appearing in boundary layers subjected to free-stream turbulence and the bursting of streaks in the sublayer of turbulent boundary layers are due to similar mechanisms.

In order to model the streaky structures Westin *et al.* (1998) introduced finite-time disturbances into a laminar boundary layer and followed their subsequent development. In this case the maximum disturbance level decreased with downstream distance, however, the length of the disturbance increased. The spanwise scale on the other hand was more or less constant. In a theoretical study, Landahl (1990) showed that a convected eddy of finite length in a shear flow will elongate and at the same time decrease its amplitude. Although the behaviour is qualitatively correct with respect to what has been observed in the experiments it is not straightforward to do quantitative comparisons with the model of Landahl.

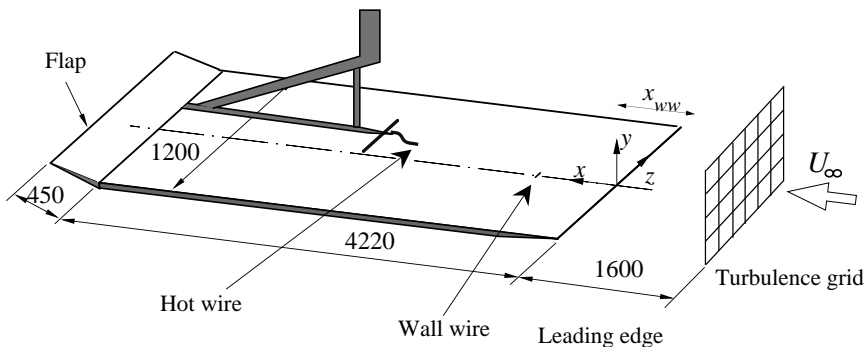


FIGURE 2. Experimental setup.

Single-point measurements by Matsubara & Alfredsson (2001) showed that the streamwise scale (obtained from temporal spectra by a Taylor’s hypothesis) of the disturbances increases in the downstream direction in linear proportion to the boundary-layer thickness (which grows as the square root of the streamwise distance for a Blasius flat-plate boundary-layer). The use of Taylor’s hypothesis in this context is, however, somewhat questionable. In the present study, streamwise correlation measurements, using a wall probe and a traversed hot wire, are used to give a more accurate picture of the streamwise structure of the disturbances. These measurements confirm the earlier findings that the length increases in linear proportion to the boundary-layer thickness. This indicates that the structures develop in a self-similar manner, since they grow also in the direction normal to the wall and thereby extend across the boundary layer from the wall to its outer edge.

In section 2, the experimental setup is described. A kinematical observation regarding inclined structures is described in section 3 before the experimental results are presented in section 4. Finally, the conclusions are given in section 5.

## 2. Experimental setup

The experiments were performed in the MTL wind-tunnel at KTH. The setup was the same as the one used by Matsubara & Alfredsson (2001) with the addition of a wall wire, see figure 2. The measurements of the boundary layer forming on the plate give a shape factor of  $2.6 \pm 0.1$  (Blasius boundary layer solution: 2.59), which is similar to previous measurements in the present setup.

Upstream of the leading edge of the flat plate, different grids were installed in order to generate the free-stream turbulence. Two different grids were used, giving FST levels, defined as

$$Tu = \frac{u_{rms}(x^* = 0)}{U_\infty} \quad (1)$$

of 1.1% and 1.8%, respectively, where the free-stream velocity  $U_\infty$  was 4.8 m/s during the measurements.

The dimensional coordinates are  $(x^*, y^*)$  for the streamwise and wall-normal directions, respectively, whereas the non-dimensional coordinates are denoted  $(x, y)$  and scaled by

$$\delta = \sqrt{\frac{\nu x^*}{U_\infty}} \quad (2)$$

where  $\nu$  is the kinematical viscosity of the air.

The wall wire was mounted in a plug. The wall-wire position, denoted  $x_{ww}^*$ , could be chosen to be 214, 414, 484, 764 or 834 mm downstream of the leading edge.

For each wall-wire position, the signals from the hot wire and wall wire were sampled simultaneously with the hot wire positioned at 41 streamwise and 8 wall normal positions with  $y$  ranging from 0.3 to 5.7. The wall-wire fluctuation signal used in all processing,  $W(t)$ , is obtained from the raw voltage from the anemometer,  $E_{ww}(t)$ , as

$$W(t) = \frac{E_{ww}(t) - \overline{E_{ww}}}{E_{ww,rms}}. \quad (3)$$

Even though the wall-wire signal is a nonlinear function of the shear stress, the signal  $W(t)$  is a good approximation of the (normalized) wall shear-stress fluctuations as long as the response is close to linear around the working point  $\overline{E_{ww}}$ .

### 3. A kinematical observation

As will be shown from the experimental results, an inclined structure develops inside the boundary layer. Assume that the slope of the structure is similar at different streamwise positions if both the streamwise and vertical coordinates are scaled with the local boundary layer thickness (see figure 3(a)) and that the slope of the structure can be defined by a straight line. This makes it possible to derive, from pure kinematical arguments, how the propagation speed of the structure changes in the wall-normal and downstream directions.

Consider a structure at time  $t_1$  and  $t_2 = t_1 + \Delta t$ . Within the structure we identify two points traveling with the structure as indicated in figure 3(b). The points are separated by the non-dimensional distance  $\Delta y$  in the vertical direction. Denote the  $y$ -coordinate of the lower point  $y^l$  and the upper  $y^u$ . Defining  $u^u$  and  $u^l$  as the propagation speed of the structure at  $y^u$  and  $y^l$ , respectively, we can now write

$$u^u = \frac{x_2^u - x_1^u}{\Delta t} \quad (4)$$

Scaling of streaks in boundary layers subjected to FST

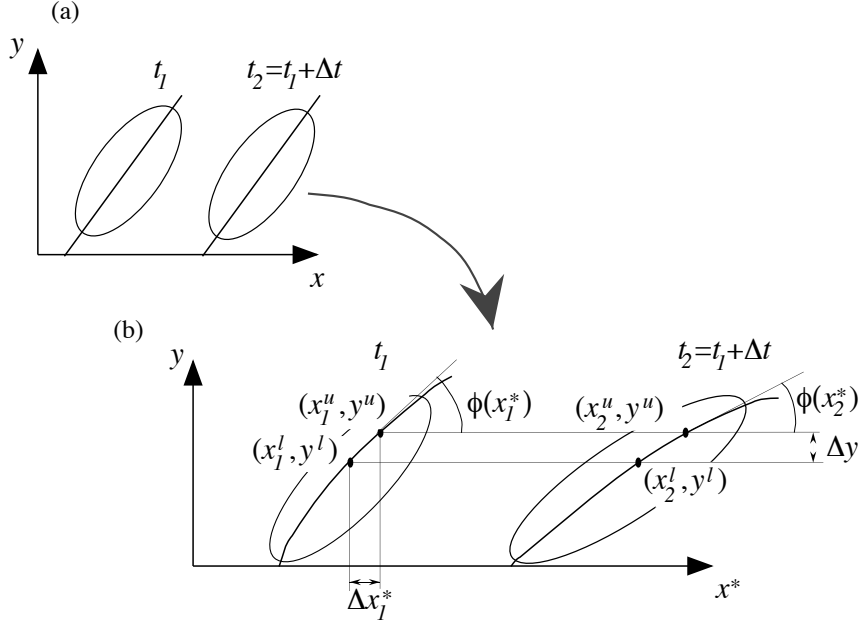


FIGURE 3. Sketch of the situation studied in the derivation in equation (4-11).

and similarly for  $u^l$ . We aim at an equation for  $U_{struc}(x^*, y)$  and start with

$$\frac{u^u - u^l}{\Delta y} = \frac{\Delta U_{struc}}{\Delta y} = \frac{x_2^u - x_1^u - (x_2^l - x_1^l)}{\Delta y \Delta t} = \frac{\Delta x_2^* - \Delta x_1^*}{\Delta y \Delta t} \quad (5)$$

where  $\Delta x_i^* = x_i^u - x_i^l$ .

Define the inverse slope  $k$  of the structure by

$$k = \frac{\Delta x^*}{\Delta y} \quad (6)$$

which for small separations  $\Delta y$  and  $\Delta t$  obeys

$$k = \frac{1}{\tan \phi} \quad (7)$$

where  $\phi$  is defined in figure 3(b). The angle  $\phi$  is a function of  $x^*$  since the lines  $y = C_1(x - x_0)$  in the  $(x, y)$  plane transforms to the curves  $y = C_1((x^* U_\infty / \nu)^{0.5} - (x_0^* U_\infty / \nu)^{0.5})$  in the  $(x^*, y)$  plane. Therefore, the local slope of the structure becomes

$$\tan \phi = \frac{dy}{dx^*} = \frac{1}{2} C_1 (U_\infty / \nu x^*)^{0.5}. \quad (8)$$

This means that at a given  $x^*$  the observed  $\phi$  of the structure, as it passes by, is independent of  $y$ .

In the limit of small  $\Delta y$  and  $\Delta t$ , using the fact that  $k$  is a function of  $x^*$  only, equation (5) and (6) gives

$$\lim_{\Delta y, \Delta t \rightarrow 0} \frac{\Delta U_{struc}}{\Delta y} = \frac{\partial U_{struc}}{\partial y} = \lim_{\Delta y, \Delta t \rightarrow 0} \frac{\Delta k}{\Delta t} = \frac{dk}{dx^*} \frac{dx^*}{dt}. \quad (9)$$

Since  $x^*$  is the streamwise position of the structure, the derivative  $dx^*/dt$  is the structure propagation speed  $U_{struc}(x^*, y)$  and we can thus arrive at a differential equation for  $U_{struc}$ :

$$\frac{\partial U_{struc}}{\partial y} = U_{struc}(x^*, y) f(x^*) \quad (10)$$

where  $f(x^*) = dk/dx^* \sim (x^*)^{-0.5}$ . The solution is

$$U_{struc}(y) = A(x^*) \exp[yf(x^*)] \quad (11)$$

and the arbitrary function  $A(x^*)$  appearing in the integration is the propagation speed of the structure near the wall, *i.e.*  $U_{struc}(x^*, y = 0)$ .

Later, the experimentally determined propagation speed of the structure will be compared to equation (11).

#### 4. Experimental results

From the measurements, simultaneous time series of the wall shear stress and the velocity at various positions straight downstream of the wall wire were available. In order to quantify the structures appearing in the boundary layer, correlations between these signals were used.

The correlation between the wall wire, positioned at  $x_{ww}^*$ , and the velocity measured at  $(x^*, y)$  by the hot wire, is defined as

$$R_{u,ww}(x^*, y, \tau; x_{ww}^*) = \frac{1}{T} \int_0^T \frac{u(x^*, y, t + \tau)}{u_{rms}} W(t; x_{ww}^*) dt \quad (12)$$

where  $\tau$  is a time delay between the wall wire and the hot-wire signals.

In order to study the scaling of the correlations from different wall-wire positions ( $x_{ww}^*$ ) and at different time delays ( $\tau$ ), a coordinate moving with the structures was introduced. For this reason,  $x_{ref}^*(\tau; x_{ww}^*)$  is defined as the  $x^*$  maximizing

$$R_{u,ww}(x^*, y = 2.6, \tau; x_{ww}^*). \quad (13)$$

The vertical position  $y = 2.6$  was chosen since this is the position where  $u_{rms}$  has its maximum. In order to describe the development of the structure it is useful to introduce a streamwise coordinate  $\chi^*$ , which is fixed to the structure and defined as

$$\chi^* = x^* - x_{ref}^* \quad (14)$$

Scaling of streaks in boundary layers subjected to FST

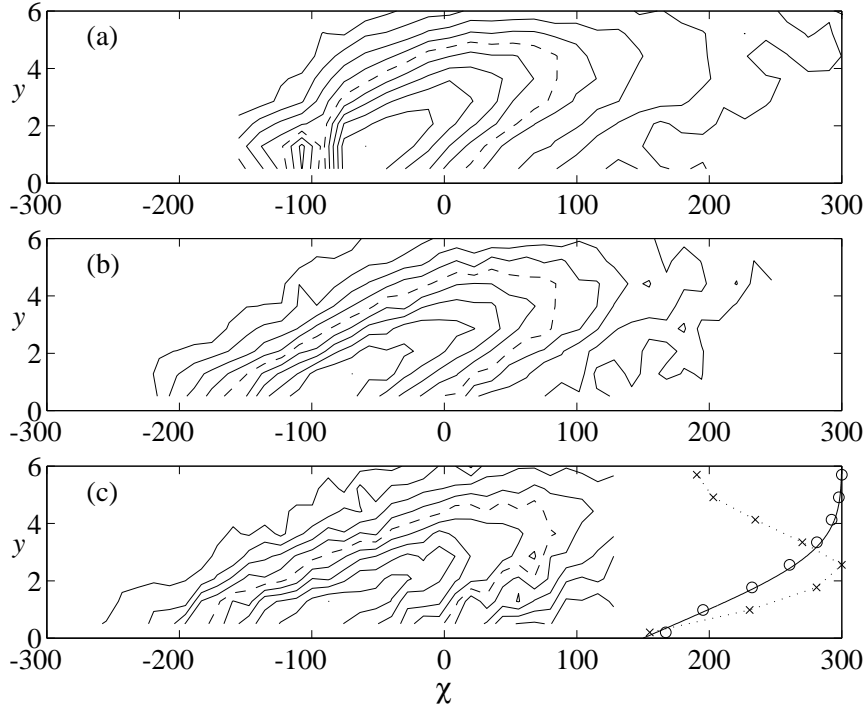


FIGURE 4. Normalized correlations between the wall wire at  $x_{ww}^* = 414$  mm,  $R_{u,ww}(x^*, y, \tau; x_{ww}^* = 414$  mm),  $\chi = (x^* - x_{ref}^*)/\delta(x_{ref}^*)$ . In each figure, the correlation is normalized with its maximum value. (a)  $\tau = 0$ ,  $x_{ref}^* = 509$  mm, (b)  $\tau = 58$  ms,  $x_{ref}^* = 734$  mm and (c):  $\tau = 99$  ms,  $x_{ref}^* = 900$  mm. Contour level is 0.1 and the contour denoting 0.5 is dashed. In (c), the normalized velocity profile (o) is shown together with the Blasius profile (line) and the normalized  $u_{rms}$ -profile (+). The dotted line is for visual aid only.

and non-dimensionalized by  $\delta(x_{ref}^*)$ , *i.e.*

$$\chi = \frac{\chi^*}{\delta(x_{ref}^*)}. \quad (15)$$

For a given  $x_{ww}^*$  and time delay  $\tau$ , the correlation distribution  $R_{u,ww}(x^*, y)$  shows an inclined structure through the boundary layer. For increasing time delays, the structure propagates downstream while the maximum correlation decreases. In figure 4, the correlations obtained with the hot wire at  $x_{ww}^* = 414$  mm is shown for three different time delays. In figure 4, the streamwise

coordinate is transformed to the structure fixed coordinate  $\chi$ . The distributions show self similarity for the three cases, except around the wall wire where probe interference affects the correlation for zero time delay (figure 4(a)). At  $y = 2.6$ , the correlation maximum occur at  $\chi = 0$  due to the definition of  $\chi$ . The height, width and length of the structure thus scales as  $\delta$ , *i.e.* with the boundary layer thickness and therefore the structure inclination angle becomes constant with this scaling (and in the physical coordinates).

The correlation structures shown in figure 4 are seen to extend above  $y = 6$ . This is probably because the boundary layer gets “corrugated”, *i.e.* locally, the boundary layer thickness varies with the disturbance in it. The boundary layer thickens due to low velocity disturbances and get thinner due to high speed disturbances in a manner similar to boundary layers in which cross-flow or Görtler vortices are present.

In figure 4(c), an example of the boundary-layer velocity profile and the normalized disturbance profile is shown. The velocity profile is seen to agree well with the Blasius boundary-layer solution. The disturbance profile is found to be zero at the wall, have a maximum around  $y = 2.6$  and approach the level of the free-stream turbulence further out.

In figure 5, correlations at the reference height  $y = 2.6$  obtained for all parameter values studied: five wall-wire positions, two free-stream turbulence levels and three  $\tau$  values, are presented. The total number of correlation traces is 21 (for  $Tu = 1.1\%$ , the measurements were only performed for  $x_{ww}^* = 214$  and 484 mm). Using physical units, as shown in (a), the width for which the correlations drop to zero vary from 0.15 to 0.4 m. If scaled by  $\delta(x_{ref}^*)$  (where  $x_{ref}^*$  is determined individually for each of the correlation traces), it is seen that the correlations collapse in (b). The streamwise width of the structures in the boundary layer is thus seen to scale as  $(x^*)^{0.5}$ .

Defining the width,  $\mathcal{W}^*$ , as the streamwise length, for which the normalized correlation at  $y = 2.6$  is larger than 0.5, the result from figure 5 can be quantified. In figure 6(a) and (b),  $\mathcal{W}^*$  and  $\mathcal{W} = \mathcal{W}^*/\delta(x_{ref}^*)$  are shown as functions of downstream position. The dimensional data in (a) is seen to follow the curve  $\mathcal{W}^* = 0.32(x_{ref}^*)^{0.5}$  fairly well. If non-dimensionalized, this curve transforms to  $\mathcal{W} = 183$ . In figure 6(b), the non-dimensional  $\mathcal{W}$  is seen to be around this value for all  $x^*$ .

Thus, having established the scaling of the structures, the 21 correlation structures (out of which three are shown in figure 4) can be averaged. The result of such an averaging is shown in figure 7(a). Before averaging, the amplitude of each correlation has been normalized with its maximum value. The resulting mean structure is very similar to the samples of individual structures seen in figure 4, further demonstrating the self similarity of the structures. The mean structure is seen to be very long (note the scales, the figure has to be stretched

Scaling of streaks in boundary layers subjected to FST

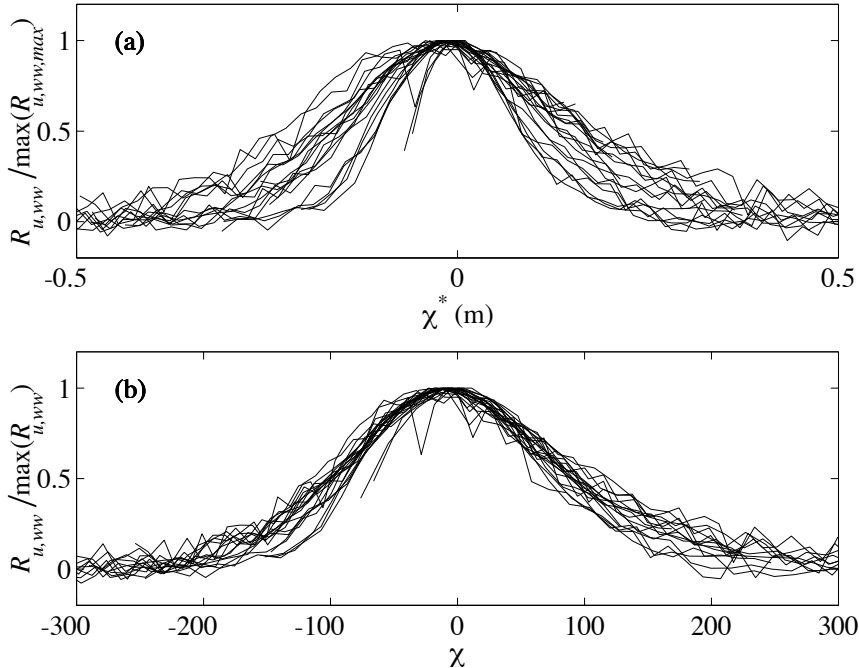


FIGURE 5. Normalized correlations as a function of the structure-following coordinate  $\chi^*$  at  $y = 2.6$ ; (a) dimensional  $\chi^*$ , (b) nondimensional  $\chi$  scaled by  $\delta(x_{ref}^*)$ .

22 times in the horizontal direction in order to obtain the physical aspect ratio) and inclined through the boundary layer.

In figure 7(b), the propagation speed along constant  $y$  of the correlation maxima,  $U_{struc}$ , at various  $y$  is shown and compared to the Blasius profile of the mean flow. The markers are for different  $x_{ww}^*$  and the trend is that the propagation speed of the structure varies less throughout the boundary layer further downstream. At  $y = 2.6 \pm 0.2$ ,  $U_{struc}$  is seen to be close to constant at all  $x_{ww}^*$  and  $Tu$ . In addition, the constant velocity seem to agree with the local mean velocity of the flow. This vertical position ( $y = 2.6$ ) is close to the position of maximum  $u_{rms}$ .

The variation of  $U_{struc}$  through the boundary layer and with the streamwise position is understood by the analysis in section 3, leading to equation (11). From the measured values of  $U_{struc}$  in figure 7(b), the parameters  $U_{struc}(x^*, 0)$  and  $f(x^*)$  in equation (11) can be determined by curve fitting. The resulting parameters are shown in figure 8. In figure 8(a), it is seen that the expected relation  $f \sim (x^*)^{-0.5}$  is fulfilled. Also, the numerical values of  $f$  turn out to be

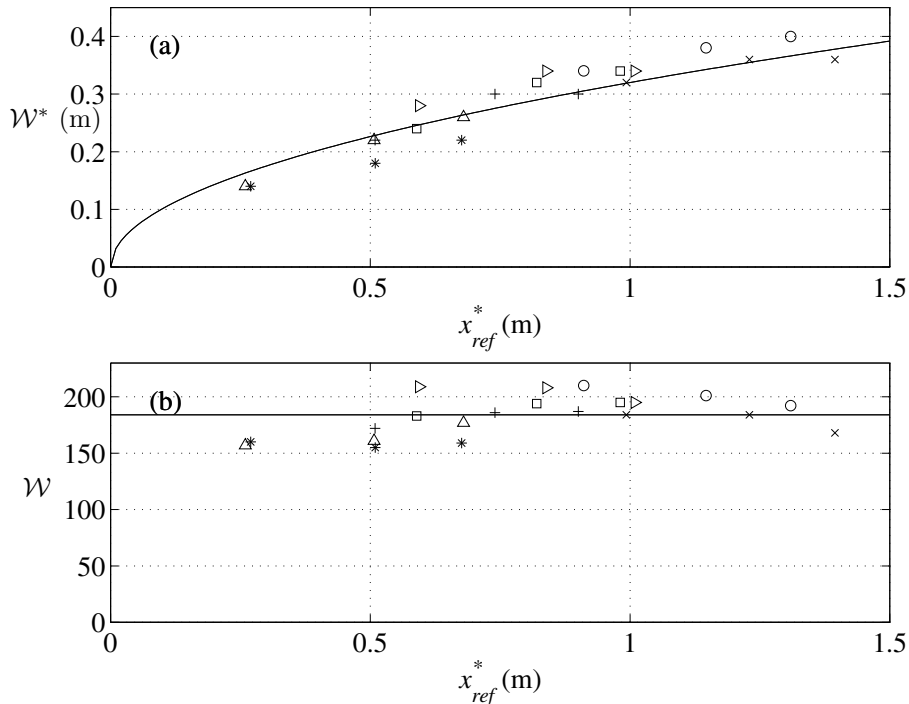


FIGURE 6. Streamwise extent during which the velocity–shear stress correlation  $R_{u,ww}(x^*, 2.6, \tau; x_{ww}^*)$  is over 50 % of its maximum value, (a) physical scaling, (b) nondimensional scaling according to equation (4.3). Symbols are  $Tu=1.8\%$ ,  $x_{ww}^*=214$  (\*), 414 (+), 484(□), 764(○), 834 mm (×) and  $Tu=1.1\%$ ,  $x_{ww}^*=214$  (△), 484 mm (▷). For each symbol,  $\tau$  is 0, 58 and 99 ms increasing downstream. For curve and line see text.

small, allowing a series expansion of equation (11) around  $y = 0$ . In the series expansion, the variation of the propagation speed with  $y$  turn out to be close to linear, which is also seen in figure 7(b).

Furthermore, in figure 8(b) the measured speed of the structure close to the wall,  $U_{struc}(x^*, 0)$ , shown with the markers, is seen to increase with  $x^*$ . The curve is obtained from equation (11) assuming that there is a height,  $y_c$ , at which the speed of the structure is constant ( $U_c$ ) for all  $x^*$ . With these assumptions,  $U_{struc}(x^*, y = 0)$  is obtained as  $U_c \exp[-y_c f(x^*)]$ . The values chosen in the figure are  $y_c = 2.6$  (the position where the propagation speed equals the mean flow velocity) and  $U_c = 0.81$  (the mean flow velocity at  $y =$

*Scaling of streaks in boundary layers subjected to FST*

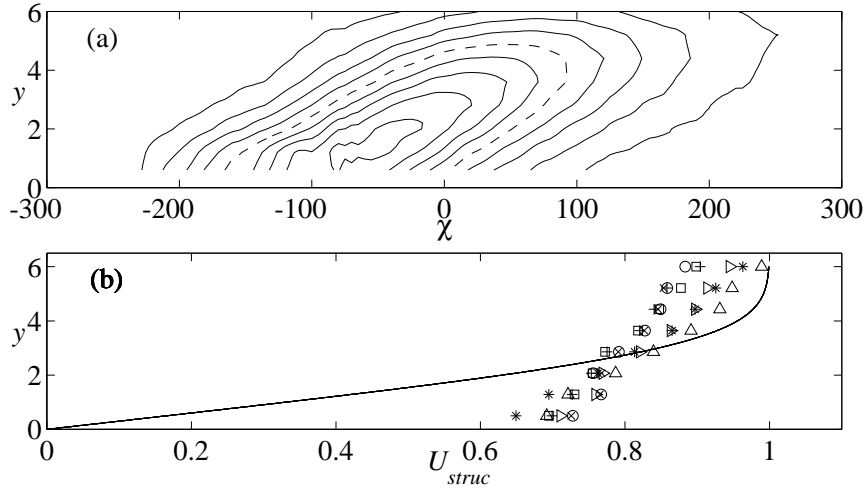


FIGURE 7. Mean correlation distribution in (a) and structure propagation speed for different  $x_{ww}^*$  and  $Tu$  in (b). The contour levels in (a) are 0.1, 0.2,  $\dots$ , 0.9 and the dashed contour is 0.5. The symbols in (b) refer to the same parameter values as in figure 6 and the solid line is the Blasius solution.

2.6). The results are consistent with the  $(x^*)^{0.5}$  scaling and equation (11) together with the assumption of a constant velocity (equal to the mean flow velocity) close to  $y_c = 2.6$ .

## 5. Conclusions

The streamwise correlation between the velocity in the boundary layer and the wall-shear stress at a fixed position was measured by a wall wire and a hot wire traversed in the boundary layer. The correlations were obtained for five wall-wire positions, two levels of the free-stream turbulence and three time delays between the signals.

The correlation structure was found to:

- i)* be self similar in the coordinates  $(\chi, y)$ , where  $\chi$  is the streamwise coordinate translated to the streamwise position of maximum correlation at  $y = 2.6$ , denoted  $x_{ref}^*$ , and scaled by  $\delta(x_{ref}^*)$  and
- ii)* propagate downstream with a constant speed along non-dimensional  $y = 2.6$ ; the constant velocity was found to be around  $0.81U_\infty$ .

At first thought, it might seem contradictory that the propagation speed of the structures varies through the boundary layer, while the slope is constant. The solution to this apparent contradiction is the *streamwise* variation of the

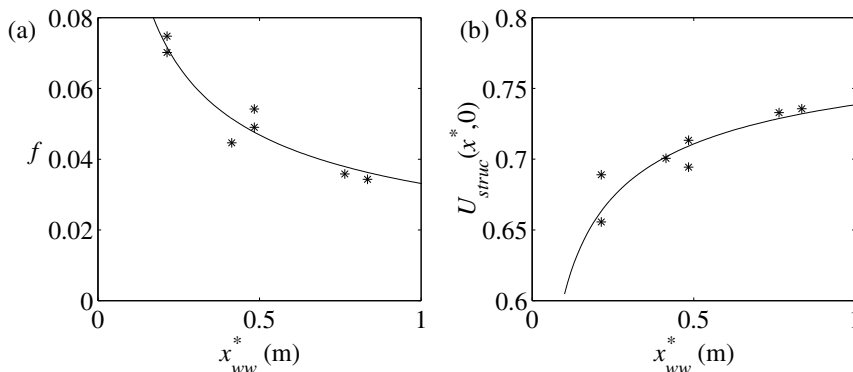


FIGURE 8. The function  $f(x^*)$  from equation (11) in (a) and  $U_{struc}(x^*, 0)$  in (b) as functions of the wall-wire position  $x_{ww}^*$ . The curve in (a) is  $f(x^*) = 0.033(x^*)^{-0.5}$ . The curve in (b) is  $U_{struc}(x^*, 0) = U_c \exp[-y_c f(x^*)]$  with  $U_c = 0.81$  and  $y_c = 2.6$ .

propagation speed (illustrated in figure 8(b)) and the wall-normal growth of the structure.

The variation of the propagation speed with the streamwise and the non-dimensional wall-normal position was derived from a simple kinematical model and found to agree with the measurements. At  $y = 2.6 \pm 0.2$ , the propagation speed of the correlation structure agrees with the local mean velocity. This position is very close to the position of maximum  $u_{rms}$ .

In short, it has been found that the length of the high and low velocity streaks appearing in a boundary layer subjected to free-stream turbulence grows as the boundary-layer thickness. This confirms the results of Matsubara & Alfredsson (2001), who draw the same conclusion using Taylors' hypothesis and scaled frequency spectra.

### Acknowledgment

Marcus Gällstedt and Ulf Landén are acknowledged for manufacturing parts of the setup. Jens Fransson and Junichiro Shiomi are acknowledged for discussions and reading of the manuscript. Economical support has been received from the Swedish Research Council.

## References

- ALFREDSSON, P. H. & MATSUBARA, M. 2000 Free-stream turbulence, streaky structures and transition in boundary layer flows. *AIAA-paper 2000-2534*.
- ANDERSSON, P., BERGGREN, M. & HENNINGSON, D. S. 1999 Optimal disturbances and bypass transition in boundary layers. *Phys. Fluids* **11**, 134–150.
- JACOBS, R. G. & DURBIN, P. A. 2001 Simulations of bypass transition. *J. Fluid Mech.* **428**, 185–212.
- KENDALL, J. M. 1998 Experiments on boundary-layer receptivity to freestream turbulence. *AIAA-paper 98-0530*.
- LANDAHL, M. T. 1990 On sublayer streaks. *J. Fluid Mech.* **212**, 593–614.
- LUCHINI, P. 1996 Reynolds-number-independent instability of the boundary layer over a flat surface. *J. Fluid Mech.* **327**, 101–115.
- LUCHINI, P. 2000 Reynolds number independent instability of the boundary layer over a flat surface: optimal perturbations. *J. Fluid Mech.* **404**, 289–309.
- MATSUBARA, M. & ALFREDSSON, P. H. 2001 Disturbance growth in boundary layers subjected to free stream turbulence. *J. Fluid Mech.* **430**, 149–168.
- WESTIN, K. J. A., BAKCHINOV, A. A., KOZLOV, V. V. & ALFREDSSON, P. H. 1998 Experiments on localized disturbances in a flat boundary layer. Part 1. The receptivity and evolution of a localized free stream disturbance. *Eur. J. Mech. B/Fluids* **17**, 823–846.



Paper 3

**P3**



# Streak oscillations of finite length: disturbance evolution and growth

By **Fredrik Lundell**

KTH Mechanics, 100 44 Stockholm, Sweden

Secondary instabilities of velocity streaks are studied in a plane channel flow. At first, the secondary instability is forced by a random signal, creating wave packets of various frequencies and durations. Thereafter, the secondary instability is forced by a sinusoidal signal consisting of  $N$  periods, where  $N$  ranges from 0.5 to 30. It is found that the disturbance distribution of the secondary instability is similar to distributions previously obtained for streaks forced by infinitely long wave trains. The growth of the *localized* secondary instabilities studied in the present work is found to be exponential but the growth rate is smaller for short ( $N < 3.5$ ) wave packets as compared to infinite wave trains. During the breakdown process, incipient spots are formed. At this point, the finite disturbances have a non-periodic three-dimensional distribution.

---

## 1. Introduction

It is known from flow visualizations and measurements (Kendall 1998; Matsubara & Alfredsson 2001) that if the turbulence level outside a boundary layer is large, laminar-turbulent transition might be preceded by the formation and growth of streamwise streaks with alternating high and low velocity. The growth mechanism for such streaks is so called *transient growth*, studied theoretically by Ellingsen & Palm (1975), Landahl (1980), Butler & Farrell (1992), Luchini (2000) and Andersson, Berggren & Henningson (1999). Further downstream, breakdown occurs due to wave-like secondary instabilities of the streaks. For a Blasius boundary layer, this transition scenario is dominant for Free-Stream Turbulence (FST) levels ranging from about 1% to 7%. With lower disturbance levels, T-S waves interact with the streaks giving a more complex transition scenario. With higher disturbance levels turbulent spots can be produced directly by disturbances injected locally in the boundary layer by the free-stream turbulence.

The secondary instability scenario sketched above is not the only candidate for the breakdown. From the data of a direct numerical simulation, Jacobs & Durbin (2001) found that the breakdown was triggered by small scale disturbances in the free stream interacting with low-speed streaks in the boundary layer. Fasel (2002) speculated that oblique T-S waves are the source of high frequency disturbances.

The flow visualizations of transition induced by FST by Matsubara & Alfredsson (2001) clearly show the appearance of anti-symmetric secondary instabilities acting on the low-velocity streaks. This agrees with the theoretical analysis of Andersson, Brandt & Henningson (2001), who found that a low-speed streak generated in a Blasius boundary layer by the optimal disturbance is subject to an anti-symmetric instability. Asai, Minagawa & Nishioka (2002) performed a controlled experiment, in which the secondary instability of low-speed streaks was studied. The streaks were generated by small fences on a flat plate in a Blasius boundary layer and disturbed with speakers through holes. The spanwise width of the streak was varied and it was found that the most unstable mode varies with the width. Wide streaks are more susceptible to the symmetric mode while narrow streaks are more susceptible to the anti-symmetric mode.

Elofsson, Kawakami & Alfredsson (1999) did measurements in the same channel-flow apparatus as the one used in the present study. They generated streaks and forced the secondary instability by earphones. It was found that in the channel, the dominant mode of the secondary instability was the anti-symmetric one. It was also found that the growth of the secondary instability was linearly related to the peak-to-peak amplitude of the streaks. The cross-flow distribution of the secondary disturbance consisted of two peaks, positioned symmetrically around the low-speed streak in the spanwise direction. The wall-normal maximum of the disturbance was located slightly above the centre of the channel.

Instabilities of velocity streaks are of interest not only in the study of transition induced by free-stream turbulence. Görtler vortices break down due to secondary instabilities, see *e.g.* Saric (1994) or Bottaro & Klingmann (1996). As a Görtler vortex develops downstream, the most unstable mode can change from one symmetry to the other. Also, the pressure gradient affects the preferred mode. Secondary instabilities of “velocity streaks” also appear in the analysis of breakdown to turbulence of cross-flow vortices. An example is Malik, Choudarhi & Chang (1999) who used linear stability analysis and predicted the frequencies and growth measured in experiments by Kohama, Onodera & Egami (1996) correctly. As opposed to the streaks of the present study, streaks generated from a linearly unstable vortex change rapidly downstream, an effect complicating the analysis.

### *Streak oscillations of finite length: disturbance evolution and growth*

The process sketched above: growth of streamwise streaks followed by the amplification of secondary instabilities and finally breakdown, has been proposed to be a vital ingredient in the process of growth and bursting of streaks in turbulent, wall-bounded shear flow by Waleffe (1995). Hamilton, Kim & Waleffe (1995) observed this cycle in a DNS data base of low Reynolds number turbulent flow. In a recent paper based on DNS studies and stability calculations, Schoppa & Hussain (2002) report that the secondary instability of near-wall streaks in wall-bounded turbulence can be subject to transient growth.

All experiments and theory cited above have investigated infinitely long wave trains. In a real boundary layer undergoing transition, flow visualizations indicate that the secondary disturbances occurring naturally are limited to a duration of a few periods. In the present work, a forcing which simulates a turbulent free stream affecting streaks in a laminar boundary layer has been used to disturb streaks in a laminar flow. This leads to localized, secondary disturbances developing on the streaks, which then can be studied in detail. Furthermore the present paper also presents results regarding a one frequency disturbance of limited length. The experiments have been performed in the apparatus also used by Elofsson *et al.* (1999). The similarities (disturbance distribution) and differences (disturbance growth) between an infinite wave train and a finite wave packet are extracted and elucidated.

In section 2, the experimental setup is described. The results are presented in section 3 and 4. In section 3, the streaks are forced by a random signal and in section 4m they are forced by a signal with a predetermined number of wavelengths. The conclusions are summarized in section 5.

## **2. Material and methods**

### *2.1. Flow apparatus and streak generation*

The flow apparatus (figure 1), is a plane channel, consisting of two glass plates separated by 8.2 mm thick aluminum bars. The air is blown through the channel by a centrifugal fan. Before entering the channel region, the air passes a silencer, a stagnation chamber with two turbulence damping screens and finally a plane contraction. The aspect ratio of the channel is 1:100 and the first instrumental plug is positioned 95 channel heights downstream of the channel inlet.

Five laminar streamwise velocity streaks are generated by applying suction through streamwise slots at one of the channel walls. Close to the generation, the streaks grow rapidly and reach a maximum amplitude, whereupon they decay slowly downstream. The spanwise wavelength of the streaks is 15 mm (3.7*h*). The same width was used by Elofsson *et al.* (1999).

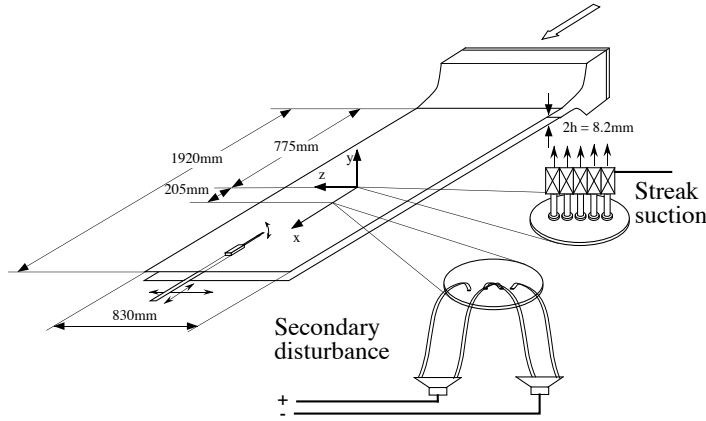


FIGURE 1. Experimental setup.

The streamwise velocity in the channel is measured by a single hot wire which can be traversed to any point in the flow field. The hot wire was calibrated against a total pressure tube utilizing the parabolic velocity profile. The coordinates are  $x$ ,  $y$  and  $z$  for the streamwise, wall-normal and spanwise direction, respectively. All lengths are normalized with the half-channel height  $h$  (4.1 mm) and the origin is positioned at the centre of the channel. The spanwise position of the origin is at the centre of a low-velocity streak; the streamwise position of the origin is at the position of streak generation. The velocity is decomposed into a mean,  $U$ , and a fluctuating part,  $u$ . In the present work,  $u$  denotes the fluctuation after ensemble averaging. The fluctuation of each realization is denoted  $u_k$ . All velocities are normalized with the centreline velocity,  $U_{CL}$ .

## 2.2. Streak characteristics

The streaks generated by suction through the streamwise slots persist throughout the channel as seen in figure 2, where the variation of the mean velocity in the  $xz$ -plane at  $y = 0.36$  is shown (the position is approximately one third towards the upper wall from the channel centre). This  $y$ -position is shown since the secondary instability has its maximum amplitude at this height (will be demonstrated later). The contours in the figure show the velocity after subtraction of the spanwise mean at each  $x$ . The peak-to-peak amplitude ( $\Delta U$ ) is approximately 55% of the centreline velocity,  $U_{CL}$ , and the streaks persist throughout the test section. In figure 2, three lines mark the centre part of the area at  $x = 88$ , 112 and 161. These regions will be used as example regions throughout the paper.

*Streak oscillations of finite length: disturbance evolution and growth*

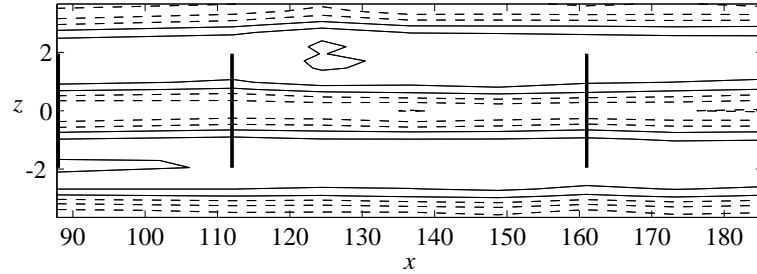


FIGURE 2. Mean flow variation in the  $xz$ -plane at  $y = 0.36$ . Contour levels are 10% of the centreline velocity,  $U_{CL}$ , and negative contours are dashed. The thick solid lines show the position of the data presented in figures 3, 6 and 10.

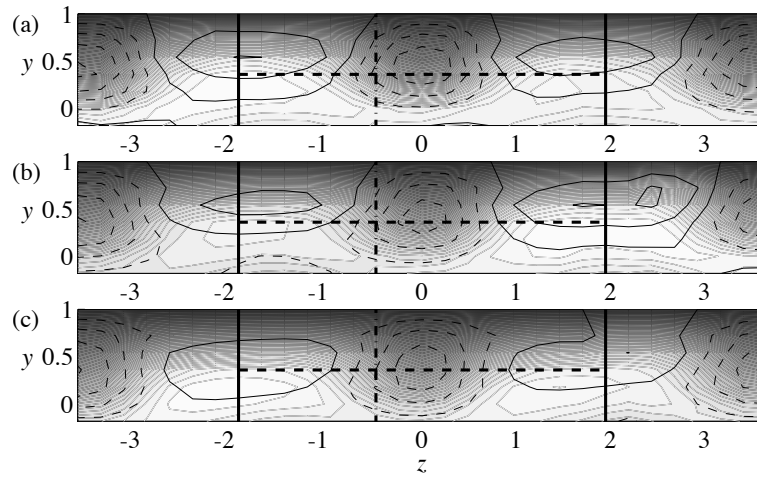


FIGURE 3. Mean flow deviation from the parabolic velocity profile (contours) and mean flow (gray scale) in the upper half of the channel at (a)  $x = 88$ , (b) 112 and (c) 161. Contour lines are 10% of  $U_{CL}$  and negative contours are dashed. For the gray scale, black is 0 and white is  $U_{CL}$ . The lines indicate the areas studied in figures 4–10.

The cross-stream ( $yz$ ) distributions of the streaks at  $x = 88, 112$  and  $161$  are shown in figure 3. Note that  $y = 0$  and  $1$  correspond to the centre and upper wall of the channel, respectively, *i.e.* only the upper half of the channel is shown. The gray scale shows the absolute velocity, black denotes zero and light gray is the maximum velocity. To be able to show the velocity distribution up

to the wall at  $y = 1$ , the velocity was interpolated to zero at the wall. The measurements extend to  $y = 0.75$ . The contours in figure 3 show the deviation from the laminar (parabolic) velocity profile. The low-speed streaks are seen as the regions of negative (dashed) velocity defect and in between them, high-speed streaks (the positive, solid, peaks) are situated. The straight bold lines in figure 3 show the regions and cuts from which the example disturbance in figures 4–9 are shown.

The random forcing experiments are a spin-off from a control experiment. In order for the control experiment to work properly, the velocity had to be fairly high, 13.5 m/s, giving a Reynolds number  $Re = U_{CL}h/\nu$  of 3600. In the definition of the Reynolds number,  $\nu$  is the kinematical viscosity of the air. For the subsequent measurements with a controlled forcing the velocity was lower, 10.9 m/s ( $Re = 2900$ ) in order to be comparable to what was used by Elofsson *et al.* (1999). The streak amplitude and spacing was however similar during the two experiments. The streaks shown in figures 2 and 3 originate from the random forcing experiments.

The streak amplitudes of the present work are not directly comparable with those of Elofsson *et al.* (1999). They measured the streak development from generation to downstream decay and defined the streak amplitude as the maximum spanwise peak-to-peak velocity difference occurring at some  $x$ -position. With the current forcing system, it was not possible to measure as far upstream as the streak generation. The amplitude used in the present measurements, 55% at  $x = 88$ , corresponds to  $\Delta U_{max} = 71\text{--}74\%$  in Elofsson *et al.* (1999). With this streak amplitude, the maximum growth factor (varies with frequency) of the secondary instability was around 0.02 in their experiment.

### 2.3. "Random" forcing of the secondary instability

The disturbance generation of the random disturbance experiments reported in section 3 is inspired by the experiment of Shaikh (1997), who generated Tollmien-Schlichting (T-S) wave packets in a boundary layer using a random signal connected to a speaker to produce perturbations through a hole in the plate. Repeated measurements using the same disturbance signal and ensemble averaging made it possible to study repeated and non-repeated features of the boundary layer response to the forcing.

During the random forcing experiments of the present work, the secondary instability of the streaks was forced through spanwise slots. PVC-tubes connected the slots to speakers, which were driven by a known white-noise sequence, digitally bandpass filtered in a suitable frequency band (100–500 Hz). Two speakers, driven with the original and inverted signal, respectively, were used. By connecting tubes from the two speakers to different slots, symmetric and anti-symmetric modes of the secondary instability could be forced. In the present setup, anti-symmetric disturbances grow much faster than symmetric

### *Streak oscillations of finite length: disturbance evolution and growth*

ones. The streamwise position of the secondary forcing is at  $x = 50$  (*i.e.*  $50h$  downstream of the streak generation).

#### *2.4. Controlled forcing of the secondary instability*

For the controlled disturbance experiments, the secondary instability of the central streak was forced by two earphones. The earphones were positioned symmetrically over the low-speed streak under study at  $x = 50$ ,  $z = \pm 1.2$ . The forcing signal was a harmonic oscillation,  $\sin(2\pi ft)$ , for  $0 < t < N/f$  and zero elsewhere. The two earphones were driven with signals of opposite sign. The parameter  $N$  is the number of periods to be generated and the frequency  $f$  was chosen to be the frequency giving the largest growth of the disturbance if the streak was forced by an infinite wave train.

### **3. Random forcing results**

During the experiments with random forcing of the secondary instability, measurements were performed at 9 streamwise, 7 vertical and 31 spanwise positions. At each position, the disturbance sequence was run 30 times whereupon ensemble averaging was used in order to investigate repeated features of the response of the flow. The amplitude of the secondary instability forcing was chosen so that a few (3-7) turbulent spots appeared at the most downstream measurement positions during one realization of the disturbance sequence.

First, the growth and initial breakdown of a single wave packet, generated by the random forcing, will be studied in figures 4-9. Thereafter, the frequency, propagation velocity and growth of all the wave packets identified in the measurements will be extracted from the data and presented.

#### *3.1. An example disturbance*

The fluctuation of the ensemble-averaged velocity signal from  $x = 112$ ,  $y = 0.36$  and  $z = -0.49$  is shown in figure 4. In (a), the full, 1.2 s long sequence is shown. In this sequence, quite a few strong oscillations of the velocity are seen, especially around  $t = 300$  ms and  $t = 750$  ms. It is seen in (b) (where the time axis is zoomed around  $t = 300$  ms), that the high amplitude oscillations are of various lengths: some consist of one or two periods only, while others persist for seven periods or more. The frequency inside different wave packets varies only with  $\pm 20\%$ . In (c) and (d) the zooming in continues, finally showing a single wave packet, which will be studied in more detail in the following.

In figure 5, the 30 individual realizations from three  $x$ -positions,  $x = 88$ , 112 and 161, of this wave packet are shown. The traces originate from the point where the secondary instability is found to reach its maximum amplitude, *i.e.*  $(y, z) = (0.36, -0.49)$ . Note that the vertical scale changes, as the wave packet grow in amplitude downstream. It is seen that the offset level of the traces varies slightly (approximately  $\pm 0.7\%$  of  $U_{CL}$ ) around the mean value. The

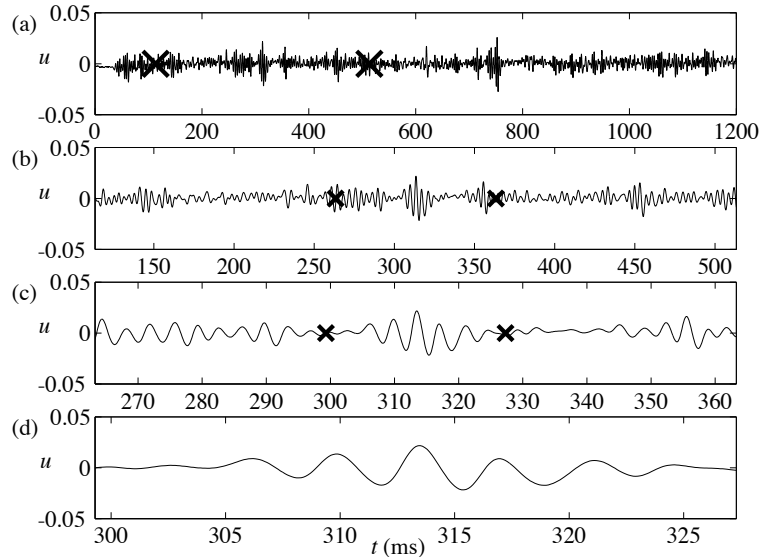


FIGURE 4. Ensemble-averaged velocity signal from  $x = 112$ ,  $y = 0.36$  and  $z = -0.49$ . In (a) the complete sequence is shown whereas (b–d) zoom in on the period marked with crosses in the plot above.

oscillation is due to the large values of  $\partial U/\partial y$  and  $\partial U/\partial z$  at the position of the hot wire: a small, low frequency meandering of the streaks thus gives a fairly large amplitude oscillation in  $u$ . Apart from this variation of the zero level, the traces at the two most upstream positions in figure 5(a) and (b) show small variations over the realizations. The wave packet is seen to grow in amplitude from (a) to (b), but there are five distinguishable peaks at both positions. There is no indication of temporal elongation of the disturbance from  $x = 88$  to  $x = 112$ . Further downstream, as shown in figure 5(c), the later (upstream) parts of the disturbance turn into more irregular and non-repeated oscillations. However, even if the traces in figure 5(c) show a non-repeated behaviour for  $t > 333$  ms, the initial oscillations are repeated for all the traces. The non-repeated features are due to the non-linear development of an incipient spot (frequency mixing eventually leading to turbulence).

The spanwise structure of the wave packet is shown in figure 6. Contours of the streamwise velocity is shown as contours in the  $zt$ -plane. Again, the data are taken from  $x = 88$ , 112 and 161 in (a) through (c). At all three positions, the asymmetrical nature of the disturbance is seen: a high velocity (solid) peak at one side is mirrored by a low velocity (dashed) valley on the other side. At the two upstream positions, the distributions are very similar: five peaks along

*Streak oscillations of finite length: disturbance evolution and growth*

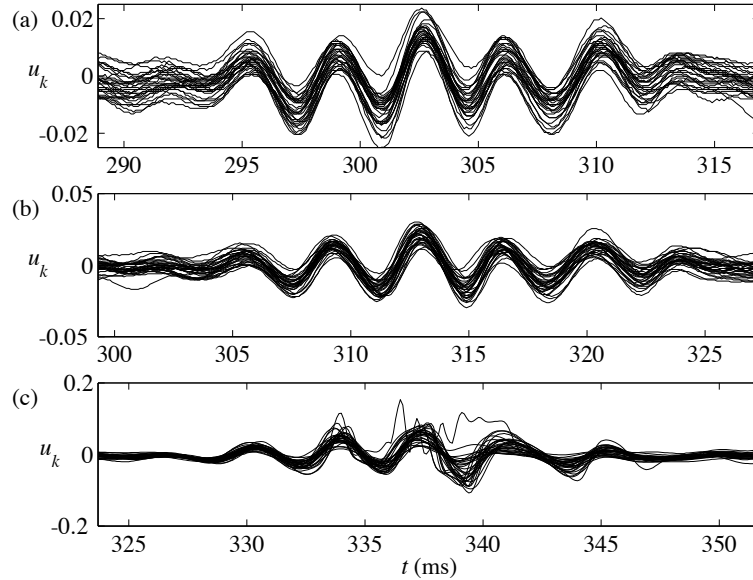


FIGURE 5. Raw signals before ensemble averaging at  $y = 0.36$ ,  $z = -0.49$  and (a)  $x = 88$ , (b) 112 and (c) 161. The traces in (b) are the ones averaged in figure 4(d).

lines of constant  $z = \pm 0.49$ . The peaks are stretched so that the disturbance reaches the hot wire earlier further out from the centre of the low velocity streak at  $z = 0$ , this gives the regions of disturbed velocity an angle to the spanwise direction. Finally, it is seen that at  $x = 161$  (figure 6(c)), the relative amplitude of the central peak at  $t = 337$  ms to the others has increased, as compared to the upstream distributions in (a) and (b) (see around  $t = 302$  and 311 ms, respectively).

The vertical disturbance distributions from the spanwise position at which the secondary instability shows its maximum value ( $z = -0.49$ ) are shown in figure 7. The stretching due to the mean-velocity gradient is seen here as well: at the centre of the channel ( $y = 0$ ), where the velocity is larger, each peak and valley reach the hot wire earlier as compared to closer to the wall ( $y = 1$ ). For the rest, the distributions show the same features as before: amplitude growth from  $x = 88$  (a) to  $x = 112$  (b) and thereafter a more radical change until  $x = 161$  (c). In (c), there is a large high velocity tail close to the wall, again a part of the development of the incipient spot. Such a feature would not be seen if the streak was forced by an infinite wave train. In that case, a turbulent wedge is formed rather than individual incipient spots.

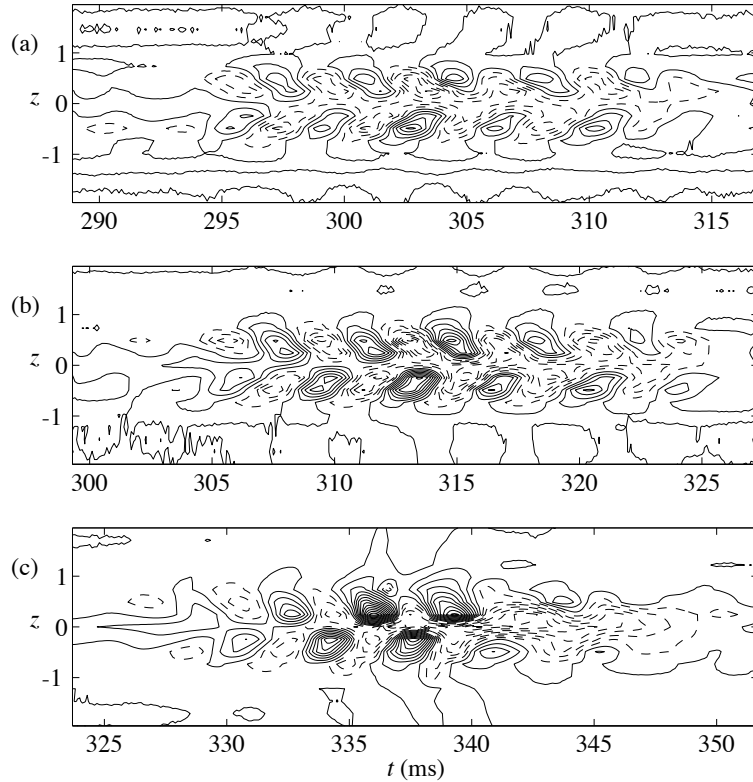


FIGURE 6. Ensemble-averaged disturbance velocity  $u$  at  $y = 0.36$  and (a)  $x = 88$ , (b)  $112$  and (c)  $161$ . Contour levels are (a, b)  $0.3\%$  and (c)  $1\%$  of  $U_{CL}$ . Negative contours are dashed. To get a physical aspect ratio of the figure, the time axis has to be stretched by a factor of three.

The change from an amplified wave packet to an incipient spot is even more dramatic if the energy of the disturbance is studied in the  $yz$ -plane. This is done in figure 8 where the distributions are shown as contours. At each spatial point  $(y, z)$ , the energy ( $u^2$ ) is integrated in time over the duration of the wave packet. In each diagram, the maximum amplitude of  $u$  is indicated as a percentage of  $U_{CL}$ . The two upstream positions in figure 8(a) and (b) show the typical distribution for an asymmetric mode of a velocity streak (created by transient growth or an exponentially growing vortex) subjected to a continuous disturbance: two peaks at the positions of maximum spanwise shear. Such distributions have been obtained experimentally by *e.g.* Matsubara & Alfredsson (1998) (rotating channel flow), Elofsson *et al.* (1999) (streaks in the

*Streak oscillations of finite length: disturbance evolution and growth*

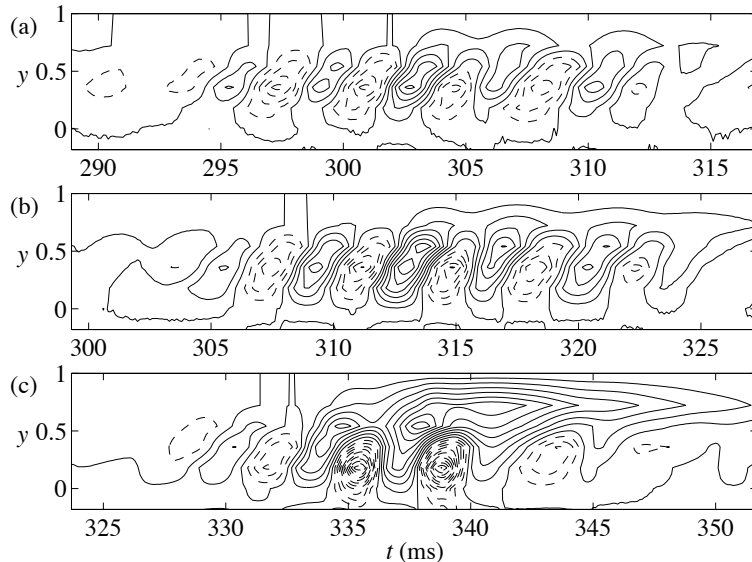


FIGURE 7. Ensemble-averaged disturbance velocity  $u$  at  $z = -0.49$  and (a)  $x = 88$ , (b) 112 and (c) 161. Contour levels are (a, b) 0.3% and (c) 1% of  $U_{CL}$ . Negative contours are dashed. A physical aspect ratio of the distribution is achieved by stretching the time axis a factor of eight.

present channel) and Asai *et al.* (2002) (streaks in a Blasius boundary layer) and theoretically by Reddy *et al.* (1998) (theory and DNS of streaks in plane channel flow), Andersson *et al.* (2001) (theory on optimal streaks in a Blasius boundary layer). Further downstream, during the breakdown, energy maxima are found at three positions: the first being at the centre of both the channel ( $y = 0$ ) and the streak ( $z = 0$ ) and the two others are close to the wall symmetrically around the centre of the streak.

The change in energy distribution from  $x = 112$  to  $x = 161$  is mainly due to low frequency modifications of the flow. This is demonstrated in figure 9, where the individual traces from the two peaks appearing at the most downstream position,  $x = 161$  (the crosses in figure 8(c)), are shown. In figure 9(a) the 30 velocity traces from the position of the left cross in figure 8(c) are shown. The high value of the energy arises from a low frequency acceleration of the flow. In all except one of the traces, no high frequency oscillations are present. In figure 9(b) the realizations at the position of the central cross in figure 8(c) are shown. It is seen that in the centre, the disturbance energy is partly originating from a low frequency oscillation and partly due to multi-frequency quick oscillations. Interestingly, the point of strongest acceleration is not the

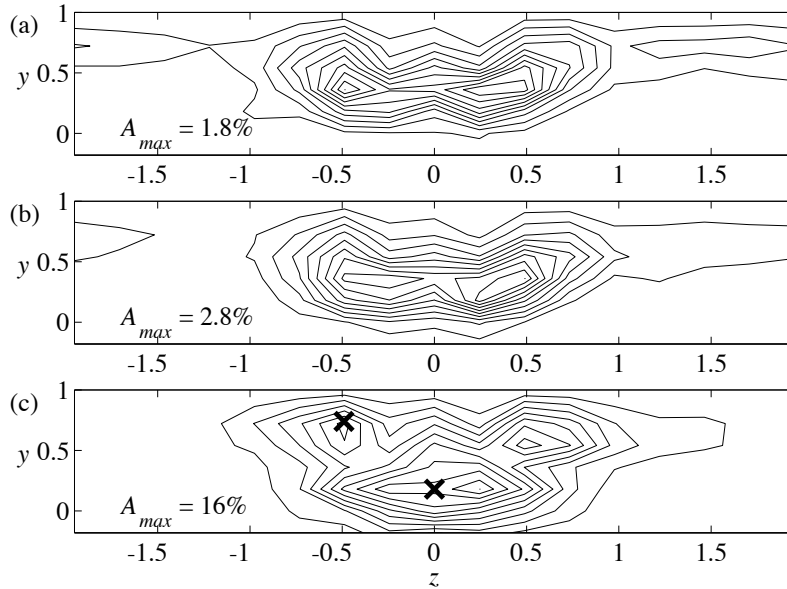


FIGURE 8. Distribution of disturbance energy at (a)  $x = 88$ , (b) 112 and (c) 161. Contour levels are 10 % of the total energy in each figure. The maximum amplitude of  $u$  is indicated in each figure.

point of lowest velocity deviation (the centre of the streak) but merely two positions close to the wall on the streak flanks. The strong velocity deviations also appear spatially and temporally separated from the strong oscillations seen at  $x = 161$  in figure 5(c).

### 3.2. Disturbance properties and their variation

Having studied a single wave packet in some detail and found that the disturbance distributions agree with what have been reported for endless wave trains, 13 wave packets will be extracted and analyzed from the data.

In order to detect the wave packets, the local variance  $\text{Var}(x, t; \Delta t)$ , defined as:

$$\text{Var}(t, x; \Delta t) = \max_{y,z} \left[ \frac{1}{\Delta t} \int_{t-\Delta t/2}^{t+\Delta t/2} u^2(t, x, y, z) dt \right], \quad (1)$$

is used. In the present case, an integration time  $\Delta t$  of 16 ms was the shortest giving a single, well-defined peak for each wave packet. This definition of the local variance is somewhat different from the definition of Blackwelder & Kaplan (1976), where the instantaneous mean is subtracted in the integrand.

*Streak oscillations of finite length: disturbance evolution and growth*

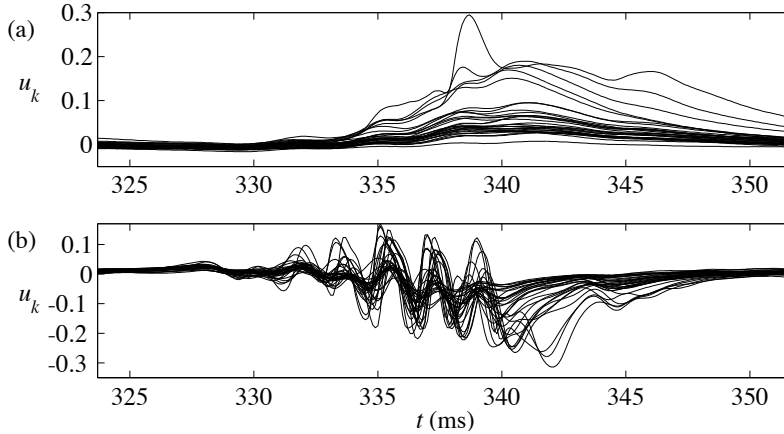


FIGURE 9. Velocity traces at  $x = 161$  from the positions marked with crosses in figure 6. The position is (a)  $y = 0.74$ ,  $z = -0.49$  and (b)  $y = 0.18$ ,  $z = 0$ .

In the present case, the high frequency oscillations appear around the overall mean value, why the definition above is sufficient to capture high frequency activity.

The temporal development of  $\text{Var}(x, t; 16 \text{ ms})$  at  $x = 88$ ,  $112$  and  $161$  is shown in figure 10. The example disturbance studied above in figures 4–9 occurs at  $t \approx 320 \text{ ms}$  and is marked with a cross. In figure 10(a), it is seen that the local variance exhibits distinguishable maxima at certain times. Further downstream (figure 10(b)) the energy of these peaks increase while the relative amplitude of the background noise decreases (note the change of the vertical axis). Also, the amplification varies from peak to peak; their relative amplitude is not constant. At the most downstream position, shown in (c), the local variance is dominated by two peaks, corresponding to the wave packet studied above and a later, even stronger, disturbance. Upon comparing the three traces in figure 10, it is seen that the peaks arrive at later times at the more downstream position. However, there is no difficulty to identify peaks corresponding to the same disturbance at the three positions.

For the 13 most pronounced peaks in  $\text{Var}(x, t; 16 \text{ ms})$ , the properties defined below were extracted. The disturbances are indexed by the subscript  $i$ . The properties are:

- time of occurrence,  $t_i(x)$ , defined as the time at which the local maximum of  $\text{Var}(x, t; 16 \text{ ms})$  occurs.
- amplitude  $A_i(x)$ , defined as the local maxima of  $\text{Var}$ , *i.e.*  $A_i(x) = \text{Var}(x, t_i(x); 16 \text{ ms})$

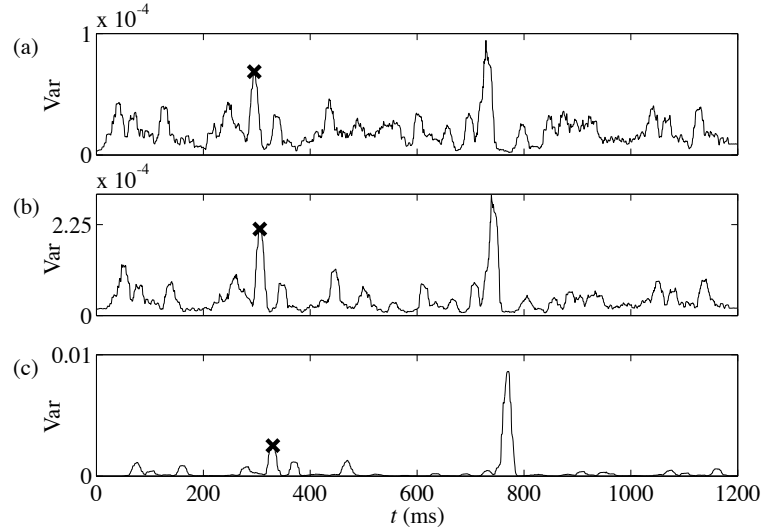


FIGURE 10. Time trace of  $\text{Var}(x, t; 16 \text{ ms})$  defined by equation (1) at (a)  $x = 88$ , (b) 112 and (c) 161. The centre of the disturbance studied in figures 4–9 is marked with a cross.

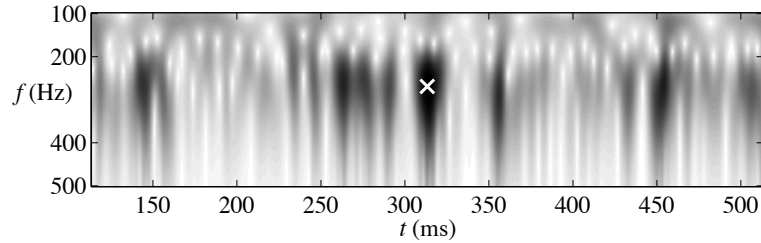


FIGURE 11. The wavelet transform of the second signal from the top in figure 4. White is the minimum value whereas black is maximum. The cross marks the time of maximum  $\text{Var}$  and the frequency at which the energy is maximum of the wave packet studied in figures 4–9.

- growth factor  $\gamma_i$ , defined as  $\frac{\ln(A_i(x_1)/A_i(x_0))}{x_1 - x_0}$
- propagation velocity  $u_{p,i}$ , defined as  $(x_1 - x_0)/(t_i(x_1) - t_i(x_0))$
- duration  $\tau_i$ , defined as the duration around  $t_i(x)$  during which the local variance  $\text{Var}(x, t; 16 \text{ ms})$  stays above 80% of the maximum  $A_i(x)$
- frequency,  $f_i$ , determined from the Morlet wavelet of the signal as described below.

*Streak oscillations of finite length: disturbance evolution and growth*

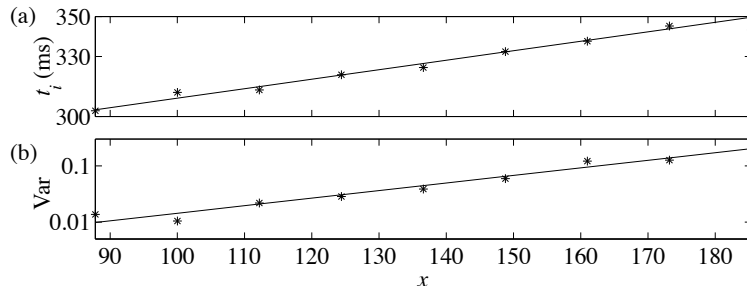


FIGURE 12. Streamwise development of time of occurrence  $t_i$  (a) and amplitude  $A_i$  in logarithmic scale (b) for the example wave packet.

In order to determine the individual frequency of each wave packet, wavelet analysis using the Morlet wavelet was used. In the wavelet, the frequency content of the signal is analyzed at each instant. In figure 11, in which the wavelet transform of the signal in figure 4(b) is shown, black is indicating the highest energy and white low. In figure 11, there are a number of black regions, corresponding to different wave packets, one of them marked with a white cross. The cross marks the wave packet studied in figures 4–9. The frequency of a wave packet,  $f_i$  is determined as the frequency at which the wavelet transform exhibits a maximum at time  $t_i$ .

The streamwise development of the time of occurrence and amplitude for the example wave packet is shown in figure 12. The slope of the lines correspond to  $u_{p,i}$  and  $\gamma_i$ , respectively.

In figure 13, the exponential growth factors for the 13 individual disturbances are plotted as a function of their frequency. The disturbance used as example is marked with a ring, the others with filled symbols. The size of the symbols is proportional to the length of the disturbance in full wavelengths as indicated in the upper right corner. The growth factor is seen to be between 0.004 and 0.014 for the 13 disturbances. This value is in the same range as the value 0.02 obtained for streaks of the same amplitude by Elofsson *et al.* (1999). The 13 disturbances are too few to draw any definite conclusions, but some comments will be made. Only three disturbances have a growth factor larger than 0.008. Two around  $f = 270$  Hz and one around  $f = 305$  Hz. A possible explanation for this could be that  $f = 270$  Hz is close to the frequency maximizing the growth ( $f = 273$  Hz) and that the disturbance at  $f = 305$  Hz is longer (marker larger) than the other disturbances. The large-growth disturbance at  $f = 305$  Hz inspired the idea that the length of the disturbance also affects the growth. This question was specifically addressed in the experiments with controlled forcing, reported in section 4.

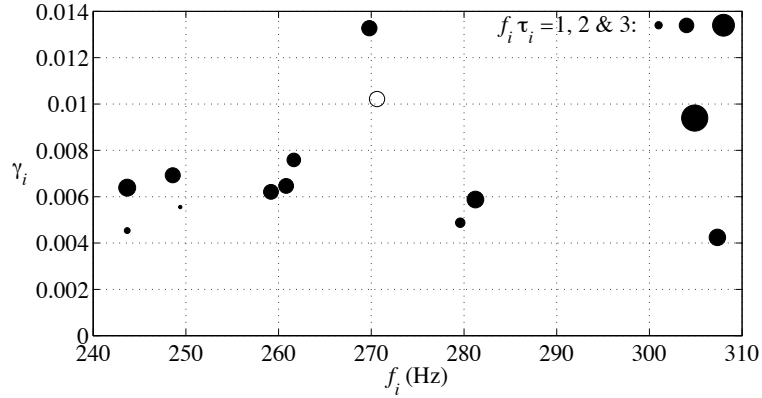


FIGURE 13. Streamwise growth factor  $\gamma$  of  $u_{rms,\Delta t}(t_i)$  as a function of  $f_i$ . The size of each marker indicates the length in full wavelengths ( $f_i \tau_i$ ), of the corresponding disturbance as indicated by the three explanatory markers in the upper right corner. The disturbance studied in figures 4–9 is shown with an open symbol.

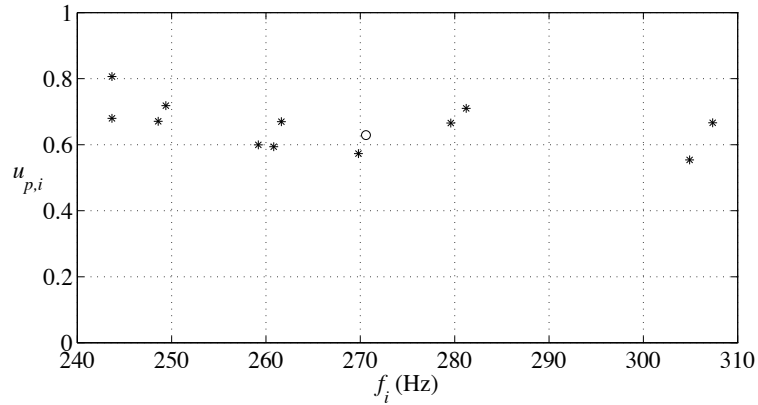


FIGURE 14. Streamwise propagation velocity  $u_{p,i}$  as a function of  $f_i$ .

When it comes to the propagation velocity  $u_{p,i}$ , shown in figure 14, it seems to be approximately constant and roughly 65% of  $U_{CL}$ , in good correspondence with the phase speed obtained by Elofsson *et al.* (1999) for disturbances of a streak forced by an infinite wave train (69%). This value is slightly lower than

*Streak oscillations of finite length: disturbance evolution and growth*

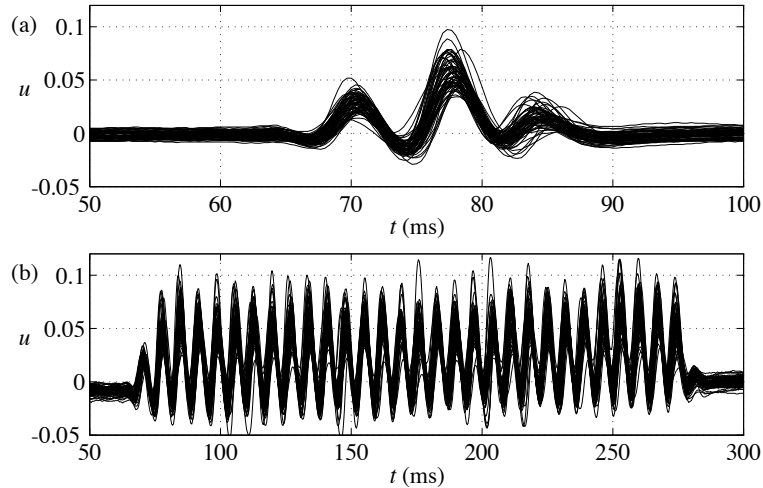


FIGURE 15. The 60 individual realizations for (a)  $N = 2.5$  and (b)  $N = 30$  at  $x = 112$ ,  $y = 0.36$  and  $z = 0.49$ .

the local velocity at the point where the secondary instability has its maximum velocity.

#### 4. Controlled forcing

##### 4.1. Disturbances

The experiments with a controlled forcing, during which the secondary instability was forced by a predetermined number of wavelengths ( $N$ ), were done in order to study the growth of wave packets of various length. The aim was to determine whether there is a decrease in growth of short disturbances as indicated in figure 13. The measurements were made at the position at which the secondary instability had its maximum amplitude. At each streamwise position, the disturbance sequence was run 60 times for each  $N$ . Ensemble averaging of these signals, as above, extracted the repeated features of the disturbances.

The 60 traces of the velocity fluctuation for  $N = 2.5$  and  $N = 30$  with  $f = 270$  Hz at  $x = 112$  are shown in figures 15(a) and (b). All features of the disturbances are seen to be repeated in all the realizations. Note that the time scale differs in (a) and (b). The frequency is the same for the two cases. The peak-to-peak amplitude of the wave disturbance is seen to be approximately  $0.15 U_{CL}$  for the case with  $N = 30$  in (b) and a little bit less for  $N = 2.5$  in (a). At the present position, no turbulence is seen in the traces. Furthermore, a small acceleration of the mean flow at large times can be observed for  $N = 30$ : at  $t = 300$  ms the velocity is increased a few percent of  $U_{CL}$  as compared to the velocity at  $t = 0$ . This is due to a large turbulent area created downstream

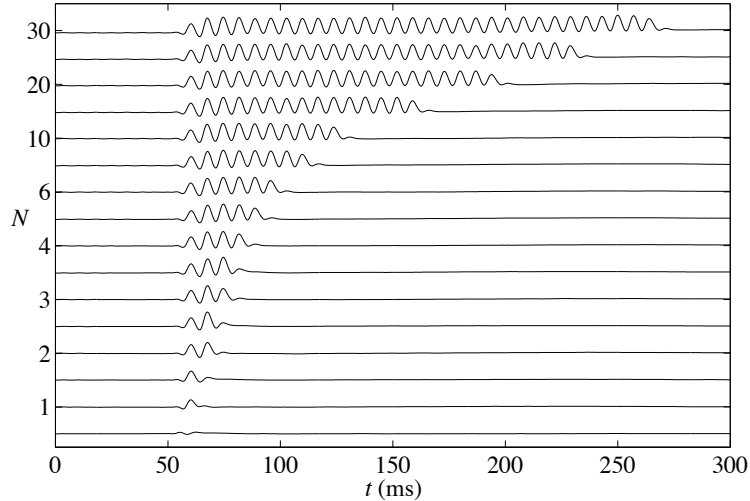


FIGURE 16. Ensemble-averaged velocity traces at  $x = 112$ ,  $y = 0.36$  and  $z = 0.49$ . The number of wavelengths,  $N$ , is 0.5, 1, 1.5, 2, 2.5, 3, 3.5, 4, 5, 6, 8, 10, 15, 20, 25 and 30 from the bottom and up. The traces are all scaled with the same amplitude. The maximum amplitude is 11 % of  $U_{CL}$ .

in the channel (due to the earlier parts of the disturbance). The downstream turbulence affects the pressure gradient in the channel and thus the streak suction in such a way that the mean velocity at the present position increases. This effect is not visible until the disturbance has convected downstream, grown and established the turbulence, why it is not visible when  $N = 2.5$ .

In figure 16 the ensemble averages for all  $N$ -values are shown. For the first seven traces from the bottom,  $N$  increases with a half from one trace to the next. For this reason the first seven traces are ending with a small valley and peak, alternately. The top nine traces are all ending with a small peak.

The spectral content of the forcing signals generating the disturbances in figure 16 is illustrated in figure 17. The gray area shows that for  $N = 2.5$ , the energy is smeared out from  $f = 230$  Hz to  $f = 570$  Hz while for  $N = 10$  or higher, a much more narrow frequency band around  $f = 270$  Hz is sufficient to contain most of the fluctuation energy.

#### 4.2. Amplitude growth

To calculate the growth rate, the amplitude of the disturbance at various streamwise positions ( $x$ -values) has to be measured at a suitable ( $y, z$ ) position. For that purpose, a complete  $yz$ -plane was measured at  $x = 112$ . The

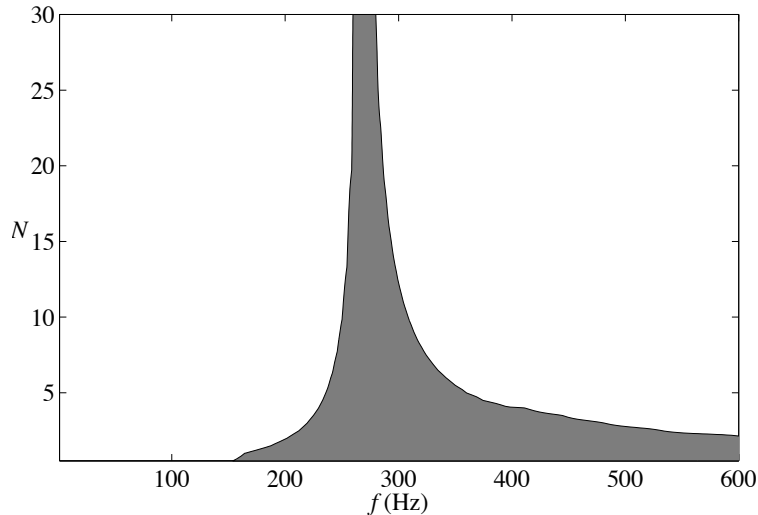


FIGURE 17. Spectral content of the signals in figure 16. The gray area shows the region within which 90% of the energy appears.

$yz$ -position of the fluctuation maximum in this plane (*c.f.* 8) was chosen as the reference position whereupon measurements were done at three  $x$ -positions (separated  $4.9h$ ) upstream and downstream of  $x = 112$  (*i.e.* totally seven  $x$ -positions). The parameter  $N$  was 0.5, 1, 1.5, 2, 2.5, 3, 3.5, 4, 5, 6, 8, 10, 15, 20, 25 and 30. The characteristics obtained for  $N=30$  is taken as the ones that would be obtained for an infinite wave train.

From traces such as the ones shown in figure 16, the amplitude was determined as the maximum difference between two consecutive extreme points (for small  $x$ , the acceleration effect mentioned in the discussion of figure 15 and the limited extent of the disturbances complicates simpler statistical, such as straightforward *rms*-calculations, methods). The amplitude grows exponentially in  $x$ , and the growth factors are shown as a function of  $N$  in figure 18. Short wave packets ( $N < 3.5$ ) indeed show a lower growth rate as compared to wave packets of larger  $N$ , confirming the vague indication from figure 13 that short wave packets exhibit a smaller growth rate compared to infinite wave trains.

The decay of  $\gamma$  as  $N$  decreases can be explained by the spectral content of the wave packets with low  $N$ . The frequencies (or streamwise wavenumbers) of anti symmetric streak instabilities that grow are known to be limited (Elofsson *et al.* (1999), Asai *et al.* (2002), Andersson *et al.* (2001)). Theoretically, low frequencies are always amplified (or neutral) whereas high frequencies are

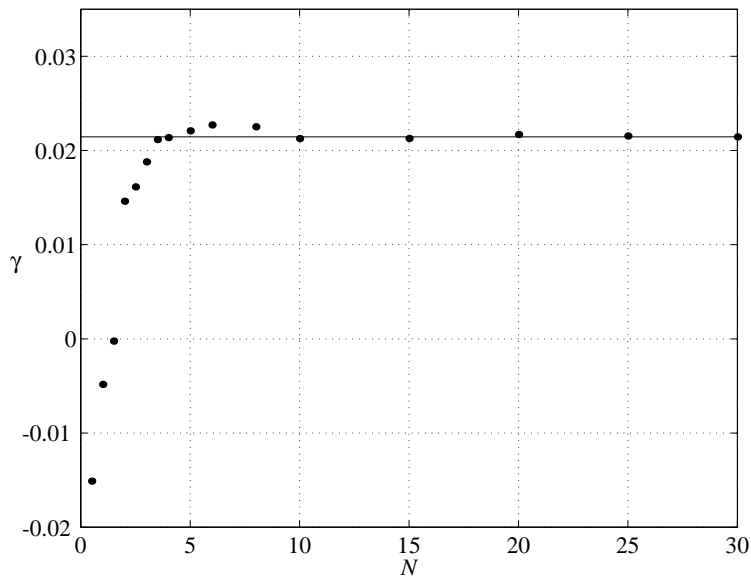


FIGURE 18. Growthfactor as a function of number of wavelengths. The line denotes the value obtained for  $N = 30$ .

damped. From figure 17 it is known that the spectral region in which the vast majority energy is found varies with  $N$ . For high enough  $N$ , the gray region in figure 17 is a narrow band around the amplified forcing frequency (270 Hz). For lower  $N$ , however, the contribution from higher, damped frequencies increases. With this in mind, the small growth factors of wave packets with small  $N$  in figure 18 is quite natural.

## 5. Conclusions

The secondary instability of laminar velocity streaks has been studied. Straight laminar velocity streaks were created in a plane channel flow. The secondary instability of the streaks was forced in two ways, (i) by a random signal band-pass filtered in a suitable frequency band and (ii) by a signal exhibiting a predetermined ( $N$ ) number of wavelengths. The parameter  $N$  was varied from 0.5 to 30.

The random forcing of the streaks created localized wave packets of finite duration. The properties of these disturbances were seen to be similar to these of an infinitely long wave train as investigated by Elofsson *et al.* (1999): the  $yz$ -distribution shows two maxima at  $y = 0.36$  and  $z = \pm 0.49$  and the propagation speed of the wave packets was found to be 65% of  $U_{CL}$  (the phase speed measured by Elofsson *et al.* (1999) was 69% of  $U_{CL}$ ). The amplitude of the

*Streak oscillations of finite length: disturbance evolution and growth*

disturbances grew exponentially and the growth factor was seen to vary with frequency, exhibiting a maximum for a well defined frequency. In addition to these similarities with what have been observed for streaks disturbed by infinite wave trains, the data also indicated that short disturbances have a smaller growth rate than long ones.

After the exponential growth of the disturbance, breakdown to turbulence was initiated. The first stages of the development to incipient spots could be followed. It was found that if a disturbance is followed downstream, the major part of the disturbance energy moved to three positions: two long regions of accelerated flow close to the wall at  $z = \pm 0.49$  and a shorter region of decelerated flow at the centre of both the channel and the streak. The regions at  $z = \pm 0.49$  showed a low frequency modulation of the flow, while in the centre, there were both high and low frequency oscillations.

The experiment with a controlled forcing confirmed that the observation regarding the relation between disturbance length and growth (lower growth factors for short disturbances) was correct. The growth factor was seen to decrease towards negative values for  $N < 3.5$ . This phenomenon was explained by the large energy contribution from high frequencies for low  $N$ .

### **Acknowledgments**

I thank my brother Mr. H. M. Henrik Lundell for spending two summer months performing the measurements reported in section 4. Lic. Luca Brandt is gratefully acknowledged for the discussions and explanations regarding the spectral distribution of wave packets. Professor P. Henrik Alfredsson is acknowledged for inspiration, guiding, reading and comments. Lic. Kristian Angele and Lic. Jens Fransson are also acknowledged for reading and commenting the manuscript. Mr. Marcus Gällstedt has been invaluable in the workshop.

## References

- ANDERSSON, P., BERGGREN, M. & HENNINGSON, D. S. 1999 Optimal disturbances and bypass transition in boundary layers. *Phys. Fluids* **11**, 134–150.
- ANDERSSON, P., BRANDT, L. & HENNINGSON, D. S. 2001 On the breakdown of boundary layer streaks. *J. Fluid Mech.* **428**, 29–60.
- ASAI, M., MINAGAWA, M. & NISHIOKA, M. 2002 The instability and breakdown of a near-wall low-speed streak. *J. Fluid Mech.* **455**, 289–314.
- BLACKWELDER, R. F. & KAPLAN, R. E. 1976 On the wall structure of the turbulent boundary layer. *J. Fluid Mech.* **76**, 89–112.
- BOTTARO, A. & KLINGMANN, B. G. B. 1996 On the linear breakdown of Görtler vortices. *Eur. J. Mech. B/Fluids* **15**, 301–330.
- BUTLER, K. M. & FARRELL, D. F. 1992 Three dimensional optimal perturbations in viscous shear flow. *Phys. Fluids A* **4**, 1637–1650.
- ELLINGSEN, T. & PALM, E. 1975 Stability of linear flow. *Phys. Fluids* **18**, 487–488.
- ELOFSSON, P. A., KAWAKAMI, M. & ALFREDSSON, P. H. 1999 Experiments on the stability of streamwise streaks in plane Poiseuille flow. *Phys. Fluids* **11**, 915–930.
- FASEL, H. F. 2002 Numerical investigation of the interaction of the Klebanoff-mode with a Tollmien-Schlichting wave. *J. Fluid Mech.* **450**, 1–33.
- HAMILTON, J. M., KIM, J. & WALEFFE, F. 1995 Regeneration mechanisms of near-wall turbulence structures. *J. Fluid Mech.* **287**, 317–348.
- JACOBS, R. G. & DURBIN, P. A. 2001 Simulations of bypass transition. *J. Fluid Mech.* **428**, 185–212.
- KENDALL, J. M. 1998 Experiments on boundary-layer receptivity to freestream turbulence. *AIAA-paper 98-0530*.
- KOHAMA, Y., ONODERA, T. & EGAMI, Y. 1996 Design and control of crossflow instability field. In *IUTAM Symposium on Nonlinear Instability and Transition in Three-Dimensional Boundary Layers, Manchester, UK* (ed. P. W. Duck & P. Hall), pp. 4.1–4.13. Kluwer.
- LANDAHL, M. T. 1980 A note on an algebraic instability of inviscid shear flows. *J. Fluid Mech.* **98**, 243–251.
- LUCHINI, P. 2000 Reynolds number independent instability of the boundary layer over a flat surface: optimal perturbations. *J. Fluid Mech.* **404**, 289–309.
- MALIK, R. M., LI, F., CHOUDHARI, M. M. & CHANG, C. 1999 Secondary instability

- of crossflow vortices and swept-wing boundary-layer transition. *J. Fluid Mech.* **399**, 85–115.
- MATSUBARA, M. & ALFREDSSON, P. H. 1998 Secondary instability in rotating channel flow. *J. Fluid Mech.* **368**, 27–50.
- MATSUBARA, M. & ALFREDSSON, P. H. 2001 Disturbance growth in boundary layers subjected to free stream turbulence. *J. Fluid Mech.* **430**, 149–168.
- REDDY, S. C., SCHMID, P. J., BAGGETT, J. S. & HENNINGSON, D. S. 1998 On stability of streamwise streaks and transition thresholds in plane channel flows. *J. Fluid Mech.* **365**, 269–303.
- SARIC, W. S. 1994 Görtler vortices. *Annu. Rev. Fluid Mech.* **26**, 379–409.
- SCHOPPA, W. & HUSSAIN, F. 2002 Coherent structure generation in near-wall turbulence. *J. Fluid Mech.* **453**, 57–108.
- WALEFFE, F. 1995 Hydrodynamic stability and turbulence: beyond transients to a self-sustained process. *Stud. Appl. Math.* **95**, 319–343.



# Paper 4

**P4**



# Experiments on control of streamwise streaks

By **Fredrik Lundell & P. Henrik Alfredsson**

KTH Mechanics, S-100 44 Stockholm, Sweden

Control of streamwise velocity streaks are studied experimentally in a plane channel flow. High and low-velocity streaks are created by suction through streamwise slots and further downstream, the secondary instability of the streaks is forced by speakers. The streaks are controlled by localized suction downstream of the disturbance generation. In a modified setup, reactive control is used in order to delay transition of low-velocity regions appearing at known spanwise positions randomly in time. As expected, the growth rate of the secondary instability decreases when localized suction is applied below a low-velocity streak. With control applied, transition is substantially delayed. The suction position and, in the case of reactive control of randomly appearing disturbances, the time instants at which control suction was turned on/off, were varied. The parameter study shows that the control suction has to be applied within a narrow area (10% of a streak width) around the centre of a low-velocity streak. The timing of the control suction is seen to be less critical.

---

## 1. Introduction

For wall bounded flows, as *e.g.* flow along vehicles (ships, airplanes) or in piping systems, skin friction drag can be the major source for the resistance to be overcome by the propulsion system. This has led to various proposals on how to decrease the drag. Examples in the past are for liquid flows polymer additives and microbubbles, whereas boundary-layer suction, cooling (or heating) the surface, Large Eddy Break Up-devices (LEBU:s) or grooved surfaces have been proposed for flows independent of the fluid. These methods are all distributed, in the sense that the full flow field is affected. This is in contrast to selective methods which aim at control of specific and thereby localized (in time and space) events or structures. During the last ten years ideas have been presented based on local reactive control, where the idea is to detect and then selectively use control on flow structures which are identified to be responsible for transition to turbulence or turbulence production.

Several reviews (Bushnell & McGinley 1989, Gad-El-Hak 1996, Bewley 2001) have been published recently describing the developments within the area of control. The development of refined control methods have mainly been done from a theoretical/numerical viewpoint and much less from a viewpoint of physical implementation. Most studies aim at controlling T-S waves or turbulent boundary layers. T-S waves may be controlled by periodic suction/blowing through a spanwise slot or heating a strip out-of-phase with the wave. When trying to control turbulent boundary-layer flows one focuses on the streamwise-oriented structures of high and low-velocity streaks in the near-wall region which are assumed to be the starting point for the bursting sequence. Usually the idea is to decrease the spanwise variation of streamwise velocity and thereby decrease the number or strength of the bursting sequences. This can be achieved by localized suction below low-velocity streaks and blowing below high-velocity streak.

In this context it is interesting to note that laminar-turbulent transition of boundary layers influenced by free-stream turbulence (FST) is preceded by the growth of streaky structures in the boundary layer (*e.g.* Kendall 1998, Matsubara & Alfredsson 2001 and Jacobs & Durbin 2001). These streaks are the result of three-dimensional disturbances growing transiently in the boundary layer. The transient disturbance growth is due to non-orthogonality of the eigenmodes, which may give rise to large disturbance growth even at subcritical Reynolds numbers (Butler & Farrell 1992, Andersson, Bergren & Henningson 1999 and Luchini 2000). It has been proposed that the growth mechanism behind the streaks in FST-induced transition is similar to the mechanism giving rise to streaks close to the wall in turbulent flows (Johansson, Alfredsson & Kim 1991), and therefore plays a key role also in self-sustained turbulence (Waleffe 1995).

An investigation of streamwise streaks was made by Elofsson, Kawakami & Alfredsson (1999) in a model experiment in which streaks were created in a laminar Poiseuille channel flow. They concentrated on the secondary instability which develops on the streaks and found that the most unstable mode of the secondary wave instability was anti-symmetric with a wavenumber slightly smaller than the spanwise wavenumber of the streak. This is consistent with the analysis for streaks in a boundary layer performed by Andersson, Brandt & Henningson (2001). The theoretical results show that the secondary instability originates from the inflectional spanwise velocity profile developing as the streaks grow. The experimental findings of Elofsson, Kawakami & Alfredsson (1999) support this conclusion for the streaks in the channel. After the growth of the secondary instability waves, incipient spots are seen to appear and further downstream, the flow becomes fully turbulent.

## *Experiments on control of streamwise streaks*

### *1.1. Experimental and numerical flow control*

The results discussed above show that a control strategy which could be successful for boundary-layer control is one where the streaky structures are affected by the control. Localized suction has been used in order to decrease the growth of streamwise vortices or to control bursting events by *e.g.* Myose & Blackwelder (1995) (controlling streamwise Görtler vortices) and Gad-El-Hak & Blackwelder (1989) (controlling artificially generated bursts). Bakchinov *et al.* (2000) controlled transiently growing disturbances in a boundary layer by localized suction and blowing. A demonstration of a different control concept is Breuer, Haritonidis & Landahl (1989), who used an array of moving wall elements to cancel a disturbance introduced by an initial wall movement (in the opposite direction from the one used for cancellation). All these studies aimed at, and succeeded in, delaying transition by acting locally on artificially generated structures in the flow.

For reactive control, localized sensing of the status of the flow is also necessary. For practical reasons wall information is usually the only possible alternative, either in form of the wall pressure or the shear stress. An example is the study by Fan, Herbert & Haritonidis (1995), where a neural network was trained to give a phaseshift of the signal from a sensing microphone to the actuating speaker, minimizing pressure fluctuations at the wall downstream of the actuator.

Rathnasingham & Breuer (1997) used pulsating jets driven by a resonance cavity in order to generate vortices inhibiting the bursting in a turbulent boundary layer. In the experiments, a linear system identification scheme was used in order to determine when and with what amplitude to turn on the actuators utilizing the information from upstream wall-wire sensors. Pressure sensors at the wall downstream of the actuating jets were used to tune the system. In the turbulent boundary layer under study, estimations from the mean-velocity profile show a shear-stress reduction of up to 7%. A blowing jet created by a piston-type actuator was used by Rebeck & Choi (2001) and reduced the strength of the sweep motion towards the wall during bursts.

An actuator, consisting of a moving beam above a cavity in the wall, can generate streamwise vortex structures. Such an actuator was constructed by Jacobsson & Reynolds (1998). Properly applied the actuator was shown to decrease the strength of streamwise structures in a boundary layer. They used wall-mounted hot films as sensors and showed successful control of streamwise vortices and streaks, but obtained no considerable increase of the control effect using neural networks as compared to much simpler, proportional controllers.

Choi, Moin & Kim (1994) performed numerical simulations in which a proportional control scheme was used in order to decrease the strength of streaks in turbulent channel flows. In a numerical simulation the limitations of physical sensors and actuators are not present and in this case the control algorithm

used the normal velocity at a certain height over the wall, prescribing the opposite of this velocity at the wall. Later simulations by Lee *et al.* (1997) show that a neural network trained on the same problem adopted the same kind of control. Reductions in shear stress of up to 25% were obtained. By coupling the velocity at a specific height over the wall to the pressure variations at the wall, it will be possible to use wall-mounted pressure sensors in a physical implementation.

A general result from the studies above is that a complicated control algorithm based on system identification (using neural networks or linear system identification) does not show better results than the ones obtained with simple proportional controllers. It is also obvious that the typical physical implementation and the cases studied numerically differ in the sense that the physical implementation utilizes a limited number of sensors and actuators, whereas numerical studies may use information from all over the wall (or in the whole flow field) together with proper actuator output over the whole wall area (or in the whole flow field). In order for the knowledge from numerical/theoretical studies to be useful for physical implementation of reactive control, the theoretical/numerical knowledge needs to be complemented with physical or numerical experiments exploring the limitations of physically realizable actuators. On the other hand progress in sensor and actuator manufacturing has given a hope to produce a large number of sensors and actuators allowing individual structures in the flow to be controlled, (Ho & Tai 1996; Löfdahl & Gad-el-Hak 1999).

### 1.2. *Present work*

In this paper we attempt to describe how breakdown to turbulence in a model flow with streaky structures resembling that of a boundary layer subjected to free-stream turbulence or the near-wall region of a turbulent boundary layer, *i.e.* flow with streamwise orientated regions of high and low velocity, can be delayed in a physical experiment. The experimental situation is similar to the one of Elofsson *et al.* (1999). In this setup, the effects of the control could be measured in a detailed manner. Also, the parameter space in which the control is effective was studied. Together with the knowledge of the disturbance structure in the boundary layer, the experiences from the model experiment will be used in order to design a control system for boundary layers subjected to FST, similar to the systems described above but comprising a larger number of sensors and actuators.

In section 2, the experimental apparatus and in section 3, experiments on the control of velocity streaks by localized suction are described. First, fundamental studies of the control are reported and after that, reactive control of randomly generated disturbances is presented. Finally, the results are summarized in section 4.



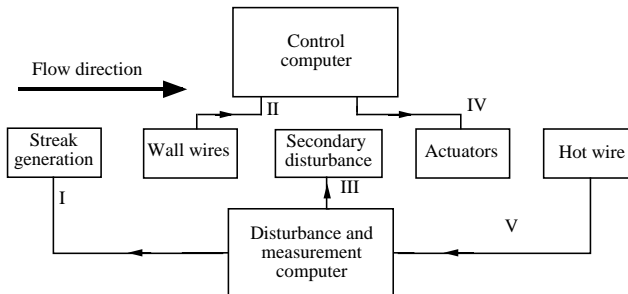


FIGURE 2. Block diagram of the experimental setup for reactive streak control. The Roman numerals I-V refer to figure 1(b).

The coordinates are  $x$  (streamwise),  $y$  (vertical) and  $z$  (spanwise). All lengths are normalized with the half channel-height  $h$  (4.1 mm) and the velocity is scaled by the centreline velocity,  $U_{CL}$ . The channel walls are at  $y = \pm 1$ . The Reynolds number is defined as  $Re = U_{CL}h/\nu$  where  $\nu$  is the kinematical viscosity of the air.

The total pressure on the centreline was measured by a conical total-pressure tube inserted from the open downstream end of the channel and a static-pressure hole in the channel wall at the streamwise position of the conical tube. The maximum velocity in the channel was just above 13 m/s, corresponding to a Reynolds number of 3500. With no external disturbances applied, the flow was laminar at this Reynolds number.

The streamwise velocity was measured utilizing constant-temperature hot-wire anemometry. The single hot wire used could be traversed to any position in the flow field where streaks were present (with stepper motors in the  $y$ - and  $z$ -directions and manually in the  $x$ -direction). Fast and reliable calibration of the hot wire was obtained by using the parabolic laminar velocity profile in the channel.

## 2.2. Disturbance generation

2.2a. *Continuous suction control.* Streamwise streaks were created by localized suction from slots in the upper channel wall. Five streamwise-oriented slots, each with the dimensions  $15 \times 1.5 \text{ mm}^2$ , with a separation of 15 mm in the spanwise direction, created five high-speed streaks at the upper wall, with low-speed streaks between them. The streaks were created when high-speed air was moved towards the wall in order to replace the low-velocity air removed by the suction slot. The position of the suction slot was 980 mm, or 239 half channel-heights, downstream of the channel inlet. The streak amplitude could be varied and in the present experiment, the velocity difference between the high and low

### *Experiments on control of streamwise streaks*

velocity region was 55% of  $U_{CL}$ . The streak generation is positioned at  $x = 0$  and  $z = 0$  corresponds to the centre of a low-velocity streak.

High quality earphone-speakers (Sony) were used in order to force the secondary instability of the streaks. The disturbance was introduced through two narrow holes, positioned symmetrically over the centre of the low-velocity streak at  $y = 1$ ,  $z = \pm 1.2$ . The earphones were driven by a sinusoidal signal from a signal generator. By applying the original disturbance signal to one of the earphones and either the same or the inverted signal to the other, symmetrical (same) or anti-symmetric (inverse) modes of the streak oscillation could be triggered. The forcing was positioned 285 mm, *i.e.*  $70h$ , downstream of the streak generation. At the forcing position, the streaks had reached their maximum amplitude and were in a laminar, slowly decaying, phase.

*2.2b. Reactive control.* In order to create time-dependent disturbances to be tackled by the reactive control system, solenoid valves were used to turn each high-speed streak on and off individually. The valves were controlled by the computer and the pattern with which the valves were turned on and off could be chosen as either predetermined or random. With repeated disturbances, phase-locked measurements utilizing a single hot wire could give information from the whole flow field. For the results reported here, a fixed pattern was used.

To fully complete the experimental simulation of time-dependent disturbances in a real boundary layer subjected to free-stream turbulence, not only the streaks themselves have to be time-dependent, but also the forcing of the secondary instability. This was done by using a number of spanwise oriented slots (0.5 mm wide in the streamwise and 10 mm long in the spanwise direction, respectively), connected to speakers creating a blowing/suction action through the slot forcing the secondary instability. The speakers were driven by band-pass filtered (50–500 Hz) white-noise signals. The original signal and its reverse (since the signal is random, a phase shift is not possible) were connected to different slots, so that symmetric as well as anti-symmetric forcing was obtained. This forcing simulates the forcing by free-stream turbulence on streaks in a real boundary layer. Repeated signals, synchronized with the valves regulating the streak suction, gave the possibility of ensemble-averaged measurements.

### *2.3. Control system*

*2.3a. Continuous suction control.* The objective of the control was to affect the low-speed streaks by localized suction and thereby reduce the growth of the secondary disturbance introduced by the earphones. The control suction was established through a 0.5 mm hole situated off-centre in a circular plug 85 mm ( $21h$ ) downstream of the earphones forcing the secondary disturbance. In non-dimensional coordinates, the default control position was  $(x_a, y_a, z_a) = (90, 1, 0)$ . When rotating the plug, the off-centre hole moved in the spanwise

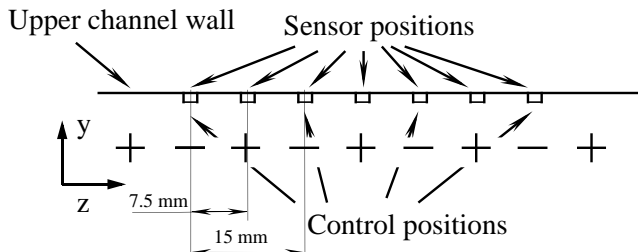


FIGURE 3. Spanwise positioning of sensors and actuators. In the real setup the wire prongs are flush with the wall.

direction so that the spanwise position of the hole,  $z_a$  ( $a$  for actuation), was altered. The flow through the control-suction hole was maintained by a small vacuum cleaner. It was around 0.5 l/min and was measured by a thermal mass-flow meter.

2.3b. *Reactive control.* For reactive control, time-dependent localized suction was used to control the randomly occurring disturbances. In order to gain experience in control-system design, and to study the use of different control-algorithm parameters, the control system was complemented with sensors sensing the streamwise shear-stress at the wall and fast (300 Hz) solenoid valves for turning the control suction on and off. The sensors were platinum wall wires, 2.5  $\mu\text{m}$  in diameter and 0.5 mm in length, welded to prongs, which were flush with the wall. The wires were bent, so that the centre of the wires were positioned 25–50  $\mu\text{m}$  above the wall.

The spanwise positions of the sensors and actuators are shown in figure 3. As can be seen, the sensors are positioned with a spanwise separation of  $\lambda/2$ , with  $\lambda$  being the spanwise wavelength of the streaks. The actuators are positioned over the known positions of low-velocity streaks. The reaction time of the control system from sensing via processing to actuator output was 10–15 ms, most of which was the time for full control-suction strength to be established after the control-suction valves were opened.

The control algorithm was based on the spanwise difference of the streamwise shear. The shear-stress difference between two adjacent sensors,  $\Delta_i$ , was calculated as

$$\Delta_i(t) = \frac{(s_i(t) - s_{i+1}(t))}{\Delta_{max}} \quad (1)$$

with

$$\Delta_{max} = \max |s_i(t) - s_{i+1}(t)|, i = 1 \dots 6. \quad (2)$$

The quantity  $s_i(t)$  is the shear stress measured by sensor  $i$  and  $\Delta_{max}$  is the maximum shear-stress difference that can be created by the streak suction.

Whenever

$$|\Delta_i(t)| > \Delta_{thr} \quad (3)$$

with  $\Delta_{thr}$  being a threshold value between 0 and 1, the control suction was turned on at the spanwise position of low shear after a time delay  $\tau$ . When  $|\Delta_i|$  decreased below the threshold, control was turned off, again with the delay  $\tau$ . The two extreme cases of  $\Delta_{thr}$ , 0 and 1, correspond to continuous suction and no suction, respectively.

### 3. Results

#### 3.1. Continuous suction control

This part reports results where continuous localized suction is performed below a low-velocity streak, and it is shown that the breakdown can be delayed. For each measurement station, measurements were performed twice: first without and then with control applied, in order to keep experimental conditions as constant as possible and allowing a direct comparison for the case with and without control. All measurements reported in the present section were made with a centreline velocity of 7.6 m/s giving a Reynolds number of 2000. The Reynolds number was chosen to match Elofsson *et al.* (1999). The case with no control applied is referred to as the reference case.

The reported data s at  $y = 0.6$ , *i.e.*  $0.4h$  from the upper wall. The previous study by Elofsson *et al.* (1999) shows that the secondary disturbance has its maximum amplitude at this height. The secondary disturbance was introduced at  $x = 70$  and the frequency (260 Hz) was in the range of the most unstable frequencies for the present streaks. The earphones were situated symmetrically over the centre streak (at  $z = \pm 1.2$ ) and the forcing was anti-symmetric. Elofsson *et al.* (1999) found that even with the symmetric triggering, the anti-symmetric mode appears and grows faster.

In figure 4, the mean velocity (a, c) and amplitude of the secondary instability (b, d) ( $u_{rms}$ ) are shown in the  $xz$ -plane at  $y = 0.6$ . The two left graphs, (a) and (b), show the flow field with no control applied whereas (c) and (d) to the right show the flow field for the case with control applied. Note that the  $x$ -coordinate is compressed with a factor 2.5 compared to the  $z$ -coordinate. The measurement grid consists of 10 positions in  $x$  and 45 in  $z$ . At each measurement point, 32 768 velocity values were sampled at a sampling rate of 3 kHz. The average velocity, calculated as the average over  $90 < x < 180$ ,  $-3.6 < z < 3.6$  (two wavelengths in the spanwise direction), is subtracted why the streaks appear as regions of positive and negative velocity (figure 4(a, c)). The maximum peak-to-peak amplitude of the velocity streaks is larger than 50% of the centreline velocity in the case with no control suction. Comparing figure 4(a) and (c), it is seen that in the case with control applied, (c), the streaks are of lower amplitude as compared to the reference case. Also, the controlled streaks are more or less unchanged throughout the measurement

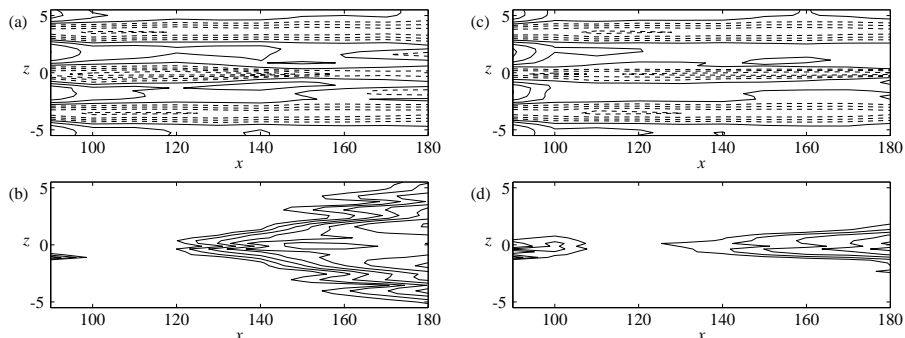


FIGURE 4. Mean velocity disturbance (a, c) and velocity *rms* (b, d) of the streaks in the channel with (a, b) and without (c, d) control applied. The velocity contours in (a) and (c) are  $\pm 5\%$ ,  $\pm 15\%$  of  $U_{CL}$  after subtraction of the mean velocity in the region  $90 < x < 180$ ,  $-3.6 < z < 3.6$ ; the *rms*-contours in (b) and (d) are logarithmic 1.75%, 2.5%, 3.8%... of  $U_{CL}$ . Data taken at  $y=0.6$ .

region, in contrast to the situation in (a), where the streaky structure is less apparent for the downstream part of the measurement area.

The contours of figure 4(b) and (d) indicate the disturbance level without and with control applied. Note that the disturbance contours are logarithmic so that equidistant contours show exponential growth. With no control applied, the downstream ( $x > 145$ ) development of the secondary disturbance, figure 4(b), shows saturation as well as spreading of the secondary instability to neighbouring streaks, with the largest amplitude between high and low-velocity regions. Even further downstream,  $x > 160$ , the *rms*-level is smeared out in the central part which is an indication of transition. Another sign of transition is seen in the mean-velocity distribution, becoming increasingly homogeneous in the spanwise direction.

If, however, the control suction is applied below the central low-velocity streak at  $x = 90$ , figure 4(d) shows that the control suction introduces some local disturbances at  $x = 90 - 110$ . Further downstream, the growth of the secondary instability is seen. As for the reference case with no control applied in figure 4(b), the disturbance has its maximum value between the region of high and low velocity. The contour levels are the same in figures 4(b) and (d), and it is seen that the disturbance growth in the streamwise direction as well as the spreading of the secondary instability in the spanwise direction substantially decrease with the control turned on. The signs of laminar-turbulent transition in figure 4(a, b): disappearance of the streaks and levelling of region of high

*Experiments on control of streamwise streaks*

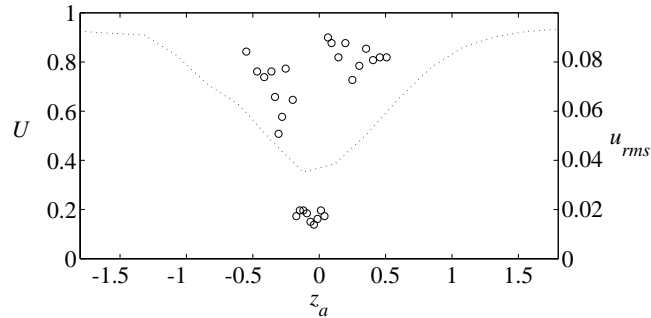


FIGURE 5. Velocity fluctuations as a function of actuator position  $z_a$ , (...)  $U(x = 145, y = 0.6, z = z_a)$  (left scale) and ( $\circ$ )  $u_{rms}(x = 145, y = 0.6, z = 1)$  with control suction applied at  $z_a$  (right scale).

$rms$ , are not present in figure 4(c, d). This indicates that the control suction decreases the growth of the secondary instability and thus delays the process of breakdown to turbulence of the streak.

In the experiment above, the suction was applied directly below a low-speed streak. In a realistic situation, where disturbances appear randomly, this will not be the case. Therefore the dependence of the control effect on the spanwise control position was studied. By rotating the control plug the control suction hole could be moved in the spanwise direction. As a diagnostic, the disturbance level at a fixed position downstream of the control, in this case  $(x, y, z) = (145, 0.6, 1)$ , was measured. This position was chosen because, for the reference case, the disturbance distribution has a maximum there (see figure 4(b)). At this position, the flow is transitional with no control applied. In figure 5 the disturbance level at this position is shown with various  $z_a$ . In the figure, the spanwise velocity profile at the streamwise position of control and  $z$ -values corresponding to  $z_a$  is shown. From the figure it is obvious that for successful control to be achieved, the suction can only be applied to a narrow region close to the centre of the low-velocity streak. The width of the region where control is to be applied is seen to be  $0.25h$ , corresponding to less than 1 mm in the physical setup.

Increasing the strength of the control suction, the width of the region for which control is successful becomes narrower. Decreasing the suction strength, the control effect rather abruptly disappears. If the flow rate through the control suction hole is non-dimensionalized by the centreline velocity and the area where laminar flow is maintained with control as compared to that without control, a non-dimensionalized suction coefficient can be obtained as  $C_q = q/AU_{CL}$  where  $C_q$  is the suction coefficient,  $q$  the flow rate, and  $A$  the controlled area (the area where transition is inhibited by the control). In the present case

the area is a triangle with corners in  $(x, z) = (150, 0)$ ,  $(180, 3)$  and  $(180, -3)$  (see figure 4), and a suction coefficient less than  $4 \times 10^{-4}$  is obtained with a flow rate of  $4.2 \text{ cm}^3/\text{s}$  (the approximate flow rate used in the experiments). The amount of fluid withdrawn from the flow by the control suction is about 0.25% of the flow through the part of the channel occupied by the streak (one streak wavelength times half the channel height). In the present experiment, the control suction was applied fairly far downstream of the streak generation. It is believed, and indicated in boundary layer experiments by Bakchinov *et al.* (2000), that the suction necessary for successful control decreases if the control suction is applied further upstream.

In figure 6 the velocity and disturbance distributions without control applied are studied in detail at each streamwise position.

In figure 6(a–e), the mean velocity profile is seen to be more or less constant. However, in (f–i), an increasing modification is seen to appear. Since this modification starts to appear right after the *rms*-value reaches its maximum in the centre at  $x = 150$  (figure 6(f)), it is believed that transition to turbulence plays an important part in the modification of the mean velocity profiles. Even further downstream, it is seen that the mean velocity in the region  $-3.6 < z < 3.6$  increases, indicating development of the fuller turbulent velocity profile. It is also seen that the smearing of the mean velocity profile mentioned in the discussion of figure 4 is actually a “streak doubling”. In figure 6, the onset of the secondary instability between the regions of high and low velocity is clearly seen. As the secondary instability spreads in the spanwise direction, it is seen that it first appears at the new inflection point arising due to the streak doubling (see figure 6(g) at  $z = -1$ ) and as it grows, the maximum moves towards the centre of the newly created low-velocity streak, similar to the behaviour of the original, central low-velocity streak from figure 6(c) to (f).

A similar, but delayed, behaviour is seen in the case with control applied in figure 7. The control makes a small modification of the mean velocity distribution, as compared to the case without control applied (compare the dashed line in figures 6 (no control) and 7 (with control) (a–d)). The control suction is seen to increase the minimum velocity from 0.3 to 0.5, thus decreasing the maxima value of  $\partial U/\partial z$  and the amplification of the secondary instability.

From previous figures it is clear that the growth of the secondary instability decreases for the continuous suction control case. In figure 8 the maximum of the *rms*-level for the two cases are compared. For each of the two cases, the *rms*-level has been normalized with its minimum value, obtained at  $x = 110$ . The decreased growth of the secondary instability in the controlled case is clearly seen. The two lines in the figures are the least-square fits to the *N*-values in the region where the exponential growth of the secondary disturbance occurs ( $x = 120$ – $140$  in the case of no control and  $x = 110$ – $180$  in the case with control applied). From the figure it is obvious that the control decreases the

*Experiments on control of streamwise streaks*

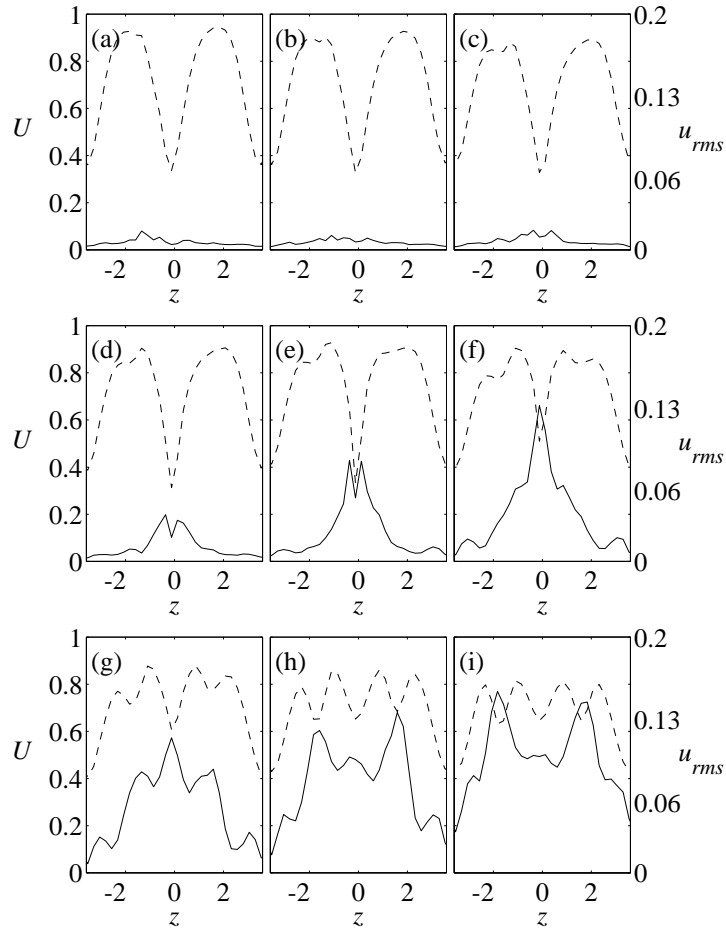


FIGURE 6. Spanwise mean velocity ( $\cdots$ , left scale) and disturbance ( $—$ , right scale) distribution at (a)  $x = 100$  to (i)  $x = 180$  *without* control applied. All data are taken at  $y = 0.6$ .

disturbance growth. The logarithmic growth factor becomes 0.082 without and 0.029 with control applied, *i.e.* the growth factor is smaller by a factor of 3 in the controlled case.

### 3.2. Reactive control

All results in this section were obtained at a Reynolds number of 3300, corresponding to a centreline velocity of 12.5 m/s. This higher Reynolds number was chosen in order to get an illustrative, positive control result with a reasonable control suction rate.

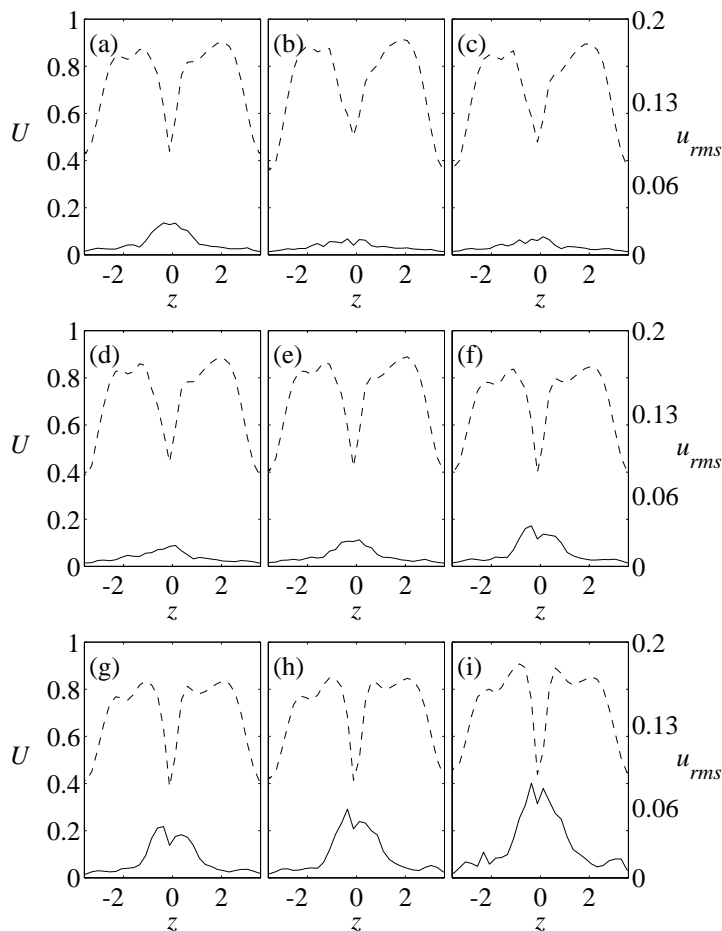
FIGURE 7. Same as figure 6 but *with* control applied.

Figure 9 shows the streaks generated by turning the streak suction on and off. For the figure, a predetermined streak pattern has been used in order to create the streaks, so that repeated measurements give a picture of the flow pattern. As can be seen, elongated structures are created, with varying amplitude and length. The maximum peak-to-peak amplitude of the disturbances are approximately 65%, in the region of to the values seen Westin *et al.* 1994 in measurements from boundary layer subjected to FST prior to breakdown. The measurements shown in figure 9 were done without artificial forcing of the secondary instability. It is seen that the resulting streak pattern is of rather varying amplitude, despite the fact that when the suction is turned on, the

*Experiments on control of streamwise streaks*

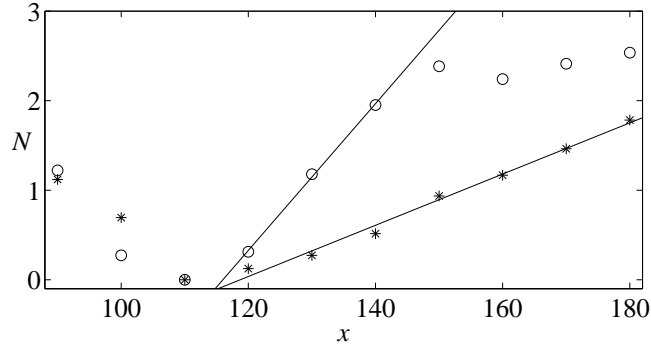


FIGURE 8. Growth of the secondary disturbance without (○) and with (\*) control applied. The lines have slopes of 0.082 and 0.029, respectively.  $N$  is calculated as  $\ln(u_{rms}/u_{rms,min})$ . The disturbance level is chosen as the maximum of  $u_{rms}$  in the spanwise direction at  $y = 0.6$ .

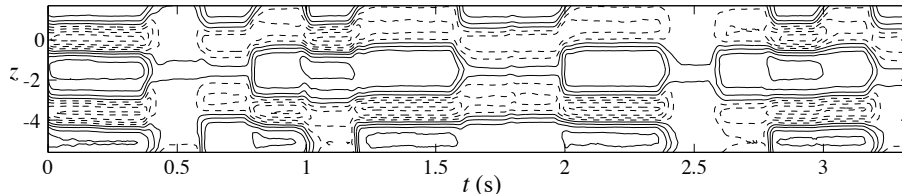


FIGURE 9. Streaks produced at  $(x, y) = (200, 0.6)$  by turning the streak suction on and off. A time period  $\delta t$  of 1 s corresponds to approximately  $\delta x = 2000$ , why the time axis should be stretched 150 times in order to get a physical aspect ratio of the disturbances. Contour spacing is  $\pm 10\%$  of  $U_\infty$  with negative contours dashed.

suction velocity is constant. It is also seen that depending on whether one single or two neighbouring streaks are turned on, the structures appear at different spanwise positions. In order to generate laminar structures such as the ones seen in figure 9, care has to be taken so that the streamwise gradients of the velocity,  $\partial U/\partial x$  (corresponding to  $\partial U/\partial t$  in figure 9), do not become too large at the leading and trailing edges of the disturbance. Most critical are the leading edge of a high-velocity structure and the trailing edge of a low-velocity structure, since the high velocity tends to catch up with the slower fluid in front of it and thereby sharpen the gradients. For a low-velocity structure the same is valid for the faster fluid behind it and the trailing edge of the structure.

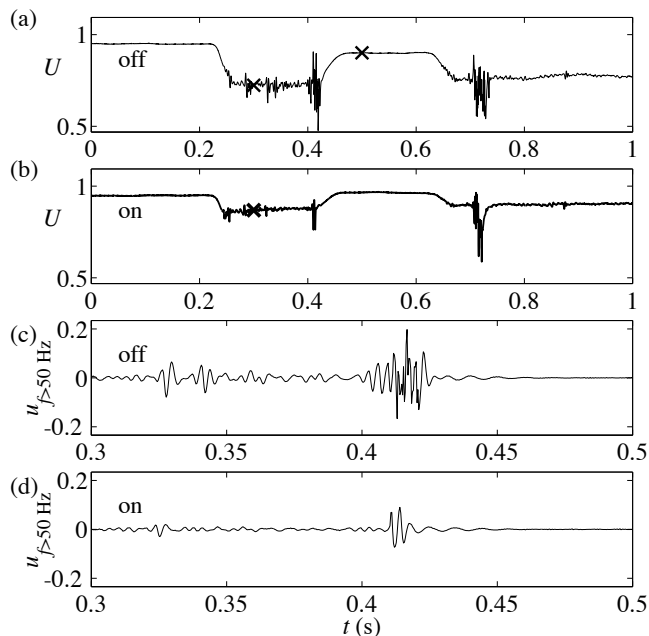


FIGURE 10. Velocity traces from the setup with triggering of the secondary instability. In (a) and (c) no control was applied, in (b) and (d) reactive control was applied so that the control suction was turned on during the passing of the low-velocity streak in question. In (c) and (d), the signal has been high-pass filtered at 50 Hz in order to isolate the high frequency oscillations. The position is  $(x, y, z) = (200, 0.2, 0)$ . In the controlled case the controller parameters are  $\tau = 0$  and  $\Delta = 0.6$ .

Velocity traces from  $(x, y, z) = (200, 0.2, 0)$  with triggering of the secondary instability are shown in figure 10. In figure 10(a), the velocity with no control applied is shown, showing two low-velocity streaks passing the hot wire ( $0.2 < t < 0.45$  and  $t > 0.65$ ). It is seen that the low-velocity streaks oscillate strongly during some periods, the strongest for  $0.4 < t < 0.43$  and  $0.7 < t < 0.75$ . This is possibly due to the receptivity of the streaks; whenever the forcing signal triggers an unstable frequency, the resulting disturbance will grow, giving rise to large amplitude velocity oscillations further downstream. In figure 10 it is also seen that the secondary disturbance only appears when there is a low-velocity streak present. For the periods when the velocity is undisturbed (12 m/s), there are no signs of high frequency disturbances (observed throughout the full time records). With the control applied, figure 10(b),

*Experiments on control of streamwise streaks*

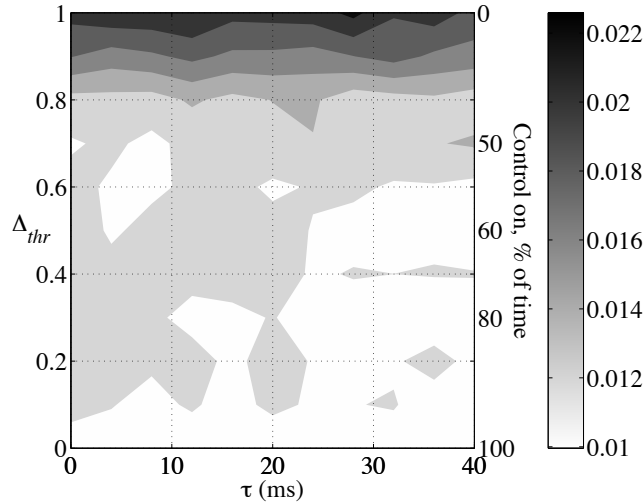


FIGURE 11. Control effect for various control parameters. Hot-wire position is  $(x, y, z) = (200, 0.2, 0)$ .

it is seen that the amplitude of the low velocity disturbance has decreased, as well as the number, amplitude and length of the high-frequency oscillations. The forcing conditions were the same during the two measurements shown in figure 10.

In figure 10(c, d), the portions between the crosses in figure 10(a, b) have been high-pass filtered so that only the oscillations due to the secondary instability of the streaks remain; the low-frequency passages of the streaks are filtered out. It is seen that the large amplitude, high frequency oscillation is stronger and more intermittent/turbulent in the case with no control applied as compared to the controlled case.

During the measurements, it was desirable to have an easy-to-calculate indicator of whether the flow was disturbed/turbulent or laminar. In order to obtain such a measure the *rms* of the high-pass filtered ( $f > 50$  Hz) velocity signal at the centre of the low-velocity streak was calculated. The height  $y = 0.2$  was chosen since the high-frequency oscillations at this height were found to be the best indicator of whether the flow is disturbed/turbulent or not. Closer to the wall, *e.g.* at  $y = 0.6$ , as used in the previous section, it is not possible to distinguish a turbulent flow from a laminar one on the basis of this measure. At  $y = 0.6$  the maximum *rms*-value is namely obtained for an intermittent transitional flow; at  $y = 0.2$  the maximum *rms* is obtained for a fully developed turbulent flow.

The control effect for different controller parameter settings is shown in figure 11. The two parameters are the threshold value of the streak detection,

$\Delta_{thr}$  and the time delay from detection to actuation,  $\tau$ , as discussed in section 2.2b. The control effect is measured as the high-frequency oscillation at  $(x, y, z) = (200, 0.2, 0)$ . The total number of parameter settings shown in the figure is 121 ( $11 \times 11$ ). It is clearly shown that for  $\Delta_{thr} < 0.7$  there is a strong reduction of the high frequency fluctuations independent of the time delay and that the effect is insensitive to the exact value of  $\Delta_{thr}$ . With  $\Delta_{thr} = 0.6$  the suction is turned on approximately 50% of the time. This coincides with the time during which the low-speed streaks are turned on at their maximum amplitude, and indicates that control has to be applied for all times at which streaks exist for the control to be efficient. The exact timing of the control is however less critical.

#### 4. Summary

The present study is part of a larger effort in order to understand, predict and control transition induced by free-stream turbulence. Streaks, modeling the disturbances in a boundary layer subjected to free-stream turbulence, were created in a channel flow. Successful delay of transition was obtained, probably by decreasing the spanwise velocity gradient,  $\partial U/\partial z$ , which drives the inviscid inflection-point instability.

Similar effects have also been demonstrated by Myose & Blackwelder (1995) (Görtler vortices) and Egami & Kohama (1999) (crossflow vortices). As in the present study, they both report transition delay obtained by localized suction applied at the position of low velocity. We have demonstrated that the spanwise position at which control suction is applied has a large impact on the control effect. The control suction has to be applied at a narrow region close to the centre of a low-velocity streak in order to obtain the control effect.

A measure of the control effort is the suction coefficient,  $C_q = V/U_\infty$ , where  $V$  is the suction velocity at the wall. Classical results by Gad-El-Hak (1986) show that no T-S waves will be amplified if the suction coefficient is  $1.18 \times 10^{-4}$  in the case of evenly distributed suction. However, if free-stream turbulence induced transition is to be inhibited, recent experiments by Fransson (2001) show that the suction coefficient has to be increased substantially over this value if transition is to be avoided. With a free-stream turbulence level of 1.6%, a suction coefficient of  $2.5 \times 10^{-3}$  was needed to avoid transition. For localized actuation, the suction coefficient at the location of the control is much higher, but a more relevant suction coefficient is obtained if the suction is averaged over the area where the control action has the desired effect. The effective suction area has been obtained in various ways. Myose & Blackwelder (1995) used the area from the leading edge to the suction position. Other investigators (*e.g.* Blackwelder & Gad-El-Hak (1989) and Egami & Kohama (1999)), calculated the area from the streamwise length and spanwise separation of their suction slits. The well-defined disturbances and detailed measurements of the control effect used in the present experiment gave the possibility to calculate the suction

### *Experiments on control of streamwise streaks*

coefficient based on the area over which the control suction inhibits transition (*i.e.* the area laminarized by the control). With such a definition of the effective suction area, the suction coefficient obtained from the present experiment ( $4 \times 10^{-4}$ ) is a fifth of the critical value obtained by Fransson (2001).

Control experiments on time-varying streaks, randomly forced, have also been reported. Such disturbances are similar disturbance induced by FST laminar boundary layers. A reactive control system was designed and evaluated. As in the previous case, transition was delayed by the control. The control system consisted of seven upstream wall-wire sensors, detecting the streamwise shear stress at the wall. Further downstream, suction through four streamwise slots, turned on and off by fast solenoid valves, was used in order to control breakdown to turbulence of the disturbances. As in the case with time independent streaks, transition delay was obtained by decreasing the growth of the secondary disturbance acting on the streaks. It was seen that if only the control suction was turned on for sufficiently long time periods, the timing, *i.e.* the delay between sensing a structure and proper actuator output, did not have a large impact on the control effect.

This reactive control system should be able to control similar random streaky structures in a boundary layer in a wind-tunnel over an area which comprises several streaky structures in the spanwise direction. As compared to earlier experiments on reactive transition control by localized suction, the present study presents more detailed measurements of the control effect and employs a larger number of sensors and actuators. Visualization results of Matsubara & Alfredsson (2001) show that the structures seen in grid-generated FST induced transition appear and disappear at various positions, but once created, a disturbance move only slowly in the spanwise direction during its development. Such a behaviour highly simplifies control, since a once detected structure basically convects straight downstream while growing/decaying.

In the reactive control experiments, it was not possible to vary the streamwise position of the control, also the current control was applied on already formed streaks. However, experiments in a boundary layer by Bakchinov *et al.* (2000), indicate that applying the control as close as possible to the position at which the disturbance is introduced gives the most reduction in growth of transiently growing structures (such as the streaks in the present experiment). This means that a control system to be used in a real boundary layer has to identify disturbances potentially leading to large transient growth and transition at an early stage, indicating the need for adaptive controllers with system identification. Such controllers have been used to control turbulence by Rathnasingham & Breuer 1997. It is our intention to use the experience gained from the experiments reported here together with earlier results to build a multi-input/multi-output reactive control system and use it to delay transition in boundary layers subjected to free-stream turbulence.

*Fredrik Lundell & P. Henrik Alfredsson*

### **Acknowledgments**

The work of earlier experimentalists (especially Dr. Per Elofsson and Dr. Mitsuyoshi Kawakami) in the channel gave the present project a flying start! Mr. Marcus Gällstedt is an excellent tutor in designing and constructing experimental equipment. Dr. Jens Österlund gave some invaluable time-saving advice on the manufacturing of wall wires. Dr. Johan Westin carefully read an early version of the manuscript. Michaela Agoston proof read the manuscript. The persons mentioned above are all acknowledged. So is financial support from VR (the Swedish Research Council) and KTH (Royal Institute of Technology, Stockholm).

## References

- ANDERSSON, P., BERGGREN, M. & HENNINGSON, D. S. 1999 Optimal disturbances and bypass transition in boundary layers. *Phys. Fluids* **11**, 134–150.
- ANDERSSON, P., BRANDT, L. & HENNINGSON, D. S. 2001 On the breakdown of boundary layer streaks. *J. Fluid Mech.* **428**, 29–60.
- BAKCHINOV, A. A., KATASONOV, M. M., ALFREDSSON, P. H. & KOZLOV, V. V. 2000 Control of streaky structures by localized blowing and suction. In *IUTAM Symposium on Laminar-turbulent transition* (ed. H. F. Fasel & W. S. Saric), pp. 159–164. Heidelberg: Springer Verlag.
- BEWLEY, T. R., MOIN, P. & TEMAM, R. 2001 DNS-based predictive control of turbulence: an optimal benchmark for feedback algorithms. *J. Fluid Mech.* **447**, 179–225.
- BREUER, K. S., HARITONIDIS, J. H. & LANDAHL, M. T. 1989 The control of transient disturbances in a flat plate boundary layer through active wall motion. *Phys. Fluids A* **1**, 574–582.
- BUSHNELL, D. M. & MCGINLEY, C. B. 1989 Turbulence control in wall flows. *Annu. Rev. Fluid Mech.* **21**, 1–20.
- BUTLER, K. M. & FARRELL, D. F. 1992 Three dimensional optimal perturbations in viscous shear flow. *Phys. Fluids A* **4**, 1637–1650.
- CHOI, H., MOIN, P. & KIM, J. 1994 Active turbulence control for drag reduction in wall-bounded flows. *J. Fluid Mech.* **262**, 75–110.
- EGAMI, E. & KOHAMA, Y. 1999 Control of crossflow instability field by selective suction system. In *IUTAM Symposium on Mechanics of Passive and Active Flow Control* (ed. G. E. A. Meier & P. R. Viswanath), pp. 171–176. Dordrecht: Kluwer Academic Publishers.
- ELOFSSON, P. A., KAWAKAMI, M. & ALFREDSSON, P. H. 1999 Experiments on the stability of streamwise streaks in plane Poiseuille flow. *Phys. Fluids* **11**, 915–930.
- FAN, X., HERBERT, T. & HARITONIDIS, J. H. 1995 Transition control with neural networks. *AIAA-paper 95-0674*.
- FRANSSON, J. H. M. 2001 Investigation of the asymptotic suction boundary layer. TRITA-MEK 2001:11. Department of Mechanics, Royal Institute of Technology.
- GAD-EL-HAK, M. 1996 Modern developments in flow control. *Appl. Mech. Rev.* **49**, 365–379.

- GAD-EL-HAK, M. & BLACKWELDER, R. F. 1989 Selective suction for controlling bursting events in a boundary layer. *AIAA J.* **27**, 308–314.
- GAD-EL-HAK, M. & HUSSAIN, A. K. M. F. 1986 Coherent structures in a turbulent boundary layer. part 1: Generation of "artificial" bursts. *Phys. Fluids* **29**, 2124–2139.
- HO, C.-M. & TAI, Y.-C. 1996 Review: MEMS and its applications for flow control. *J. Fluids Eng.* **118**, 437–447.
- JACOBS, R. G. & DURBIN, P. A. 2001 Simulations of bypass transition. *J. Fluid Mech.* **428**, 185–212.
- JACOBSON, S. A. & REYNOLDS, W. C. 1995 An experimental investigation towards the active control of turbulent boundary layers. TF 64. Department of Mechanical Engineering, Stanford University.
- JACOBSON, S. A. & REYNOLDS, W. C. 1998 Active control of streamwise vortices and streaks in boundary layers. *J. Fluid Mech.* **360**, 179–211.
- JOHANSSON, A. V., ALFREDSSON, P. H. & KIM, J. 1991 Evolution and dynamics of shear-layer structures in near-wall turbulence. *J. Fluid Mech.* **224**, 579–599.
- KENDALL, J. M. 1998 Experiments on boundary-layer receptivity to freestream turbulence. *AIAA-paper 98-0530*.
- LEE, C., KIM, J., BABCOCK, D. & GOODMAN, R. 1997 Application of neural networks to turbulence control for drag reduction. *Phys. Fluids* **9**, 1740–1747.
- LÖFDAHL, L. & GAD-EL-HAK, M. 1999 MEMS applications in turbulence and flow control. *Prog. Aerospace Sci.* **35**, 101–203.
- LUCHINI, P. 2000 Reynolds number independent instability of the boundary layer over a flat surface: optimal perturbations. *J. Fluid Mech.* **404**, 289–309.
- MATSUBARA, M. & ALFREDSSON, P. H. 2001 Disturbance growth in boundary layers subjected to free stream turbulence. *J. Fluid Mech.* **430**, 149–168.
- MYOSE, R. Y. & BLACKWELDER, R. F. 1995 Control of streamwise vortices using selective suction. *AIAA J.* **33**, 1076–1080.
- RATHNASINGHAM, R. & BREUER, K. S. 1997 System identification and control of a turbulent boundary layer. *Phys. Fluids* **9**, 1867–1869.
- REBBECK, H. & CHOI, K.-S. 2001 Opposition control of near wall turbulence with a piston-type actuator. *Phys. Fluids* **13**, 2142–2145.
- WALEFFE, F. 1995 Hydrodynamic stability and turbulence: beyond transients to a self-sustained process. *Stud. Appl. Math.* **95**, 319–343.
- WESTIN, K. J. A., BOIKO, A. V., KLINGMANN, B. G. B., KOZLOV, V. V. & ALFREDSSON, P. H. 1994 Experiments in a boundary layer subjected to free stream turbulence. Part 1. Boundary layer structure and receptivity. *J. Fluid Mech.* **281**, 193–218.

# Paper 5

P5



# Reactive control of free-stream turbulence induced transition: an experimental study

By **Fredrik Lundell**

KTH Mechanics, S-100 44 Stockholm, Sweden

Reactive control of free-stream turbulence induced transition on a flat plate has been studied. A control system consisting of upstream sensors (wall wires) and downstream actuators (suction through holes) has been built and an ad-hoc, threshold control algorithm has been tested. A parameter variation has been performed in order to find a working point of the control system. Detailed measurements of the flow field show how the control influence the disturbances in the boundary layer. The effect on the mean flow due to the control is minute. The control system manages to inhibit the growth of the fluctuations of the streamwise velocity component for a considerable distance downstream of the actuator position. Further downstream, however, the fluctuations grow again. Spectra show that the elongation of the structures in the downstream seem to be nearly eliminated in the controlled region. The spanwise scale of the disturbances, on the other hand, is not affected by the control.

---

## 1. Introduction

In this paper, a simple reactive control system is used to decrease disturbance growth in a boundary layer subjected to Free-Stream Turbulence (FST). This flow case has been chosen since the disturbance development is well documented, why detailed measurements of the control effect can be performed. In addition, the route to turbulence of a boundary layer subjected to free-stream turbulence: an initial growth of high- and low-speed streaks followed by high frequency oscillation and eventually the formation of turbulent spots, resembles the self-generation cycle of turbulence. In this introduction, recent development of FST induced transition and flow control will be reviewed and the present experiment motivated.

### 1.1. Streaks and their breakdown

The formation of streaks before breakdown to turbulence of a laminar boundary layer subjected to free-stream turbulence is well established. This is reported in the review of Kendall (1998). In later measurements by Matsubara & Alfredsson (2001) and Lundell & Alfredsson (2003*b*), the development of these structures is studied in detail. In the zero-pressure gradient (constant free-stream velocity) boundary layers usually studied, the *rms*-value of the streamwise velocity is seen to grow in linear proportion to the boundary layer thickness. The spanwise scale of the disturbances is of the order of the boundary-layer thickness and the structures become elongated as they propagate downstream.

The primary disturbance, the streaks, gives rise to *rms*-amplitudes of 10–15% prior to breakdown (Matsubara & Alfredsson 2001). The wall-normal profile of  $u_{rms}$  has its maximum at approximately half the boundary-layer thickness and agrees well with the distribution obtained from optimal disturbance theory of Andersson, Berggren & Henningson (1999) and Luchini (2000).

The later stages of breakdown might be due to secondary instabilities of the streaks, as proposed by *e.g.* Matsubara & Alfredsson (2001) and studied experimentally by Elofsson, Kawakami & Alfredsson (1999) and Asai, Minagawa & Nishioka (2002). Theoretical analysis of the secondary instability of streaks can be found in Reddy *et al.* (1998) and Andersson, Brandt & Henningson (2001). It has been found that if the streak amplitude is large enough, secondary instabilities will be amplified by the streak. Alternatives to the secondary instability scenario have been suggested, two possibilities are growth of two-dimensional waves (Bakchinov *et al.* 1995; Fasel 2002) or interaction between the streaks and small scales in the free stream as suggested by Jacobs & Durbin (2001) based on results from a direct numerical simulation.

The secondary instability scenario shows strong resemblance with the regeneration cycle of turbulence proposed by *e.g.* Waleffe (1995) and detected in a database from a DNS by Hamilton, Kim & Waleffe (1995). The cycle consists of three stages: transient growth of streaks, amplification of secondary instabilities and finally non-linear mixing, eventually producing vortices which can generate a new streak and thereby close the cycle.

### 1.2. Streak control

1.2a. *Numerical flow control.* Since streaks are a vital ingredient not only in free-stream turbulence induced transition, but also in the turbulence regeneration cycle, control of FST induced transition could have similarities with control of turbulence. The reason to study reactive control of turbulence is that it might be possible to save large amounts of energy by altering the flow dynamics with a small energy input. In a Direct Numerical Simulation (DNS), Choi, Moin & Kim (1994) showed that the skin friction in a turbulent channel

### *Reactive control of free-stream turbulence induced transition*

flow can be reduced by a control scheme named *opposition control*. In opposition control, the wall-normal velocity at a certain distance from the wall is measured and its opposite is applied at the wall.

A later Large Eddy Simulation (LES) study by Chang *et al.* (2002) showed that the opposition control scheme relaminarizes turbulent channel flows at low Reynolds numbers (the Reynolds number can be defined as  $Re = U_{CL}h/\nu$  where  $U_{CL}$  is the centreline velocity,  $h$  is half the channel height and  $\nu$  is the kinematical viscosity of the fluid). At higher Reynolds numbers, the skin friction was reduced, but the flow remained turbulent. The control effect decreased as the Reynolds number was increased.

Another method was used by Bewley, Moin & Temam (2001), who minimized the velocity fluctuations in a turbulent channel flow by direct optimization. The wall-normal velocity distribution at the walls was set to velocities minimizing future flow oscillations. They were able to relaminarize the flow at higher Reynolds numbers as compared to Chang *et al.* (2002). The method is time consuming and impossible to implement in a physical experiment, but illustrates the possibilities of actuation at the wall.

A final example of a numerical flow control study is the work of Högberg, Henningson & Bewley (2002), who applied controllers designed by optimal control theory to transition in spatially developing boundary layers. The optimal controllers were found to decrease the fluctuation energy of single mode disturbances very well (order of 10 or more), but work less well on optimal disturbances. Optimal disturbances were reduced only at the streamwise positions at which control was applied. Downstream of the controlled region, the disturbance amplitude increased again. Numerical flow control experiments taking physical considerations on sensing and actuation into account, such as Endo *et al.* (2000), typically report reduced effects.

1.2b. *Experimental flow control.* An experimentalist who wants to study flow control neither has access to the measurements available in a DNS nor the ability to perform amplitude modulated, fine scale structured actuation. One way to study flow control is therefore to generate disturbances in a controlled manner, and then try to cancel them with some suitable actuation. Two examples are the studies of Gad-el-Hak (1989) and Bakchinov *et al.* (1999), who used suction through holes to inhibit the growth and breakdown of streak-like disturbances in laminar boundary layers. An alternative is to adapt the method used by Rebbeck & Choi (2001), where an actuator was activated continuously at the wall in a turbulent boundary layer. By monitoring the incoming flow, Rebbeck & Choi (2001) could use conditional averaging in the post-processing of the data to study how the actuation effected the mean structure in the boundary layer.

Physical realizations of reactive control systems are however quite rare. Rathnasingham (1997) used skin friction measurements and pulsating jets to

control a turbulent boundary layer. Finite Impulse Response (FIR) filters were used to determine (i) the disturbance development from sensor to some point downstream of the actuator and (ii) how the actuator influenced the flow at the same position. The control system decreased the bursting frequency downstream of the actuator and some skin friction reduction was reported. The skin friction was however estimated from the mean velocity profiles, a method which is not very reliable in an experiment.

Jacobson & Reynolds (1998) used a flap-and-cavity vortex generator to control streamwise streaks. Randomly generated disturbances in a laminar flow were controlled by two controllers: an ad-hoc linear controller and a neural network. They showed that such a control scheme could decrease the amplitude of the disturbances.

In the present experiment, intermittent suction through holes triggered by wall-wire signals from upstream sensors was used. The same concept was used by Kerho *et al.* (2000), who used in total 25 sensors and actuators and tried the system in a turbulent boundary layer. The fluctuations of the streamwise velocity component were found to decrease due to the control and large drag reduction was reported, again based on the mean velocity profiles, why the results should be interpreted with care. Flow visualizations indicate that the control system removes the fluid of the low velocity streaks completely, rather than performs the minute modifications of the flow aimed for in the present study.

### 1.3. *Present work*

The use of a reactive control system to control free-stream turbulence induced transition has been studied both for its inherent interest, but also since the dynamics are believed to be similar to the dynamics in turbulent wall shear flow: randomly appearing streaks of high and low velocity which eventually breaks down to turbulence. Compared to turbulent flows, the time and length scales are much more convenient for a control experiment, *i.e.* they are slower and larger, respectively. From previous investigations, detailed knowledge of the disturbance growth in a laminar boundary layer subjected to FST is available, simplifying the characterization of the control effect.

In this paper, the possibilities to control streaks appearing in FST induced transition are evaluated and discussed. The aim of the paper is not to investigate intriguing parameter dependencies in a specific controller, but rather to do a careful study of the control effect, and perhaps to serve as a benchmark for future studies.

The setup, control system and controller is described in section 2. In section 3, the disturbance growth as well as the streak development with and without control is presented. Some aspects of the results are discussed in section 4 and finally the conclusions are summarized in section 5.

Reactive control of free-stream turbulence induced transition

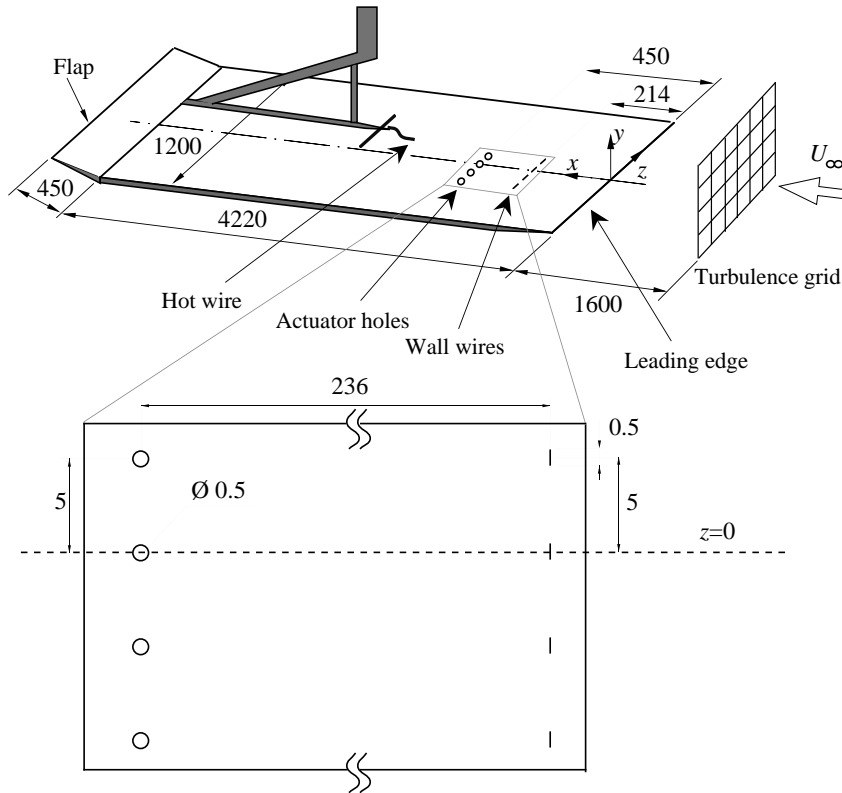


FIGURE 1. Flat plate setup used in the present experiment. Measures are in mm.

## 2. Material and methods

### 2.1. Flat-plate setup

The experiments were performed in the MTL wind-tunnel at KTH Mechanics in Stockholm. In the test section, a flat plate was placed (the setup is sketched in figure 1). The leading edge of the plate has been designed in order to minimize the pressure gradient around it (see Klingmann *et al.* (1993) for details). After the plate was mounted in the tunnel, the trailing edge flap was adjusted so that no turbulence spots, generated by separation at the leading edge, occurred in the boundary layer. After proper flow around the leading edge had been secured, the roof was adjusted in order to achieve a constant free-stream velocity along the plate. The free-stream velocity ( $U_\infty$ ) was 4.8 m/s  $\pm 1\%$  along the plate during the measurements.

The coordinates are  $x$ ,  $y$  and  $z$  for the streamwise, wall-normal and spanwise directions, respectively. The streamwise velocity is denoted  $U$  with capital

*Fredrik Lundell*

	(mm)	$\delta$	$l^+$
sensor width	0.5	0.61	5.7
separation	5.0	6.1	57.0
actuator width	0.5	0.41	4.8
separation	5.0	4.1	48.0

TABLE 1. Width and separation of the sensors at  $x = 214$  mm and the actuators at  $x = 450$  mm in the units mm,  $\delta$  and  $l^+$ .

denoting the mean value and lower case denoting the fluctuations. The leading edge is at  $x = 0, y = 0$ . The Reynolds number is  $Re = U_\infty x / \nu$  where  $\nu$  is the kinematical viscosity of the air. The non-dimensional wall-normal coordinate  $y$  is non-dimensionalized as

$$y = \frac{y^*}{\delta} \tag{1}$$

where  $y^*$  is the dimensional coordinate and  $\delta = (\nu x / U_\infty)^{0.5}$ . Velocities are normalized with the free-stream velocity,  $U_\infty$ .

The free-stream turbulence was generated by a grid placed 1600 mm upstream of the leading edge. The grid used is grid B of Matsubara & Alfredsson (2001) and Fransson (2001). The turbulence intensity,  $Tu$ , (measured by  $u_{rms}$ ) outside the boundary layer at the leading edge was 1.5% of  $U_\infty$ .

The velocity was measured by a hot wire mounted to a 3D traverse. The hot wire was made of platinum with a length of 0.5 mm and a diameter of  $2.5 \mu\text{m}$ . The hot wire was calibrated against a Prandtl tube in the free stream without the turbulence generating grid present. The hot wire was recalibrated when the free-stream velocity measured by the Prandtl tube and the wire differed more than 2%. The time between calibrations varied from 2-11 days.

The wall position was determined by fitting velocity profiles to the theoretical Blasius solution. In this case the profiles were measured without the turbulence generating grid.

## 2.2. Control system

The control system consists of four wall wires and four suction holes, positioned straight downstream of the sensors as shown in figure 1. Platinum wires, 0.5 mm long,  $2.5 \mu\text{m}$  diameter were used for the wall wires, which were welded to prongs flush with the wall. During the welding, the wire were given a bend out from the wall, so that the centre of the platinum wire was positioned 25–50  $\mu\text{m}$  above the wall. The wall wires were aligned in the spanwise direction. The dimensions of the control system are given in table 1, measured in (mm), the local boundary layer scale ( $\delta$ ) and the friction length scale of a Blasius boundary layer ( $l^+$ ) at the position of the sensing and actuation, respectively.

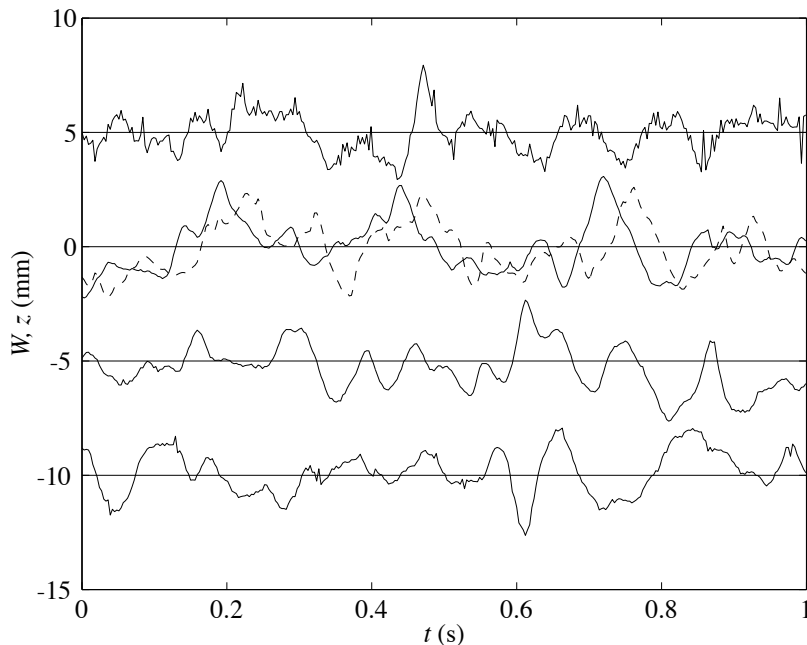


FIGURE 2. Simultaneous signals from the wall wires ( $W$ ) at  $x = 214$  mm,  $z = -5, 0, 5, 10$  mm (solid) and the simultaneously velocity measured by the hot wire at  $x = 400$  mm,  $y = 2.1$  (dashed around  $z = 0$ ). The velocity signal has been transformed and scaled as  $W$  (see equation (2)) and the signals are separated so that they fluctuate around the value corresponding to their  $z$ -position.

### 2.3. Controller

For the control logic, the raw signal from the wall wire,  $E_{ww}$ , was normalized according to

$$W(t) = \frac{E_{ww}(t) - \overline{E_{ww}}}{E_{ww,rms}} \quad (2)$$

where  $\overline{E_{ww}}$  is the temporal mean of the raw signal from the anemometer. After this normalization,  $W(t)$  is a good approximation of the (normalized) fluctuations of the wall-shear stress.

In figure 2, simultaneous time traces of the signals from the wall wires (positioned at  $x = 214$  mm) and the hot-wire signal from  $x = 400$  mm,  $y = 2.1$ , (dashed) are shown. It is seen that the velocity signal and the wall-wire signal at the same spanwise position are correlated with a time delay: a period of low shear stress at  $x = 214$  mm (solid curve) is soon followed by a period of low

velocity at  $x = 400$  mm,  $y = 2.1$  (dashed curve), showing the convective nature of the disturbances. The maximum correlation between the signals at  $z = 0$  is 86% with a delay of 34 ms. All the wall-wire signals show similar low frequency variations. The correlations between the wall-wire signals are between -10 and 0% for a separation of 5 mm and around -20% with 10 mm separation.

The control scheme was such that the control suction was turned on with a delay  $d_c$  if the normalized wall-wire signal  $W$  was below (or above in some parameter variation tests) a preset threshold value. In the presentation of the results to follow, the threshold value is not given explicitly, instead the time fraction during which control is turned on is given for each threshold value.

The physical rationale for the control scheme is that a low value of the shear stress indicates a streak of low velocity passing above the sensor. After a time delay  $d_c$ , this streak has been convected to the suction holes, where the suction through the narrow hole generates streamwise vorticity, which can use the mean shear as a lever to redistribute the momentum so that the streak stops growing or ultimately disappears.

### 3. Results

The results section is divided into four parts. In the first, information accessible from the streamwise velocity and its *rms*-value is presented. The second part presents the parameter variation performed to find an working point of the control system. Finally the development of structures in the boundary layer is studied in two subsections on the velocity-signal spectra and the correlations between the wall-wire signal and the movable hot wire.

The sampling speed was 2 kHz and the sampling period 60 s for all measurements. The hot wire was sampled together with the four wall-wire signals used in the controller.

In all cases where measurements with and without control are compared, the measurements were performed in sequence within 16 hours without opening the wind-tunnel in between.

#### 3.1. Velocity statistics and disturbance growth

First the mean and disturbance structure of the basic flow, *i.e.* a boundary layer subjected to FST, will be presented. This is followed by the response of the mean flow to the control.

The mean-flow characteristics of the boundary layer without control applied is summarized in figure 3. Velocity profiles measured by the hot wire at 19 streamwise positions ranging from  $x = 200$  to 1600 mm without control are shown in figure 3(a). The Blasius boundary layer solution is shown as a solid line in the figure. The profiles agree well with the theoretical solution, showing that the boundary layer under study is close to a Blasius boundary layer.

Reactive control of free-stream turbulence induced transition

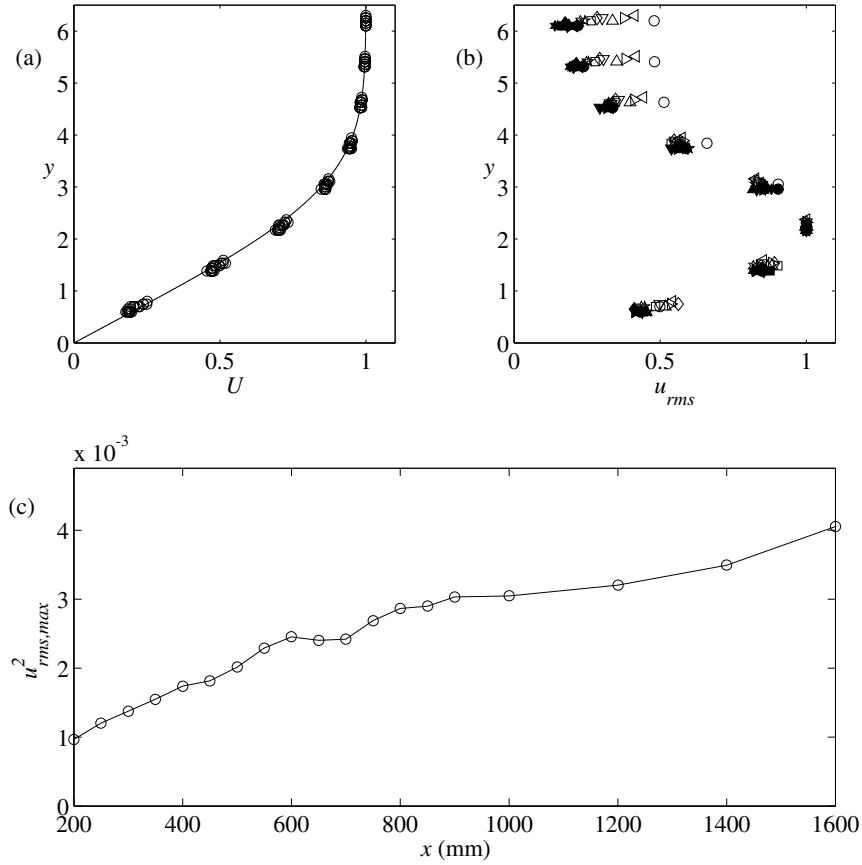


FIGURE 3. Mean flow without control applied, (a) mean velocity  $U$  at different  $x$  ranging from 200 mm to 1600 mm, (b) normalized profiles of  $u_{rms}$  and (c) streamwise development of  $u_{rms,max}^2$ .

The disturbance evolution is shown as the  $u_{rms}$  profiles in figure 3(b). The  $u_{rms}$  profile is self similar and in good agreement with earlier data (Kendall 1998): a maximum is found around  $y = 2.1$ . The profile agrees well with the optimal growth theory (not shown) of Andersson *et al.* (1999) and Luchini (2000). In the upper parts of the boundary layer, the disturbance approaches the free-stream turbulence level, which is decreasing downstream.

The streamwise growth of the maximum  $u_{rms,max}^2$  is shown in figure 3(c). The  $u_{rms,max}^2$  increases from 3% at  $x = 200$  mm to 6% at  $x = 1600$  mm. The flow is thus far from transitional in the region under study. Matsubara & Alfredsson

(2001) and others report that  $u_{rms}^2$  grows linearly with  $x$ . In the present setup, the growth is somewhat slower, especially at large  $x$ . The reason for this might be that  $Tu$  is in the lower range of previous studies and that the number of data points in  $y$  are too few to capture the exact maximum.

Having established the agreement between the present boundary layer and previous investigations, it is time to turn to the control results. The controller is run under the conditions to be presented in section 3.2. At  $x = 200 - 350$  mm, measurements were performed without control only, since the effect of the control could not be detected at these upstream positions. At  $x = 400 - 1600$  mm, measurements were performed both with and without control.

The mean velocity profiles with and without control are shown in figure 4(a). At  $x = 450$  and  $500$  mm, *i.e.* just above the control suction hole, there is a deviation between the measurement without control applied (o) as compared with the results with control (\*). At all other streamwise positions, the effect on the mean velocity profile due to the control is small.

Even though the control has a small effect on the mean flow, the effect on the disturbance growth is substantial. In figure 4(b) the profiles of  $u_{rms}$  at subsequent streamwise positions are shown. At each streamwise position, the profile is normalized with the maximum  $u_{rms}$  without control applied. At  $x = 450$  and  $500$  mm, the control is seen to decrease  $u_{rms}$  in the centre of the boundary layer while there is an increase closer to the wall. Further downstream, there is a consistent decrease at the centre of the boundary layer and no increase closer to the wall. The increase closer to the wall appears because of the actuation and the fact that the hot wire cannot distinguish between streamwise and wall-normal velocity. The fluctuating wall-normal velocity over the control suction hole thus gives an increase in the measured  $u_{rms}$ .

The small change of the mean velocity profile is further illustrated in figure 4(c) where the streamwise variation of the change in shape factor,  $H = \delta^*/\theta$ , with and without control is shown. The symbols  $\delta^*$  and  $\theta$  denote the displacement and momentum-loss thicknesses, respectively and for a Blasius boundary layer the shape factor is 2.59. With control applied, the shape factor is seen to decrease about 0.1 at  $x = 450$  to  $x = 600$  mm but further downstream, the shape factor is not changed by the control.

In order to obtain a consistent measure of the control effect, the disturbance energy in the boundary layer is calculated as

$$E(x) = \frac{1}{U_\infty^2} \int_0^6 [u_{rms}(x, y)]^2 dy \quad (3)$$

where the integral is discretized as a sum for the discrete measurements. The measurements were made with only eight points through the boundary layer in order to speed up the measurements. The consistency of  $E$  calculated from the sparse data as a measure of the disturbance level was confirmed by measuring the disturbance profile with and without control at  $x = 600$  mm and two point

Reactive control of free-stream turbulence induced transition

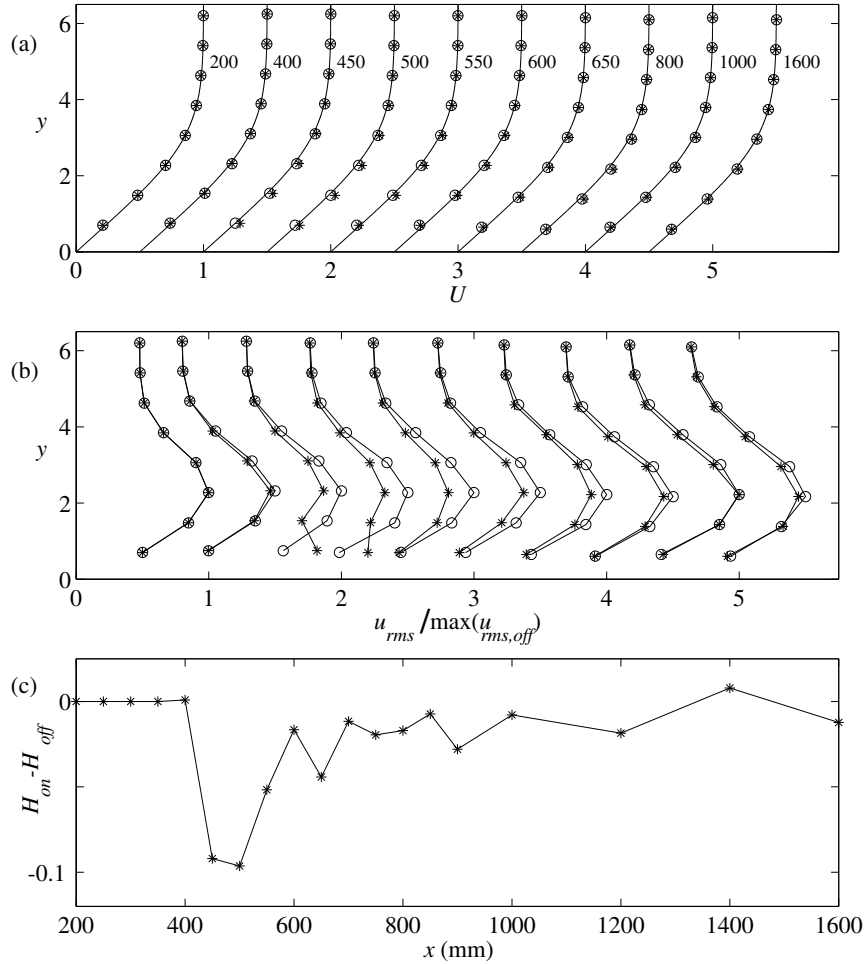


FIGURE 4. Mean flow and fluctuation with and without control applied, (a) velocity profiles with control ( $*$ ) on and ( $\circ$ ) off at the  $x$ -positions indicated around  $y = 5$  together with the theoretical Blasius solution ( $-$ ), (b) disturbance distributions from the positions in (a), at each  $x$  normalized with the maximal  $u_{rms}$  without control applied and (c) variation of the shape factor  $H$  with and without control applied. Consecutive profiles in (a) and (b) are off-set 0.5.

distributions, one being the standard one (eight points between  $y = 0.5$  and  $y = 6$ ) and the other one being 30 points from closer to the wall to  $y = 6$ .

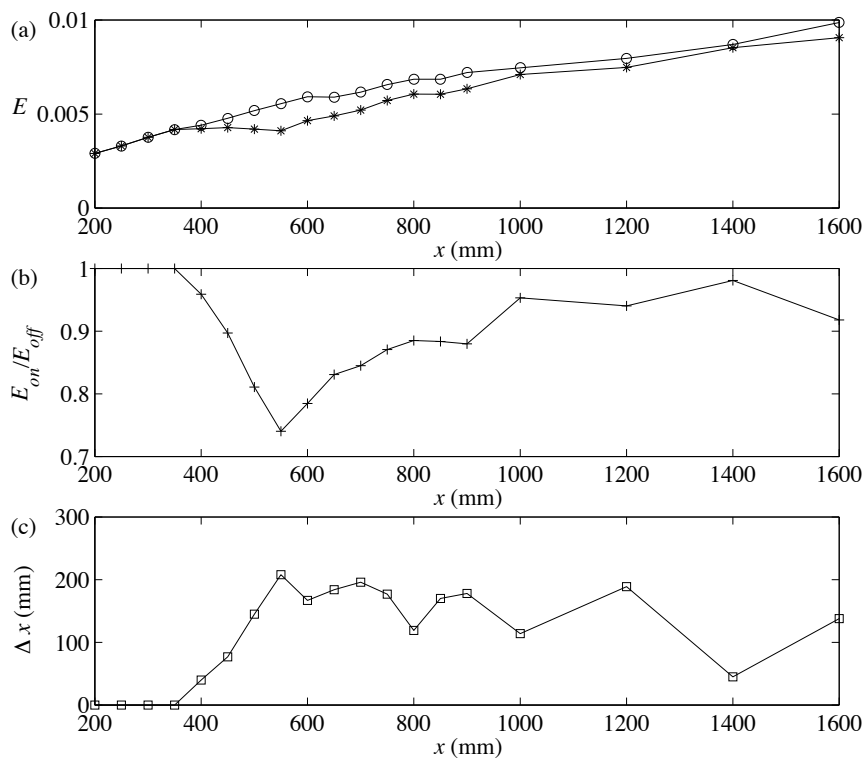


FIGURE 5. Streamwise development of  $E$ ; (a) control ( $*$ ) on and ( $o$ ) off, (b)  $E_{on}/E_{off}$  ( $+$ ) and (c) distance disturbance development is delayed by the control, defined by equation (4).

The values of  $E$  obtained with the two point distributions differs only a few percent.

In figure 5(a), the streamwise development of  $E$  is shown with and without control applied. Without control,  $E$  is seen to grow almost linearly with the streamwise position. If control is turned on, the disturbance energy is found to be constant from the control position at  $x = 450$  mm and almost 200 mm downstream. Compared to the values without control applied, the maximum energy reduction is found to be 26% (figure 5(b)). The growth of  $E$  downstream of  $x = 600$  mm with control applied is probably a combination of disturbances already in the boundary layer entering from the sides, new disturbances being introduced by the free stream and continued growth of the initial disturbances. The numerical study of Högberg & Henningson (2002) shows that optimal controllers, which manage to reduce the energy of single-mode disturbances a factor of 10, only give a reduction of about a factor of 3 when applied to optimal

Reactive control of free-stream turbulence induced transition

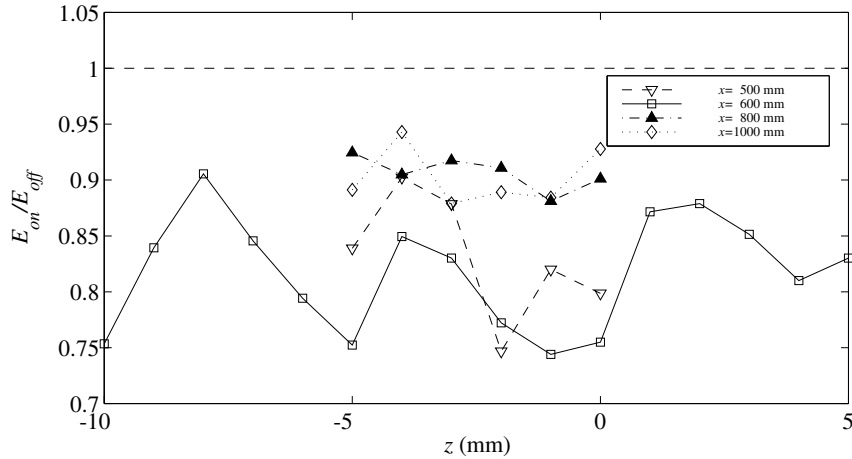


FIGURE 6. Spanwise variation of  $E_{on}/E_{off}$  at  $x = 500, 600, 800$  and  $1000$  mm as indicated in the label. The dashed line shows 1, the value obtained with no control.

disturbances. The numerical results show that the reduction of energy is limited to the region where control is applied, similar to the present experimental result. However, the results of Lundell & Alfredsson (2003a) show that substantial transition delay can be obtained also by decreasing the strength of streamwise streaks, complete cancellation is not necessary.

One way to quantify the control effect is to study the distance the disturbance development is delayed by the control, *i.e.* to determine  $\Delta x$  so that

$$E_{on}(x) = E_{off}(x - \Delta x). \quad (4)$$

This measure is shown in figure 5(c), where it is seen that  $\Delta x$  reaches a value of approximately 200 mm at  $x = 450$  mm decreases slowly downstream. There is a tendency that  $\Delta x$  starts to decrease downstream of 1000 mm, but the data is too sparse to draw any firm conclusions in this region. Even if the disturbance amplitude starts to grow again downstream of  $x = 550$  mm, the "disturbance development distance"  $\Delta x$  gained by the control remains close to constant.

So far, measurements have been presented for positions straight downstream of the control suction hole at  $z = 0$  only. In figure 6, the reduction in  $E$  due to the control is shown as a function of  $z$  at four streamwise positions. At  $x = 500, 800$  and  $1000$  mm, the measurements have been performed at  $-5 < z < 0$  only, while at  $x = 600$  mm, the measurements span  $-15 < z < 5$ . The data has been normalized with the uncontrolled value, so that all values lower than 1 indicate a positive control effect. At all points, there is a reduction in the fluctuation energy thanks to the control. In figure 6 it is observed that at

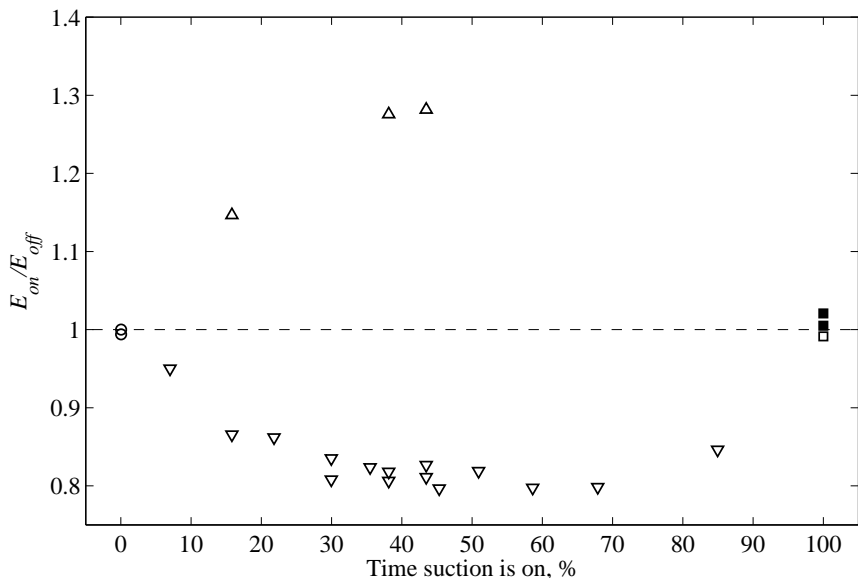


FIGURE 7. Control effect ( $E_{on}/E_{off}$ ) as a function of the time control suction is applied; suction on low velocity ( $\nabla$ ), suction on high velocity ( $\Delta$ ) ( $x = 600$  mm), no (0%) suction ( $\circ$ ) ( $x = 600$  mm) and continuous (100%) suction ( $\square$ ) ( $x = 600$  mm) and ( $\blacksquare$ ) ( $x = 500$  and  $800$  mm).

$x = 500$  mm, only 50 mm downstream of the actuators, there is a strong spanwise variation of the control effect. This is due to the vicinity to the actuation and the mixture of streamwise and wall-normal velocity disturbances detected by the hot wire. Further downstream, at  $x = 600$  mm (the solid line), the reduction has a maximum at the spanwise positions of the sensors and control suction holes ( $z = -10, -5, 0$  and  $5$  mm). At these positions, the reduction is around 25%. In between the control positions, the effect is smaller and the reduction is around 10–15%. Continuing to  $x = 800$  and  $1000$  mm, the control effect seems to be smeared out in the spanwise direction.

### 3.2. Parameter variation

The controller involves three parameters: the delay  $d_c$  between detection and actuation, the flow rate through the control suction hole and finally the threshold value of the wall shear stress signal  $W$ , below which control suction is turned on. These parameters have to be tuned to get a good control effect. The initial state for the parameter study presented in figures 7–9 was found by trial and error. Once a parameter combination giving a detectable control effect was found, the three parameters were tuned, aiming to find an optimum.

*Reactive control of free-stream turbulence induced transition*

3.2a. *Threshold.* The open symbols in figure 7 show the control effect at  $x = 600$  mm for various threshold values. As filled symbols, the data obtained at  $x = 500$  and  $800$  mm with continuous suction through the control holes is shown. The control effect is measured as  $E_{on}/E_{off}$  and the threshold value is not shown explicitly, instead the resulting fraction of time that control was turned on is shown. The four different symbols in figure 7 stand for different cases. The reference, no control, (0%) case is marked by circles ( $\circ$ ) and the squares ( $\square$ ) show the control effect obtained with continuous suction (100%) through the control suction hole. One notes that with continuous suction, there is no control effect: the disturbance level is the same as without suction applied. This excludes the possibility that the control effect is due to mean-flow modification rather than streak cancellation, since if this was the case, the control effect would increase with the time the suction was turned on.

It is also seen that the disturbance level was the same with no and continuous suction also at  $x = 500$  and  $800$  mm, confirming that the effect is not limited to  $x = 600$  mm only.

With the two limiting cases of no and continuous suction studied and understood, the attention is turned to the cases in between, marked with triangles pointing upwards ( $\triangle$ ) and downwards ( $\nabla$ ). They differ so that the upwards pointing triangles ( $\triangle$ ) denote suction applied when  $W$  is larger than threshold, whereas the downwards pointing triangles ( $\nabla$ ) denote suction applied when  $W$  drops below the current threshold. Upwards pointing triangles thus denote the result when suction is applied to high-speed streaks while downwards pointing triangles denote suction applied to low-speed streaks.

Studying the downwards pointing triangles in figure 7 from 0% to 100%, one sees that as suction is applied to regions of negative velocity deviations, the disturbance level is initially decreased. As the threshold value is increased, and suction is applied also to regions of less extreme velocity deviations, the effect flattens out at 30%, becomes approximately constant until 70% suction time whereupon the disturbance energy increases towards the continuous suction value. Observe that from 50% and up, suction is applied also at periods of positive velocity disturbances, why the increase in the disturbance level is natural. The return to unity is however not obvious.

Finally, the attention will be turned to the upwards pointing triangles. They show the response of the flow if suction is applied at instances of high velocity. Doing so, the disturbance level increases, presumably because the high velocity streaks are amplified and the low velocity streaks are left as they are. There is a tendency of a flat area above 40% suction. Larger time fractions with suction on high-speed structures have not been measured, since the main interest of the present study is to delay transition and reduce the strength of the streaks, rather than promoting it. When the time fraction increases towards

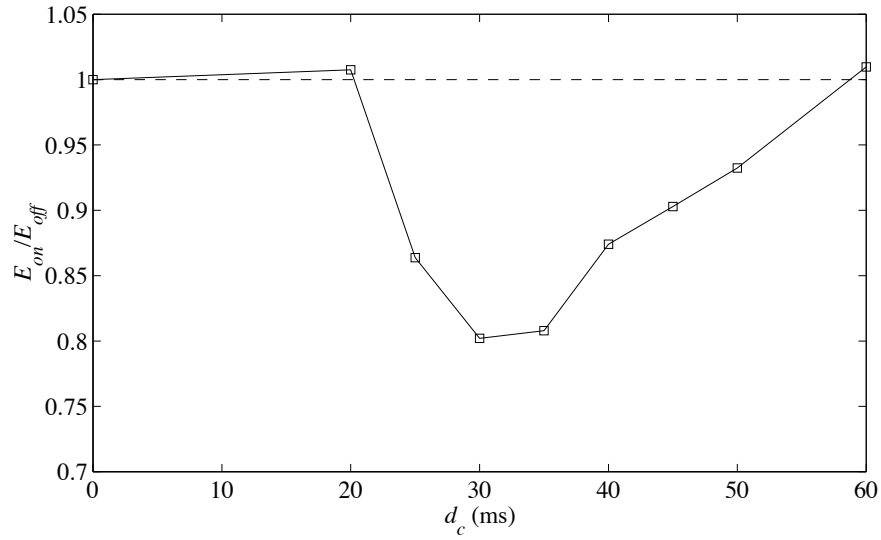


FIGURE 8. Control effect ( $E_{on}/E_{off}$ ) as a function of delay  $d_c$  between detection and actuation.

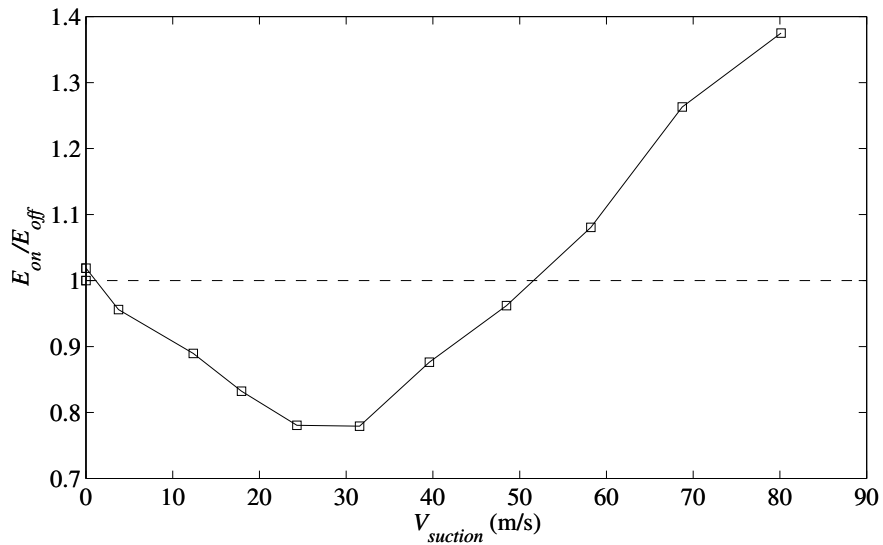


FIGURE 9. Control effect ( $E_{on}/E_{off}$ ) at  $x = 600$  mm as a function of velocity through the suction holes.

100%, the disturbance level must approach the value obtained for continuous suction, *i.e.* 1.

### *Reactive control of free-stream turbulence induced transition*

3.2b. *Delay.* The delay between sensor and actuation was found to have an optimal value around 32 ms as shown in figure 8. The control effect decreases somewhat differently for longer and shorter delays, respectively. For longer delays, the control effect decreases and disappears at a delay of 60 ms. If, however, delays shorter than the optimal one is considered, there is no effect already at 20 ms, 12 ms shorter than the optimal one. This asymmetry might seem puzzling at first sight, but is explained by the anti-disturbances introduced by the control suction. The control suction generates a region of high velocity. If this anti-disturbance is turned on a little bit late (large delays), it can catch up with the low velocity streak to be controlled, now downstream of it. If the anti-disturbance instead is turned on too early, the high velocity anti-disturbance appears downstream of the low velocity streak, and the distance between them will increase as they propagate downstream.

3.2c. *Suction strength.* Also when it comes to suction strength, there is a clear optimum as seen in figure 9. Increasing the suction strength from zero, the control effect increases and reaches an optimum whereupon the disturbance level increases again. Increasing the suction rate far above the optimal value, the disturbance level increases and for high enough suction rates, transition to turbulence is forced by the control suction.

3.2d. *Parameter settings.* During the control experiments, the threshold was set such that suction occurred 30% of the time and the delay was chosen as 32 ms. The suction velocity was 28 m/s, except for figure 7 where it was 18 m/s, since the optimal value was not known when that data was taken. A further variation of the threshold and suction velocity is not expected to give a substantial improvement of the control effect.

### 3.3. *Spectra*

3.3a. *Streamwise development.* With the control effect carefully determined (inhibited growth of  $E$  from the position of the actuator and 200 mm downstream) and the optimal working point of the controller detected, structure development with and without control can be studied. First, straightforward spectra of the streamwise velocity at different streamwise positions with control on and off are shown in figure 10. The spectra are taken from close-to-constant  $y = 2.1$ . The energy has been multiplied by the frequency, so that the area under the curve in the semi-logarithmic plot is the total fluctuation energy in the frequency band under study. Matsubara & Alfredsson (2001) reported that the streamwise lengthscale increases with the boundary-layer thickness. This was concluded by the fact that the spectra for low frequencies could be made to collapse if the frequency was non-dimensionalized with the boundary-layer thickness and the free-stream velocity. In figure 10(a), an increasing importance of low frequencies further downstream is seen: without control, the peak

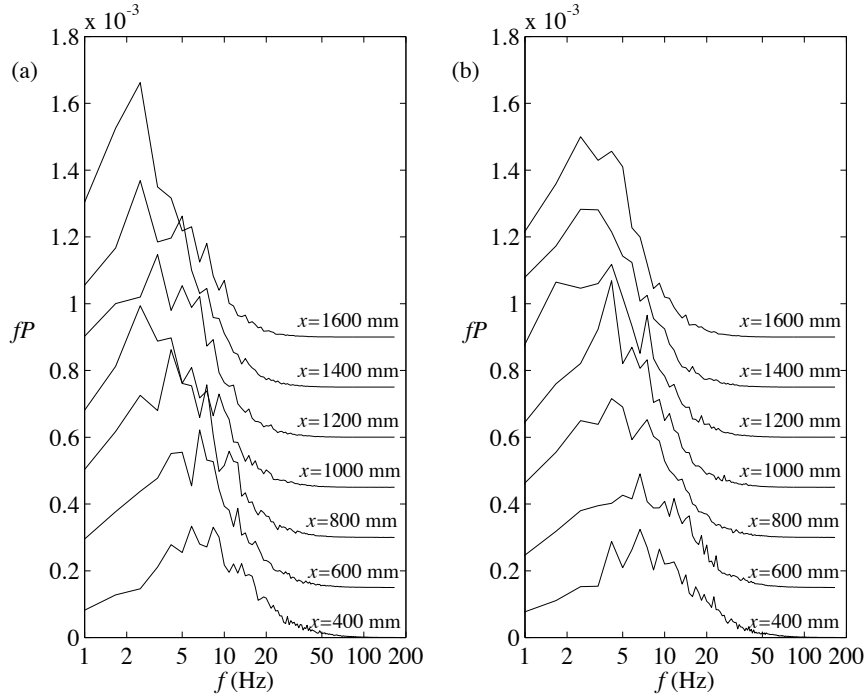


FIGURE 10. Spectra of the velocity at  $y = 2.1$  and  $x = 400, 600, 800, 1000, 1200, 1400$  and  $1600$  mm with control (a) off and (b) on.

moves to lower frequencies while getting narrower as  $x$  increases. Under reactive control, as shown in figure 10(b), the situation is similar, although the movement to lower frequencies seems to be delayed by the control.

A measure of this effect is shown in figure 11, where the frequency below which 90% of the energy appears,  $f_{90}$ , is shown for various  $x$  with and without control. Without control ( $\circ$ ), the value decreases from 16 Hz at  $x = 400$  mm to just below 6 Hz at  $x = 1600$  mm. When control is applied,  $f_{90}$  is almost constant from  $x = 400$  to 600 mm, the region during which fluctuation growth is inhibited by the control. After  $x = 600$  mm, the values with control approaches the values obtained without control. As opposed to the disturbance energy, the frequency is returning to a certain distance, instead it is constant for some distance downstream of the control, further downstream no difference between the two cases can be detected.

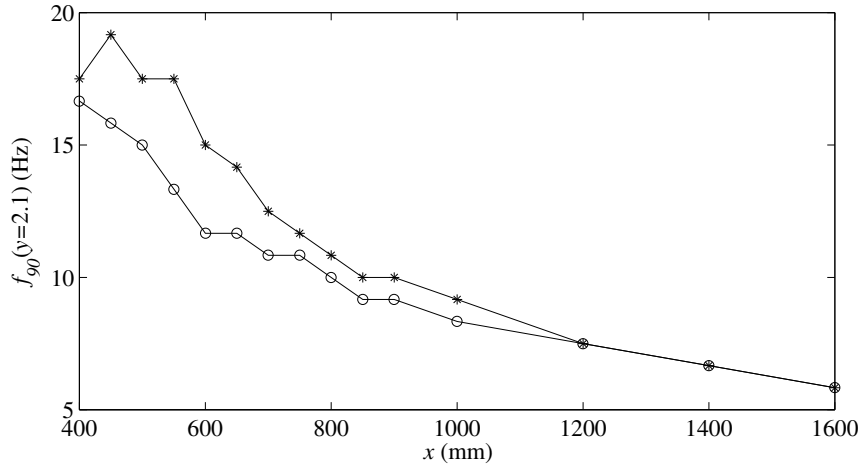


FIGURE 11. Streamwise variation of the frequency below which 90% of the energy appears,  $f_{90}$ , at  $y = 2.1$  with control on (\*) and off (o).

3.3b. *Wall-normal structure.* Velocity signal spectra at different heights in the boundary layer at  $x = 600$  mm are shown in figure 12. Close to the wall most energy is found for low frequencies and up through the boundary layer, the dominant frequency increases. The spectra are concentrated around lower energy without control than with, especially close to the wall (compare figure 12(a) and (b)).

In figure 13,  $f_{90}$  is shown at various heights through the boundary layer and at different streamwise positions. Without control, figure 13(a), the boundary layer is seen to filter out the high frequencies from the free stream and amplify the low ones. There is a monotonous decrease towards the wall from  $y = 6$ , where  $f_{90}$  is around 170 at all streamwise positions, down to the wall where the minimum value of  $f_{90}$  is reached at the most downstream position and reads around 8 Hz. The curves from the three streamwise positions appear side by side. With control applied, figure 13(b), the curves for  $x = 400$  and 600 mm collapse close to the wall. Further out towards the free stream, the behaviour with and without control is more similar.

### 3.4. Correlations

Finally, correlations between the signal from the wall wire positioned at  $x = 214$  mm and the hot-wire signal are shown. In figure 14 the streamwise development of the maximum correlation (at the delay between the signals maximizing the correlation) at  $y = 2.1$  is shown with and without control. The correlation is seen to be close to unity at  $x = 250$  mm, *i.e.* almost straight above

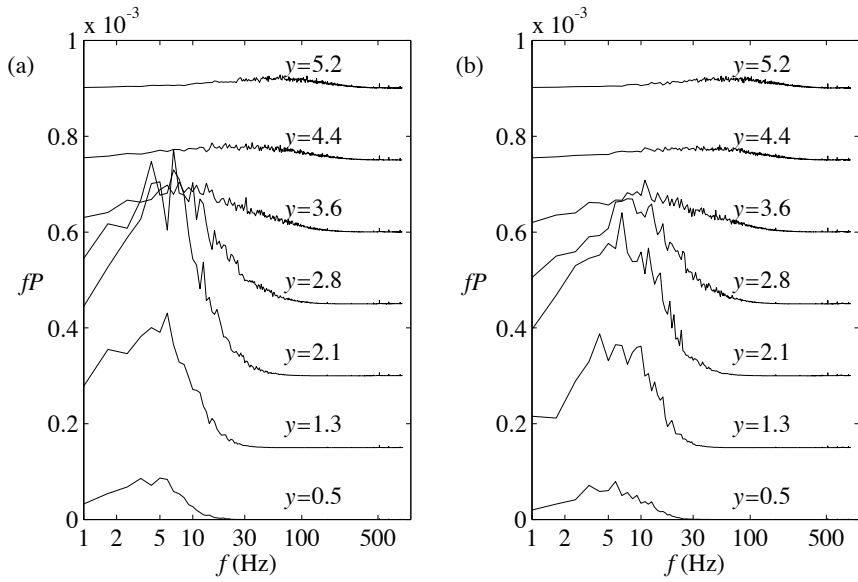


FIGURE 12. Spectra of the velocity at  $x = 600$  mm and  $y = 0.5, 1.3, 2.1, \dots, 6$  with control (a) off and (b) on.

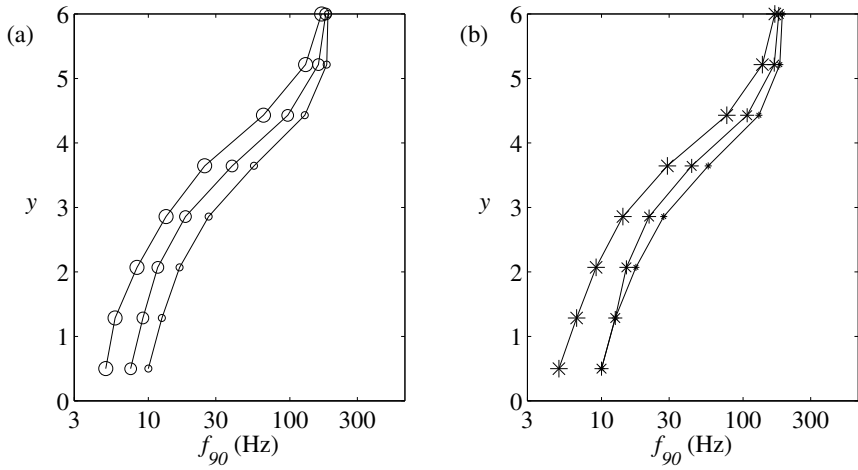


FIGURE 13. Wall-normal variation of the frequency below which 90% of the energy appears,  $f_{90}$ , at  $x = 400, 600$  and  $1200$  mm (increasing with marker size) with control (a) off and (b) on.

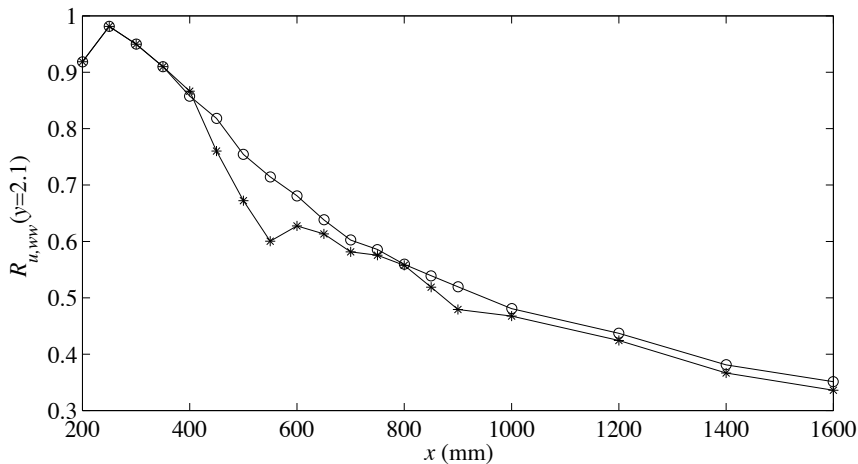


FIGURE 14. Correlation between the wall wire and the hot wire at  $(x = 600 \text{ mm}, y = 2.1)$  with (\*) and without (o) control applied.

the wall wire, demonstrating that the flow structures detected by the wall wire are coherent across the boundary layer up to at least  $y = 2.1$  where the same structure is detected by the hot wire. Moving the hot wire downstream, the correlation decreases. At the streamwise position of the actuator,  $x = 450 \text{ mm}$ , the correlation has dropped to just above 0.80. Further downstream, the correlation continues to decrease and becomes 0.35 at  $x = 1600 \text{ mm}$ . With control applied, the correlation is slightly decreased in the region where the growth of disturbance amplitude is inhibited ( $x = 450$  to  $600 \text{ mm}$ ). Apart from this region, the control does not have a large effect on the correlation between signals from the wall wire and the hot wire.

Larger effects due to the control are found in the delays maximizing the correlation,  $\tau_{max}$ , which are shown in figure 15 (not to be confused with the delay  $d_c$  used in the controller). Without control,  $\tau_{max}$  grows linearly in the downstream direction, a result indicating that the structures in the boundary layer propagate downstream with constant velocity. The effect due to the control is not large in figure 15(a), even though it can be seen that the delay becomes somewhat lower from  $x = 450 \text{ mm}$  and downstream with control applied. The difference is accentuated in figure 15(b), where the difference in delay,  $\tau_{max,off} - \tau_{max,on}$  with and without control is plotted. The delay is found to be up to 8 ms shorter when control is applied, showing that the disturbances correlated with the wall-wire signal appear 8 ms earlier at  $x = 600 \text{ mm}$  as compared to the case without control applied.

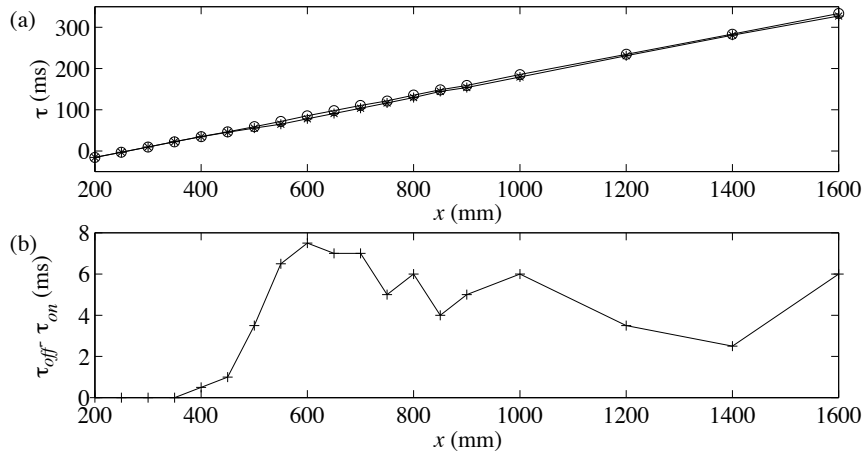


FIGURE 15. Delay maximizing  $R_{u,ww}(x, y = 2.1)$  as a function of  $x$ , (a) control (\*) on and (o) off and (b) its difference with control on and off in (b).

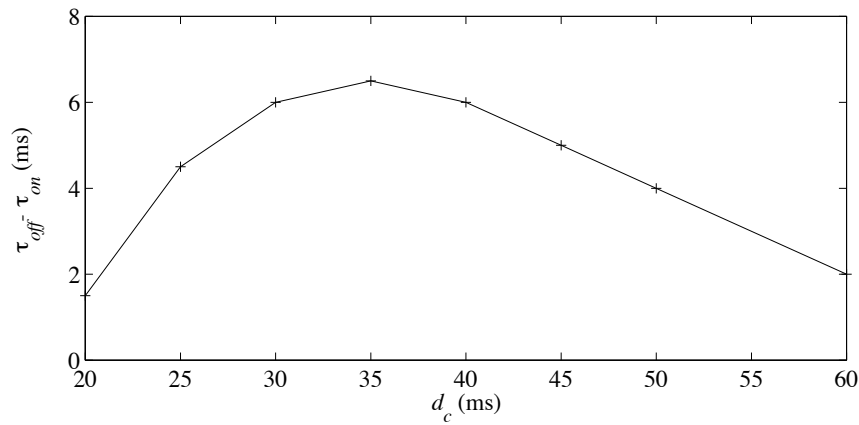


FIGURE 16. Delay maximizing  $R_{u,ww}(x = 600 \text{ mm}, y = 2.1)$  as a function of the delay in the control loop,  $d_c$ .

Figure 16 shows the difference in  $\tau$  maximizing the correlation as a function of  $d_c$ , the delay between sensing and actuation. For all  $d_c$ , the disturbances are seen to arrive to the hot wire at  $x = 600 \text{ mm}, y = 2.1$  earlier with control applied than without. The advancement in time is found to have a maximum at a delay close to the one maximizing the control effect (compare figure 8).

*Reactive control of free-stream turbulence induced transition*

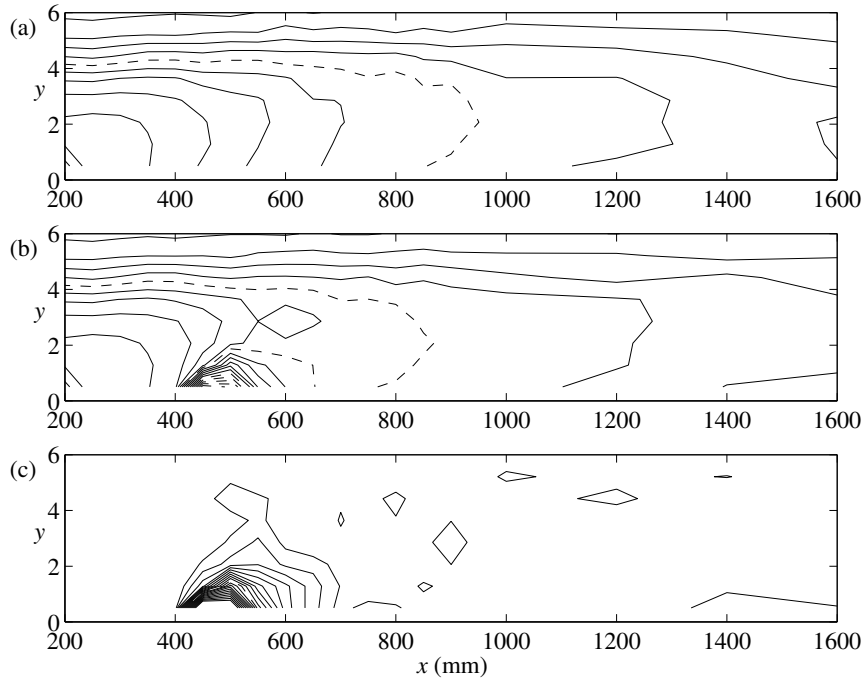


FIGURE 17. Maximum correlation between the wall wire and the hot wire (a) without, (b) with control and (c) difference between (a) and (b). Contour separation is 10%, the contour at 50% and the negative contours are dashed.

This indicates that the advancement in arrival time is directly related to the cancellation of the streaks when the control is successful.

The contours in figure 17 show the maximum correlation obtained with the hot wire positioned in different positions. The contour denoting 50% correlation is dashed, and the contour spacing is 10%. With control applied, shown in (b), there is a strong negative correlation in the region  $400 < x < 500$  mm, which is due to the control suction (which of course is negatively correlated with the sensor signal). Comparing the case with control in figure 17(b) with the case without control in (a), the dashed 50% contour is found to be slightly more upstream with control applied. Apart from the negative correlation around the control suction hole, there are no substantial between the two cases, as is also illustrated in figure 17(c) where the difference between the two cases is shown.

In figure 17 the correlation between the disturbance at the sensing position,  $x = 214$  mm, is found to have a correlation of 80% with the disturbances at the actuation position,  $x = 450$  mm. By applying linear system identification

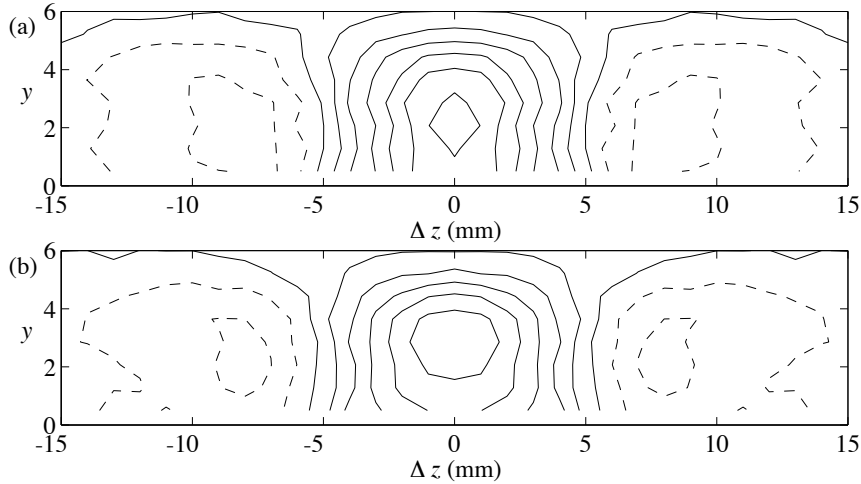


FIGURE 18. Cross-flow distribution of the maximum correlation at  $x = 600$  mm with control (a) off and (b) on. Contour spacing is 10% and negative contours are dashed. The correlation has been calculated for positive separations, averaged over the four wall wires and mirrored at  $z = 0$ .

(*e.g.* Wiener filters as used by Amonlirdviman & Breuer (2000)) it is possible to increase this value to 82–83%. The benefit from using linear system identification is thus very small in the present case, and was not further pursued. This also indicates that the fluctuation energy appearing at  $x = 450$  mm, which is uncorrelated with the wall-wire signal, is due to noise entering the system or non-linear dynamics. If they were the result of linear dynamics, such a development should be possible to catch with the linear system identification. One important non-linear mechanism of the streaks is probably that high- and low-speed streaks might travel with different velocities. An important consequence of figure 17(b), which must be taken into account when designing control systems with even more sensors, is that the information obtainable at the wall just downstream of the control does not reflect the developments in the flow above, due to the strong, localized actuation. This problem might disappear if the actuation is more distributed.

The cross-stream structure of the disturbances is illustrated in figures 18 and 19. In figure 18, the maximum correlation between the wall-wire sensor and the hot wire at  $x = 600$  mm is shown. To obtain the correlation for different  $\Delta z$  in minimum time, the hot wire was traversed in between two of the wall wires, whereupon the correlations were calculated between the hot-wire signal and the signal from suitable wall wires. In order to increase the visual impact of the data, the data has been mirrored around  $\Delta z = 0$ . In figure 18, the

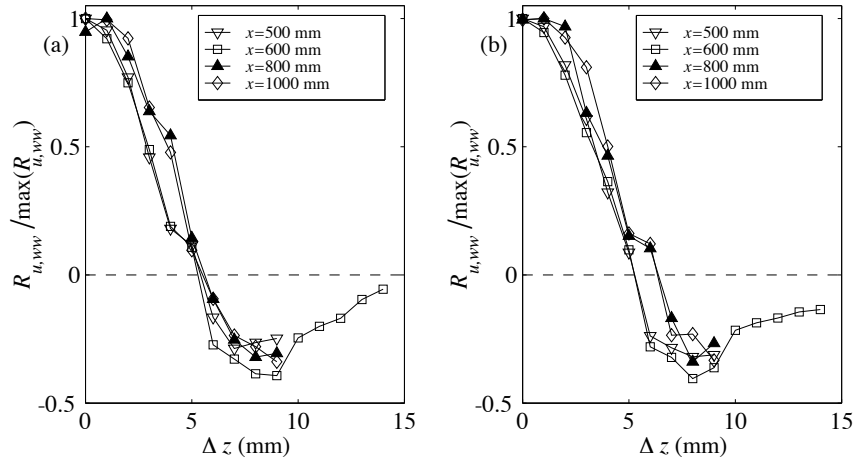


FIGURE 19. Cross-flow distribution of the maximum correlation between the wall wire at  $(x, y, z) = (214 \text{ mm}, 0, 0)$  and the velocity at  $(y, z) = (2.1, \Delta z)$  at  $x = 500, 600, 800$  and  $1000 \text{ mm}$  without control applied normalized so that the maximum of each correlation is 1.

cross-stream distribution is seen to be insensitive to the control. Neither the spanwise width nor the height of the structures are changed by the control. The only detectable difference is that without control in figure 18(a), the structure is seen to extend all the way down to the wall, whereas with control applied, the correlation is lower close to the wall.

In figure 19, the spanwise structure of the correlation (a) without control and (b) with control applied is shown at different streamwise positions. Each correlation has been normalized by its maximum value, found in figure 14. Figure 19(a) shows that while the disturbances travel from the wall wire, the spanwise scale remain constant. When control is applied, as seen in (b), there is a tendency of widening of the structure far downstream. The widening is however fairly small and further measurements are needed if the streamwise development of the spanwise structure without and with control are to be detected accurately.

Finally, the temporal evolution of the correlation structures are shown in figures 20 (no control) and 21 (control). Without control, the structure is seen to develop downstream. At first, the structure is short and as it develops downstream, it grows in length. The structures have been found to grow as the boundary layer thickness, *i.e.* as  $x^{0.5}$  (Matsubara & Alfredsson 2001; Lundell & Alfredsson 2003b). When control is applied, the length of the structure is seen to increase much less, as also deduced from the spectra above.

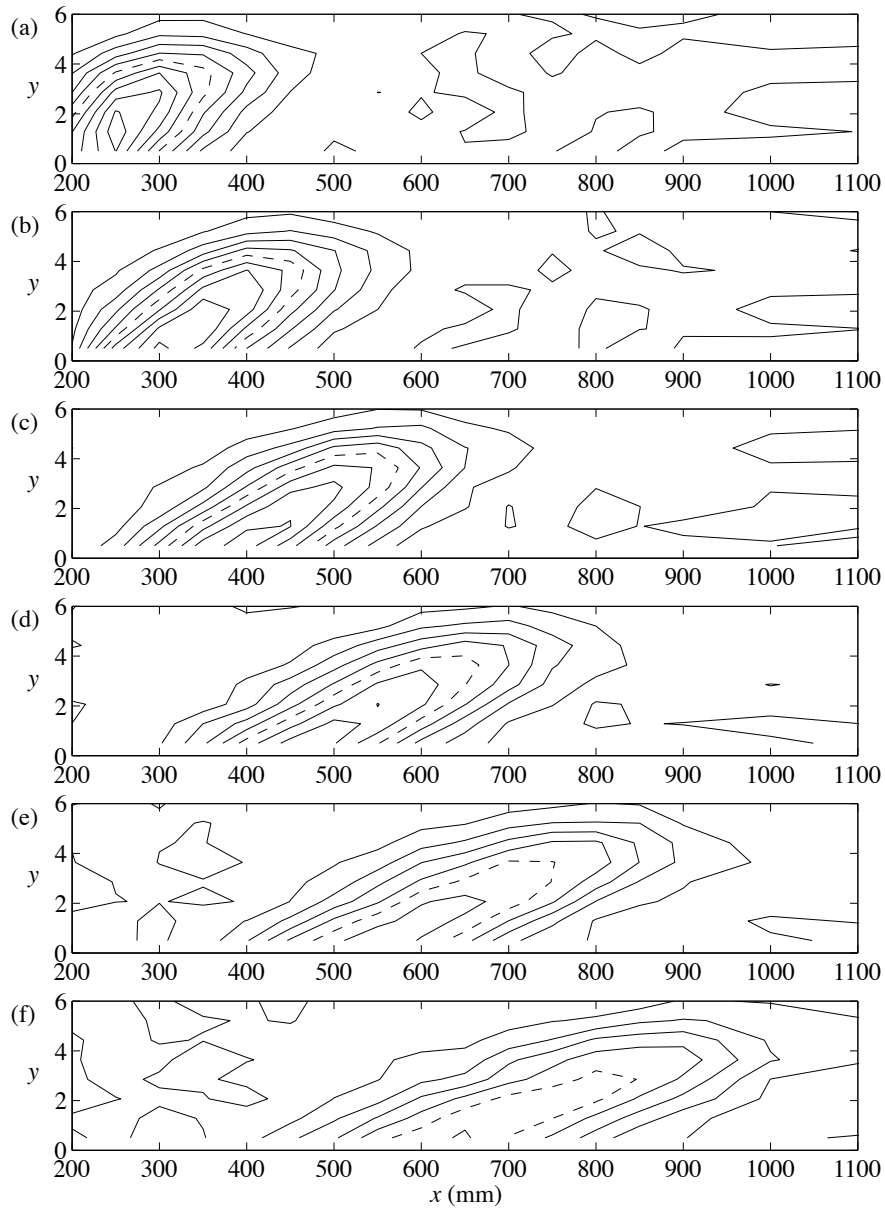


FIGURE 20. Correlation between the wall wire and the hot wire,  $\tau = 0$ –125 ms from (a) through (f). Contour separation is 10%, the 50% contour is dashed.

*Reactive control of free-stream turbulence induced transition*

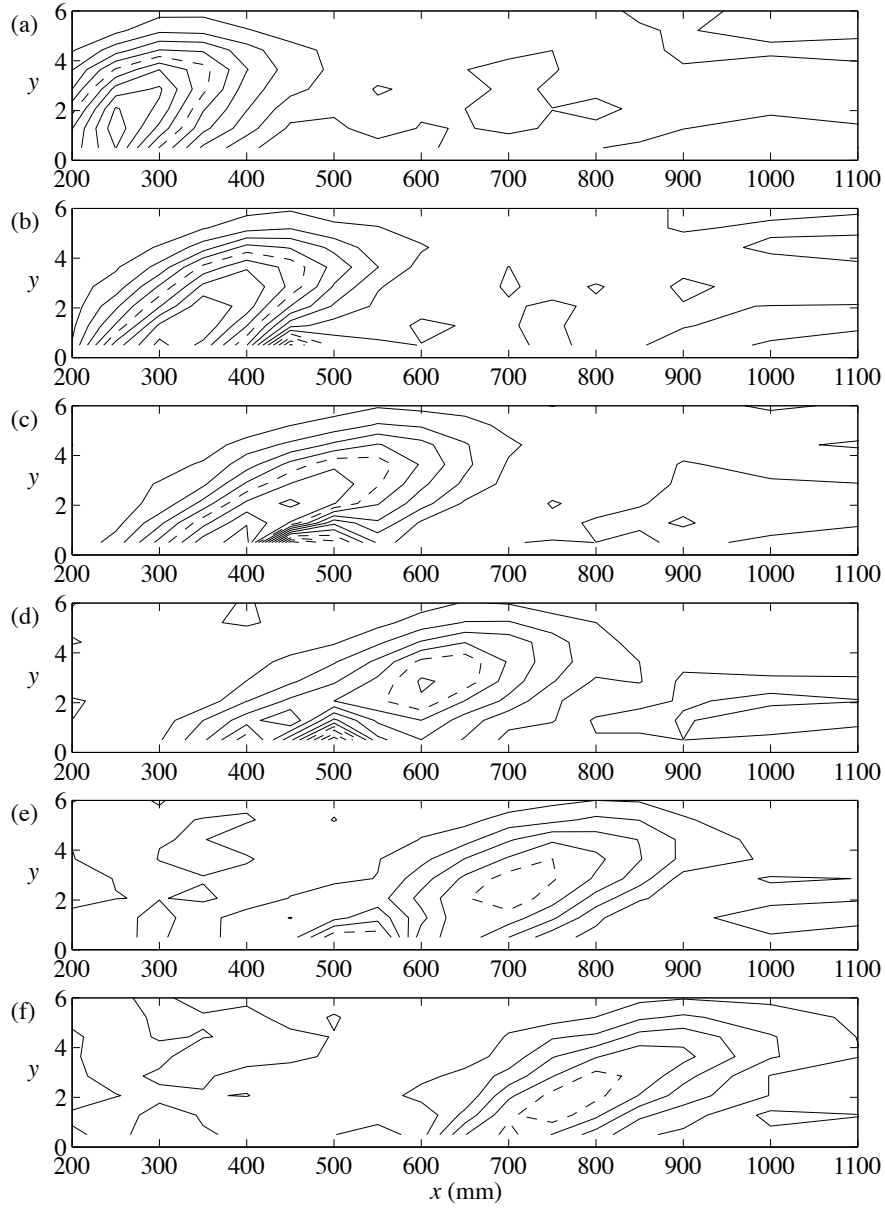


FIGURE 21. Correlation between the wall wire and the hot wire,  $\tau = 0$ –125 ms from (a) through (f). Contour separation is 10%, the 50% contour is dashed.

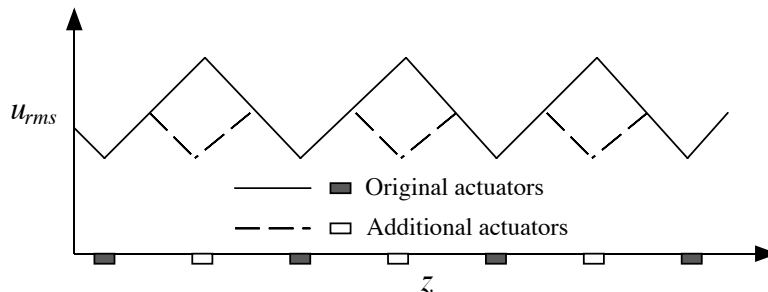


FIGURE 22. Schematic of spanwise disturbance distribution with increased numbers of sensors and actuators.

#### 4. Discussion

Even though the main control result, that the disturbance amplitude development is hindered for 200 mm, is very clear in figure 5(b), there are a few aspects of the results that deserve further discussion.

From figure 6, showing the spanwise distribution of disturbance energy, it can be conjectured that increasing the sensor and actuator density by a factor of two can improve the spanwise control result substantially (*cf.* figure 22). Allowing some speculation, the spanwise profile at  $x = 600$  mm (figure 6) would then have a maximum around 0.82 rather than 0.92 as it is now. Consequently, the level at which the fluctuation energy is smeared out further downstream should also be reduced. Increasing the sensor/actuator density even further will probably give smaller gains in the disturbance attenuation. The physical reason for this might be that with such a density, most (low-speed) streaks can be reduced. In the present experiment, the sensor separation is just large enough for a streak to pass in between two sensors without detection. In this context it should also be noted that Lundell & Alfredsson (2003a) showed that in order to delay transition of streaks in a channel flow with localized suction, it has to be applied within a rather narrow region around the centre of the streaks.

If doubling the actuator density, the actuator separation would be approximately  $25 l^+$  or  $2\delta$  (see table 1), *i.e.* slightly wider than half the boundary-layer thickness. Previous correlation measurements and analysis of flow visualization images show that the width of the streaks is around  $2\delta^*$ , or  $3.4\delta$ . The cross-stream correlation measurement from the present experiment shows that the streaks have a width of  $6\delta$  at the position of the actuation. It might thus be necessary that the spanwise actuator separation is considerably smaller (factor of 3) than the width of the streaks.

The results from the variation of the threshold in figure 7 serve as a good illustration of the most important differences of the present work compared

*Reactive control of free-stream turbulence induced transition*

to two of the previous experimental studies on reactive flow control, namely Rathnasingham & Breuer (1997) and Kerho *et al.* (2000).

In the study of Rathnasingham & Breuer (1997), reactive control was applied to a turbulent boundary layer and the bursting frequency, pressure fluctuations and friction drag, measured from the mean velocity profiles, was decreased. However, their actuator could produce actuation with one sign only, while their controller resulted in control signals of both signs. In the present setup, this would correspond to applying suction to both high- and low-speed streaks, which of course would reduce the positive effect of the control (or actually cancel it completely). The results of Rathnasingham & Breuer (1997) might however be of large engineering importance, but the physical interpretation of the control effect gets blurred by the single-signed actuation.

As compared to Kerho *et al.* (2000), who used reactively controlled intermittent suction to decrease the drag in a turbulent boundary layer, the present study reports no control effect for continuous suction. In the case of Kerho *et al.* (2000), the control effect was only slightly increased for reactively controlled suction, as compared to continuous suction through the same suction ports. Even though the turbulent boundary layer might be of greater engineering importance, the clear and logic results of the present experiment allow a detailed study of the control effect.

If the flow rate used during the control experiments,  $q$ , through one of the control holes is averaged over the area,  $A$ , where the control has an effect,  $5 \text{ mm} \times 200 \text{ mm}$  (*i.e.* the actuator separation times the disturbance development delay,  $\Delta x$ ), the suction coefficient defined by  $C_q = q/U_\infty A$  becomes  $3.4 \times 10^{-4}$ . This suction coefficient is almost equal to the suction coefficient necessary to delay breakdown of streaks in a plane channel flow as studied by Lundell & Alfredsson (2003a). It is approximately one third of the uniform suction necessary to inhibit disturbance growth in a boundary layer subjected to similar levels of FST (Yoshioka *et al.* 2003).

Some space will also be devoted to a hypothetical explanation of the early arrival of structures reported in figures 15 and 16. If it is due to pure acceleration of the structures, the structures have to increase their velocity due to the control and gain 8 ms from  $x = 450$  (the control position) to  $x = 550 \text{ mm}$ . After this initial and quick acceleration, the structures would move with the same velocity as without control applied. Such a direct explanation seems unlikely: why would the disturbances suddenly accelerate and decelerate like that?

A possible scenario will be given based on the sketch in figure 23. Consider the boundary layer over the flat plate, subject to disturbances in the free stream. Initially, a disturbance in the free stream (illustrated by the vertical arrow) introduces a small amplitude streak (the horizontal arrow) in the boundary layer at  $x_1$ . The streak is growing in amplitude and length while

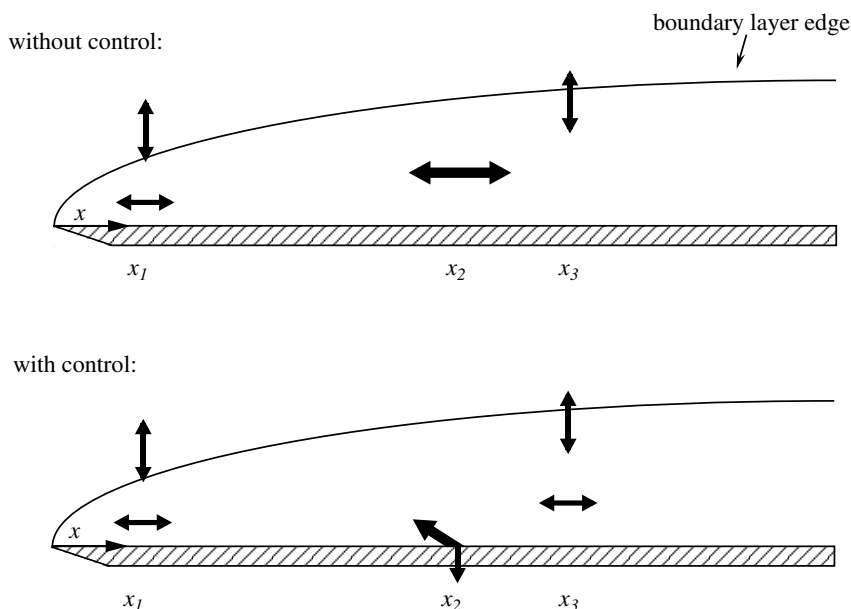


FIGURE 23. Illustration of the attempt to explain the decrease in delay maximizing the correlation due to the control.

propagating downstream with a velocity around  $0.8U_\infty$  (Lundell & Alfredsson 2003b), whereas the free-stream disturbance is convected with the velocity  $U_\infty$ . When the streak has moved to  $x_2$ , the faster free-stream disturbance has reached  $x_3$ , as indicated in figure 23. The velocity signal at  $x_2$  will of course be correlated to the wall-shear disturbance detected at  $x_1$  with a proper time delay between the signals. A moment later, the streak will reach  $x_3$ , giving a correlation between the velocity at this position and the shear stress at  $x_1$ .

When control is applied, the situation becomes somewhat different. Assuming that the control suction, positioned at  $x_2$ , completely removes the streak introduced at  $x_1$  (not by forcing it into the wall as indicated in figure 23, but by rearranging the momentum in the boundary layer), the main contribution to the correlation between the shear stress at  $x_1$  and the velocity at  $x_3$  could be a new, weak, streak, generated by the free-stream disturbance downstream of  $x_2$  and thereby not attacked by the control. At  $x_3$ , the new streak has not yet grown to high amplitudes, but with the control suction removing the streak generated upstream, it may give a considerable contribution to the correlation between the signals. This correlation will of course be obtained with a shorter delay between the signals as compared to the case without control applied. Once created, the streak created at  $x_3$  will propagate with the typical structure velocity.

### *Reactive control of free-stream turbulence induced transition*

However, the numbers must be correct if some belief is to be put into this explanation. Assume that the disturbance at  $x_1$  is created at  $t = 0$  and that  $x_1$  is somewhere close to the leading edge, *e.g.* at  $x = 100$  mm. Without control, the streak will arrive at  $x_3$  (which we assume to be at  $x = 500$  mm) at  $t_{off} = 0.8U_\infty/(x_3 - x_1)$ . Inserting the numbers we get  $t_{off} = 100$  ms. For the case with control, the new streak created at  $x_3$  will appear at  $t_{on} = U_\infty/(x_3 - x_1)$ , giving  $t_{on} = 80$  ms. The difference is thus 20 ms, about twice the change seen in the measurements. The observed value is 7–8 ms, which seems plausible since the effect of the control on disturbance energy was around 25%.

The physical situation differs from the discussion above so that in the real situation there is a continuous forcing on the boundary layer from the free-stream. The disturbances observed at a specific  $x$  are thus the integrated result of the continuous forcing and the amplification of disturbances by the boundary layer. To fully understand the mechanism behind the early arrival with control applied, a better understanding of the fundamental physics of how disturbances in the free stream forces streaks in the boundary layer is needed.

The near-constant correlation with and without control (see figure 14(a)) together with the change in arrival time indicate that at least some of the energy appearing downstream of  $x = 600$  mm (figure 5) with control applied is due to new streaks created by disturbances in the free stream. The reasoning behind this assumption is that streaks entering from the sides would not be correlated with the wall wire why the downstream correlation should decrease with control applied if such streaks were the source of the disturbance growth downstream of the control.

## **5. Conclusions**

A reactive control system has been used to control disturbances in a boundary layer subjected to free-stream turbulence. Wall wires were used to sense disturbances in the boundary layer and further downstream, suction through narrow holes were used to decrease the strength of structures of low velocity passing over the hole. A parameter variation was performed in order to find the optimal working conditions of the control.

The effect of the control are summarized below.

- Applying the control did not change the mean flow, except very close to the control suction hole, where the velocity profile became fuller.
- The growth of the amplitude of the streamwise velocity fluctuations were inhibited from the actuation position and 200 mm downstream, corresponding to approximately 40 boundary-layer thicknesses.
- The streamwise development of the spectra towards lower frequencies were inhibited in the region in which the fluctuation level is constant.
- The correlation between the sensor and the velocity decreased in a narrow neighbourhood of the control hole only.

- The maximum correlation between the upstream wall wire and the downstream hot wire occurred at shorter delays with control applied, *i.e.* the structures appeared earlier with control applied.
- The spanwise structure of the disturbances seemed not to be changed by the control.

Based on the facts above, it was concluded that the low velocity streaks are removed by the control, giving the decrease in energy growth. The growth of disturbance energy appearing downstream of  $x = 600$  mm could be explained with an analogy to the results of Högberg & Henningson (2002), who found that optimal disturbances in a spatially developing boundary layer starts growing again downstream of the control. The mechanism might also be streaks entering from the sides. This can however not explain why the downstream values of the correlation between the hot wire and the wall wire show similar values with and without control applied. A third alternative is that the growth is due to new streaks entering from the free stream.

If the growth is due to disturbances entering from the sides, actuators at one streamwise position might be enough to delay transition. If, however, new streaks are created by the free stream, or by the disturbances remaining after the control, rows of actuators and sensors must be placed after each other in the streamwise direction. A problem which then arises is that downstream of an actuator, the state of the flow in the boundary layer cannot be detected at the wall, since the suction through the hole destroys the correlation between the shear stress at the wall and flow in the boundary layer.

From the parameter study, it was found that high-speed streaks were amplified by the suction while the amplitude of low-speed streaks was decreased. If suction was applied continuously, the two effects canceled each other. The flow response to the timing of the control suction was however asymmetric: when controlling a low velocity streak, being late is better than being early. If the opposite version of this asymmetry applies when controlling high velocity streaks by blowing, the delay has to be chosen dependent on the sign of the disturbance to be canceled.

The spanwise disturbance distributions indicate that the control effect would be almost uniform in the spanwise direction if the actuator spacing is half the spacing used in the present experiment. This means that an actuator spacing of  $25 l^+$  or  $2\delta$  is needed to control streaks such as the present ones. The resulting spacing, 2.5 mm, is about one third of the streak spacing found by spanwise correlation measurements.

## **Acknowledgments**

Professor P. Henrik Alfredsson is acknowledged for inspiration and comments on the manuscript. The craftsmanship of Marcus Gällstedt and Ulf Landén has been a great help in designing and building the setup. Timmy Sigfrids proof

*Reactive control of free-stream turbulence induced transition*

read the manuscript. Economical support from the Swedish Research Council is also acknowledged.

## References

- AMONLIRDVIMAN, K. & BREUER, K. S. 2000 Linear predictive filtering in a numerically simulated turbulent flow. *Phys. Fluids* **12**, 3221–3228.
- ANDERSSON, P., BERGGREN, M. & HENNINGSON, D. S. 1999 Optimal disturbances and bypass transition in boundary layers. *Phys. Fluids* **11**, 134–150.
- ANDERSSON, P., BRANDT, L. & HENNINGSON, D. S. 2001 On the breakdown of boundary layer streaks. *J. Fluid Mech.* **428**, 29–60.
- ASAI, M., MINAGAWA, M. & NISHIOKA, M. 2002 The instability and breakdown of a near-wall low-speed streak. *J. Fluid Mech.* **455**, 289–314.
- BAKCHINOV, A. A., GREK, G. R., KLINGMANN, B. G. B. & KOZLOV, V. V. 1995 Transition experiments in a boundary layer with embedded streamwise vortices. *Phys. Fluids* **7**, 820–832.
- BAKCHINOV, A. A., KATASONOV, M. M., ALFREDSSON, P. H. & KOZLOV, V. V. 1999 Control of boundary layer transition at high FST by localized suction. In *IUTAM Symposium on Mechanics of Passive and Active Flow Control* (ed. G. E. A. Meier & P. R. Viswanath), pp. 159–164. Dordrecht: Kluwer Academic Publishers.
- BEWLEY, T. R., MOIN, P. & TEMAM, R. 2001 DNS-based predictive control of turbulence: an optimal benchmark for feedback algorithms. *J. Fluid Mech.* **447**, 179–225.
- CHANG, Y., COLLIS, S. S. & RAMAKRISHNAN, S. 2002 Viscous effect in control of near-wall turbulence. *Phys. Fluids* **14**, 4069–4080.
- CHOI, H., MOIN, P. & KIM, J. 1994 Active turbulence control for drag reduction in wall-bounded flows. *J. Fluid Mech.* **262**, 75–110.
- ELOFSSON, P. A., KAWAKAMI, M. & ALFREDSSON, P. H. 1999 Experiments on the stability of streamwise streaks in plane Poiseuille flow. *Phys. Fluids* **11**, 915–930.
- ENDO, T., KASAGI, N. & SUZUKI, Y. 2000 Feedback control of wall turbulence with wall deformation. *Int. J. Heat Fluid Flow* **21**, 568–575.
- FASEL, H. F. 2002 Numerical investigation of the interaction of the Klebanoff-mode with a Tollmien-Schlichting wave. *J. Fluid Mech.* **450**, 1–33.
- FRANSSON, J. H. M. 2001 Investigation of the asymptotic suction boundary layer. TRITA-MEK 2001:11. Department of Mechanics, Royal Institute of Technology.
- GAD-EL-HAK, M. 1989 Flow control. *Appl. Mech. Rev.* **42**, 261–292.

- HAMILTON, J. M., KIM, J. & WALEFFE, F. 1995 Regeneration mechanisms of near-wall turbulence structures. *J. Fluid Mech.* **287**, 317–348.
- HÖGBERG, M. & HENNINGSON, D. S. 2002 Linear optimal control applied to instabilities in spatially developing boundary layers. *J. Fluid Mech.* **470**, 151–179.
- JACOBS, R. G. & DURBIN, P. A. 2001 Simulations of bypass transition. *J. Fluid Mech.* **428**, 185–212.
- JACOBSON, S. A. & REYNOLDS, W. C. 1998 Active control of streamwise vortices and streaks in boundary layers. *J. Fluid Mech.* **360**, 179–211.
- KENDALL, J. M. 1998 Experiments on boundary-layer receptivity to freestream turbulence. *AIAA-paper 98-0530*.
- KERHO, M., HEID, J., KRAMER, B. & NG, T. 2000 Active drag reduction using selective low rate suction. *AIAA-paper 2000-4018*.
- KLINGMANN, B. G. B., BOIKO, A., WESTIN, K. J. A., KOZLOV, V. V. & ALFREDSSON, P. H. 1993 Experiments on the stability of Tollmien-Schlichting waves. *Eur. J. Mech., B/Fluids* **12**, 493–514.
- LUCHINI, P. 2000 Reynolds number independent instability of the boundary layer over a flat surface: optimal perturbations. *J. Fluid Mech.* **404**, 289–309.
- LUNDELL, F. & ALFREDSSON, P. H. 2003a Experiments on control of streamwise streaks. *Eur. J. Mech. B - Fluids* Submitted.
- LUNDELL, F. & ALFREDSSON, P. H. 2003b Streamwise scaling of velocity streaks in a boundary layer subjected to free-stream turbulence. *J. Fluid Mech.* Submitted.
- MATSUBARA, M. & ALFREDSSON, P. H. 2001 Disturbance growth in boundary layers subjected to free stream turbulence. *J. Fluid Mech.* **430**, 149–168.
- RATHNASINGHAM, R. 1997 System identification and active control of a turbulent boundary layer. PhD thesis, Dep. of Aeronautics and Astronautics, Massachusetts Institute of Technology.
- RATHNASINGHAM, R. & BREUER, K. S. 1997 System identification and control of a turbulent boundary layer. *Phys. Fluids* **9**, 1867–1869.
- REBBECK, H. & CHOI, K.-S. 2001 Opposition control of near wall turbulence with a piston-type actuator. *Phys. Fluids* **13**, 2142–2145.
- REDDY, S. C., SCHMID, P. J., BAGGETT, J. S. & HENNINGSON, D. S. 1998 On stability of streamwise streaks and transition thresholds in plane channel flows. *J. Fluid Mech.* **365**, 269–303.
- WALEFFE, F. 1995 Hydrodynamic stability and turbulence: beyond transients to a self-sustained process. *Stud. Appl. Math.* **95**, 319–343.
- YOSHIOKA, S., FRANSSON, J. H. M. & ALFREDSSON, P. H. 2003 Evolution of disturbances in a boundary layer with wall suction. In *Turbulence Shear Flow Phenomena 3*. To appear.



# Paper 6

**P6**



# Streak control by a surface-mounted piezo-ceramic flap

By Fredrik Lundell<sup>1,3</sup>, Ayumu Inasawa<sup>2</sup>, Satoshi Kikuchi<sup>3</sup> & Yasuaki Kohama<sup>3</sup>

<sup>1</sup>KTH Mechanics, KTH, S-100 44 Stockholm, Sweden

<sup>2</sup>Aeronautics and Space Engineering, Tohoku University, 980-8579 Sendai, Japan

<sup>3</sup>Institute of Fluid Science, Tohoku University, 980-8577 Sendai, Japan

Transitional structures, generated in a Blasius boundary layer, are suppressed by moving a piezo-ceramic flap. The structures are generated by a speaker through a hole in a flat plate. Downstream of the disturbance hole, a piezo-ceramic flap is positioned. Small (50  $\mu\text{m}$ ) and fast (1.3 ms), repeated movements of the flap are found to be sufficient to inhibit breakdown of the structure.

---

## 1. Introduction

The possibility to decrease friction drag in turbulent flows or delay transition by clever manipulation of the flow has been demonstrated in many numerical studies (see *e.g.* Choi, Moin & Kim 1994 or Högberg, Bewley & Henningsson 2002). Experimental realization of such schemes is currently impossible due to the sensor density, computational power and distributed actuation necessary. If such schemes are to be realized in physical experiments, sensors and actuators with a high density have to be designed and constructed.

In this paper, a flap mounted in a shallow cavity on the surface without other connections than the electrical wire needed to drive it, is used to generate a controlled perturbation. The potential of such an actuator to control a streaky disturbance is demonstrated. The control performance are similar to those of Gad-el-Hak (1989) and Bakchinov *et al.* (1999), who implemented control by localized suction.

In contrast to most actuators studied previously, the flap used in the present experiment can be mounted in a shallow deepening in the surface. Previous experimental studies on flow control have used actuators demanding constructions reaching deeper down into the wall. Examples of actuators are

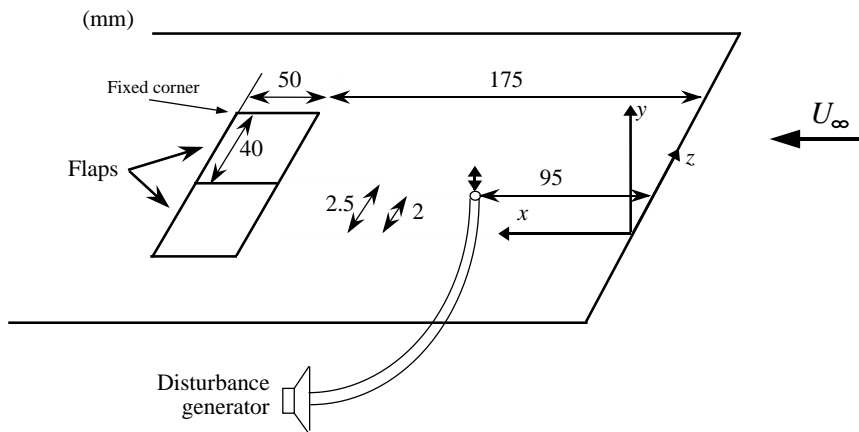


FIGURE 1. Experimental setup.

(i) suction through holes, Kerho *et al.* (2000), (ii) fluctuating jets (demanding resonance chambers in the structure under the actuator), Rathnasingham (1997), (iii) flaps with cavities beneath them, Jacobson & Reynolds (1998) and (iv) the piston type actuator examined by Rebbeck & Choi (2001).

## 2. Experimental setup

The experiments were performed in the MTL wind-tunnel at KTH with the setup sketched in figure 1. The coordinates are  $x$ ,  $y$  and  $z$  as indicated in the figure. The wall-normal coordinate is scaled with  $\delta = (x\nu/U_\infty)^{0.5}$  where  $\nu$  is the kinematical viscosity of the air and  $U_\infty$  is the free-stream velocity. An elongated structure of low velocity with a high frequency oscillation was created by blowing through a 0.5 mm hole at  $x = 95$  mm,  $z = 2$  mm, using a speaker.

Downstream of the hole through which the streak was generated, two piezo-ceramic flaps were positioned. The upstream side of the flap was fixed and the downstream side free to move. By applying a voltage over the flap, it bends out of the plane. During the measurements, only one flap was used. One of the downstream corners of the flap was fixed so that when applying the voltage over the flap, the other corner was lifted, thereby generating a localized velocity perturbation.

A hot wire measuring the streamwise velocity could be traversed in the flow field. At each hot-wire position, 20 realizations of the speaker/flap sequence were sampled and ensemble averaged.

*Streak control by a surface-mounted piezo-ceramic flap*

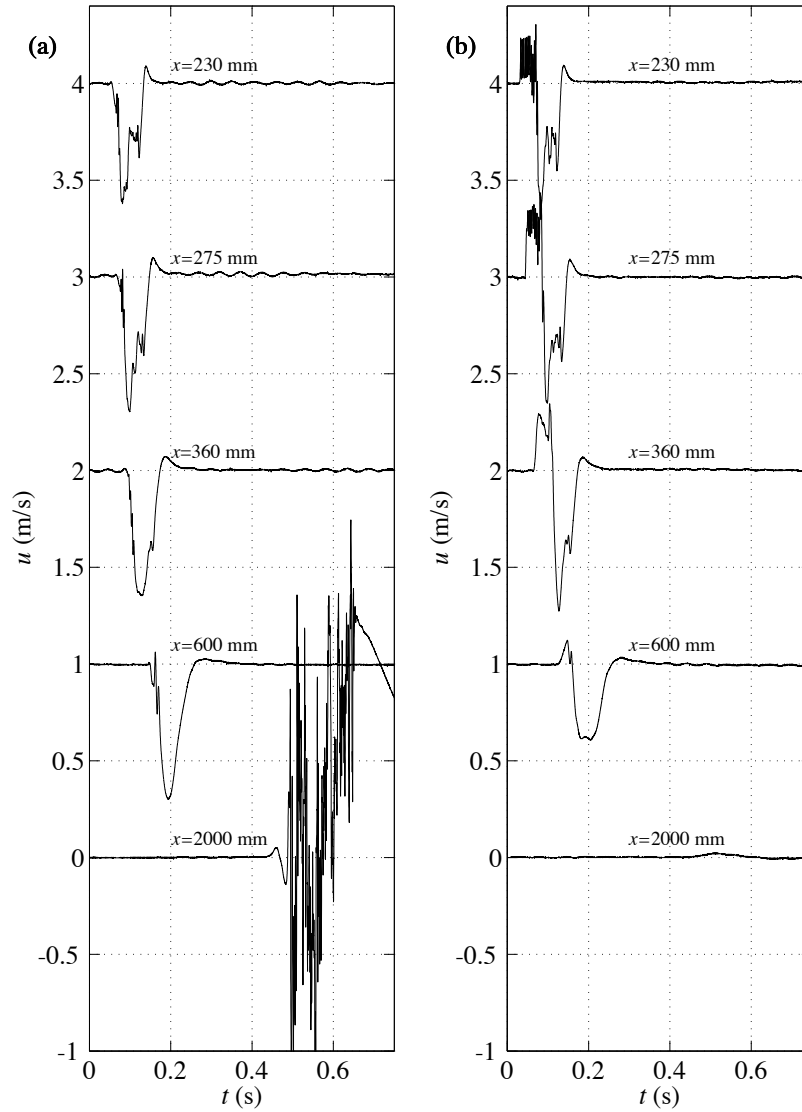


FIGURE 2. Velocity signal (a) without control applied and (b) with. Traces are separated 1 m/s.

### 3. Results

The success of the flap as an actuator is illustrated in figure 2. In (a), velocity traces of the disturbance velocity from the centre of the low velocity structure

( $z = 2$  mm) created by the speaker are shown. At  $x = 230$  mm a low velocity disturbance is seen. As the disturbance develops downstream, the amplitude of the low velocity increases and a high frequency oscillation appears at early times. Finally the signature of a turbulent spot is observed at  $x = 2000$  mm.

If the flap is positioned such that an anti perturbation is created when the flap is activated, the breakdown of the low velocity streak can be inhibited. An example of this is seen in figure 2(b). At  $x = 275$  mm, the high velocity perturbation generated by the flap is seen at  $t < 0.07$  s. Further downstream, a comparison of the traces with and without the flap control applied show that the breakdown of the structure is inhibited.

In figure 3 detailed data of the perturbation and disturbances generated by the speaker and the flap are shown. The subfigures are arranged such that the ensemble-averaged velocity variation at various streamwise positions, when using the flap, is shown in the first column. The second column shows the disturbance generated by the speaker and finally, the result when both the speaker and flap are used is shown in the third column. In each column, the plates are arranged in pairs, each pair corresponding to a streamwise position. The top plate of each pair shows the wall-normal distribution of the disturbance at  $z = 0$  and the second shows the spanwise distribution at  $y = 2$ .

The first column of figure 3 shows that the flap generates an asymmetric perturbation, consisting of one high and one low-velocity streak positioned next to each other. The perturbation is seen to exist from the wall up to  $y = 4$ . The flap was activated twelve times with a short time interval in between. The amplitude of the flap corner was  $50 \mu\text{m}$  (measured with a laser distance meter), the duration of each rise and return was 1.3 ms and the interval between rises was 12 ms. The maximum vertical velocity of the flap was around 0.1 m/s, *i.e.* 2% of  $U_\infty$ .

Initially, each upward motion of the flap corner is seen as a velocity variation. At  $x = 360$  mm the twelve peaks merge to one single perturbation. Further downstream, the amplitude of the perturbation decreases.

Studying the second column, the speaker is seen to generate a low-velocity streak flanked by two high-velocity streaks. At the downstream end of the disturbance (appearing at early times) a high frequency oscillation is amplified, ultimately leading to breakdown as seen in figure 2(a).

If the flap and speaker are actuated in sequence, the breakdown is inhibited (see figure 2). The third column in figure 3(b) shows some details of the interaction between the high-velocity perturbation generated by the flap and the low-velocity streak from the speaker. The high-velocity structure from the flap is seen to interact with the low-velocity disturbance, decreasing the velocity gradients so that the growth of the secondary instability is inhibited. The details of the interaction are intriguing and not simply additive.

*Streak control by a surface-mounted piezo-ceramic flap*

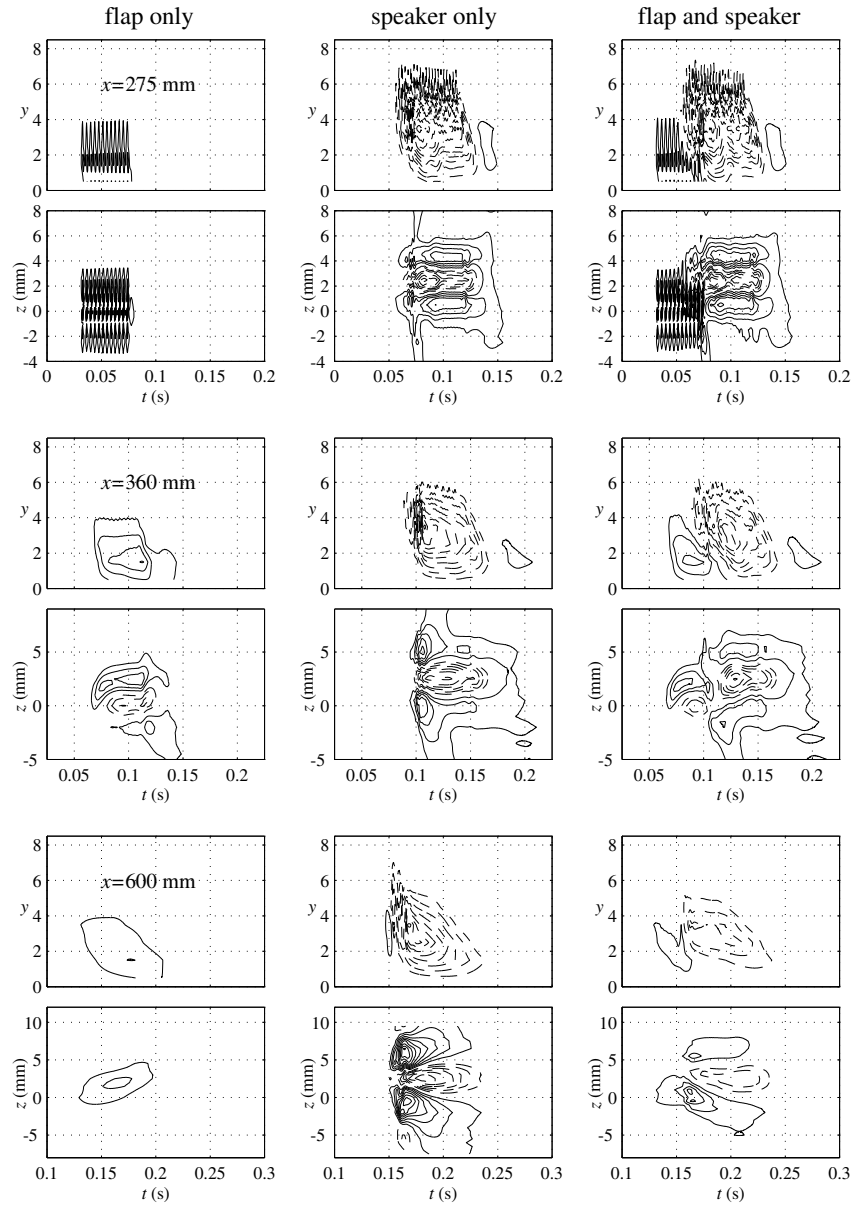


FIGURE 3. Contours of streamwise velocity at  $x = 230, 360$  and  $600$  mm from top to bottom. The columns are the perturbation and disturbance produced by flap only, speaker only and both flap and speaker respectively. Contour separation is 2.5%, negative contours are dashed.

#### **4. Discussion**

This paper follows one of the traditions in experimental flow control studies, namely the study of how an actuator interacts with a generated disturbance as previously outlined by Gad-el-Hak (1989) and Bakchinov *et al.* (1999). In contrast to previous studies, the present study demonstrates the use of surface-mounted actuators.

If used in reactive systems, amplitude modification can be obtained either by varying the amplitude of each flap movement or by pulse-width modulation, *i.e.* varying the pause between the movements of the flap.

The results presented here show successful control of generated disturbances, bound to develop into turbulent spots. Compared to suction, the perturbation generated by the flap is more complicated. Therefore careful modeling of not only the flow response to the actuation, but also of the interaction of the flap perturbation with the disturbances to be controlled has to be performed. An alternative to the chosen methodology would be to do as Rebbeck & Choi (2001), *i.e.* use the actuator a number of times in a random disturbance environment and monitor both the incoming disturbances upstream of the actuator and the downstream result after using the actuator.

## References

- BAKCHINOV, A. A., KATASONOV, M. M., ALFREDSSON, P. H. & KOZLOV, V. V. 1999 Control of boundary layer transition at high FST by localized suction. In *IUTAM Symposium on Mechanics of Passive and Active Flow Control* (ed. G. E. A. Meier & P. R. Viswanath), pp. 159–164. Dordrecht: Kluwer Academic Publishers.
- CHOI, H., MOIN, P. & KIM, J. 1994 Active turbulence control for drag reduction in wall-bounded flows. *J. Fluid Mech.* **262**, 75–110.
- GAD-EL-HAK, M. 1989 Flow control. *Appl. Mech. Rev.* **42**, 261–292.
- HÖGBERG, M., HENNINGSON, D. S. & BEWLEY, T. R. 2002 Localized feedback control and estimation of transition in plane channel flow. *J. Fluid Mech.* **470**, 151–179.
- JACOBSON, S. A. & REYNOLDS, W. C. 1998 Active control of streamwise vortices and streaks in boundary layers. *J. Fluid Mech.* **360**, 179–211.
- KERHO, M., HEID, J., KRAMER, B. & NG, T. 2000 Active drag reduction using selective low rate suction. *AIAA-paper 2000-4018*.
- RATHNASINGHAM, R. 1997 System identification and active control of a turbulent boundary layer. PhD thesis, Dep. of Aeronautics and Astronautics, Massachusetts Institute of Technology.
- REBBECK, H. & CHOI, K.-S. 2001 Opposition control of near wall turbulence with a piston-type actuator. *Phys. Fluids* **13**, 2142–2145.



# Paper 7

P7



# Pulse-width modulated blowing/suction as a flow control actuator

By **Fredrik Lundell**

KTH Mechanics, S-100 44 Stockholm, Sweden

The effect of Pulse-Width Modulated (PWM) blowing/suction through a hole in a flat plate, above which a Blasius boundary layer develops, is studied. A hot wire is used to measure the streamwise velocity downstream of the hole. The PWM blowing/suction is found to create amplitude-modulated variations in the streamwise velocity, well correlated with the generated signal.

---

## 1. Introduction

In fluid systems, possibilities to obtain energy savings appear in cases where separation, laminar/turbulent transition or turbulence occurs. A good reference for methods and results is Gad-el-Hak (2000). The flow can be influenced in the desired direction by non-reactive methods, such as vortex generators, riblets, polymer additives or distributed suction. Another possibility, especially in the case of control of laminar/turbulent transition and turbulence, is the use of reactive control systems.

Among the first to study the possibility to control transitional or turbulent structures, were Gad-el-Hak & Blackwelder (1989). They showed that intermittent suction at the wall can be used to inhibit the breakdown of artificially created low-speed streaks. Later progress has mainly been obtained in numerical studies, notably the demonstration of the possibility to decrease the skin friction by counteracting near-wall vortices in turbulent flow by Choi *et al.* (1994) ("opposition control") and the capability of optimally distributed blowing/suction to relaminarize turbulent channel flow (Bewley *et al.* 2001).

Experimental progress is less spectacular. Rathnasingham (1997) used linear Finite Impulse Response (FIR) filters to design controllers and a pulsating jet as actuator to decrease the bursting in a turbulent channel flow. A different kind of actuator, based on a flap oscillating over a cavity, was used by Jacobson & Reynolds (1998). It was used together with both *ad-hoc* proportional

controllers and neural networks and showed the possibility to decrease the amplitude of generated streaks and vortices in laminar boundary layers. Another experiment was reported by Kerho *et al.* (2000), who used suction through holes, triggered by signals from wall wires upstream of the actuators, to decrease the *rms*-fluctuations in a turbulent boundary layer. Rebbeck & Choi (2001) studied the effect of a piston-type actuator on structures in a turbulent boundary layer.

There are a number of important differences between the experimental and numerical studies. Numerical studies tend to use distributed sensors and modulated actuation. Among the experimental studies, none is even close to live up to this demand on sensor/actuator density. When it comes to the modulated actuation, Rathnasingham (1997) and Jacobson & Reynolds (1998) used actuators allowing a modulation of the output amplitude; it was however limited to one sign: actuation of the opposite sign could not be created and in the first study, this fact was not considered by the controller.

In the present work we study the effect of pulse-width modulated (PWM) blowing/suction on a laminar boundary layer. The pulse-width modulation gives the possibility to modulate the amplitude with a binary actuator and the blowing/suction enables actuation of both signs. In section 2 the concept of pulse-width modulation is described and the experimental setup is introduced. The results are presented in section 3 and finally the conclusions are given in section 4.

## **2. Pulse-width modulation and experimental setup**

The principle of the PWM is described in figure 1. First the original, analog signal is shown in figure 1(a). An excerpt of the signal is shown in (b) and the PWM signal is shown in (c). The last signal is created by varying the duty cycle of a square wave with a fixed frequency so that the relative duty time during each cycle equals to the current value of the analog signal in (b).

In the present work PWM was used to obtain an amplitude-modulated blowing/suction using two pressure chambers, one with high pressure and one with low pressure. An air-pump was used to maintain the pressure difference between the chambers. The two chambers were connected to a hole in a flat plate via a three-way solenoid valve, so that blowing and suction were applied alternately according to the PWM-signal shown in figure 1(c). When the PWM signal was zero, blowing through the hole was applied and consequently, suction was applied when the signal was one. This should create a positive velocity deviation of the mean velocity in the boundary layer downstream of the hole when the control signal has a high value and a negative deviation when the control signal is low.

The measurements were performed in the MTL wind-tunnel at KTH Mechanics in Stockholm in a laminar flat-plate boundary layer. The coordinate

*Pulse-width modulated blowing/suction*

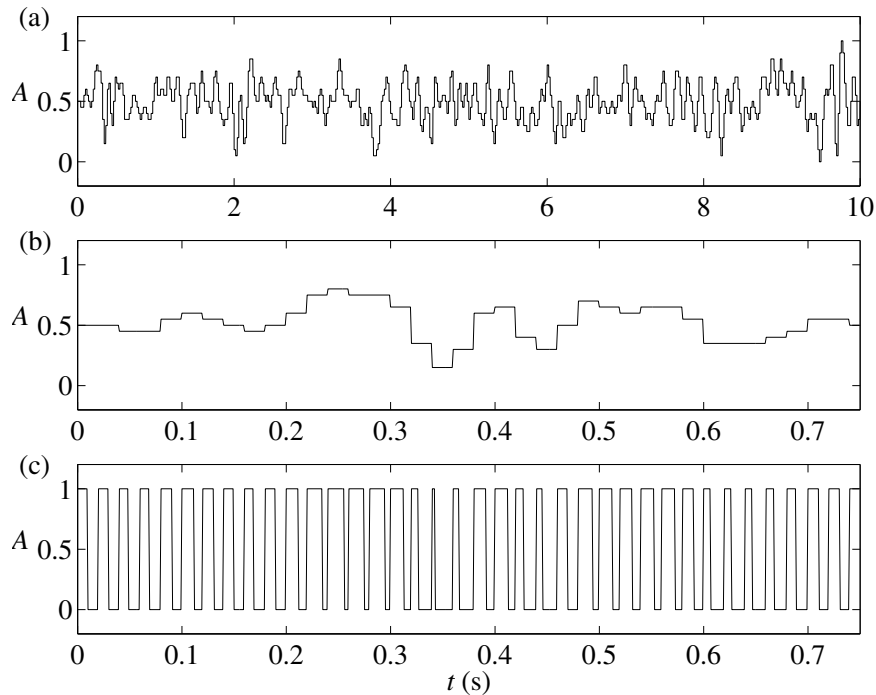


FIGURE 1. Pulse width modulation, (a) original signal, (b) excerpt of the signal in (a), (c) pulse width modulated signal created from the signal in (b).

system is  $x$ ,  $y$  and  $z$  for the streamwise, wall normal and spanwise direction respectively and origin is positioned at the leading edge. The wall-normal coordinate  $y$  is non-dimensionalized with the boundary-layer length scale  $\delta = (x\nu/U_\infty)^{0.5}$ .

The fluctuation of the streamwise velocity is denoted  $u$  and all velocities are normalized with the free-stream velocity  $U_\infty$  ( $=4.8$  m/s). The position of the hole connected to the common port of the solenoid valve was  $x = 450$  mm,  $z = 0$  mm.

In order to study the flow response to the PWM blowing/suction, a Pseudo-Random Binary Signal (PRBS) is used as input to the PWM. Such a signal exhibits certain properties which are beneficial when used for system identification Ljung (1999). The output of the system is the fluctuations of the streamwise velocity measured at different positions downstream of the actuator. The response of the flow to the actuation is characterized by the spatial distribution of the *rms*-amplitude of the output and the correlation between the input and the output.

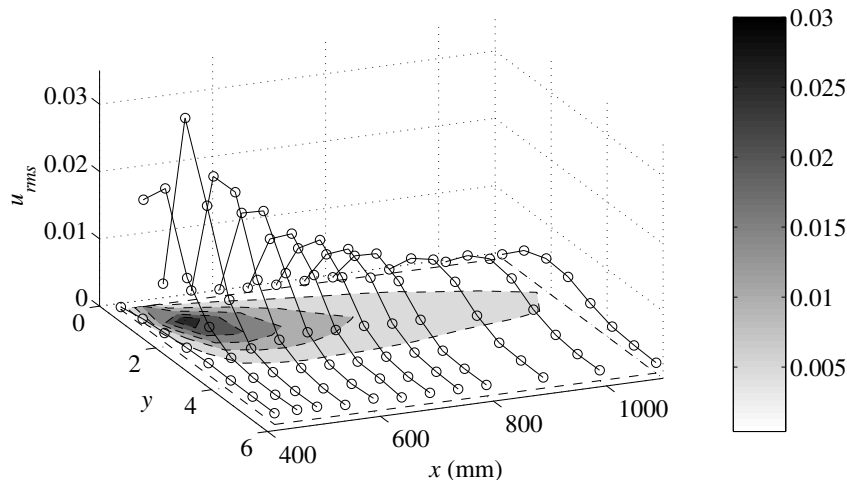


FIGURE 2. Wall-normal distribution of amplitude at  $z = 0$ . Note the direction of the  $y$ -axis.

### 3. Results

In figure 2 and 3 the *rms*-value of the streamwise velocity downstream of the actuation hole is shown. At each measurement point, the blowing/suction from the hole was controlled (via PWM) by the 10 s long signal shown in figure 1(a). In the  $xy$ -plane shown in figure 2, it is seen that the maximum velocity variation is observed close to the wall at  $x = 450$  mm (*i.e.* right above the hole) and moves outward in the downstream direction. At  $x = 600$  mm, the maximum has reached  $y = 2.2$ , where it remains throughout the measurement region. The maximum *rms*-amplitude is reached at  $x = 500$  mm and is about 3% of the free-stream velocity.

The  $xz$ -distribution shown in figure 3 shows that the perturbation is limited to a narrow region with a width of a few millimeters straight downstream of the actuation hole. The amplitudes of the perturbation profiles in figure 3 are lower than what is seen in figure 2 because the data is taken at  $y = 2.6$ .

The spatio-temporal development of the structure created by the blowing/suction is indicated in figure 4. The correlation between the generating signal from figure 1(a) and the hot-wire signal straight downstream of the hole is shown. Figure 4 shows the distribution of the correlation with increasing delays between the signals. At zero delay, as shown in 4(a), the blowing/suction creates a perturbation which stands straight up from the actuation hole at  $x = 450$  mm. Increasing the delay, the correlation distribution moves downstream while being tilted by the shear. The correlation distributions also show that the perturbation exists throughout the boundary layer.

*Pulse-width modulated blowing/suction*

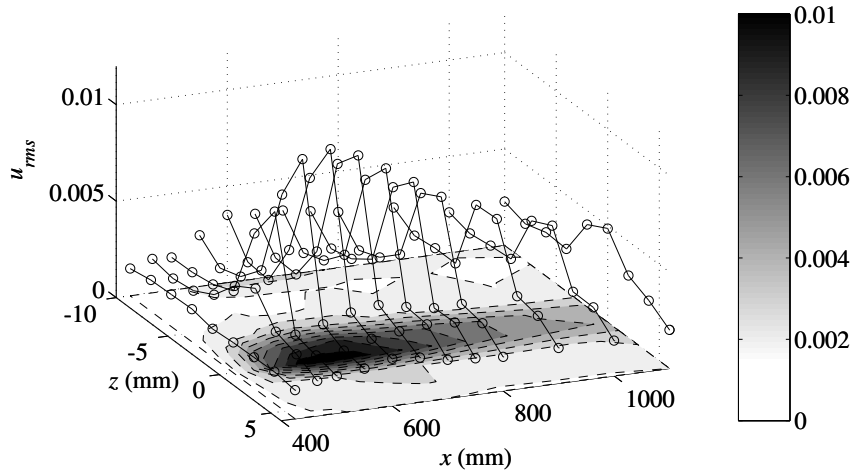


FIGURE 3. Spanwise distribution of amplitude at  $y = 2.6$ .

In order to get an understanding of the structure created by the blowing/suction, the correlation distributions in figure 4 have to be multiplied with the perturbation amplitude in figures 2 and 3. Doing so, it is seen that the pulse-width modulated-width-modulated blowing/suction can be used to generate a structure in the flow which is tilted through the boundary layer and reaching its maximum amplitude 50–100  $\delta$  (*i.e.* 10–20 boundary-layer thicknesses) downstream of the position of actuation.

#### 4. Conclusion

The pulse-width modulated blowing/suction was studied in order to evaluate whether it can be used as a flow control actuator. High (>80%) correlation between the generating signal and the velocity variation in the boundary layer shows that the blowing/suction generates a predictable velocity perturbation in the boundary layer, hence it should be possible to use for flow control purposes.

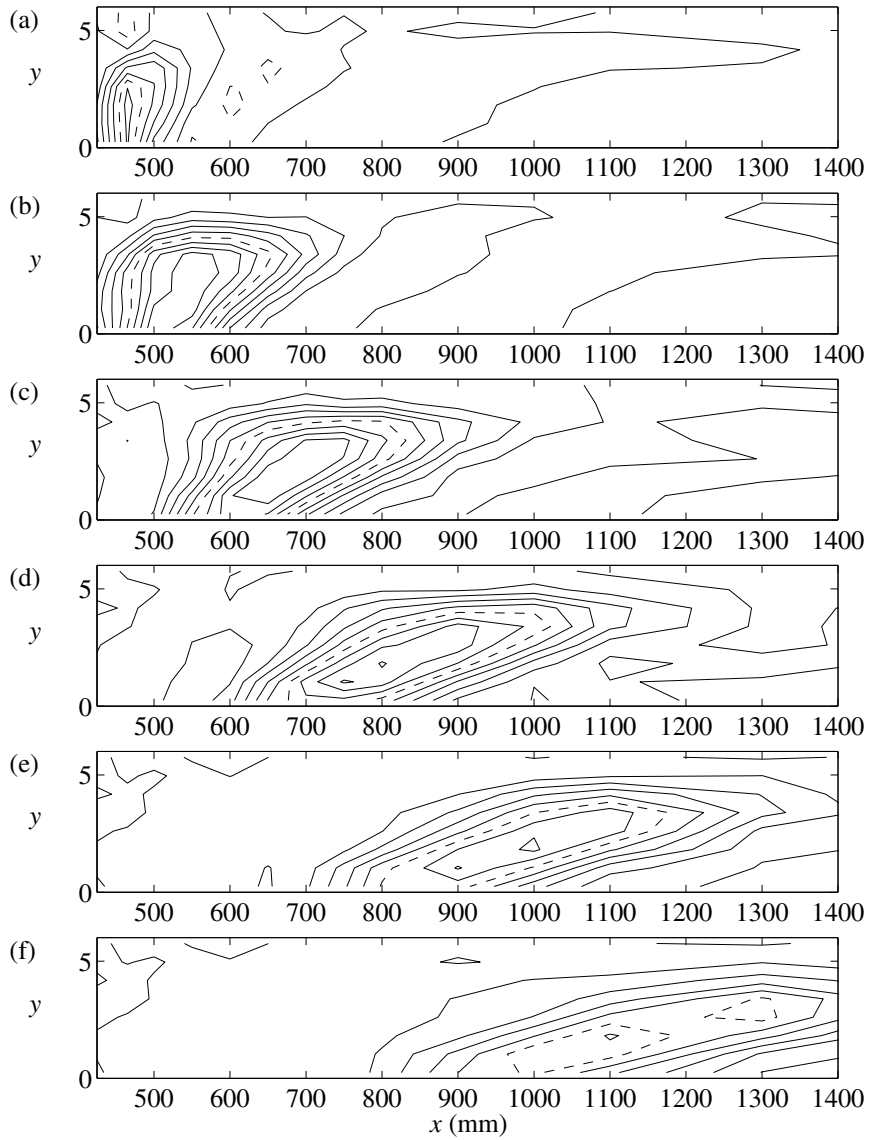


FIGURE 4. Spatio-temporal development of correlation. Delay between signals are 0 (a), 25 ms, (b), ... 125 ms (f). Contours are 10% apart and the 50% contour is dashed.

## References

- BEWLEY, T. R., MOIN, P. & TEMAM, R. 2001 DNS-based predictive control of turbulence: an optimal benchmark for feedback algorithms. *J. Fluid Mech.* **447**, 179–225.
- CHOI, H., MOIN, P. & KIM, J. 1994 Active turbulence control for drag reduction in wall-bounded flows. *J. Fluid Mech.* **262**, 75–110.
- GAD-EL-HAK, M. 2000 *Flow control*. Cambridge University Press.
- GAD-EL-HAK, M. & BLACKWELDER, R. F. 1989 Selective suction for controlling bursting events in a boundary layer. *AIAA J.* **27**, 308–314.
- JACOBSON, S. A. & REYNOLDS, W. C. 1998 Active control of streamwise vortices and streaks in boundary layers. *J. Fluid Mech.* **360**, 179–211.
- KERHO, M., HEID, J., KRAMER, B. & NG, T. 2000 Active drag reduction using selective low rate suction. *AIAA-paper 2000-4018*.
- LJUNG, L. 1999 *System Identification, theory for the user*. Prentice Hall.
- RATHNASINGHAM, R. 1997 System identification and active control of a turbulent boundary layer. PhD thesis, Dep. of Aeronautics and Astronautics, Massachusetts Institute of Technology.
- REBBECK, H. & CHOI, K.-S. 2001 Opposition control of near wall turbulence with a piston-type actuator. *Phys. Fluids* **13**, 2142–2145.